Aminoxyl Radicals -
Pure Organic Materials with Tunable Magnetic and Sensing Properties

Dissertation

zur Erlangung des Grades

“Doktor der Naturwissenschaften”

im Promotionsfach Chemie

am Fachbereich Chemie, Pharmazie und Geowissenschaften der

Johannes Gutenberg-Universität Mainz

Yulia B. Borozdina

Geboren in Irkutsk, Rußland

Mainz (2012)

Dedicated to my family

Table of Contents

Symbols and Abbreviations

Symbols

A_{ij}	hyperfine coupling constant
A_{iso}	isotropic hyperfine splitting
A_N	nitrogen hyperfine splitting constant
B_o	applied external magnetic field tensor
B_r	magnetic field at the center of the spectrum
C_m	Curie constant
D	zero-field splitting parameter
ΔE	difference in energy
ΔE_{ST}	singlet-triplet energy difference
g_e	electron g-factor - 2.0023192778 ± 0.0000000062*
g	observed g-value
h	Planck's constant $\hbar = h/(2\pi) = 1.0545\times10^{-27}$ erg s
$\hat{H}$	spin Hamiltonian
$\hat{H}_{exch}$	Heisenberg-Dirac-van Vleck Hamiltonian (HDVV)
$\hat{H}_{EZ}$	electron-Zeeman interaction
$\hat{H}_{HF}$	hyperfine interaction
J	total quantum number
J	spin-spin exchange coupling constant
L	orbital angular momentum
M	magnetization
N_A	Avogadro number
r	distance between two atoms
S	spin quantum number
$\hat{S}_a$, $\hat{S}_b$	electron-spin operators
T_C	Curie temperature
ε	extinction coefficient
θ	Weiss constant

* Taken from B. N. Taylor, W. H. Parker, D. N. Langenberg, *Rev. Mod. Phys.*, **1969** (41), 375.

μ_B	Bohr magneton* - $\beta = e\hbar/(2mc) = 9.2740 \times 10^{-24}\ J/T$
μ	effective magnetic moment
υ	frequency
χ_{mol}	molar magnetic susceptibility

Abbreviations

AFM	atomic force microscopy
BHA	2,3-dimethyl-2,3-bis(hydroxylamino)-butane
CV	cyclic voltammetry
DCM	dichloromethane
DMF	*N*,*N*-dimethylformamide
DMSO	dimethylsulfoxide
DPPH	*N*,*N*'-Diphenyl-*N*'-picrylhydrazyl
EPR	electron paramagnetic resonance
FD-MS	field desorption mass spectrometry
HOMO	highest occupied molecular orbital
LUMO	lowest unoccupied molecular orbital
NBS	*N*-bromosuccinimide
NMR	nuclear magnetic resonance
PL	photoluminescence
QY	relative quantum yield
SOMO	singly occupied molecular orbital
SQUID	superconducting quantum interference device
TDAE	tetrakis(dimethylamino) ethylene
TFA	trifluoroacetic acid
TLC	thin layer chromatography
THF	tetrahydrofuran
UV-Vis	ultraviolet-visible spectroscopy
zfs	zero field splitting

Chapter 1

Introduction and Motivation

1.1 Introduction into stable radicals

Free radicals are a kinetically independent species characterized by the presence of an unpaired electron. The highly reactive, often transient nature of radicals is a reflection of the fact that their major reactivity pathways—dimerization (1), combination (2), disproportionation (3) - are strongly favored thermodynamically, and these reactions typically occur with little to no activation barrier at very high rates:

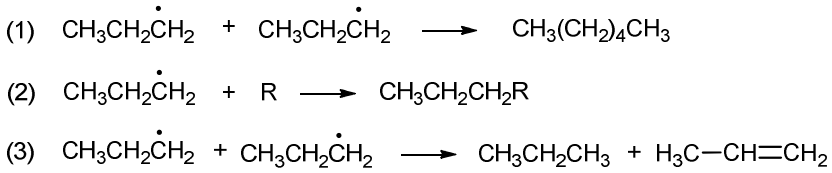

Scheme 1.1. The main types of radical reactions.

Several radical classes are currently in active use towards building organic based magnets. For example, carbenes, nitrenes, phenoxides and ketyl based radicals (*Fig. 1.1 (a)*). Although application of these radicals is often complicated by high lability and reactivity of these compounds at normal conditions. The radicals from the sub-group *(b)* in *Figure 1.1* posses much higher stability at ambient conditions.[1] From now on we will use the term *stable radicals* to describe radicals, which do not react with oxygen or moisture and, from a practical perspective, which can be isolated, handled, and stored (for prolonged time) as pure compounds under normal laboratory conditions.[2,3] Stable radicals are recognized for over a century, and some were in fact synthesized over 150 years ago. Classical examples of such radicals are Gomberg's triphenylmethyl radical, Fremy's salt, *N*,*N*'-diphenyl-*N*'-picrylhydrazyl (DPPH), nitroxides such as (2,2,6,6-tetramethyl-piperidin-1-yl)oxyl (TEMPO), verdazyl (VZ), nitronyl (NN) and imino nitroxides (IN), *tert*-butylnitroxide radical (TBN) etc., which partially are presented in *Fig.1.1 (b)*.

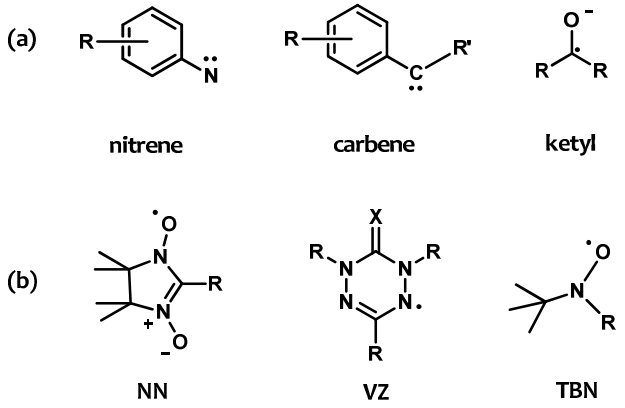

Figure 1.1. Examples of radical units frequently used as spin-carrying blocks.

Much of the current interest in stable radical chemistry arises from their status as "novelty acts" and, more essentially, from the fundamental structure and bonding issues that naturally arise with this class of compounds. Nevertheless, there are many areas of chemistry that take advantage of the properties afforded by the specific combination of open-shell configuration and chemical stability. Certain kinds of radicals are widely used as (co)catalysts for the oxidation of alcohols to carbonyl compounds,[4] while other radicals are exploited for their ability to act as *anti*oxidants.[5] The transition metal coordination chemistry of radicals has been an active area of interest to inorganic chemists for the last decades;[6,7] and polymer synthesis has received a significant boost after the development of stable-radical-mediated living radical polymerization processes.[8] Recently, there have been widespread efforts aimed at developing new materials with technologically relevant properties (magnetism, conductivity) for which stable radicals are excellent building blocks due to the presence of unpaired electrons.[9,10]

Initially established employment of stable radicals in physicochemistry, biochemistry and medicine was restricted to their application in spin-labelling chemistry.[11] Techniques such as spin trapping[12] and, more recently, EPR imaging[13] can provide plenty of information on systems into which stable radicals have been introduced. Radical reactions are implicated in a huge range of biological processes, and stable radicals are often the key players — from simple radicals such as NO and O_2 to tyrosyl[14] and flavine[15]-based compounds. Nowadays, they play an important role as spin probes for investigation of microstructure and membrane dynamics,[16] metabolism and

oxygenation,[17] pH and redox status in cellular systems,[18] for studying the dynamics in biological systems,[18] *etc*. However, the application of the reported probes is often complicated by low selectivity, unsatisfactory sensitivity and the difficult processability. In this regard, elaboration of new efficient and versatile sensors providing reliable information about the state of the studied system by means of real-time monitoring is of great interest. A reasonable approach employing nitroxide radicals, which seems to be able to fulfill such a challenging task, is described in the last section of the current chapter. Furthermore, this chapter represents a brief overview of some stable radical families, with the focus on nitroxides, which are commonly involved in the study of molecular-based magnetic materials. Some aspects of metal complexation are highlighted as well, and the origins of magnetism in diradicals and polyradicals are discussed.

1.1.1. Triphenylmethyl and related radicals

Gomberg's synthesis of the triphenylmethyl (TPM) radical **1** in 1900 was a landmark discovery as it marked the beginning of the organic free radical chemistry.[19]

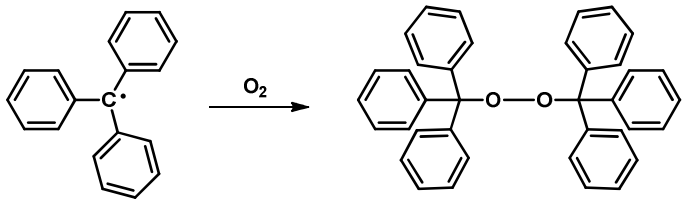

1 **2**

Scheme 1.2. Reaction of the TPM radical with oxygen.

There was much of dispute as to the identification of **1**, since the radical is air-sensitive and rapidly forms peroxide **2** upon reaction with oxygen, but Wilhelm Schlenk and coworkers in 1910 obtained tris(4-biphenyl)methyl **3**, which confirmed the existence of **1**. Heteroaromatic analogues of **1** in which one or more of the phenyl groups is replaced by, *e.g.*, pyridyl,[20] thienyl,[21] or benzotriaozlyl[22] do not show dramatically different stability from the parent compound. The tendency to dimerize can be attenuated and, in some cases, completely hindered through the proper substitution. The perchlorinated triphenylmethyl **4** is not only stable, but essentially chemically inert. For example, reaction of the derivative **4** with concentrated sulfuric acid or bromine takes

several days.[23] Such extraordinary stability of the radical **4** originates from steric shielding of the central carbon by the six *ortho* chlorine atoms (*Fig. 1.2*).

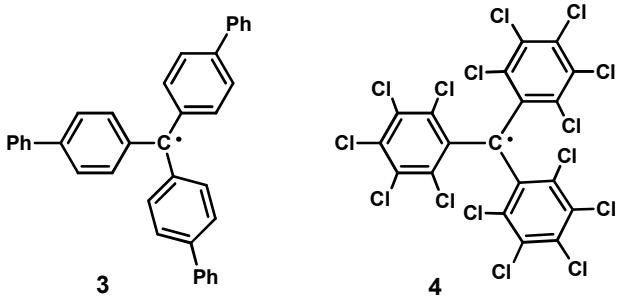

Figure 1.2. Examples of triphenylmethyl radicals.

Compound **4** is the prototype of a large number of stable polychlorinated triphenylmethyl (PTM) radical derivatives.[24] More recent work on partially chlorinated derivatives reveals that the six chlorines in the *ortho* positions appear to be sufficient and necessary for radicals of this type to be exceptionally stable.[25,26]

1.1.2. Hydrazyl and verdazyl radicals

N,*N*'-Diphenyl-*N*'-picrylhydrazyl (DPPH) **5** is by far the best known derivative among hydrazyl radicals [$R_2NNR^{\bullet}$].[27] In general, hydrazyl radicals are only persistent, and often are not very long-lived in solution. For instance, closely related analogues of **5** in which only the *p*-nitro or one of the *o*-nitro groups is removed are not stable, despite their otherwise close structural resemblance to DPPH. From the other hand, substitution of the *p*-nitro group in DPPH for a nitrone or imino nitroxide moiety leads to a number of stable multifunctional derivatives, which could be used as spin-traps or pH-sensitive probes.[28]

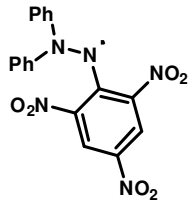

Figure 1.3. Structure of *N*,*N*'-diphenyl-*N*'-picrylhydrazyl radical **5**.

Hydrazyl radicals,[29] including the unique DPPH,[27] were discovered in the 1920s by Goldschmidt.[28a] The scientific activity associated with hydrazyl radicals has become

completely dominated by DPPH itself, mainly owing to its widespread use as (i) an EPR standard,[30] (ii) a radical scavenger in polymer chemistry,[8] and (iii) an indicator for antioxidant chemistry.[31] For instance, radical **5** is widely used to estimate radical scavenging activity of various bioactive natural products.[32]

In contrast to the relatively poor stability of most hydrazyls, there are several kinds of stable radicals in which the hydrazyl subunit is incorporated into a delocalized (and often cyclic) π system. For example, radicals **6**, **7** represented in *Figure 1.4* are sufficiently stable for R = Ar.[33,34] V*erdazyls* could be referred as another type of stable hydrazyl radicals.

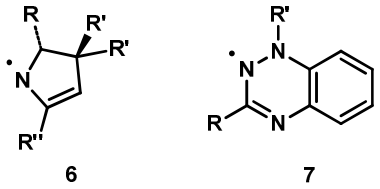

Figure 1.4. Stable hydrazyl radicals **6**, **7**.

Verdazyl radicals (Vz) have general structure **8** shown in *Fig. 1.5* and can be categorized according to the nature of the C-6 ring carbon atom. Verdazyls **9** ("*Kuhn verdazyls*") have a saturated carbon at C-6 and nearly always have aromatic substituents on each of the nitrogen atoms (R' and R''). Verdazyls containing a carbonyl (oxo-verdazyls **10**), or thiocarbonyl (thioverdazyls **11**) group at C-6 were developed in the 1980s by Neugebauer.[35]

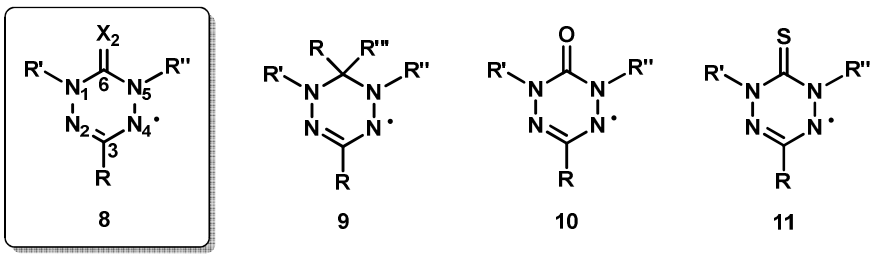

Figure 1.5. Different types of verdazyl radicals.

One major property that effects magnetic characteristics covering all size scales, from molecules to bulk materials, is how unpaired electrons, or spins, interact. Due to the light nature of elements composing organic compounds, only the intramolecular magnetic exchange interactions determine the magnetic behavior in the range of temperatures well above 0.1 K. Other kinds of magnetic interactions (such as hyperfine or

spin-orbital interactions) as well as sources of magnetic anisotropies can be considered as negligible above this temperature in most open shell organic materials. Consequently, magnetic organic system may be described at zero applied magnetic fields by the effective spin Hamiltonian approach:

$$H = -2 \sum J_{ij} S_i S_j \qquad (\mathbf{1})$$

where J_{ij} represents the effective exchange interaction parameter for the magnetic centers *i* and *j* – the spin-containing units – which have total quantum spin numbers S_i S_j, respectively. According to the formalism of *equation (1)*, when J_{ij} is *positive* the two spins tend to be parallel to each other in the ground state and the magnetic coupling is ferromagnetic. On the contrary, if J_{ij} is *negative* the two spins align in an antiparallel fashion and the interaction is antiferromagnetic.

Most organic magnetic materials exhibit paramagnetic behaviors at high temperatures where the spins of the material behave independently of each other. However, as lower temperatures, the neighboring spins tend to align in accordance with the signs of their J_{ij} parameters. Alignment of spins can be propagated along one, two or three dimensions of the solid, but only if the alignment occurs in three dimensions a real long range magnetic ordering can appear. In this case the solid exhibits a cooperative magnetic property below its critical temperature (T_C), behaving as a bulk magnet. For a magnetic material to be technologically useful, T_C should be at least as high as above liquid nitrogen, ideally above room temperature. In a molecular magnetic material this property is primarily determined by the dimensional exchange of electrons on individual components, *i.e.* the stronger the components exchange in three dimensions, the higher the ordering temperature is.

Verdazyls are potentially bridging through two nitrogen atoms carrying large spin densities.[36] In that respect, they resemble nitroxides because, depending on the metal ion, magnetic interactions are large and ferromagnetic (Cu(II), Ni(II), Co(II)) or antiferromagnetic (Mn(II)).[37] Hicks reported the preparation of the first verdazyl radical complexes of open-shell ions with Ni(II) and Mn(II).[37a] Reactions of a pyridine-based verdazyl **12** (*Fig. 1.6*) with $Mn(hfac)_2 \times 2H_2O$ afforded air-stable complexes **13a** (M = Ni) and **13b** (M = Mn). Preliminary X-ray crystallographic data confirmed the mononuclear, pseudo-octahedral nature of complexes **13a** and **13b**, both of which contain a fully planar, chelating ligand **12** as shown in *Figure 1.6*. The susceptibility of Mn complex **13b** can be

explained by a model in which the verdazyl and manganese spins are antiferromagnetically coupled with J_{AB} = -65 K. Therefore, the ground spin state of the complex may be sketched as one parallel Mn (S = 5/2) spin and one antiparallel radical (S = 1/2) spin, leading to $S_{complex}$ = 2.

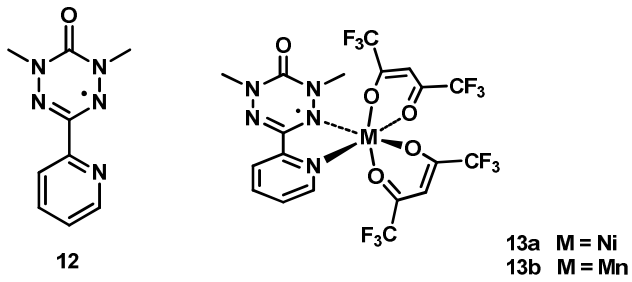

Figure 1.6. Molecular structure of pyridine-based verdazyl radical and its complexes with $M(hfac)_2$.[37a]

The magnetic behavior of Ni complex **13a** is consistent with that of a ferromagnetically coupled S_A = ½, S_B = 1 pair with J_{AB} = +345 K. It was concluded, that in the case of Ni(II) the verdazyl-metal coupling was strong and ferromagnetic. Although the ground state of this Ni(II) complex is rather low (3/2), it illustrates a general synthetic approach, where the choice of ancillary ligands is important. These results indicate the potential of creating new magnetic materials based on coordinated verdazyl radicals and paramagnetic metal ions.

1.1.3. Nitroxide radicals

Nitroxides $[R_2NO]^{\bullet}$ are the most well-known class of stable radicals. The first nitroxide - an "inorganic" derivative, Fremy's salt **14** - is known over 150 years, and the first "organic" nitroxide - 1-imidazolidinyloxy-2,4-diimino-5,5-dimethyl-porphyrexide **15** - was discovered very shortly after the triphenylmethyl radical at the beginning of the 20th century. Nitroxide chemistry has a long and rich history, and there are many derivatives which are stable with respect to air, water, dimerization, and other radical-involving reactions. The versatility of these radicals is further enhanced by the fact that a fairly diverse range of organic chemistry can be carried out on remote sites of molecules carrying a nitroxide group without affecting the radical site itself. Nitroxide radical chemistry has been compiled in a number of books and reviews.[31a,38,39]

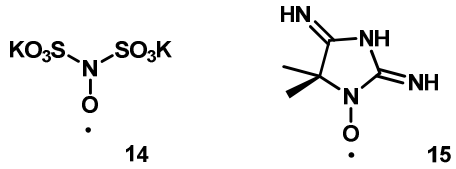

Figure 1.7. The first nitroxide radicals.

Nitroxides have substantial spin density on both N and O, which can be illustrated by one of two resonance structures **16a** and **16b**. In the language of molecular orbital theory, the electron resides in an NO π^* orbital. It is interesting to compare the stability of these two tautomers. The NO bond in nitroxide does not suffer from the conformationally-driven destabilizing effects, because the oxygen atom carries no substituent.

Figure 1.8. Resonance stabilization of the nitroxides.

Nitroxides with two quaternary carbon-based substituents are quite robust, *e.g.* (2,2,6,6-tetramethyl-piperidin-1-yl)oxyl **17** (TEMPO), *tert*-butyl nitroxides (TBN) **18**, **19** and **20**. Several nitroxides of this type are commercially available, often with a remote functional group for modification for spin-labeling applications.

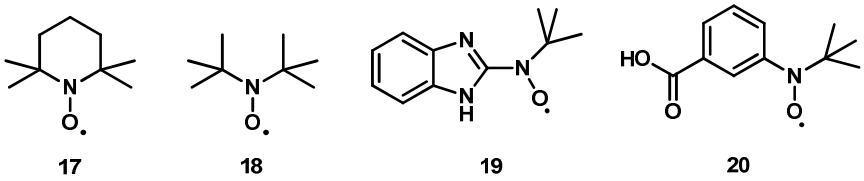

Figure 1.9. Stable nitroxide radicals.

To control the intermolecular exchange interactions and the resultant magnetic behavior of the compounds, one should be able to arrange molecules in a predictable fashion. Therefore, much interest in the field of organic-based magnetic materials was focused on studying the magneto-structural correlations and finding the way to adjust them.

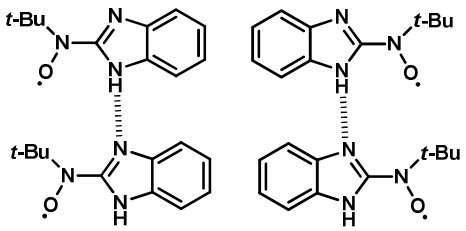

Figure 1.10. Schematic diagram of packing pattern for radical **19**.

Hydrogen bonding, as well as π-stacking, covalent and noncovalent interactions are commonly involved in directed crystal packing formation. 2-(*N-tert*-butylaminoxyl)benzimidazole **19** and 3-(*N-tert*-butylaminoxyl)benzoic acid **20** are some of the model compounds, synthesized to gather more information about the relationship between crystallographic assembly and exchange interactions.[40] Radical **19** was shown to be a bulk antiferromagnet with a Neél temperature[*] of 1.7 K.[41] The system forms hydrogen bonded chains involving the benzimidazole N-H unit,[40a] as demonstrated in *Figure 1.10*.

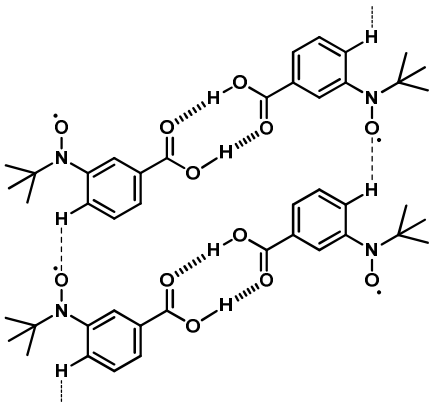

Figure 1.11. Schematic representation of close contacts in nitroxide **20**.

Interestingly, radical acid **20** forms dimer aggregates by the complementary association of two carboxylic groups through the hydrogen bonding in solid state (*Fig. 1.11*).[40b] Due to such arrangement in the crystal there are no close direct spin pairing contacts between radical fragments. Therefore, the magnetic interactions are transmitted presumably through noncovalent hydrogen bonding.[40b,c]

[*] The *Néel temperature* or *magnetic ordering temperature*, T_N, is the temperature above which an antiferromagnetic material becomes paramagnetic - that is, the thermal energy becomes large enough to destroy the macroscopic magnetic ordering within the material.

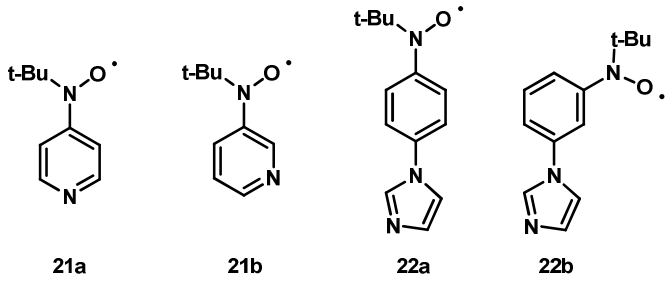

Figure 1.12. Examples of some TBN ligands.

The oxygen atom of the nitroxide group exhibits weak basicity; therefore, it demonstrates coordinating ability with respect to transition metal ions, which allows assembling metal ions and nitroxide radicals in low dimensional materials in order to obtain bulk magnets.[42-46] Iwamura has described TBN functionalized pyridines **21a**,**b** and imidazoles **22a**,**b** (*Fig. 1.12*), which were used for the preparation of a number of metal complexes.[47]

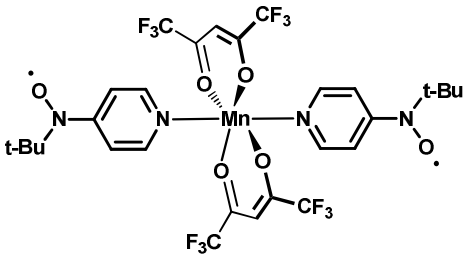

Figure 1.13. Structure of a complex formed between **21a** and $Mg(hfac)_2$.

Notably, for all complexes the primary mode of binding between a ligand and bis(hexafluoroacetylacetonato)manganese (II) ($Mn(hfac)_2$) through the pyridyl nitrogen was observed, as shown in *Figure 1.13* on example of 4-(*N*-oxy-*N*-*tert*-butylamino)pyridine **21a**. Furthermore, magnetic interactions between the radical and metal could be controlled by varying the position of the nitroxide group. Thus, the interactions were ferromagnetic when the nitroxide was attached in the *para* position (compounds **21a**, **22a**), and antiferromagnetic for the *meta* isomers (radicals **21b**, **22b**). Moreover, it was shown, that the magnitude of the magnetic interactions decreases from pyridines **21a**,**b** to imidazoles **22a**,**b** serie, due to the increase of the relative distance between the radical moiety and the metal center.

Nitronyl nitroxides (**NN**) represent another class of stable radicals (*Fig. 1.14*), which are extensively used as building blocks for organic magnetic materials and in spin

labeling of small molecules.[48] Ullmann first reported nitronyl nitroxides nearly 40 years ago.[49] The fundamental aspects of their electronic structure are well-established.[12a] These radicals incorporate the necessary features for stability (*e.g.*, no α-hydrogens) typical for nitroxides, and can thus be made with a wide variety of *R* groups. The stability of nitronyl nitroxides generally rivals the most stable examples of nitroxides. The π SOMO spans both NO groups and has a nodal plane passing through the central carbon atom, although spin polarization leads to nearly negligible spin on carbon, which can be influenced by electron withdrawing or donating groups (*Fig. 1.14*). As a result the spin distribution is symmetrically disposed about the two NO groups and is only slightly affected by the substituent *R*.

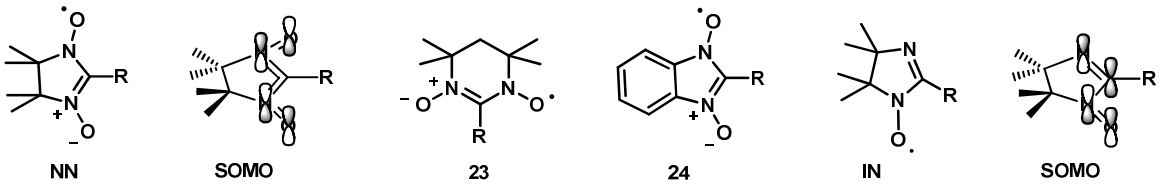

Figure 1.14. Some examples of nitronyl **23**, **24** (NN) and imino nitroxide (IN) radicals, together with the SOMOs of the first and the last cases.

Nitronyl nitroxide radicals based on other structural templates are known. For example, *Rey* has developed the synthesis of pyrimidinyl nitronyl nitroxides **23**,[50] whose electronic structures are generally quite similar to those of the more familiar imidazoline-based nitronyl nitroxides **NN**. Benzannelated analogues **24** have not yet received much attention,[51] though recent experimental and computational studies indicate that there is at least partial delocalization of spin from the ONCNO moiety onto the annelated ring.[52]

Nitroxide radicals in which the NO group is conjugated to a C=N moiety, so-called "*imino nitroxides*" (**IN**) (*Fig. 1.14*), generally posses higher stability compared to the corresponding nitronyls.[53] EPR spectroscopy, neutron diffraction, and computational studies indicate that spin on the nitroxide nitrogen is substantially larger than on the imino nitrogen, though the latter nitrogen does possess substantial spin density.[53,54a] In contrast to the NN in the imino nitroxides the carbon atom of the NCNO moiety is not necessarily a node of the SOMO (*Fig. 1.14*), but experimentally negative spin population is observed on this carbon atom.[54] Nevertheless, the effect is less pronounced than in the NN radicals.

Since magnetism is a bulk property spin carrying ligands, such as nitronyl- (**NN**) and imino- (**IN**) nitroxides, are particularly attractive.[55,56] They both bear several oxyl groups and unsaturated structures allowing correlation of the unpaired spin density over the different coordination sites. They are the cornerstones of the metal–radical approach toward molecular magnets.[57,58]

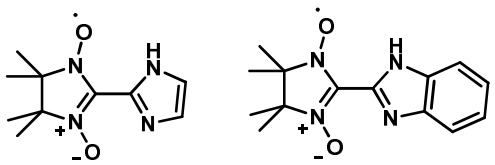

25 26

Figure 1.15. Examples of NN radicals with additional chelating sites.

For example, Luneau has described a set of ligands based on functionalization of imidazole **25** and benzimidazole **26** (*Fig. 1.15*).[59] These compounds have been successfully employed as bridging ligands in either one- or two-dimensional complexes with $Mn(hfac)_2$. Spin-spin interactions between the metal and ligand are typically moderately strong and antiferromagnetic in nature. The two-dimensional structures based on **26** exhibited evidence for bulk magnetization at 40 K, which far outpaced the similar complex with **25**, where magnetization was observed only at 1.4 K.

There are cyclic transition metal complexes with nitroxide or nitronyl nitroxide radicals. The number of spins in such complexes is finite, therefore, the systems can be described by a rigorous solution of the spin Hamiltonian to give the sign and the magnitude of the exchange coupling. These values serve as good measures for designing and analyzing of new extended systems containing two or more types of exchange coupling parameters.[60] Example of a discrete high-spin ferrimagnetic ring, formed by phenyl-nitronyl nitroxide derivative with $Mn(hfac)_2$, is shown in *Figure 1.16*.[61] $[Mn(hfac)_2NNPh]_6$ is a crown molecule with an overall S_6 symmetry. The low temperature ($5 K < T < 50 K$) magnetic measurements revealed the presence of a strong antiferromagnetic coupling between the Mn(II) spins and the NO spins, resulting in a S = 12 ground state.[†] The high temperature ($150 K < T < 300 K$) magnetic study allowed the determination of an average exchange coupling constant J/k = 480 K.[46b] Note, that free radicals are rich donors for metal ions, and perfectly suited for giving large exchange

[†] For strong antiferromagnetic coupling all the manganese (II) spins (S = 5/2) are up, and the radical ones (S = ½) are down, giving therefore for 6 Mn-NN couples 6×(5/2 - 1/2) = 12 spins.

interactions and very robust high-spin ground states. However, despite the large S value, the compound behaves as a paramagnet throughout the temperature range 5 – 300 K.[61]

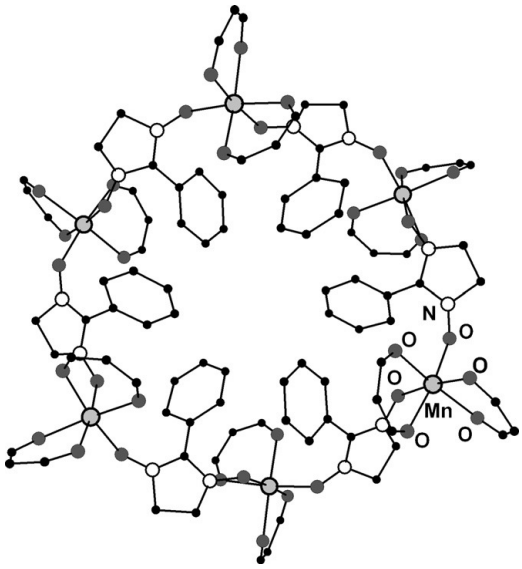

Figure 1.16. Molecular structure of the cyclic $[Mn(hfac)_2NNPh]_6$ complex. Hydrogen, fluorine atoms, and methyl groups are omitted for clarity.[61]

Multiple examples of complexes with nitroxide and nitronyl nitroxide radicals in particulary have been described during the last 20 years,[58,62] demonstrating fruitfulness of the supramolecular approach. Nevertheless, construction of high-dimensional networks using magnetic metal ions with organic free radicals serving as bridging ligands (the so-called *hybrid approach*) remains a challenging task, since the structure of the desired complexes are difficult to predict, and the design seems to depend on serendipity.[63]

1.2. Monoradicals as magnetic materials

There are several different mechanisms governing the through-space coupling of unpaired electrons in molecular systems.[64] These mechanisms can be divided in two classes: (i) spin-exchange (McConell I) and (ii) charge transfer mechanisms.[64] The McConell I mechanism predicts a ferromagnetic coupling only if the regions with positive spin densities of a given open-shell molecule are in contact with the negatively spin polarized regions of a neighboring molecule. According to the charge transfer mechanism,

a ferromagnetic coupling among two open-shell molecules only occurs if there exists an intermolecular overlap between the singly occupied molecular orbital (SOMO) of one molecule and the next highest doubly occupied MO (NHOMO) and/or the lowest unoccupied one (LUMO) of the other one and, moreover, if the overlap between SOMOs of both molecules is disfavored. From the above description it is clear that in order to produce ferromagnetic interactions in open-shell molecular solids it is required not only to choose carefully the electronic characteristics of open-shell molecules (*e.g.* molecules with large spin polarizations), but also to orient them properly relative to each other. Since all these conditions are not easy to accomplish, ferromagnetic interactions in purely organic molecular solids are extremely rare.

Almost all attempts in the design of purely organic radicals systems showing spontaneous magnetization have involved nitroxide radical derivatives as building blocks. There are several reports made by the groups of Kinoshita[65] (compound **27** in *Fig. 1.17*) and Rassat[66] (for further details see section *1.3 Biradical and polyradical systems* of the current chapter), who have succeeded in finding organic crystalline ferromagnets. The strength of the exchange interaction between free radical molecules in van der Waals contacts or in hydrogen-bonding is limited, the ordering temperatures (T_C) of the crystals among the majority of free radicals is very low (1K).

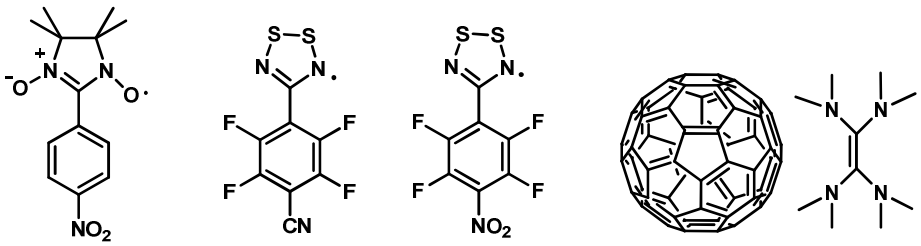

Figure 1.17. Examples of organic ferromagnets.

One approach to raise the magnetic ordering temperature utilizes the more diffuse nature of the *3p* sulphur orbitals compared to the *2p* ones of the oxygen atoms. The heterocyclic dithiadiazolyl radicals *p*-$NCC_6F_4CNSSN^{\bullet}$ (**28**) and *p*-$O_2NC_6F_4CNSSN^{\bullet}$ (**29**) have provided some promising results.[67] The main difficulty of utilizing dithiadiazolyl radicals, however, is the lack of sufficient steric protection to inhibit dimerisation. Perfluoraryl groups are commonly used as stabilizing substituents in aromatic ring. Firstly

described in 1996 dithiadiazolyl **28** (β-phase) demonstrated bulk ferromagnetic ordering at unprecedented high temperature under ambient pressure – 36K,[68,69] although this compound is known as a *weak ferromagnet*. For the nitro analogue **29** the T_C value is only 1.3K.[69]

Remarkably, that due to the charge transfer interactions between donor and acceptor molecules in purely organic compounds - tetrakis(dimethylamino) ethylene-C_{60} **30a** (TDAE-C_{60}) - a T_C as high as 16 K could be achieved.[70] TDAE-C_{60} possesses monoclinic structure (space group C2/*m*). More detailed X-ray structural analysis revealed that unusually short distances between adjacent C_{60} units are responsible for the coupling between spins localized on neighboring C_{60}^- ions and the formation of the ferromagnetically correlated spin state. The discovery of other non-TDAE fullerene ferromagnets[71] (for instance alkali fullerides AC_{60}, where A = Rb[72], Cs[73]), provided additional evidence favoring the suggestion, that it was the peculiar structure of the TDAE molecule, determining the rotational degrees of freedom of C_{60}, but not the spins, which played the crucial role on the magnetic properties of TDAE-C_{60}.

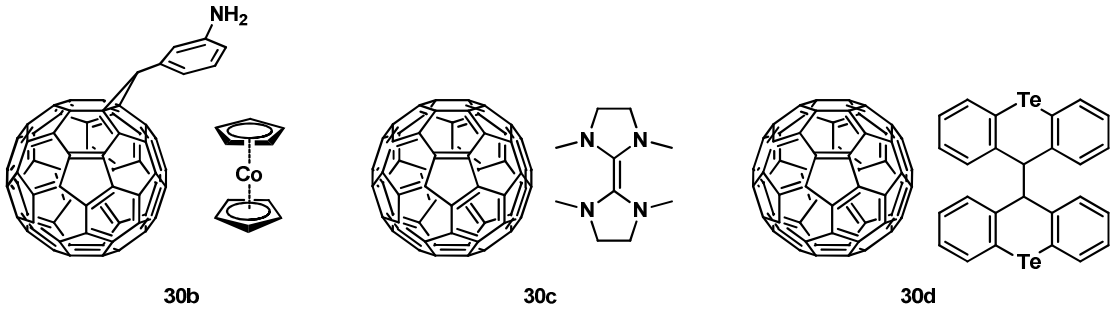

30b **30c** **30d**

Figure 1.18. Examples of fullerene-based magnetic materials.

In that vein, the replacement of TDAE by another strong donor, cobaltocene (*Fig. 1.18* **30b**), resulted in very similar magnetic properties.[74] Ferromagnetism below 19 K in a cobaltocene-doped fullerene derivative was shown to be due to the unpaired spins on the fullerene molecules. There have been reports on higher T_C, for example complex of C_{60} with 1,1',3,3'-tetramethyl-$\Delta^{2,2'}$-bi(imidazolidine) (TMBI) (*Fig. 1.18* **30c**) was found to have a transition at 140 K,[75] but the results were not reproducible.[75,76] It was shown recently,[77] that the molecular complex between fullerene C_{60} and an organic donor 9,9'-trans-bis(telluraxanthenyl) (BTX) (*Fig. 1.18* **30d**) exhibits anomalously high magnetic susceptibility at temperatures above 130 K. The susceptibility value exceeds the one

calculated under the assumption that each molecule bears one paramagnetic spin ½. From the analysis of the ESR signal, the authors make a suggestion on ferromagnetic or superparamagnetic behaviour of the samples. Magnetic properties are ascribed to the electron transfer from donor molecule BTX to C60, which generates electron spins in the system. The anomalously high magnetism is supposed to be due to ferromagnetic correlations in the system of these spins.

The replacement of methyl groups in the NN **27** for a 1,2-phenylene fragment affords benzoimidazol-1-oxyl 3-oxide **31**. The planar structure of NN **31** in combination with effective spin density delocalization, promotes the formation of channels in the crystal ensuring rather strong both antiferromagnetic and ferromagnetic interactions between unpaired electrons depending on the character of the substituents in the aromatic core. The peak value of ferromagnetic exchange energy J/k_B = 66 K was recorded in one of the crystal modifications of benzoimidazol-1-oxyl 3-oxide with 2,6-difluorophenyl substituent in *2* position (**31a**).[78]

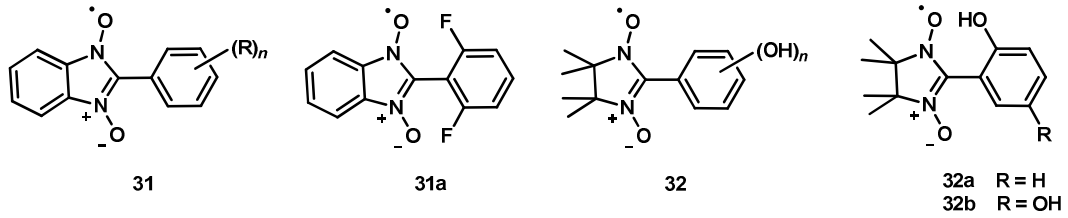

Figure 1.19. Examples of NN radicals with additional sites for H-bonding.

Exchange interaction channels between the paramagnetic centers also arise upon the formation of intermolecular hydrogen bonds between the oxygen atoms of the radical units in nitroxides and OH groups of neighboring molecules. For example, such *H*-bonds are formed in the crystals of nitronyl nitroxides **32**. Depending on the number and position of the OH groups, primary zero-, one-, two- or three-dimensional exchange-bound clusters are formed, which accounts for the diversity of the magnetic properties of derivatives **32**,[79] in particular, their capability for magnetic ordering. The *o*-hydroxy-phenyl-substituted isomer **32a** (T_C = 0.45 K) and 2,5-dihydroxyphenyl-substituted nitronyl nitroxide **32b** (T_C = 0.5 K)[80] became the first examples of organic ferromagnets whose primary structure is specified by intermolecular *H*-bonds.

As follows from this brief introduction, the unpaired electron distribution in the free radicals and the crystal packing play a crucial role in the magnetic behaviour of the

free-radical solids. A favorable packing to achieve a long-range magnetic order must allow the proximity of the spin density of different free radicals and the propagation of the magnetic interactions through the solid. In addition, the nature of the magnetic interactions depends strongly on the relative geometry between the interacting magnetic orbitals which is also determined by the crystal packing. Hence, the unique examples of purely organic compounds showing bulk ferromagnetism represented earlier in *Fig. 1.17* are molecular solids - the β-phase of 2-(p-nitrophenyl)nitronyl nitroxide **27**,[81] dithiadiazolyl radical **28**[69] and the 1:1 complex of C_{60} with tetrakis(dimethylamino)ethylene **30a**,[70,82] which exhibit transitions towards bulk ferromagnetic ordered states below 0.65, 36 and 16.1 K (at ambient pressure), respectively.

1.3. Biradical and polyradical systems

An important goal in the field of organic molecular magnetism is to prepare synthetically a compound incorporating more than one unpaired electron with appreciably large ferromagnetic coupling between them, resulting in a molecule which has a triplet (S = 1) or higher (S > 1) ground state.[83] In unconjugated radicals, such as TEMPO, the NO group bearing the free electron is comparatively isolated from the rest of the molecule by saturated hydrocarbon groups and, therefore, bears the vast majority of the spin density. Spin-polarization leads to the high stability of the radical of such type, but, as the main drawback, the magnetic properties of unconjugated derivatives can't be tuned through the rational design or precisely predicted.

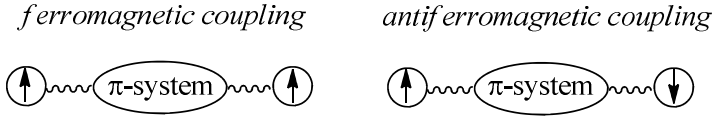

Figure 1.20. Schematic representation of ferromagnetic and antiferromagnetic spin alignment within material.

Therefore, it is necessary to use a "*ferromagnetic coupler*" or spacer, which provides a pathway for the transmission of the interactions between two or more unpaired electrons within the molecule, leading to extensive delocalization of the free electrons

over the aromatic core. Ferromagnetic interactions occur when the electrons have the same spin orientation, and conversely, antiferromagnetic coupling describes antiparallel spin-spin interactions. The possibility to control the through bond exchange in conjugated molecules is the first step towards obtaining bulk magnetic properties.

The simplest model of a π -conjugated diradical[‡] is trimethylenemethane **33** (TMM), first observed by Dowd.[84] Spectroscopic studies suggested a triplet ground state for TMM.[85,86] Diradical **33** can be considered as two methyl radicals connected to the same end of ethylene (*1,1*-connection) as shown in *Fig. 1.21*. Alternatively, two methyl radicals may be formally connected to the opposite sites of ethylene (*1,2*-connection) to give butadiene **34**, which has singlet ground state.[87] The ethylene moiety acts as a strong ferromagnetic and strong antiferromagnetic coupling unit when 1,1- and 1,2-connected, respectively. In other words, connectivity (*topology*) determines the type of spin coupling (bonding).[88] The concept of spin coupling unit is widely used in both organic diradicals and metal complexes.[82,89 ,90]

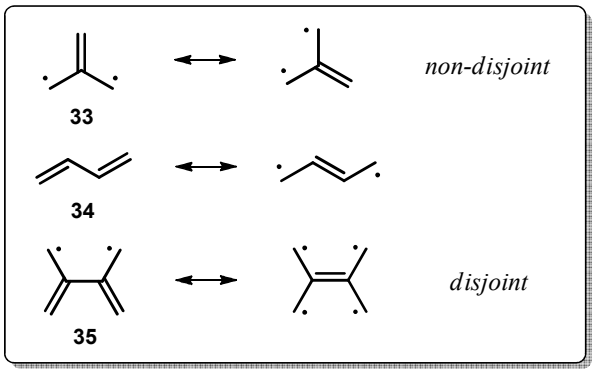

Figure 1.21. The influence of topology on the spin-coupling.

Trimethylenemethane **33** and tetramethyleneethane **35** (TME) are the simplest non-Kekulé even alternant hydrocarbons for which the Longuet-Higgins' rule dictates the occurrence of two nonbonding molecular orbitals (NBMO) that have zero π-bond energy and therefore both are diradicals. Two NBMO's each of which is represented by a linear combination of 2*p*-atomic orbitals have common atoms in TMM (non-disjoint), but can be confined as two different sets of atoms in TME (disjoint).[91] Borden and Davidson predicted in their molecular orbital theory[92] that, while TMM should have a ground state triplet, singlet and triplet states of TME are nearly degenerate and higher order terms

[‡] However, its practical implementation required many efforts.

favor the singlet ground state.[93] It is noted that any non-Kekulé alternant hydrocarbons of extended π-conjugation may be regarded as a vinylog or phenylog of TMM or TME (including pentamethylenepropane).[94,95] It is only the former which can have high-spin ground state.[96]

Strong ferromagnetic coupling may also be achieved via a benzene moiety. In so called non-Kekulé structures,[97] such as *m*-xylene (1,3-dimethylene-benzene), no double-bond between the unpaired electrons can be formed. The *p*- and *o*-xylene, in contrast, allow spin pairing towards the more stable quinoid structures in the Kekulé forms as shown in *Fig.1.22 B*, and therefore the low spin state (S = 0) is expected. For *m*-xylene the ground state is anticipated to be a triplet (S = 1). This is due to the presence of degenerate non-bonding molecular orbitals (NBMOs) of a non-disjoint type.

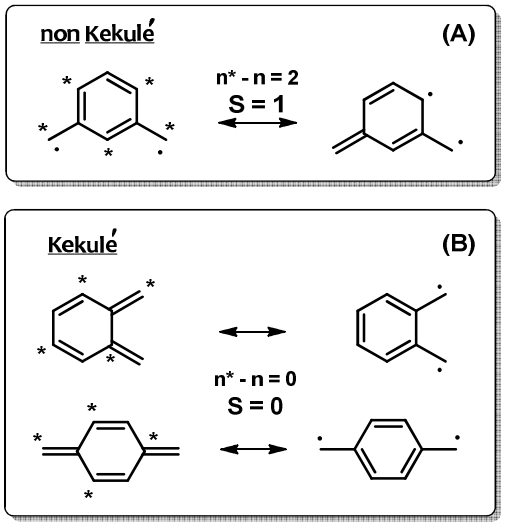

Figure 1.22. Non- Kekulé vs Kekulé structures.

In 1950, Longuet-Higgins[98] proposed a *topological model*, which makes it possible to predict the ground spin state in a π-conjugated molecule on the basis of Hund´s rule. *Equation* (*2*) describes this relation:

$$n\mathrm{NBMO} = (\mathrm{N} - 2\mathrm{T});\ \mathrm{S} = 0.5\ (\mathrm{N}\text{-}2\mathrm{T}) \qquad (\mathbf{2})$$

where, **N** is the number of π-centres and **T** - the number of double bonds.

Thus, the presence (non-Kekulé structures) or absence (Kekulé structures) of open-shell resonance structures leads to strong ferromagnetic or strong antiferromagnetic coupling for diradicals with one coupling unit.

Another approach, proposed by Ovchinnikov,[99] is to invoke the concept of *spin polarization*, which arose from valence bond theory and Pariser-Parr-Pople Hamiltonian. Following this concept the conjugated carbon framework can be divided in alternant "starred" n***** and "unstarred" n (spin polarized) centers, in such a way that each starred atom faces contacts with only unstarred ones. Then through the *equation* (*3*), and by counting half of the difference between n***** and n, the value of the net spin S in the system can be anticipated.

$$S = 0.5\ (n^* - n) \qquad (\mathbf{3})$$

The Ovchinnikov rule also predicts triplet ground state for non-Kekulé molecules, since the spin multiplicity is expressed as $2S+1$.

A classical example of a ferromagnetic coupler of this type is *m*-phenylene, which plays the role of a bridging unit in a great variety of radicals.[100,101] Typically, carbene species lack the stability for characterization under ambient conditions and have an inherent drawback for further extension to usable magnetic materials. To overcome the problems of *m*-phenylenecarbene units Iwamura designed and prepared bis[3-*tert*-butyl-5-(*N*-oxy-*tert*-butylamino)phenyl]nitroxide **36** demonstrated in *Figure 1.23*. Compound **36** was shown to be stable under ambient temperature. Notably, triradical **36** has a quartet ground state and possesses large intramolecular ferromagnetic exchange coupling J/K_B = +240 K.[102]

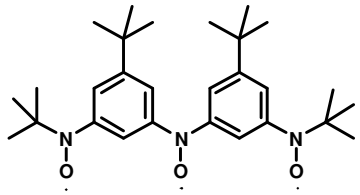

36

Figure 1.23. Nitroxide triradical **36**, S = 3/2.

Megumi et al. suggested other type of triradical in which *tert*-butyl nitroxide in **36** was replaced with Ullman's nitronyl nitroxide for the terminal spin sources (**37**).[103] Nitronyl nitroxides are more stable than *tert*-butyl nitroxide and modifiable to other organic radicals such as imino nitroxide **39**, thus enabling the construction of organic radicals having two different kinds of nitroxide species. The intramolecular coupling in **37** is guided by efficient π-conjugation, resulting in an extremely strong exchange coupling between the central nitroxide and the terminal nitronyl nitroxides J/K_B = +231 K.[103]

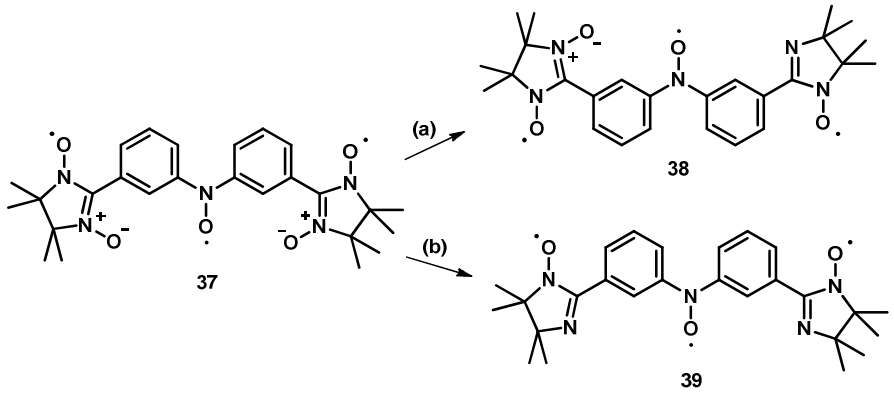

Scheme 1.3: (a) p-toluenesulfonyl isocyanate, CH_2Cl_2; (b) $NaNO_2$, acetic acid, H_2O, CH_2Cl_2.

Such organic heterospin systems have a number of interesting aspects. The singly occupied MOs (SOMOs) have different spatial distribution and energy levels, and the magnitude of the exchange coupling between them is different. The difference of the ionization potential or shape of the orbital contributing to the coordination bond may produce various coordination patterns to transition metals. Thus, for the construction of a molecular magnet, it is important to investigate the intramolecular interaction of a polyradical consisting of different spins.

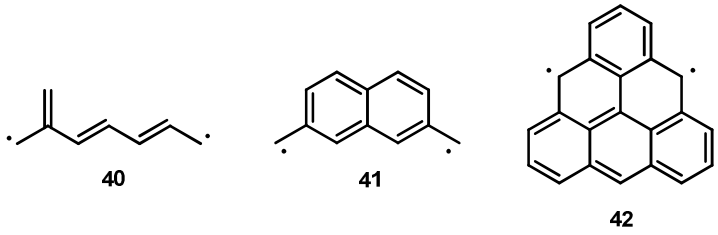

Figure 1.24. Examples of high-spin spin-bearing building blocks.

Following these approaches many high spin molecules connected by different coupling units, such as derivatives of heptatriene **40**, non-Kekulé quinodimethane **41** and triangulene **42**, shown in *Figure 1.24*, have been designed and synthesized.[104,105] Nontheless, there are several known exceptions, so-called "Violations of Hund's Rule in Non-Kekulé Hydrocarbons".[106] Demonstrating thereby, that molecular magnetism is a complex subject.[93,107]

Keeping in mind the characteristics described previously, the design of organic molecular materials showing bulk magnetic properties involves three main conditions: (i) stability of the spin-containing units; (ii) coupling routes or magnetic interaction

mechanisms between the neighboring spin-containing building blocks; (iii) propagation of the magnetic interactions along the three dimensions of the material. Rigid adamantine-based diradicals designed and synthesized by Rassat and Chiarelli (*Fig. 1.25)* fulfilled the requirements listed above.[108,109] In all obtained compounds within this family intramolecular ferromagnetic interactions are present.[110] However, while radicals **43b** and **43c** show dominant antiferromagnetic interactions in the bulk state, the diradical **43a** (which a priori is the most symmetric (D_{2d}) among the derivatives) is a bulk ferromagnet with T_C = 1.48K. As dictated by the small magnetic anisotropy of this compound no hysteresis could be observed, which is typical for a "soft" magnet behavior. To date this value of ferromagnetic transition temperature remains the highest among nitroxides.[66,111]

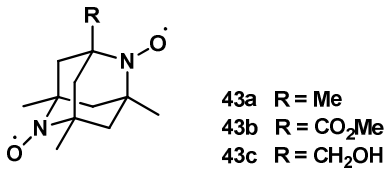

Figure 1.25. Example of dinitroxide pure organic magnet.

Numerous concepts have been established to organize low-dimensional spin-carrying units into a higher-dimensional assembly. A rare and unique approach was implemented by co-crystallization of two different species: monoradical **44** (S = ½) and biradical **45** (S = 1), and thus prepared a solid phase consisting from stacks of alternating radicals **44** and **45** with ferromagnetic spin ordering within the columns at *T* < 10 K according to EPR data.[112,113]

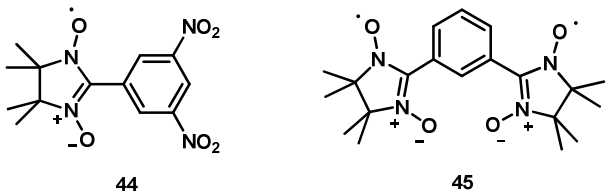

Figure 1.26. Material formed by co-crystallization of two different spin-carrying species: monoradical **44** and biradical **45**.

Co-crystallization of different paramagnetic molecules is an uncommon strategy. It is more rational to link the high-spin and low-spin components by a particular system of chemical bonds, in other words to fabricate a ferrimagnetic molecular block. Following

this idea a series of polyradicals was obtained. As an example, polyradicals **46** and **47** are represented in *Figure 1.27*.

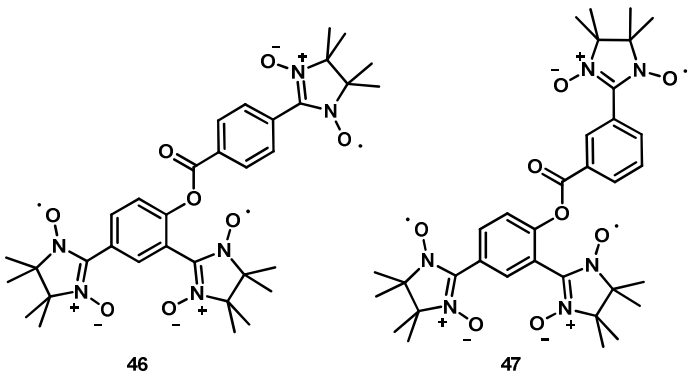

Figure 1.27. Nitroxides containing high- and low-spin units within one molecule.

Here the biradical fragment with the triplet ground state is linked by a system of covalent bonds to more remote monoradical fragment.[114,115] It has been found from the X-ray crystal structure analysis that the biradical and monoradical moieties are packed in a one dimensional chain in the crystal. According to the magnetic susceptibility measurements for **46** and **47** radicals the existence of the ferromagnetic exchange interactions of $2J/k_B \sim +20$ K and 9.5 K, respectively, was observed, as the temperature was decreased. However, below 10 K the magnetic susceptibility values decreased, which was attributed to the intermolecular antiferromagnetic interactions along the chain. Observed at around 0.26 K minimum and upturn of $\chi_p T$ proved the ferrimagnetic behavior of the radicals **46** and **47**.

Another possible way to ensure the propagation of the ferromagnetic interactions is to prepare a polymer, consisting of coupled spins.[116,117] The basic principle underlying the design is the desire to endow organic molecules with many half-filled orthogonal orbitals. Their presence is dictated by symmetry and can be achieved in two ways: orthogonality in space and topological symmetry. Carbenes in triplet ground states are examples of the former. In π-biradicals, parallel alignment of the two spins can become favored if the radical centers are placed in phase with the spin polarization of the intervening π-bonds. The Schlenk hydrocarbon in the triplet ground state is such an example.[118] One-dimensional poly(*m*-phenylenecarbenes) **48**[119] were proposed as the first prototype of organic ferromagnets and investigated extensively for some time.[120] However, in the one-dimensional systems, the first excited state lies $\sim 2J$ above the

ground state, is of lower-spin and favored statistically. As a result one-dimensional spins do not order at finite temperature ($T_C = 0$).

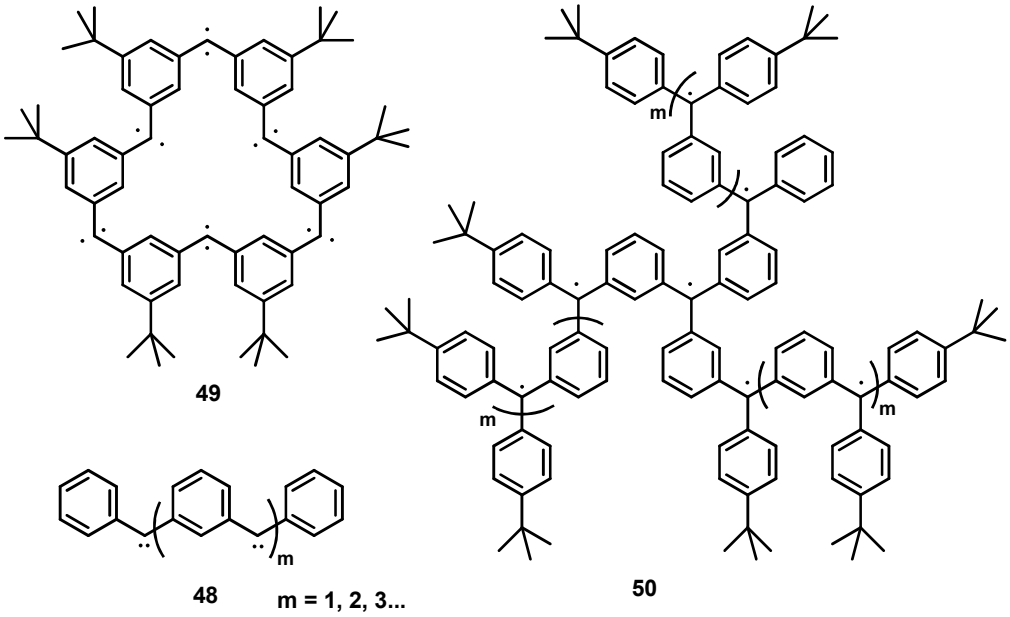

Figure 1.28. Examples of high-spin macromolecules.

To realize the long-range order at finite temperatures, increasing the dimension of the aligned spins is required. This can be achieved either by imposing the proper stacking orientation and therefore magnetic interaction between the molecular chains of **48** as in crystals,[121] or by increasing the dimension of **48** itself. For that reason, highly branched dendritic structures, including hexacarbene, expected to give S = 6 species have been prepared, even though the observed spin states were lower than the theoretical values. This occurrence is explained in terms of a facile interbranch recombination of the carbene centers, due to the congested and flexible structures.[111,122] The most promising cyclic candidate for constructing a high-spin network is a hexacarbene **49** shown in *Figure 1.28*.

Poly(arylmethyl) radicals have been developed mainly by Rajca's group from one-dimensional to dendritic and then to ring structures.[123] It was concluded that the calyx[4]arene-based macrocyclic structures are the most viable building blocks not only because of high spin density but also because of the availability of multiple intramolecular coupling pathways.[124] In order to obtain high-dimensional systems the macromolecules with the branched-chain pseudo-two-dimensional structure (as the polyradical **50** demonstrated in *Figure 1.28*) and highest spin multiplicity S = 1000[124,125] known to date

were prepared.[126,127,128] Thereby it was demonstrated, that such topology of the framework was appropriate for controlling high-spin ground state of the system.

π-Conjugated polymers in which stable radical centers are attached as pendants to the main chain continue to be the aims of super-high spin materials. A combination of polymer chains as poly(acetylenes), poly(diacetylenes), poly(phenylenevinylenes), *etc*. with stable radicals such as nitronyl nitroxide, *t*-butyl aminoxyl, and phenoxyl radical have been studied. [129,130] In the poly(acetylenes) carrying nitronyl nitroxide radicals, the spin density was more than 95% intact. However, the result of the magnetic measurement was not encouraging: a paramagnet with weakly antiferromagnetic interaction was found.[129b,130]

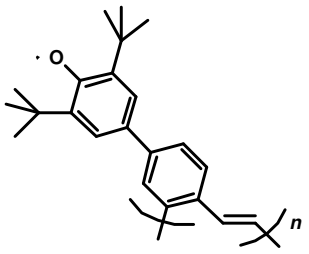

51

Figure 1.29. An example of high-spin polymer.

Up-to-date, the best choice seems to be a poly(*o*-phenylenvinylene) skeleton with phenoxyl radicals **51**. In this system the spin concentration is limited to 68% of the theoretical value but the observed spin multiplicity is more than S = 5/2. The phenoxyl radical is not as stable, as most of the nitroxides, but delocalization of the spin density is more extensive than in nitronyl or *t*-butyl aminoxyl radicals. This result suggests that the degree of the exchange interactions is more important than the spin concentration.

Poly-*o*-semiquinone (SQ) radicals bring opportunities to design high-spin polynuclear complexes. Following well-established rules, these polyradicals are designed in such a way as to obtain triplet or quartet ground states.[131,132] Some examples of such ligands are given in *Figure 1.30*. Biradical **52a** and triradical **52c** are *m*-phenylene derivatives, while biradicals **52b** belong to the TMM group.[131c] A systematic study has shown that the intramolecular coupling in the Zn complexes with **52a** is modulated by substituent effects and correlated with the angle between the semiquinone rings.[131c] However, large ferromagnetic interactions (> 43 K) are observed for angles as large as 50°. In addition, it was demonstrated that energy matching of the coupler and the SQ

orbitals, as well as modulated delocalization within mixed-valent states, contribute also to the magnetic exchange coupling.

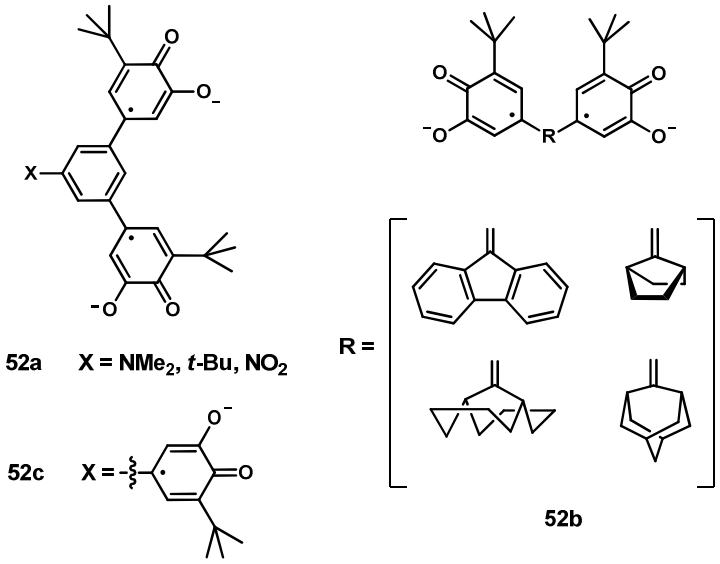

Figure 1.30. Examples of bis- and tris-*o*-semiquinone radicals having a high ground spin state.

Coordination chemistry of these ligands may be complicated by bonding requirements, which would lead to large angles between the SQ rings and intra-ligand antiferromagnetic coupling. Such features were indeed observed in Co(III) and Fe(III) complexes where the intra-ligand magnetic interaction becomes antiferromagnetic upon coordination. Nevertheless, high-spin molecules have been characterized involving these polyradicals, mostly metal complexes of **52a** (X = *t*-Bu) and **52c**, which afford binuclear and trinuclear species, respectively.[133] In Mn(II) complexes, both geometries lead to antiferromagnetic behavior, whereas for Ni(II) complexes they give antiferro- and ferromagnetic coupling, respectively. Large metal–radical interactions are observed in the range $-288 < J < 288$ K. However, in contrast to the heterospin systems, the ground state is not well stabilized because SQ–SQ interaction is rather weak.[131c]

1.4. Motivation

1.4.1. Weakly coupled spin-dimers – a strategy towards organic-based magnetic materials

It is essential to satisfy needs of the modern science engineering new materials with controlled properties. This can be achieved using pure organic materials, in which control of the interactions between spin carriers can be assured through the rational design of the molecular backbone.[134] Necessary therefore are the control of the *intra*- and *inter*molecular exchange interactions. While the former can be designed and adjusted through the synthesis of different conjugated bridges between the spin-containing sites, the latter needs supramolecular approaches as hydrogen bonding, π-stacking, or metal complexation. In nitronyl nitroxide radicals the spin density of the unpaired electron is delocalized over two sites of coordination, leaving open the possibility to arrange molecular units into a supramolecular network.[135,136]

While a large number of approaches have considered stable radicals and biradicals for ferromagnetic network formation of pure organics,[78] to our best knowledge only a few studies considered so far antiferromagnetic coupled biradicals.[138,139] Herein, a new approach towards weakly coupled organic spin-dimer systems with singlet ground state is described. It is thought that in such spin networks the population of the triplet state can be significantly increased and made predominant upon influence of an external magnetic field. To afford through space spin interactions within the network the *intra*molecular exchange interactions should be roughly double the size of the *inter*molecular interactions and in the range of 5 – 15 K to be suitable for the laboratory magnet application. For the fine tuning of the magnetic exchange interactions in biradicals we used conjugation control of the bridging unit with topologically aligned radicals in para-position. Further details of the synthesis of a series of new nitroxide biradicals, their characterization, including X-ray structural analysis, and, finally, the magnetic properties, which are discussed with respect to the quantum chemical calculations based on the DFT approach are discussed in *Chapter 3*.

1.4.2. Fluorophore-nitroxide sensing

During recent years the importance of free radical reactions occurring in biological systems has been established. Free radicals such as superoxide, hydroxyl and peroxyl radicals appearing in the living organisms as a result of redox processes can attack biological molecules including proteins, lipids and nucleic acids. These chemical processes cause the damage to mitochondria, chromosomes and cell membranes and are believed to assist or even cause arteriosclerosis, cancer, virus infections, diseases induced by cigarette smoking and cell aging.[140,141]

The biochemical oxidative damage may be delayed or prevented by natural and artificial antioxidants.[142,143] The antioxidants defending against oxidative stress in biological objects include ascorbate, uric acid, tocopherol, and SH-containing substances: serum albumin, lipoic acid and glutathione. Antioxidants function as the scavengers of free radicals and reactive oxygen species, such as hydrogen peroxide and alkyl-peroxides.

The literature contains data about several methods for a quantitative analysis of antioxidants in plasma, blood and buffers. These methods rely on different phenomena and registration techniques and suffer from several limitations. The spectrophotometric methods involve measurement of either the resultant color of products of certain reactions involving ascorbate[144] or absorbance of ascorbic acid itself (265 nm).[145] Also, the methods measuring spectroscopic absorption can not be applied directly to systems with a high optical density such as blood, fruit juices and other biological liquids. A number of sensitive and specific assays of antioxidants including ascorbic and uric acids, tocopherol have been developed based on high performance liquid chromatography (HPLC).[146] These techniques require several preliminary steps such as centrifugation, microfiltration, addition of certain chemicals, *etc*. In addition, HPLC separations require relatively long time, therefore, could not be considered as a rapid method of analysis. Several novel strategies for measurement of the total antioxidant status are based on chemical generation of free radicals which attack antioxidants.[147] Using such active reagents makes these methods non-selective and does not allow to differentiate between specific reductants.

Another group of methods is based on free radical reagents attacking reductants. Nitroxides are relatively stable towards oxidation, but they can be reduced to the

corresponding hydroxyl amines.[148,149] The hydroxylamine derivatives are oxidized directly by superoxide radicals, and catalytically by dioxygen in the presence of transition metal ions (Fe^{3+}, Cu^{2+}).[150] The values of nitroxide redox potential depend on their chemical structure. Thus, any chemical or photo-reduction of this fragment to a corresponding hydroxylamine derivative, oxidation of the nitroxide fragment, addition of an active radical, or reducing substrate (for example, antioxidant, ascorbate, semiquinone and superoxide radicals, nitric oxide) would result in a decrease of electron spin resonance (ESR) signal that should be accompanied by an increase in fluorescence. The organic synthetic chemistry allows us to optimize the sensitivity (in other words response) of such dual molecules by manipulating bridges (spacers), the structure of the fluorophore and the nitroxide fragments, *etc*.[18]. The property of stable nitroxide radical moiety to quench the excited state of the chromophore segment could be exploited not only for developing of new molecular probes, but also for modeling intramolecular photochemical and photophysical processes in the course of the light energy conversion and construction of new photoswitchable magnetic materials.[16,17,18]

The method employs hybrid molecules consisting of a fluorescent and nitroxide radical (FN) connected with a spacer. *Figure 1.30* represents some examples of the dual fluorophore compounds synthesized by the groups of Blough and Likhtenstein.[17,18,151]

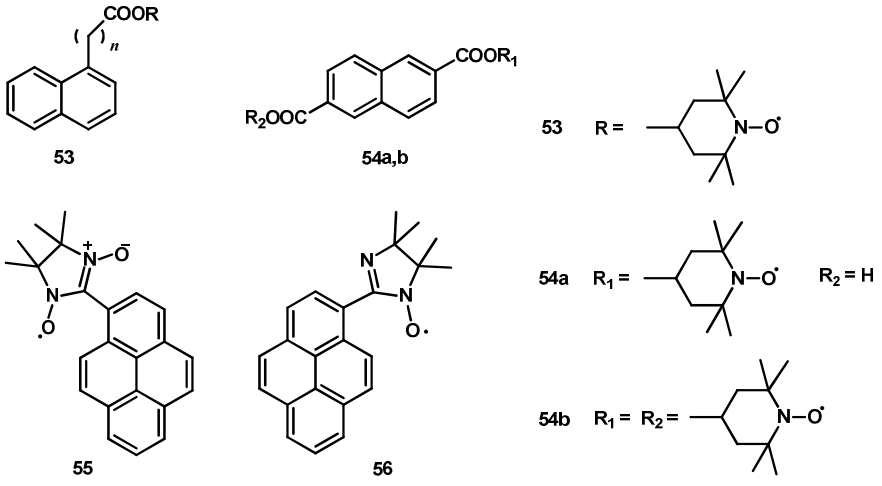

Figure 1.31. Examples of fluorophore-nitroxide probes.

Nitronyl nitroxide radical **55** linked to the pyrene core (*Fig. 1.31*) has recommended itself as a versatile analytical tool. Thus, interactions of the radical **55** with different antioxidants[152,153] and nitric oxide (NO)[154,155] were studied. Zhang found that

the fluorescence of pyrene can be tuned by virtue of chemical inputs.[156] Although the reported quantum yields are not that impressive, the relatively high increase of the fluorescence intensity makes the pyrene nitroxide **55** a promising candidate for further studies.

Searching for a way to improve the sensitivity of the known probes **55** and **56** by means of structural pattern modification and to find new attractive targets, it was suggested to examine the influence of the covalent linking between the aromatic core (e.g. pyrene, perylene) and an additional chromophore fragment, such as pyrazole,[157] on the photophysical properties and sensitivity of the model compound. Further details concerning the project are discussed in *Chapter 2*.

References

[1] D. Griller, K. U. Ingold, *Acc. Chem. Res.*, **1976** (9), 13-19.

[2] N. Jux, Y. Rubin, K. Holczer, *Angew. Chem. Int. Ed. Engl.*, **1996** (35), 1986–1990.

[3] (a) N. Wiberg, T. Blank, W. Kaim, B. Schwederski, G. Linti, *Eur. J. Inorg. Chem.,* **2000**, 1475–1481; (b) A. Armstrong, T. Chivers, M. Parvez, R. T. Boere, *Angew. Chem. Int. Ed.*, **2004** (43), 502–505; (c) Y. Ishida, A. Sekiguchi, K. Kobayashi, S. Nagase, *Organometallics*, **2004** (23), 4891–4896; (d) V. Y. Lee, A. Sekiguchi, *Eur. J. Inorg. Chem.*, **2005**, 1209–1222; (e) S. Ito, M. Kikuchi, M. Yoshifuji, A. J. Arduengo III, T. A. Konovalova, L. D. Kispert, *Angew. Chem. Int. Ed.*, **2006** (45), 4341–4345.

[4] (a) H. Zimmer, D. C. Lankin, S. W. Horgan, *Chem. Rev.*, **1971** (71), 229–246; (b) A. E. J. deNooy, A. C. Besemer, H. van Bekkum, *Synthesis*, **1996**, 1153–1174; (c) R. A. Sheldon, I. W. C. E. Arends, G. J. Ten Brink, A. Dijksman, *Acc. Chem. Res.*, **2002** (35), 774–781.

[5] (a) J. S. Wright, D. J. Carpenter, D. J. McKay, K. U. Ingold, *J. Am. Chem. Soc.*, **1997** (119), 4245–4252; (b) J. C. Scaiano, A. Martin, G. P. A. Yap, K. U. Ingold, *Org. Lett.*, **2000** (2), 899–901; (c) J. S. Wright, E. R. Johnson, G. A. DiLabio, *J. Am. Chem. Soc.*, **2001** (123), 1173–1183; (d) E. Font-Sanchis, C. Aliaga, K. S. Focsaneanu, J. C. Scaiano, *Chem. Commun.*, **2002,** 1576–1577; (e) C. Aliaga, A. Aspee, J. C. Scaiano, *Org. Lett.*, **2003** (5), 4145–4148.

[6] (a) W. Kaim, *Coord. Chem. Rev.*, **1987** (76), 187–235; (b) C. G. Pierpont, C. W. Lange, *Prog. Inorg. Chem.*, **1994** (41), 331–442.

[7] (a) A. Caneschi, D.Gatteschi, P. Rey, *Prog. Inorg. Chem.*, **1991** (39), 331–429; (b) P. Chaudhuri, K. Wieghardt, *Prog. Inorg. Chem.*, **2001** (50), 151–216.

[8] C. J. Hawker, A. W. Bosman, E. Harth, *Chem. Rev.*, **2001** (101), 3661–3688.

[9] (a) A. Rajca, *Chem. Rev.*, **1994** (94), 871–893; (b) *Magnetic Properties of OrganicMaterials* (ed.: P. M. Lahti), Marcel Dekker, New York, **1999**.

[10] J. M. Rawson, A. Alberola, A. Whalley, *J. Mater. Chem.*, **2006** (16), 2560–2575.

[11] L. J. Berliner, *Spin Labelling: Theory and Applications*, Academic Press, New York, **1979**.

[12] (a) M. J. Perkins, *Adv. Phys. Org. Chem.*, **1980** (17), 1; (b) D. Rehorek, *Chem. Soc. Rev.*, **1991** (20), 341–353; (c) A. L. J. Beckwith, V. W. Bowry, K. U. Ingold, *J. Am. Chem. Soc.*, **1992** (114), 4983–4992; (d) V. W. Bowry, K. U. Ingold, *J. Am. Chem. Soc.*, **1992** (114), 4992–4996.

[13] J. L. Zweier, P. Kuppusamy, *Proc. Natl. Acad. Sci. U.S.A.*, **1988** (85), 5703–5707.

[14] (a) J. Stubbe, W. A. van der Donk, *Chem. Rev.*, **1998** (98), 705–762; (b) J. Stubbe, *Chem. Commun.*, **2003**, 2511–2513.

[15] C. W. M. Kay, R. Bittl, A. Bacher, G. Richter, S. Weber, *J. Am. Chem. Soc.*, **2005** (127), 10780–10781.

[16] (a) G. I. Likhtenstein, A. V. Kulikov, A. I. Kotelnikov, L. A. Levchenko, *J. Biochem. Biophys. Methods*, **1986** (12), 1-28; (b) D. Marsh, *Pure Appl. Chem.*, **1990** (62), 265.

[17] G. I. Likhtenshtein, *Appl. Biochem. Biotechnol.*, **2009** (152), 135–155.

[18] G. I. Likhtenstein, K. Ishii, S. Nakatsuji, *J. Photochem. Photobiol.*, **2007** (83), 871–881.

[19] A. R. Katritzky, B. Yang, D. P. M. Pleynet, *J. Org. Chem.*, **1998** (63), 9992-9994.

[20] N. I. Tzerpos, A. K. Zarkadis, R. P. Kreher, L. Repas, M. Lehnig, *J. Chem. Soc. Perkin Trans. 2*, **1995**, 755-761.

[21] (a) N. Juzo, I. Akihiko, Y. Yurie, S. Motoaki, H. Masamatsu, *Tetrahedron Lett.*, **1990** (31), 2627–2630; (b) A. Mangini, G. F. Pedulli, M. Tiecco, *Tetrahedron Lett.*, **1968** (9), 4941–4944.

[22] A. R. Katritzky, B. Z. Yang, N. S. Dalal, *J. Org. Chem.*, **1998** (63), 1467-1472.

[23] M. Ballester, J. Riera-Figueras, J. Castaner, C. Badfa, J. M. Monso, *J. Am. Chem. Soc.*, **1971** (93), 2215-2225.

[24] M. Ballester, *Acc. Chem.Res.*, **1985** (18), 380-387.

[25] (a) J. Carilla, L. Fajarí, L. Juliá, J. Riera, L. Viadel, *Tetrahedron Lett.*, **1994** (35), 6529–6532; (c) J. Carilla, L. Fajarí, L. Juliá, J. Sañé, J. Rius, *Tetrahedron*, **1996** (52), 7013–7024.

[26] S. Gronowitz, M. Temciuc, L. Eberson, *J. Heterocycl. Chem.*, **1995** (32), 65–67.

[27] S. Goldschmidt, K. Renn, *Ber. Deutsch. Chem. Gesel.*, **1922** (B55), 628-643.

[28] (a) P. Ionita, *Lett. Org. Chem.*, **2008** (5), 42-46; (b) E. N. Hristea, I. C. Covali-Cîmpeanu, G. Ioniță, P. Ioniță, C. Draghici, M. T. Căproiu, M. Hillebrand, T. Constantinescu, A. T. Balaban, *Eur. J. Org. Chem.,* **2009**, 626–634; (c) F. Sakran, A. Copty, M. Golosovsky, N. Bontemps, D. Davidov, A. Frenkel, *Appl. Phys. Lett.*, **2003** (82), 1479-1481.

[29] (a) S. Goldschmidt, *Ber. Deutsch. Chem. Gesel.*, **1920** (B53), 44-62; (b) S. Goldschmidt, K. Euler, *Ber. Deutsch. Chem. Gesel.*, **1922** (B55), 616-628; (c) S. Goldschmidt, A. Wolf, *Ann. Chem.*, **1924** (427), 194-226; (d) S. Goldschmidt, J. Bader, *Ann. Chem.*, **1929** (473), 137-162.

[30] (a) H. Terazono, A. Kawai, K. Tsuji, K. Shibuya, *J. Photochem. Photobiol., A: Chemistry*, **2006** (183), 22-30; (b) M. Toda, N. Ohno, T. Fujita, T. Kanemaki, S. Mitsudo, T. Idehara, Y. Fujii, M. Chiba, Y.J. Lee, J. T. Markert, *J. Magn. Magn. Materials*, **2007** (310), 2713-2715; (c) I. S. Golovina, S. P. Kolesnik, I. N. Geifman, A. G. Belous, *Rev. Scien. Instruments*, **2010** (81), 044702/1-044702/6.

[31] (a) A. R. Forrester, J. M. Hay, R. H. Thomson, *Organic Chemistry of Stable Free Radicals*, Academic Press, London, **1968**, 137-179; (b) E. I. Pleskushkina, A. N. Nikolaevskii, T. A. Filippenko, *Russ. J. Appl. Chem. (Translation of Zhurnal Prikladnoi Khimii)*, **2001** (74), 792-795.

[32] (a) D.-L. Li, X.-M. Li, Z.-Y. Peng, B.-G. Wang, *Molecules*, **2007** (12), 1163-1169; (b) J. C. Luis, F. Valdés, R. Martín, A. J. Carmona, J. D. Días, *Fitoterapia*, **2006** (77), 469-471.

[33] F. A. Neugebauer, H. Fischer, C. Krieger, *Angew. Chem. Int. Ed. Engl.,* **1989** (28), 491–492.

[34] F. A. Neugebauer, I. Umminger, *Chem. Ber.,* **1980** (113), 1205–1225.

[35] (a) F. A. Neugebauer, *Angew. Chem. Int. Ed. Engl.,* **1973** (12), 455–464; (b) O. M. Polumbrik, *Russ. Chem. Rev.,* **1978** (47), 767–785.

[36] P. M. Allemand, G. Srdanov, F. Wudl, *J. Am. Chem. Soc.*, **1990** (112), 9391.

[37] (a) R. G. Hicks, M. T. Lemaire, L. K. Thompson, T. M. Barclay, *J. Am. Chem.Soc.*, **2000** (122), 8077; (b) T. M. Barclay, R. G. Hicks, M. T. Lemaire, L. K. Thompson, *Inorg. Chem.*, **2001** (40), 5581; (c) T. M. Barclay, R. G. Hicks, M. T. Lemaire, L. K. Thompson, *Inorg. Chem.*, **2003** (42), 2261.

[38] (a) E. G. Rozanstev, *Free Nitroxyl Radicals*, Plenum, New York, **1970**; (b) E. G. Rozantsev, V. D. Sholle, *Synthesis*, **1971**, 401; (c) E. G. Rozantsev, V. D. Sholle, *Synthesis*, **1971**, 190.

[39] J. F. W. Keana, *Chem. Rev.*, **1978** (78), 37–64.

[40] (a) Y. Miyazaki, A. Inaba, S. Michio, P. S. Taylor, P. M. Lahti, *J. Phys. Chem. B*, **2008** (112), 8144-8150; (b) M. Baskett, P. M. Lahti, *Polyhedron*, **2005** (24), 2645-2652; (c) D. Maspoch, L. Catala, P. Gerbier, D. Ruiz-Molina, G. Vidal-Gancedo, K. Wurst, C. Rovira, J. Veciana, *Chem. Eur. J.*, **2002** (8), 3635-3645.

[41] Y. Miyazaki, T. Sakakibara, J. R. Ferrer, P. M. Lahti, G. Antorrena, F. Palacio, M. Sorai, *J. Phys. Chem. B*, **2002** (106), 8615.

[42] C. Benelli, A. Caneschi, D. Gatteschi, *Organic and Inorganic Low Dimensional Crystalline Materials* (eds.: P.Delhaes, M. Drillon), Plenum Press, New York, **1987**, 109.

[43] A. Caneschi, D. Gatteschi, R. Sessoli, *Mol. Cryst. Liq. Cryst.*, **1989** (176), 329-336.

[44] O. P. Anderson, T. C. Kuechler, *Inorg. Chem.*, **1980** (19), 1417.

[45] (a) A. Bencini, C. Benelli, D. Gatteschi, G. Zanchini, *J. Am. Chem. Soc.*, **1984** (84), 5813; (b) A. Grand, P. Rey, R. Subra, *Inorg. Chem.*, **1983** (22), 391; (c) A. Caneschi, D. Gatteschi, J. Laugier, P. Rey, *J. Am. Chem. Soc.*, **1987** (109), 2191; (d) Caneschi, D. Gatteschi, A. Grand, J. Laugier, L. Pardi, P. Rey, *Inorg. Chem.*, **1988** (27), 1031.

[46] (a) J. Laugier, P. Rey, C. Benelli, D. Gatteschi, C. Zanchini, *J. Am. Chem. Soc.*, **1986** (108), 6931; (b) E. Belorizky, P. Rey, *Mol. Phys.*, **1992** (75), 563; (c) A. Caneschi, D. Gatteschi, J. Laugier, L. Pardi, P. Rey, C. Zanchini, *Inorg. Chem.*, **1988** (27), 2027.

[47] (a) M. Kitano, Y. Ishimaru, K. Inoue, N. Koga, H. Iwamura, *Inorg. Chem.*, **1994** (33), 6012-6019; (b) Y. Ishimaru, M. Kitano, H. Kumada, N. Koga, H. Iwamura, *Inorg. Chem.*, **1998** (37), 2273-2280.

[48] (a) J. H. Osiecki, E. F. Ullman, *J. Am. Chem. Soc.,* **1968** (90), 1078; (b) E. F. Ullman, L. Call, J. H. Osiecki, *J. Org. Chem.*, **1970** (35), 3623-3631.

[49] E. F. Ullmann, J. H. Osiecki, D. G. B. Boocock, R. Darcy, *J. Am. Chem. Soc.*, **1972** (94), 7049.

[50] (a) P. Brough, R. Chiarelli, J. Pecaut, A. Rassat, P. Rey, *Chem. Commun.*, **2003**, 2722–2723; (b) P. Brough, J. Pecaut, A. Rassat, P. Rey, *Chem. Eur. J.*, **2006** (12), 5134–5141.

[51] (a) A. T. Balaban, P. J. Halls, A. R. Katritzky, *Chem. Ind.*, **1968**, 651; (b) H. G. Aurich, W. Weiss, *Chem. Ber.*, **1973** (106), 2408–2414; (c) H. G. Aurich, K. Stork, *Chem. Ber.*, **1975** (108), 2764–2780; (d) T. E. Gough, R. Puzic, *J. Magn. Reson.*, **1976** (23), 31–38; (e) Y. Kusaba, M. Tamura, Y. Hosokoshi, M. Kinoshita, H. Sawa, R. Kato, H. Kobayashi, *J. Mater. Chem.*, **1997** (7), 1377–1382.

[52] A. Zakrassov, V. Shteiman, Y. Sheynin, B. Tumanskii, M. Botoshansky, M. Kapon, A. Keren, M. Kaftory, T. E. Vos, J. S. Miller, *J. Mater. Chem.*, **2004** (14), 1827–1837.

[53] (a) E. F. Ullman, L. Call, J. H. Osiecki, *J. Org. Chem.*, **1970** (5), 623–3631; (b) C. Stroh, F. M. Romero, N. Kyritsakas, L. Catala, P. Turek, R. Ziessel, *J. Mater. Chem.*, **1999** (9), 875–882.

[54] (a) A. Zheludev, M. Bonnet, B. Delley, A. Grand, D. Luneau, L. Örström, E. Ressouche, P. Rey, J. Schweizer, *J. Magn. Magn. Mater.*, **1995** (145), 293–305; (b) A. Zheludev, M. Bonnet, D. Luneau, E. Ressouche, P. Rey, J. Schweizer, *Physica B*, **1995** (213-214), 268–271.

[55] (a) D. Luneau, P. Rey, J. Laugier, P. Fries, A. Caneschi, D. Gatteschi, R. Sessoli, *J. Am. Chem. Soc.*, **1991** (113), 1245–1251; (b) H. Oshio, T. Ito, *Coord. Chem. Rev.*, **2000** (198), 329–346.

[56] (a) J. H. Osiecki, E. F. Ullmann, *J. Am. Chem. Soc.*, **1961** (83), 2784.

[57] (a) A. Caneschi, D. Gatteschi, P. Rey, *Progr. Inorg. Chem.*, **1991** (39), 331; (b) A. Caneschi, D. Gatteschi, R. Sessoli, P. Rey, *Acc. Chem. Res.*, **1989** (22), 392; (c) *Magnetism: Molecules to Materials II* (eds.: H. Iwamura, K. Inoue),Wiley-VCH, Weinheim, **2001**, 61.

[58] *Spin Labeling Theory and Applications* (ed.: L. J. Berliner), Academic Press: New York, **1976**.

[59] (a) K. Fegy, D. Luneau, P. Rey, *Inorg. Chem.*, **1998** (37), 4524-4532; (b) K. Fegy, D. Luneau, P. Rey, *Angew. Chem. Int. Ed.*, **1998** (37), 1270-1273; (c) K. Fegy, C. Lescop, D. Luneau, P. Rey, *Mol. Crystals and Liq. Crystals*, **1999** (334), 521-532; (d) C. Lescop, D. Luneau, P. Rey, C. Reber, *Inorg. Chem.*, **2002** (41), 5566-5574.

[60] K. Inoue, *Structure and Bonding*, **2001** (100), 61-91.

[61] A. Caneschi, D. Gatteschi, J. Laugier, P. Rey, R. Sessoli, C. Zanchini, *J. Am. Chem. Soc.*, **1988** (110), 2795.

[62] K. E. Vostrikova, D. Luneau, M. Verdaguer,W. Wernsdorfer, P. Rey, *J. Am. Chem. Soc.*, **2000** (122), 718.

[63] V. I. Ovcharenko, V. Fursova, G. Romanenko, V. Ikorskii, *Inorg. Chem.*, **2004** (43), 3332.

[64] H. Iwamura, *Adv. Phys. Org. Chem.*, **1990** (26), 179.

[65] M. Kinoshita, P. Turek, M. Tamura, *Chem. Lett.*, **1996** [ACS Symposium series 644].

[66] R. Chiarelli, M. A. Novak, A. Rassat, J. L. Tholence, *Nature (London)*, **1993** (363), 147.

[67] A. J. Banister, N. Bricklebank, I. Lavender, J. M. Rawson, C. I. Gregory, B. K. Tanner, W. Clegg, M. R. J. Elsegood, F. Palacio, *Angew. Chem*., **1996** (108), 2648-2650.

[68] A. J. Banister, N. Bricklebank, W. Clegg, M. R. J. Elsegood, C. I. Gregory, I. Lavender, J. M. Rawson, B. K. Tanner, *J. Chem. Soc. Chem. Commun.,* **1995**, 679-680.

[69] A. Alberola, R. J. Less, C. M. Pask, J. M. Rawson, F. Palacio, P. Oliete, C. Paulsen, A. Yamaguchi, R. D. Farley, D. M. Murphy, *Angew. Chem. Int. Ed*., **2003** (42), 4782-4785.

[70] P.-M. Allemand, K. C. Khemani, A. Koch, F. Wudl, K. Holczer, S. Donovan, G. Grüner, J. D. Thompson, *Science*, **1991** (253), 301.

[71] (a) T. Takenobu, T. Muro, Y. Iwasa, T. Mitani, *Phys. Rev. Lett.*, **2000** (85), 381; (b) A. Mrzel, A. Omerzu, P. Umek, D. Mihailovic, Z. Jaglicic, Z. Trontelj, *Chem. Phys. Lett.*, **1998** (298), 329-334.

[72] (a) Y. J. Uemura, K. Kojima, G. M. Luke, W. D. Wu, G. Oszlanyi, O. Chauvet, L. Forro, *Phys. Rev. B*, **1995** (52), 6991; (b) W. A. MacFarlane, R. F. Kiefl, S. Dunsiger, J. E. Sonier, J. E. Fischer, *Phys. Rev. B*, **1995** (52), 6995.

[73] L. Cristofolini, A. Lappas, K. Vavekis, K. Prassides, R. DeRenzi, M. Ricco, A. Schenck, A. Amato, F. N. Gygax, M. Kosaka, K. Tanigaki, *J. Phys. Cond. Matter*, **1995** (7), 567.

[74] D. Mihailovic, *Monatshefte für Chemie*, **2003** (134), 137-147.

[75] (a) A. Mrzel, A. Omerzu, P. Umek, D. Mihailovic, Z. Jaglicic, Z. Trontelj, *Chem. Phys. Lett.*, **1998** (298), 329; (b) H. L. Wang, D. B. Zu, J. G. Zhao, W. S. Zhan, *Synth. Met.*, **1995** (70), 1471; (c) H. L. Wang, D. B. Zhu, *J. Phys. Chem. Sol.*, **1994** (55), 437.

[76] A. Schilder, B. Gotschy, A. Seidl, R. Gompper, *Chem. Phys.*, **1995** (193), 321.

[77] (a) D. V. Konarev, R. N. Lyubovskaya, O. S. Roshupkina, Y. M. Shulga, M. G. Kaplunov, I.N. Kremenskaya, L.P. Rozenberg, S.S. Hasanov, R. P. Shibaeva, *Mendeleev Commun.*, **1996**, 3-5; (b) V. V. Kveder, E. A. Shteinman, R. N. Lyubovskaya, S. A. Omel'chenko, Yu. A. Osip'yan, *JETP Lett.*, **2001** (74), 462-465.

[78] A. Zakrassov, V. Shteinman, Y. Sheynin, B. Tumanskii, M. Botoshansky, M. Kapon, A. Keren, M. Kaftory, T. E. Vos, J. S. Miller, *J. Mater. Chem.*, **2004** (14), 1827.

[79] (a) E. Hernandez, M. Mas, E. Molins, C. Rovira, J. Veciana, *Angew. Chem., Int. Ed. Engl.*, **1993** (32), 882; (b) J. Cirujeda, E. Hernandez-Gazio, C. Rovira, J. L. Stanger, P. Turek, J. Veciana, *J. Mater. Chem.*, **1995** (5), 243; (c) J. Cirujeda, L. E. Ochando, J. M. Amigo, C. Rovira, J. Ruis, J. Veciana, *Angew. Chem., Int. Ed. Engl.*, **1995** (34), 55; (d) J. Veciana, J. Cirujeda, C. Rovira, E. Molins, J. J. Novoa, *J. Phys.*, **1996** (16), 1967.

[80] (a) T. Sugawara, M. M. Matsushita, A. Izuoka, N. Wada, N. Takeda, M. Ishikawa, *J. Chem. Soc., Chem. Commun.*, **1994**, 1723; (b) M. M. Matsushita, A. Izuoka, T. Sugawara, T. Kobayashi, N. Wada, N. Takeda, M. Ishikawa, *J. Am. Chem. Soc.*, **1997** (119), 4369.

[81] H. Tamura, Y. Nakazawa, D. Shiomi, K. Nozawa, Y. Hosokoshi, M. Ishikawa, M. Takahashi, M. Kinoshita, *Chem. Phys. Lett.*, **1991** (186), 401.

[82] T. Sugimoto, K. Ueda, M. Tsujii, H. Fujita, N. Hosoito, N. Kanehisa, Y. Shibamoto, Y. Kai, *Chem. Phys. Lett.*, **1996** (249), 304-308.

[83] H. Iwamura, *Mol. Cryst. Liq. Cryst.*, **1993** (232), 233-250.

[84] H. M. McConnell, *J. Chem. Phys.*, **1960** (33), 115.

[85] (a, *EPR spectroscopy*) R. J. Baseman, D. W. Pratt, P. Dowd, *J. Am. Chem. Soc.*, **1976** (98), 5726; (b, *IR spectroscopy*) P. Dowd, *Angew. Chem., Int. Ed. Engl.,* **1993** (32), 119.

[86] (ab initio calculations) D. A. Dixon, T. A. Dunning, D. A. Kleier, *J. Am. Chem. Soc.*, **1981** (103), 2878.

[87] B. S. Hudson, B. E. Kohler, K. Schulten, *In Excited States* (ed.: E. C. Lim), Academic Press: New York, **1982** (6), 54-55; (b) B. S. Hudson, B. E. Kohler, K. Schulten, *In Excited States* (ed.: E. C. Lim), Academic Press: New York, **1982** (6), 86.

[88] (a) H. C. Longuet-Higgins, C. W. Rector, J. R. Platt, *J. Chem. Phys.*, **1950** (18), 1174; (b) B. M. Gimarc, J. J. Ott, *J. Am. Chem. Soc.*, **1986** (108), 4298; (c) J. J. Ott, B. M. Gimarc, *J. Am. Chem. Soc.*, **1986** (108),4303.

[89] D. A. Dougherty, *Acc. Chem. Res.*, **1991** (24), 88.

[90] S. Utamapanya, A. Rajca, *J. Am. Chem. Soc.*, **1991** (113), 9242.

[91] M. Filatov, S. Shaik, *J. Phys. Chem., A*, **1999** (103), 8885-8889.

[92] W. T Borden, E. R. Davidson, *J. Am. Chem. Soc.*, **1977** (99), 4587.

[93] *Magnetic Properties of Organic Molecules* (ed.: P. M. Lathi), Marcel Dekker: New York, **1999**.

[94] W. T. Borden, H. Iwamura, J. A. Berson, *Acc. Chem. Res.,* **1994** (27), 109-116.

[95] D. C. Oniciu, K. Matsuda, H. Iwamura, *J. Chem. Soc. Perkin Trans. 2,* **1999**, 907-913.

[96] L. C. Bush, R. B. Heath, J. A. Berson, *J. Am. Chem. Soc.*, **1997** (119), 1406-1415.

[97] M. Baumgarten, *EPR of Free Radicals in Solids* (eds.: A. Lund, M. Shiotani), Kluwer Academics Publishers: Netherlands, **2003**, 491-528.

[98] H. C. Longuet-Higgins, *J. Chem. Phys.*, **1950** (18), 265.

[99] A. A. Ovchinnikov, *Theor. Chim. Acta,* **1978** (47), 297.

[100] (a) A. Calder, A. R. Forrester, P. G. James, G. R. Luckhurst, *J. Am. Chem. Soc.*, **1969** (91), 3724-3727; (b) P. G. Wenthold, J. B. Kim, W. C. Lineberger, *J. Am. Chem. Soc.*, **1997** (119), 1354-1359; (c) M. Dvolaitzky, R. Chiarelli, A. Rassat, *Angew. Chem. Int. Ed. Engl.*, **1992** (31), 180-181.

[101] (a) F. Kanno, K. Inoue, N. Koga, H. Iwamura, *J. Am. Chem. Soc.*, **1993** (115), 847-850; (b) R. Chiarelli, S. Gambarelli, A. Rassat, *Mol. Cryst. Liq. Cryst.*, **1997** (305), 455-478; (c) J. Fujita, M. Tanaka, H. Suemune, N. Koga, K. Matsuda, H. Iwamura, *J. Am. Chem. Soc.*, **1996** (118), 9347-9351; (d) K. Yoshizawa, T. Kuga, M. Hatanaka, K. Tanaka, T. Yamabe, *Synth. Met.*, **1997** (85), 1765-1766.

[102] T. Ishida, H. Iwamura, *J. Am. Chem. Soc.*, **1991** (113), 4238.

[103] M. Tanaka, K. Matsuda, T. Itoh, H. Iwamura, *J. Am. Chem. Soc.*, **1998** (120), 7168-7173.

[104] (a) K. Inoue, H. Iwamura, *Angew. Chem. Int. Ed.,* **1995** (34), 927; (b) T. Ishida, H. Iwamura, *J. Am. Chem .Soc*., **1991** (113), 4238; (c) F. Kanno, K. Inoue, N. Koga, H. Iwamura, *J. Phys. Chem.,* **1993** (97), 13267.

[105] (a) K. Inoue, H. Iwamura*, J. Am.Chem. Soc*., **1994** (116), 3173; (b) T. Itoh, K. Matsuda , H. Iwamura, *Angew.Chem*., **1999** (111), 1886.

[106] W. T. Borden, H. Iwamura, J. A. Berson, *Acc. Chem. Res.,* **1994** (27), 109.

[107] (a) *From Molecular Assemblies to the Devices* (eds.: E. Coronado, P. Delhaes, D. Gatteschi, J. S. Miller), Kluwer Academic Publishers: Amsterdam, **1996**; (b) O. Kahn, *Molecular Magnetism*; VCH Publishers Inc.: New York, **1993**; (c) *Molecular Magnetic Materials* (eds.: D. Gatteschi) Kluwer Academic Publishers: Amsterdam, **1991**.

[108] A. Rassat, *Pure & Appl. Chem.*, **1990** (62), 223-227.

[109] R. Chiarelli, A. Rassat, *Bull. Soc. Chim. Fr.*, **1993** (130), 299-303.

[110] R. Chiarelli, M. A. Novak, A. Rassat, J. L. Tholence, Y. Dromzee, Y. Jeannin, *Phys. Scr.,* **1993** (T49B), 706-710.

[111] R. Chiarelli, A. Rassat, P. Rey, *J. Chem. Soc. Chem. Commun*., **1992**, 1081.

[112] A. Izuoka, M. Fukada, R. Kumai, M. Itakura, S. Hikami, T. Sugawara, *J. Am. Chem. Soc.*, **1994** (116), 2609.

[113] M. Nishizawa, D. Shiomi, K. Sato, T. Takui, K. Itoh, H. Sawa, R. Kato, H. Sakurai, A. Izuoka, T. Sugawara, *J. Phys. Chem. B*, **2000** (104), 503.

[114] D. Shiomi, T. Kanaya, K. Sato, M. Mito, K. Takeda, T. Takui, *J. Am. Chem. Soc.*, **2001** (123), 11823.

[115] K. Maekawa, D. Shiomi, T. Ise, K. Sato, T. Takui, *J. Phys. Chem. B*, **2005** (109), 3303.

[116] H. Iwamura, *Adv . Phys. Org. Chem.,* **1990** (26), 179.

[117] H. Iwamura, N. Koga, *Acc. Chem. Res*, **1993** (26), 346-351.

[118] G. Kothe, K. H. Denkel, W. Summermann, *Angew. Chem., Int. Ed. Engl*., **1970** (9), 906.

[119] (a) Y. Teki, T. Takui, K. Itoh, H. Iwamura, K. Kobayashi, *J. Am. Chem. Soc*., **1983** (105), 3722; (b) T. Sugawara, S. Bandow, K. Kimura, H. Iwamura, K. Itoh, *J. Am. Chem. Soc.*, **1984** (106), 6449; (c) T. Sugawara, S. Bandow, K. Kimura, H. Iwamura, K. Itoh, *J. Am. Chem. Soc.*, **1986** (108), 368.

[120] (a) N. Mataga, *Theor. Chim. Acta,* **1968** (10), 372; (b) H. Iwamura, *J. Phys. (Paris)*, **1988** (49), C8 813; (c) K. Itoh, *Chem. Phys. Lett.*, **1967** (1), 235.

[121] (a) A. Izuoka, S. Murata, T. Sugawara, H. Iwamura, *J. Am. Chem. Soc.*, **1985** (107), 1786; (b) T. Sugawara, S. Murata, K. Kimura, H. Iwamura, Y. Sugawara, H. Iwasaki, *J. Am. Chem. Soc.*, **1985** (107), 5293.

[122] K. Matsuda, N. Nakamura, K. Inoue, N. Koga, H. Iwamura, *Chem. Eur. J.*, **1996** (2), 259-264.

[123] (a) A. Rajca, S. Rajka, S.R. Desai, *J. Am. Chem. Soc.*, **1995** (117), 806-816; (b) A. Rajca, S. Rajka, *J. Am. Chem. Soc.*, **1996** (118), 8121-8126.

[124] K. Matsuda, H. Iwamura, *Current Opinion in Solid State & Mat. Science*, **1997** (2), 446-450.

[125] K. Matsuda, N. Nakamura, K. Inoue, N. Koga, H. Iwamura, *Bull. Chem. Soc. Jpn.*, **1996** (69), 1483-1494.

[126] (a) I. Fujita, Y. Teki, T. Takui, T. Kinoshita, K. Itoh, F. Miko, Y. Sawaki, H. Iwamura, A. Izuoka, T. Sugawara, *J. Am. Chem. Soc.*, **1990** (112), 4074; (b) S. Murata, H. Iwamura, *J. Am. Chem. Soc.*, **1991** (113), 5547.

[127] (a) A. Rajca, *J. Am. Chem. Soc.*, **1990** (112), 5890; (b) A. Rajca, S. Utamapanya, J. Xu, *J. Am. Chem. Soc.*, **1991** (113), 3935; (c) A. Rajca, S. Utamapanya, S. Thayumanavan, *J. Am. Chem. Soc.*, **1992** (114), 1884.

[128] N. Nakamura, K. Inoue, H. Iwamura, T. Fujioka, Y. Sawaki, *J. Am. Chem. Soc.*, **1992** (114), 1484-1485.

[129] (a) A. Fujii, T. Ishida, N. Koga, H. Iwamura, *Macromol.*, **1991** (24), 1077-1082; (b) H. Nishide, T. Kaneko, T. Nii, K. Katoh, E. Tsuchida, P. M. Lahti, *J. Am. Chem. Soc.*, **1996** (118), 9695-9704; (c) R. J. Bushby, D. R. McGill, K. M. Ng, N. Taylor, *J. Mat. Chem.*, **1997**, 2343-2354.

[130] (a) H. Nishide, T. Kaneko, S. Toriu, Y. Kuzumaki, E. Tsuchida, *Bull. Chem. Soc. Jpn.*, **1996** (69), 499-508; (b) Y. Miura, T. Issiki, Y. Ushitani, Y. Teki, K. Itoh, *J. Mater. Chem.*, **1996** (6), 1745-1750; (c) H. Ragossing, R. Saf, K. Hummel, *Eur. Polym. J.*, **1996** (32), 1307; (d) M. M. Murray, P. Kaszynski, D. A. Kaisaki, W. Chang, D. A. Dougherty, *J. Am. Chem. Soc.*, **1994** (116), 8152.

[131] (a) D. A. Shultz, A. K. Boal, G. T. Farmer, *J. Org. Chem.*, **1998** (63), 9462; (b) D. A. Shultz, S. H. Bodnar, H. Lee, J. W. Kampf, C. D. Incarvito, A. L. Rheingold, *J. Am. Chem. Soc.*, **2002** (124), 10054; (c) D. A. Shultz, R. M. Fico, S. H. Bodnar, R. K. Kumar, K. E. Vostrikova, J. W. Kampf, P. D. Boyle, *J. Am. Chem. Soc.*, **2003** (125), 11761.

[132] (a) A. Caneschi, A. Dei, C. P. Mussari, D. A. Shultz, L. Sorace, K. E. Vostrikova, *Inorg. Chem.*, **2002** (41), 1086; (b) A. Caneschi, A. Dei, H. Lee, D. A. Shultz, L. Sorace, *Inorg. Chem.*, **2001** (40), 408.

[133] (a) M. Ruf, H. Vahrenkamp, *Inorg. Chem.,* **1996** (35), 6571; (b) M. Ruf, B. C. Noll, M. D. Groner, G. T. Yee, C. G. Pierpont, *Inorg. Chem.,* **1997** (36), 4860.

[134] M. Tamura, Y. Nakazawa, D. Shiomi, K. Nozawa, Y. Hosokoshi, M. Ishikawa, M. Takahashi, M. Kinoshita, *Chem. Phys. Lett.*, **1991** (186), 401.

[135] (a) G. Zoppellaro, A. Geies, K. K. Andersson, V. Enkelmann, M. Baumgarten, *Eur. J. Org. Chem.* **2008**, 1431–1440; (b) Y.-F. Wang, L.-Y. Wang, L.-F. Ma, *J. Mol. Struct.*, **2008** (877), 138–144.

[136] (a) E. Coronado, C. Gimenez-Saiz, C. J. Gomez-Garcia, F. Romero, A. Tarazón, *J. Mater. Chem.,* **2008** (18), 929–934; (b) T. Yoshida, S. Kaizaki, *Inorg. Chem.*, **1999** (38), 1054-1058.

[137] K. Awaga, Y. Maruyama, *Chem. Phys. Lett.*, **1989** (158), 556; K. Awaga, Y. Maruyama, *J. Chem. Phys.*, **1989** (91), 2743.

[138] K. Togashi, R. Imachi, K. Tomioka, H. Tsuboi, T. Ishida, T. Nogami, N. Takeda, M. Ishikawa, *Bull. Chem. Soc. Jpn.*, **1996** (69), 2821.

[139] R. Chiarelli, M. A. Novak, A. Rassat, J. L. Tholence, *Nature (London)*, **1993** (363), 147.

[140] (a) M. K. Shigenaga, T. M. Hagen, B. N. Ames, *Proc. Natl. Acad. Sci. USA*, **1994** (91), 10771–10778; (b) M. K. Shigenaga, B. N. Ames, *Basic Life Sci.*, **1993** (61), 419–436.

[141] B. Frey, L. England, B.N. Ames, *Proc. Natl. Acad. Sci. USA*, **1989** (86), 6377–6381.

[142] B. Halliwell, *Free Rad. Res. Commun.*, **1990** (9), 1–32.

[143] (a) G. W. Burton, K. U. Ingold, *Acc. Chem. Res.*, **1986** (19), 194–201; (b) L. Packer, E. H. Witt, H. J. Tritschler, *Free Rad. Biol. Med.*, **1995** (19), 227–250.

[144] S. Moore, K. A. Calder, N. J. Miller, C. A. Rice-Evance, *Free Rad. Res. Commun.*, **1994** (21), 417–425.

[145] G. R. Buettner, B. A. Jurkiewicz, *Free Rad. Biol. Med.*, **1993** (14), 49–55.

[146] P. A. Motchnik, B. Frei, B. N. Ames, *Methods Enzymol.*, **1994** (234), 269–279.

[147] C. Rice-Evans, N. J. Miller, *Methods Enzymol.*, **1994** (234), 279–293.

[148] *Imidazolin Radicals* (ed.: L. B. Volodarsky), CRC Press, Bosa Raton, **1988**.

[149] D. Meisel, G. Czapski, *J. Phys. Chem.*, **1975** (79), 1503-1509.

[150] G. D. Rozen, E. Finkelshtein, E. J. Rauckman, *Archives Biochem. Biophys.*, **1982** (215), 367-378.

[151] (a) N. V. Blough, D. J. Simpson, *J. Am. Chem. Soc.*, **1988** (110), 1915-1917; (b) S. A. Green, D. J. Simpson, G. Zhou, P. S. Ho, N. V. Blough, *J. Am. Chem. Soc.*, **1990** (112), 7337-7346.

[152] E. M. Lozinsky, V. V. Martin, T. A. Berezina, A. I. Shames, A. L. Weis, G. I. Likhtenshtein, *J. Biochem. Biophys. Methods*, **1999** (38), 29–42.

[153] N. Medvedeva, V. V. Martin, A. L. Weis, G. I. Likhtenshtein, *J. Photochem. Photobiol. A: Chemistry*, **2004** (163), 45–51.

[154] E. M. Lozinsky, L. V. Martina, A. I. Shames, N. Uzlaner, A. Masarwa, G. I. Likhtenshtein, D. Meyerstein, V. V. Martin, Z. Prie, *Anal. Biochem.*, **2004** (326), 139–145.

[155] (a) J. Joseph, B. Kalyanaraman, J. S. Hyde, *Biochem. Biophys. Res. Commun.*, **1993** (192), 926; (b) Y. Yu. Woldman, V. V. Khramtsov, I. A. Grigor'ev, I. A. Kiriljuk, D. I. Utepbergenov, *Biochem. Biophys. Res. Commun.*, **1994** (202), 195-203.

[156] H.Wang, D. Zhang, X. Guo, L. Zhu, Z. Shuai, D. Zhu, *Chem. Commun.*, **2004**, 670–671.

[157] R. D. Miller, C. R. Moylan, O. Reiser, C. A. Walsh, *Chem. Mater.*, **1993** (5), 625-632.

Chapter 2

Fluorophore-Nitroxide Probes

2.1. Introduction

An idea to combine fluorophore and nitroxide in one molecule for studying of the probe mobility was established in 1965 by Stryer and Griffith.[1] This concept was later realized by Likhtenstein[2] and Bystryak.[3] Additionally it was first demonstrated by Bystryak[3] that in such compounds the nitroxide is a strong intramolecular quencher of the fluorescence from the fluorophore fragment.[4-6]

In general most fluorophores are chemically indifferent to highly reactive radicals such as OH·. At the same time reaction between the nitronyl nitroxide fragment and a radical or other redox-active reagent leads to the transformation of the radical paramagnetic center into a diamagnetic product, either by recombination with a short-lived radical or by reduction, thereby eliminating the intramolecular quenching pathway and resulting in an increased fluorescence yield.[7,8]

However, either the sensitivity of the reported examples[5,8] was unsatisfactory or the synthetic approach was inconvenient for obtaining compounds in a reasonable scale. Herein, an alternative method for the development of the probes with high responses is described.

Continuing our interest in nitronyl nitroxides as promising targets for organic-based magnetic materials, it has been noted, that the attachment of a pyrazole ring to a radical significantly enhances the n-π^* transition components in the absorption envelope of the radical.[9] Due to the intrinsic spectroscopic properties[10] pyrazole is commonly employed for constructing nonlinear optical materials,[11] photochromic derivatives[12] and electro-optical crystals.[13] The logic suggests, that such changes would be as well reflected in the corresponding emission spectra. This finding gave rise to an elegant idea that the introduction of the pyrazole bridging unit into the fluorophore-radical assembly

would influence the fluorescence quenching. Consequently, the sensitivity of the probe could be tuned as desired through the appropriately selected spacer between radical and fluorophore fragments. Thus, models, which consist of a stable and efficient fluorophore (e.g. pyrene, perylene) and the pyrazole bridging block covalently linked to the radical unit, represented in *Figure 2.1*, were designed.

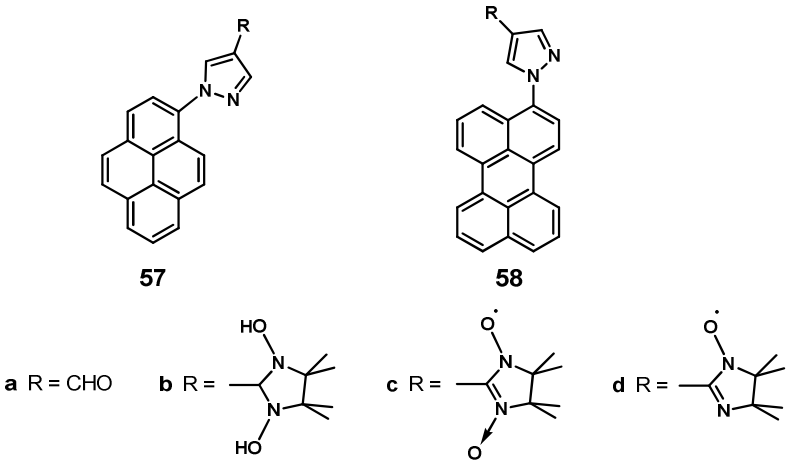

Figure 2.1. Model compounds.

In the current chapter we discuss the synthesis of the radicals 1-[4'-(3-oxide-1-oxyl-4,4,5,5-tetramethylimidazolin-2-yl)pyrazol-1'-yl]-pyrene **57c**, 1-[4-(1-oxyl-3-4,4,5,5-tetramethylimidazolin-2-yl)pyrazolyl]-pyrene **57d** and 3-[4'-(3-oxide-1-oxyl-4,4,5,5-tetramethylimidazolin-2-yl)pyrazol-1'-yl]-perylene **58c**; as well as the anthracene-based derivatives **59-62c**,**d** shown in *Figure 2.2*.

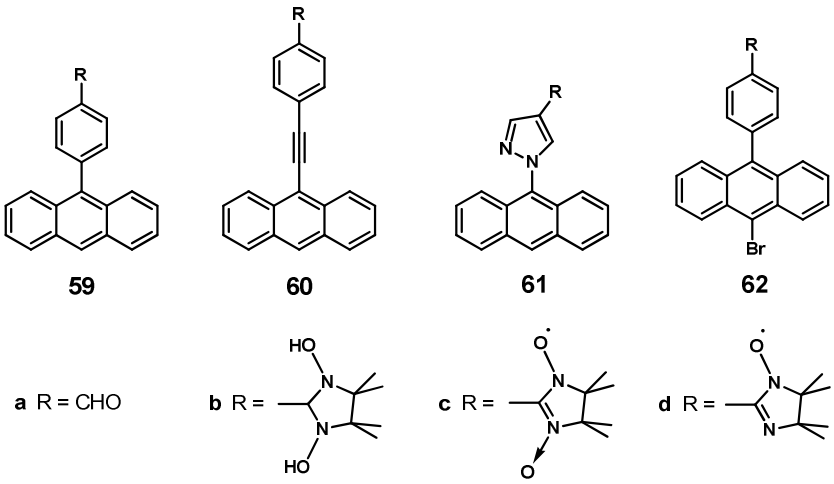

Figure 2.2. Anthracene-based models.

The radicals were characterized by UV-Vis, IR, EPR techniques and X-ray structural analysis in the case of derivatives **57c**,**d** and **59-62c**,**d**. Finally, a series of fluorescence measurements before and after addition of reactants to solution of the radical were performed. The focus of this work was to examine: (a) whether the introduction of an additional spacer into the framework could enhance the sensitivity of the probe molecule (**57**); (b) the influence of the substituent character (**59**, **61**, **62**) and the length of the distance between the radical center and the fluorophore (**60**) on the response.

2.2. Synthesis of the pyrene- and perylene-based nitroxide radicals

Inspired by the remarkable work of Zoppellaro, who obtained 2,6-bis(pyrazolyl)pyridine based nitronyl nitroxide biradical,[9,14] it was planned to synthesize 4-formyl pyrazole and attach it to a pyrene or perylene aromatic core. Despite of apparent simplicity of the molecule **64**, one should not misjudge the task. Two different routes were employed to synthesize 4-formyl pyrazole **64**.

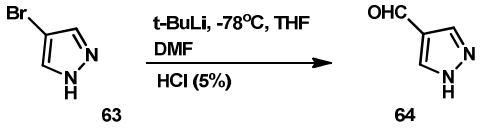

Scheme 2.1. Synthesis of pyrazole-aldehyde **64**.

The first route consisted of direct lithiation of commercially available 4-bromopyrazole **63** with 3 equivalents of *t*-BuLi, which formed intermediate 1,4-dilithiopyrazole in the course of the reaction. The latter could be converted into the formylated derivative **64** by adding dry DMF to the mixture,[15] as shown in *Scheme 2.1*. In the course of optimizing the reaction conditions, it appeared that some parameters had particularly crucial influence on the yield. The monolithiate formed immediately when adding the first equivalent of BuLi, and precipitated as a white powder from the reaction mixture. This intermediate could not further react because of its insolubility. When the mixture was warmed to a higher temperature, the lithiated compound dissolved in THF and reacted further. According to Catala,[15] prolonging the time spent at room temperature (till 3 h) increased the yield of the dilithiated derivative, and significantly diminished the amount of the starting 4-bromopyrazole **63**. However, stability of *t*-BuLi

decreased with increasing the temperature,[16] and a vast number of side-products was formed. That was the major drawback of the reaction, which led to variable and often low yields.

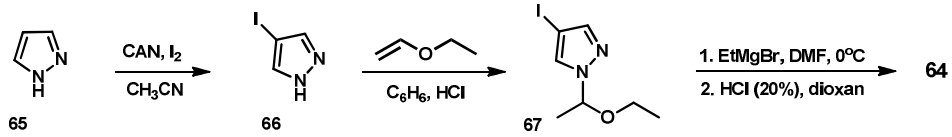

Scheme 2.2. Alternative route towards pyrazole-aldehyde **60**.

Another route towards 4-formylpyrazole derivative **64** was preferred following a multi-step approach sketched in *Scheme 2.2*.[17] At first pyrazole **65** was selectively iodinated in the presence of ceric ammonium nitrate (CAN),[17b,18] giving 4-iodo-pyrazole **66** in quantitative yield. The amino group was then protected with ethyl vinyl ether in the presence of acid catalysis. THF solution containing compound **67** was treated with Grignard reagent (EtMgBr) at ~0°C (ice bath), and after the halogen/Mg exchange was completed, dry DMF was added with small portions dropwise (to keep the temperature constantly at zero). Afterwards the mixture was decomposed with NH_4Cl saturated solution. The organic layer was collected, and the water phase was extracted with chloroform. The combined organic extracts were dried over $MgSO_4$, and the solvents were evaporated in *vacuo*. The residual pale yellowish oil contained the target aldehyde still protected with ethoxyethyl-group. Therefore, the mixture was subjected to a reaction with hydrochloric acid (10%) in dioxane. Subsequent purification using column chromatography afforded 4-formylpyrazole **64** in 80% total yield.

^{1}H NMR shown in *Figure 2.3* illustrates the changes, which happened with the pyrazole core. Thus, the broad ^{1}H-NMR signal of the free amino group (-NH) labelled with the letter *b* is present in both derivatives – iodo-pyrazole precursor **66** and the isolated product **64**, and falls at 11.64 and 12.05 ppm, respectively. Instead of this signal the NMR spectrum of the compound **67** demonstrates newly appeared peaks of CH_3- (1.57, 1.08 ppm, marked with the letters *e* and *f* in *Figure 2.3*, respectively), CH_2- (3.22-3.42 ppm, shown with the letter *d*) and CH- (5.39-5.47 ppm, labelled as *b*) groups of the ethoxyethyl fragment. Finally, the ^{1}H-resonance signal in the spectra of compound **64** at 9.85 ppm (*g*), originating from the aldehyde group, is a clear evidence confirming formation of the derivative **64**.

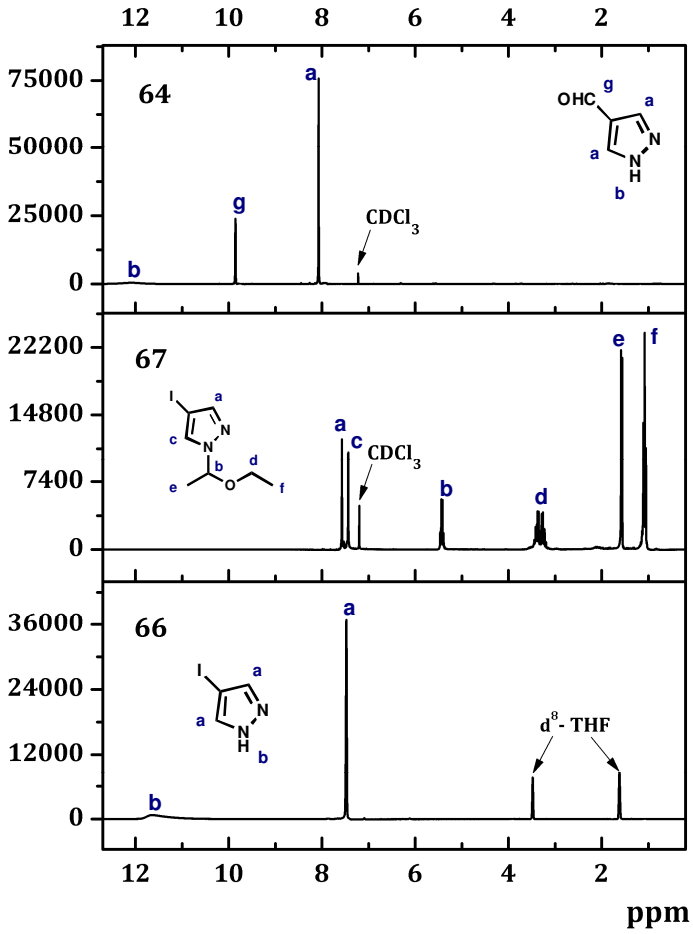

Figure 2.3. NMR spectra of the compounds **64**, **66**, **67** at 250 MHz (16 scans).[17a]

The following methods are usually applied to attach robust aromatics to the pyrazole moiety according to the literature:

- condensation between nucleophilic potassium salt of 4-formyl-1*H*-pyrazole and corresponding bromide derivative in diglyme;[13]
- coupling reaction between 4-formyl-1*H*-pyrazole and corresponding bromide derivative in the presence of NaH;[19]
- copper-catalyzed N-arylation[20,21]

So, potassium metal (2 eq.) was added to a solution of 4-formylpyrazole **64** (2 eq.) in dry diglyme, and the mixture was heated under argon at 70°C, until all of the potassium had reacted to form the pyrazolate derivative. Then, one equivalent of bromo-aryl was added through the septum under argon, and the heating was increased to 110°C. According to TLC analysis of the reaction aliquots, the main compound presented in the

mixture was the starting bromo-aryl. Continuous heating during 80 h didn't lead to significant changes in the content of the mixture.

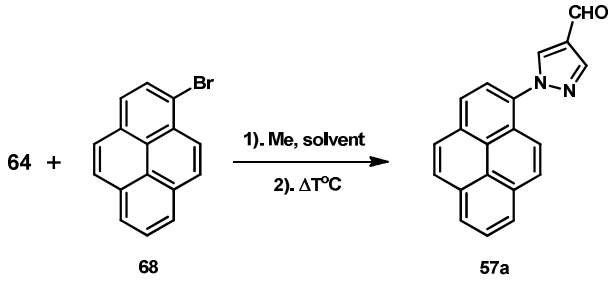

Scheme 2.3. Initial attempts to synthesize pyrazole-pyrene carbaldehyde **57a**.

Further experiments were performed varying the temperature and the reaction time, which, however, didn't lead to considerable improvements. Therefore, another route was explored. Thus, sodium hydride (2 eq.) was added to a solution of **64** (2.1 eq.) in dry THF, and the mixture was heated under argon to 50°C for 40 min. After addition of the bromo-aryl (1 eq.) the temperature was raised to 60°C and the reaction mixture was left at this temperature stirring for 24 h. In that case the yield of the desired product appeared to be also not satisfactory (varying from 5 to 15%). Furthermore, trials involving copper-catalyzed coupling reaction couldn't provide us reasonable results either. Summarizing, for all three tested methods the reaction times exceeded 24 h and the full conversion of the starting material wasn't achieved.

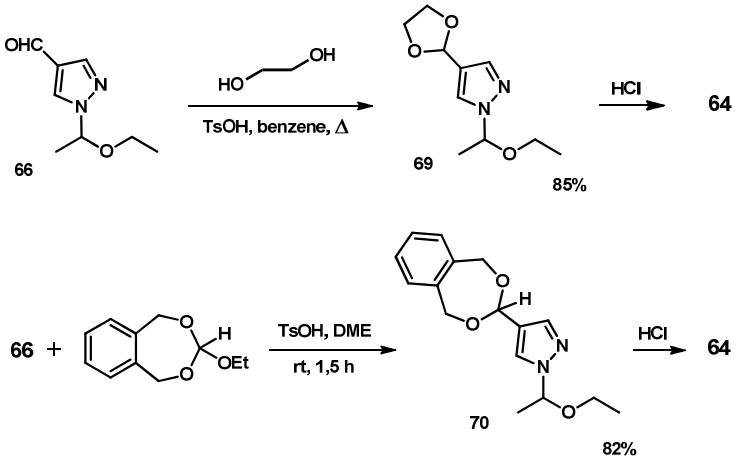

Scheme 2.4. Protection of the aldehyde function in **64** using acetals.

Both electrophilic character of the aldehyde group and the lower reactivity of the bulk ring systems in comparison to smaller molecules[13,14] were assumed to be the

reasons of our difficulties. Therefore, it was suggested to protect the aldehyde function with ethylene glycol or 3-ethoxy-1,5-dihydro-3H-2,4-benzodioxepine following the standard protocol,[22] as illustrated in *Scheme 2.4*. Protection of the aldehyde group led smoothly[22] to the target derivatives **69** and **70** in high yields. Unexpectedly, on the next step cleavage of the ethoxyethyl protective group accompanied the disclosure of the acetal ring for both compounds, although 1,5-dihydro-3H-2,4-benzodioxepine was reported to be relatively stable to acids.[23]

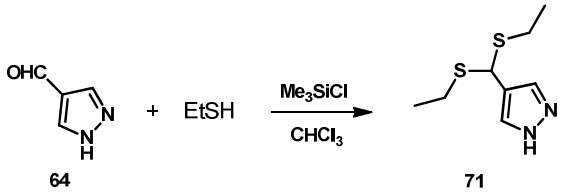

64 71

Scheme 2.5. Protection of the aldehyde function in **64** with ethanethiol.

Next, carbaldehyde **64** was subjected to a reaction with excess of ethanethiol in the presence of trimethylchlorosilane in chloroform[24] to afford 4-diethylthiol-1(*H*)-pyrazole **71**. The thiol protective group offers several advantages, for example, there was no need any more in the amino group protection, which simplifies the synthetic sequence. On the other hand, the donor character of sulfur atoms decreased the reactivity of the compound **71** in subsequent Ullman reaction.

In general, the order of introducing a carbonyl function into a framework is specified by the convenience of the particular synthetic method. Therefore, reversed reaction sequence was employed. At first, copper-catalyzed condensation between the pyrazole and bromo-pyrene was successfully realized in fairly high yield (75%). The next step was formylation at 4th position of the 1-arylpyrazole **72** under Vilsmeier–Haack reaction conditions.[25,26] The literature procedure[27,28] was slightly modified, suchwise, that to a solution of starting aryl-pyrazole derivative in dry DMF $POCl_3$ was added slowly dropwise through a septum at 95-100°C. The amount of DMF was enlarged due to the low solubility of the starting material.[28] The dense reaction mixture was stirred at this temperature and monitored by TLC. After the reaction was complete the mixture was cooled down till ambient temperature and poured on ice. The resulted dark viscous solution was neutralized with 20% aqueous sodium hydroxide. 4-Formyl-pyrazole-pyrene **57a** formed yellow precipitate which could be separated from the mother solution by filtration.

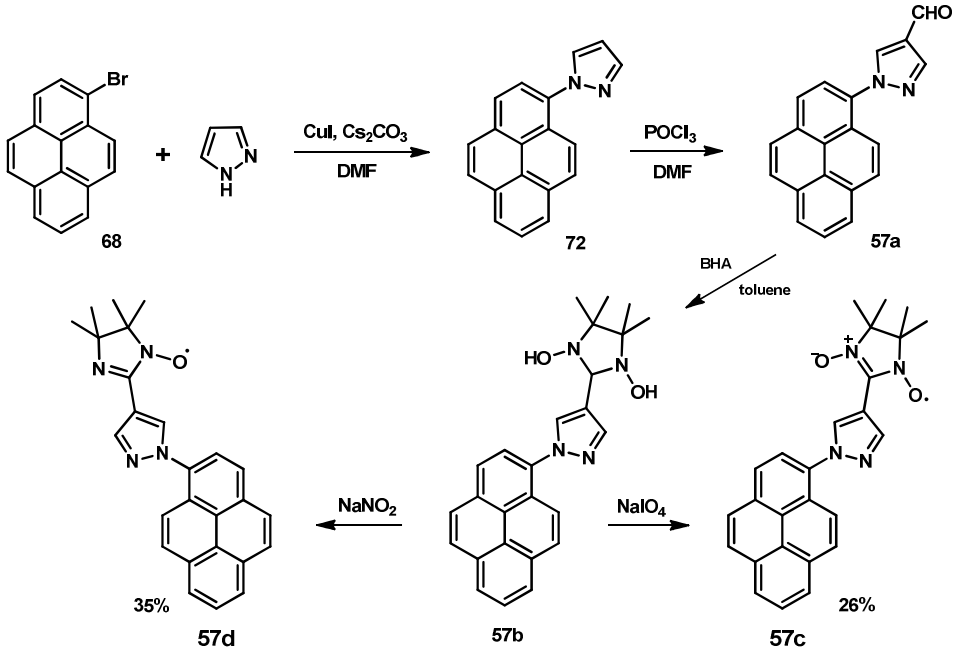

Scheme 2.6. Synthetic route towards pyrene monoradicals **57c**,**d**.

Subsequent condensation between BHA and the aldehyde **57a** in degassed toluene under argon at 110°C in 4 hours afforded the radical precursor – 4-(1,3-dihydroxy-4,4,-5,5-tetramethylimidazolidin-2-yl)-1-pyrenepyrazole **57b** - in quantitative yield. Varying the oxidation conditions nitronyl **57c** and imino nitroxide **57d** radicals were obtained. Thus, oxidation of the imidazolidine **57b** with sodium-periodate was realized in a two phase system (CH_2Cl_2/H_2O), giving after purification on a chromatographic column nitronyl nitroxide radical **57c** in 26% yield; using excess of sodium nitrite in acidic medium we achieved imino nitroxide radical **57d** in 35% yield. Summarized synthetic procedure towards pyrazole-pyrene nitronyl **57c** and imino nitroxide **57d** radicals is depicted in *Scheme 2.6*.

Although the condensation of 3-bromo-perylene **73** with pyrazole led to the desired product **74** in fairly good yield (63%), on the next step formylation of the derivative **74** didn't proceed smoothly, and we encountered a serious obstacle concerning the isolation of the product **58a**. Thus, the low solubility of the compound **58a** forced us to use stronger eluent mixtures at the expense of the separation. Crystallization from various solvents couldn't provide us pure compound. Finally, we were able to purify aldehyde **58a** using Al_2O_3 short fast flesh-column with gradient solvent mixture. Obviously

some quantity of the product remained on the column, causing the decrease of the reaction yield (only 23% according to the starting material).

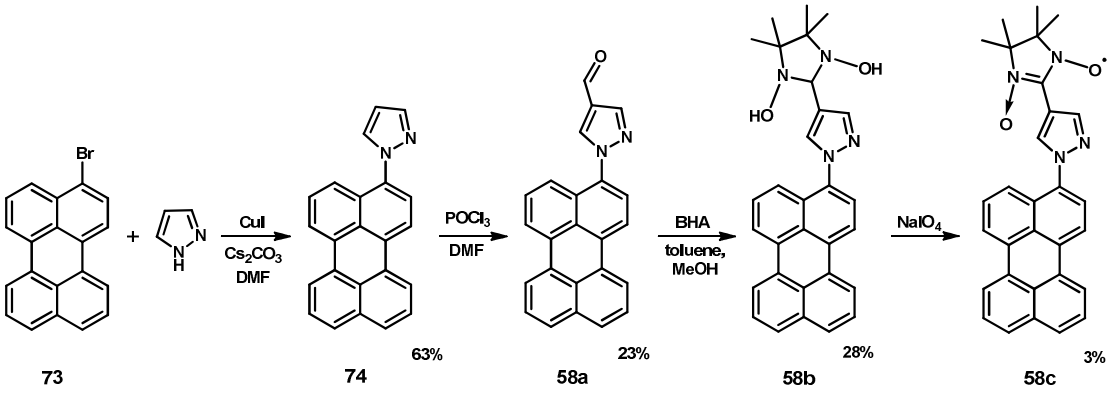

Scheme 2.7. Synthesis of the perylene-based radical **58c**.

It should be mentioned, that the low solubility is a typical problem associated with the perylene derivatives.[29] Here, carbaldehyde **58a** is poorly soluble in absolute methanol. Performing the reaction in toluene with gentle heating at 60°C destroys imidazolidine **58b**, at room temperature no traces of the product were detected. Varying solvent mixtures we achieved compound **58b** in 28% yield. Radical **58c** was obtained following the typical procedure described previously for the pyrene derivative **57c**, but with extremely low yield - 3% referring to the starting aldehyde **58a**.

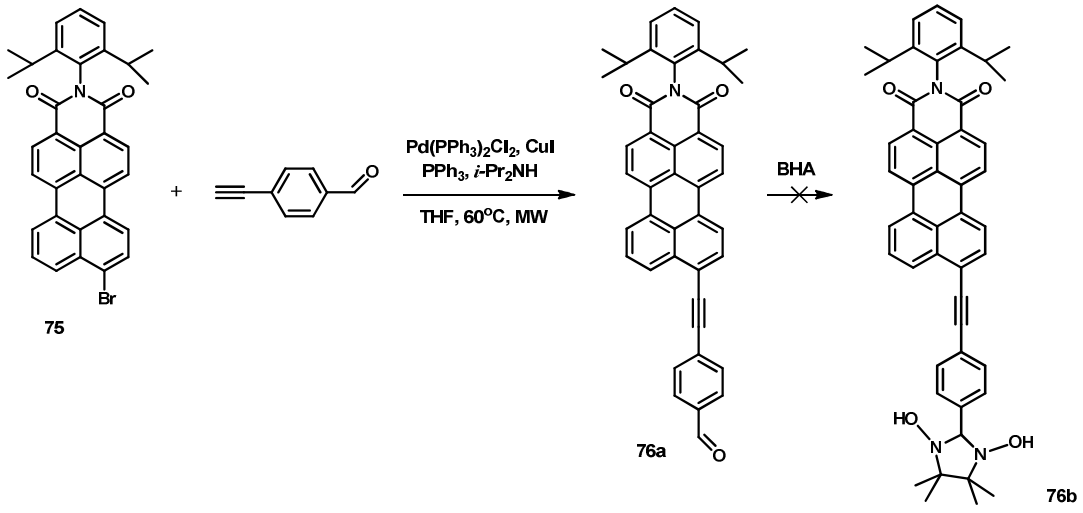

Scheme 2.8. Model with modified perylene core.

Our next target **76a** contained a modified perylene core, designed to increase the solubility of the corresponding carbaldehyde. To synthesize compound **76a** Sonogashira-Hagihara cross-coupling methodology was employed, as outlined in *Scheme 2.8*.[30] Thus,

the $Pd^{(II)}$- catalyzed reaction between N-(2,6-diisopropylphenyl)-perylene-3,4-dicarboximide **75** and 4-ethynylbenzaldehyde was carried out in the presence of strong base (*i*-Pr_2NH), and afforded the carbaldehyde **76a** in high yield (87%).

Surprisingly, among several condensation conditions tested (*Table 2.1*) none led to the formation of the imidazolidine derivative **76b**; even traces amounts of the product **76b** were not detected, while monitoring the reaction progress with TLC.

Table 2.1. Tested condensation conditions for the aldehyde **76a** and BHA.

	Solvent	Temperature	Time	**76b**
1	toluene	110°C	72h	-
2	toluene	rt	2 weeks	-
3	toluene/MeOH (1:1)	rt	2 weeks	-
4	toluene/MeOH (1:1)	50°C	48h	-
5	toluene/DCM/MeOH (2:1:1)	rt	2 weeks	-

Recently Romero demonstrated, that Pd-catalyzed cross-coupling reaction between a NN-radical bearing a halogeno function and an ethynyl functionalized aromatics is an efficient method for the preparation of novel ethynyl-bridged biradicals.[31] In this light coupling reaction between 3-ethynylperylene **77** and 2-iodo-nitronyl nitroxide radical **78** was tested, as illustrated in *Scheme 2.9*.

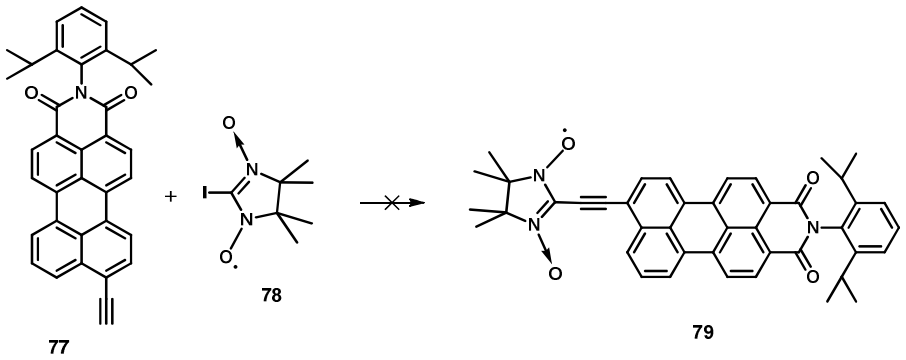

Scheme 2.9. Sonogashira-Hagihara coupling approach towards perylene-based NN.

Despite varying the experimental conditions (solvent, time, temperature) these trials failed to give viable quantities of the desired compound. Thus, after 2 days stirring at room temperature radical **78** was mainly transformed into a mixture of unidentified by-products, and was partially converted into the halogen-free NN radical (only negligible traces of a new radical species were detected by TLC analysis).

To find an ideal fluorophore is not an easy task. Here the chemical stability, fluorescence quantum yield are the parameters, which should be considered. The

objective of this study was to synthesize probes with the enhanced sensing properties, and so pyrene-based nitronyl **57c** and imino nitroxide **57d** radicals were obtained. Also perylene nitronyl derivative **58c** was achieved, the stability of the compound **58c** remained questionable. Therefore, new promising targets were designed and the work to obtain stable perylene-based nitroxides is on-going.

2.3. Crystal structure analysis of the pyrene-based nitroxide radicals

Single-crystals of the nitronyl **57c** and imino **57d** nitroxides suitable for X-ray analysis were obtained by slow diffusion of dichloromethane-hexane mixture (1:4) at room temperature. Deep-blue needle crystals of **57c** and red blocks of **57d** radicals were analyzed by X-ray diffraction and their ORTEP drawing are given in *Figures 2.4-2.5*.

Table 2.2. Crystallographic parameters of the nitronyl **57c** and imino **57d** nitroxides.

	57c	**57d**
Formula	$C_{26}H_{23}N_4O_2$	$C_{26}H_{23}N_4O$
M	423	407
crystal system	monoclinic	monoclinic
space group	$P2_1/a$	$P2_1/a$
$\boldsymbol{a}$, Å	7.4598(2)	7.3261(2)
$\boldsymbol{b}$, Å	29.3972(9)	29.7850(9)
$\boldsymbol{c}$, Å	10.0132(3)	9.8773(3)
$\boldsymbol{\beta}$, deg	109.8210(16)	109.2812(16)
$\boldsymbol{V}$, A^3	2065.78	2034.41(11)
$\boldsymbol{Z}$	4	4
$\boldsymbol{R_{factor}}(\%)$	4.47	5.08
$\boldsymbol{D_c}$, $g \times cm^{-3}$	1.362	1.330
$\boldsymbol{N_{ref}}$	5785	6159
$\boldsymbol{N_{par}}$	289	280
S	1.080	1.090
CCDC	816634	816631

The crystallographic data were collected on Nonius Kappa CCD (Mo kα, μ = 0.71073 Å) diffractometer equipped with a graphite monochromator. Pertinent crystallographic parameters and refinement data are listed in *Table 2.2*.

Regardless of many attempts employing various crystallization conditions, no suitable crystals of the derivative **58c** were achieved. Some crystalline material was obtained from the saturated solution of the radical **58c** in DCM/heptane mixture (3:5) at low (-20°C) temperature. However, the tiny crystals made under such harsh conditions were not well-defined, and, therefore, not suitable for X-ray analysis. Our attempts to grow a crystal at room temperature failed, as the radical appeared to be unstable, and on the next day the solution turned orange. Further storing the solution of the radical **58c** at room temperature led to a colorless liquid.

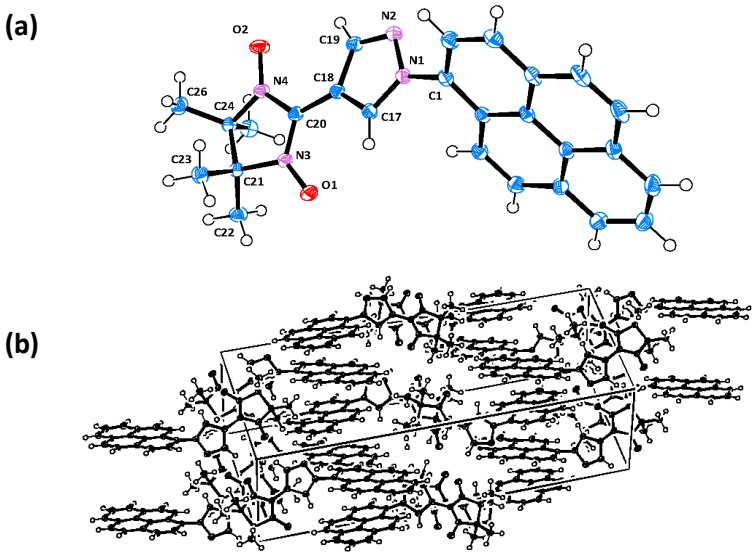

Figure 2.4. X-ray structure of **57c** with ORTEP drawn at the 50% of the probability level: (a) molecule (○ nitrogen, ● oxygen, ○ carbon); (b) crystal packing.

Single crystal X-ray diffraction study[§] confirmed the molecular structure of the pyrene-pyrazole nitronyl nitroxide **57c** (*Fig. 2.4 (a)*). This compound belongs to the monoclinic class with $P2_1/a$ space group. The dihedral angles between the plane of the pyrene core and the pyrazole ring are slightly different: C(17)-N(1)-C(1)-C(14) is 57°, while C(2)-C(1)-N(1)-N(2) is 54°. The latter angle is smaller perhaps due to the attraction of the lone pair of the nitrogen atom of the pyrazole moiety with the hydrogens of pyrene. The angle between the average plane of the radical group and the pyrazole ring is around 12°, making them fairly co-planar. Closer investigation of the crystallographic data revealed, that both NO groups are involved in the hydrogen bond formation, and have similar bond

§ X-ray structure analysis was performed by Prof. Dr. Volker Enkelmann at MPI-P (Mainz).

distances: N(3)-O(1) 1.286, N(4)-O(2) 1.279 Å. Hence, various aromatic stacking interactions assure formation of a stair-like 2D hydrogen bonded network (*Fig. 2.4 (b)*).

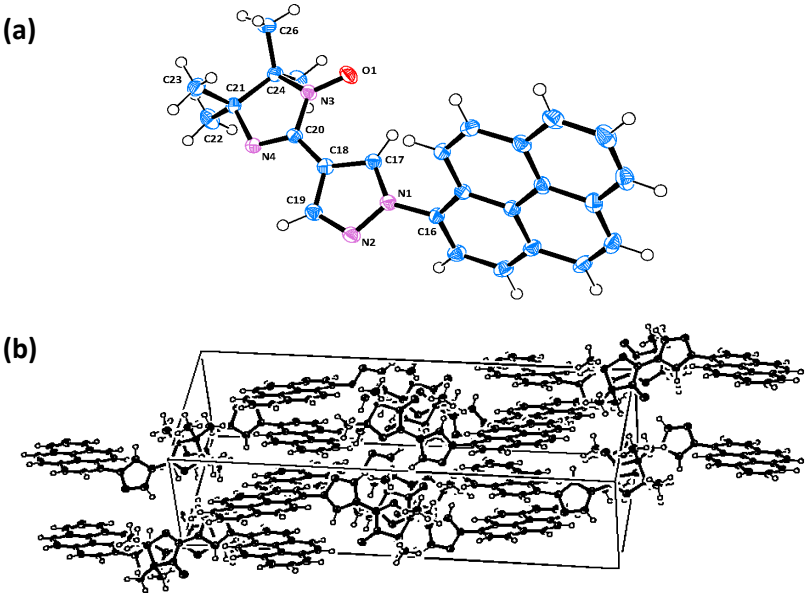

Figure 2.5. X-ray structure of **57d** with ORTEP drawn at the 50% of the probability level: (a) molecule; (b) crystal packing.

The crystal structure of the imino nitroxide derivative **57d** is similar to the one described earlier for the nitronyl analogue **57c**. Here, the radical features a $P2_1/a$ space group. Quasi planar pyrazole-nitroxide moiety is strongly tilted to the pyrene plane (~ 59°), affording, therefore, effective hydrogen bonding in a head-to-tail manner (*Fig. 2.5 (b)*). Geometrical parameters are: O1···H231' 2.55, C18···H221' 2.89, H121···H222' 2.33 Å. π-Stacking in the lattice arises mainly due to superb chelating properties of the pyrazole.[32,33]

2.4. EPR properties of the pyrene-based nitroxide radicals

2.4.1. Introduction into EPR theory and g-value determination

The phenomenon of electron spin resonance was discovered in 1944 by Zavoisky.[34] He noticed that a paramagnetic sample absorbs the energy of the electromagnetic field in a constant magnetic field. This process occurs when two conditions are fulfilled: (a) the energy of a quantum must correspond to the separation between the energy levels in the molecule; (b) the oscillating electric field component

must be able to stimulate an oscillating electric dipole in the molecule, which arises from the net spin or net orbital momentum, or from combination of those two factors.[34,35]

Magnetic properties of atoms and molecules are determined by the electron magnetic moment. Nucleus magnetic moment is significantly smaller than the electron magnetic momentum, therefore the latter basically defines the magnetic properties of the matter. Electron magnetic properties in atoms appear due to their motion around the nucleus (orbital magnetic momentum) and intrinsic orbital angular momentum of the electron, or *spin*.[34,35]

Atoms and molecules possess different magnetic properties, depending on their electronic structure. Materials consisting of the molecules with nonzero magnetic moments are called *paramagnetic*. Examples of paramagnetic materials are some gases (O_2, NO), alkali metals, various salts of the rare-earth metals, *etc*. The magnetic moment $\mathbf{M}$ of a paramagnetic sample is defined by equation (*4*),

$$\mathbf{M} = \sum i = 1^{\mathrm{N}} \mu_i \qquad (\boldsymbol{4})$$

where $\boldsymbol{\mu_i}$ – are magnetic moments of the particles, $\mathbf{N}$ - is the number of the particles. Without external magnetic field $\boldsymbol{B}$ the total magnetic moment of the sample is zero (M = 0), due to the random thermal motion of the particles.

In the majority of biological and chemical systems the orbital magnetic momentum of paramagnetic particles is negligible. Therefore, the paramagnetic properties of a sample could be attributed to the total spin S of the molecule. The energy level split into $2S$ + 1 sub-levels, corresponding to the different projections of the total spin S in direction of the vector of the applied magnetic field $\boldsymbol{B}_{\mathrm{o}}$:

$$\mathrm{E}\,(M_S) = \mathrm{g}\,\beta\,M_S\,B_{\mathrm{o}} \qquad (\boldsymbol{5})$$

According to the selection rule[34-36] two values of M_S are allowed for a system consisting of a paramagnetic center with one unpaired electron S = ½: +½ and -½, separated by an energy interval ($\Delta\mathrm{E}$) of $\mathrm{g}\beta B_{\mathrm{o}}$. Transition between two neighboring energy levels can be induced by an electromagnetic field only of the appropriate frequency υ, when the photon energy $h\upsilon$ matches the energy-level separation, i.e. $h\upsilon = \beta B_{\mathrm{o}}$. In that case the electromagnetic radiation may be regarded as the coupled electric and magnetic fields oscillating perpendicular to one another and to the direction of propagation. The separation $<\mathrm{g}\beta B>$ between the two energy levels (also referred as *Zeeman effect*) increases linearly with the magnetic field as shown in *Figure 2.6*.

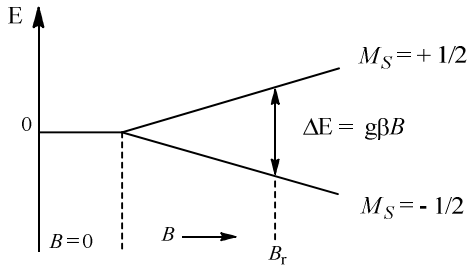

Figure 2.6. Energy-level scheme for a S = 1/2 system showing EPR absorption.

For a system in a thermodynamic equilibrium the population of the lower (N_1) and higher (N_2) levels differs. Boltzmann's law governs the relative distribution of the electrons over the two neighbouring levels, which is given by equation (*6*):

$$N_2/N_1 = \exp(-\Delta E/(kT)) \qquad (\mathbf{6})$$

where N_1 and N_2 – are the numbers of spins with M_S = -½ and the M_S = +½ states, k - Boltzmann's constant, T is the temperature. The lower level is more populated than the upper one ($N_2/N_1 < 1$).

The position of a line in the EPR spectra is characterized by the magnitude of g-factor: $g = h\upsilon/(B_r \beta)$, where $\boldsymbol{B_r}$ is the magnetic field, at which the resonance condition is met. For a free electron g_e = 2.00232. Nitroxide stable radicals and most of organic radicals show similar values of $g \approx 2.003 - 2.007$. In solution the g-factor is isotropic, while in solid state it is anisotropic and becomes orientation dependent:

$$g^2 = g_{xx}^2 I_x^2 + g_{yy}^2 I_y^2 + g_{zz}^2 I_z^2 \qquad (\mathbf{7})$$

where I_X is the direction cosine between the direction B and the principle g-axes. Among the other factors, which cause anisotropy of the g-factor and lead to serious deviations from the spin value of 2.00232, is the influence of anisotropic electric fields, surrounding the atoms, splitting of Zeeman levels in zero magnetic field, *etc*. Typically significant differences of the magnitude of the g-factor from a free electron value are observed in the presence of strong spin-orbital interactions (as in the case of transition metals).

For paramagnetic species in dilute liquid solution of low viscosity the system is apparently isotropic, due to the free molecular rotation. In such systems all the g axes $g_x = g_y = g_z$ are equal to the applied magnetic field B. Consequently, g factor is independent from the field direction and to be regarded as an effective value averaged over all orientations:

$$g_{iso} = (g_{xx} + g_{yy} + g_{zz})/3 \qquad (\mathbf{7'})$$

2.4.2. Hyperfine coupling (*hfc*)

Except the interaction of an electron with the magnetic field, additional interaction within a sample containing nucleus, which possesses an intrinsic nuclear spin angular momentum, should be considered. The interaction of an unpaired electron and a magnetic nucleus is called *nuclear hyperfine interaction* ($\boldsymbol{A}$). Hyperfine interactions are responsible for the EPR line splitting. The number of the lines depends on the magnetic nucleus number.

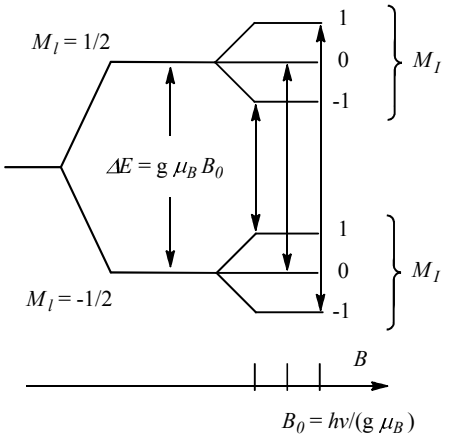

Figure 2.7. Energy-level scheme illustrating origins of *hfc* in EPR spectra of NO paramagnetic molecule.

Examples of the nucleus with non-zero nuclear spin are: ^{1}H, ^{2}D, ^{13}C, ^{14}N, ^{15}N. As an example, let us consider a nitrogen nuclei of NO paramagnetic molecule. ^{14}Nitrogen nucleus has a spin I = 1, therefore, three projections of spin are allowed: along the direction, perpendicular and against the applied magnetic field B_o. The corresponding values of the magnetic quantum number are: I_z = +1, 0, -1. It follows, that due to the interactions of a free electron with a nitrogen nuclei each Zeeman level splits in three sub-levels. According to the quantum mechanical selection rules ΔS_z = ±1 (orientation of the electron spin changes) and ΔI_z = 0 (orientation of the nuclei spin does not change). Thereby, the resulting EPR spectra of a sample containing one nitrogen nuclei and a single free electron (i.e. NO paramagnetic molecule) consist of three lines, as shown in *Figure 2.7*.

The total hyperfine interaction constant (A) consists of isotropic (A_{iso}) and anisotropic (A_{dip}) terms (*Eq. 8*):

$$A = A_{iso} + A_{dip} \quad (8)$$

The last one arises from the interactions between the electron and nuclear dipoles, and is time-averaged to zero at room temperature in solution. The anisotropic constant can be measured in solid or frozen rigid systems, when the random molecular motions are prohibited. Therefore, the observed hyperfine value in solution at ambient temperature is due to the isotropic term, which is defined by the equation (*9*):

$$A_{iso} = (A_{xx} + A_{yy} + A_{zz})/3 \quad (9)$$

For $g = g_e$ the isotropic hyperfine interaction is also called *Fermi contact*, and can be described in a precise form as:

$$A_{FC} = 8/3\pi g_e \beta_e g_n \beta_n \rho(0) \quad (10)$$

where $\rho(0) = |\psi(0)|^2$ - is the unpaired electron density at the nucleus, β_n is the nuclear magneton.

The spin energy levels of a monoradical are described by the spin-Hamiltonian $\hat{H}$ (*11*), which consider the contributions from the electron-Zeeman and the hyperfine interaction for a $S = ½$ system. Higher order terms, such as nuclear Zeeman and quadrupole contributions, are usually not considered.[35]

$$\hat{H} = g\,\beta\,\hat{S}_i\,B_o + \Sigma\,A_{ij}\,\hat{S}_i\,\hat{I}_j \quad (11)$$

The electron-Zeeman component ($g\beta\hat{S}_iB_o$) describes the interaction between the electron spin operator $\hat{S}_i$ and the applied external magnetic field tensor B_o. The hyperfine term ($\Sigma A_{ij}\hat{S}_i\hat{I}_j$) accounts for the interaction between the magnetic moment of the electron spin ($\hat{S}_i$) and the magnetic moment of the nucleus in the vicinity ($\hat{I}_j$). The coefficient A_{ij} represents the hyperfine coupling constant.

Nitronyl nitroxide and imino nitroxide monoradicals exhibit very distinct EPR resonance envelopes. In the case of NN systems, the spectrum recorded in dilute (≤ 10^{-4} M) and oxygen free DMSO solution at room temperature exhibits a clear isotropic five line pattern with g_{iso} = 2.0065(8). The five lines spectra originate from the unpaired electron interaction with the two equivalent nitrogen nuclei of the imidazolyl moiety. The relative intensity of each line follows the typical 1:2:3:2:1 ratio, as shown in *Figure 2.8 (1)*.[1,36] The best fitting of the EPR curve was obtained assuming Lorentzian/Gaussian line-width ratio = 0.66.

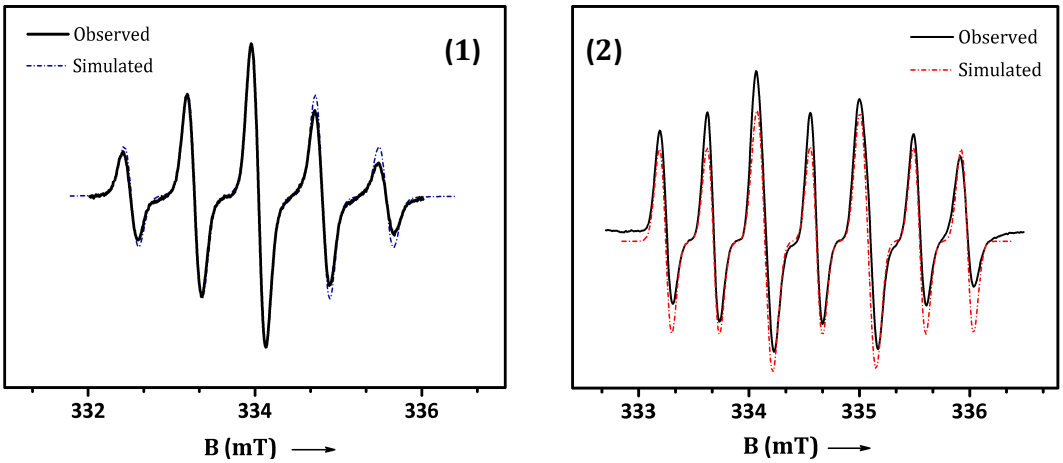

Figure 2.8. EPR spectra of the monoradicals (*1*) **57c** and (*2*) **57d** recorded in dilute (10^{-4} M) and oxygen free DMSO solution at 293 K. Experimental parameters: (*1*) 9.39753 GHz, 100 kHz modulation frequency, 0.24 mT modulation amplitude, 41 msec time constant, 42 sec sweep time, 10 mW microwave power, 2×10^4 gain; (*2*) 9.41094 GHz, 100 kHz modulation frequency, 0.52 mT modulation amplitude, 164 msec time constant, 84 sec sweep time, 0.64 mW microwave power, 8×10^5 gain. The dash-dotted line represented the computer simulation with the following parameters: (*1*) A_N = 0.749 mT, g_{iso} = 2.0065, ΔB_{pp} = 0.085 mT; (*2*) A_N = 0.885(5) mT, g_{iso} = 2.0058, ΔB_{pp} = 0.106 mT, and assuming pure Lorentzian line.

In the case of imino nitroxide monoradical, the resulting EPR spectrum represents a seven line pattern, as demonstrated in *Figure 2.8 (2)*. Such feature arises from the interaction of the unpaired electron with the two non equivalent nitrogen nuclei. The seven line pattern follows the intensities ratio of 1:1:2:1:2:1:1 and has g_{iso} = 2.0058(3).

2.4.3. Nitric oxide detection employing pyrene-pyrazole nitronyl nitroxide radical

Nitric oxide is a small molecule with an enormous physiological impact.[37,38] NO· is a gas with free radical properties, which exerts a major regulatory role as a vasorelaxant in the cardiovascular system and as a neurotransmitter in the central nervous system.[39,40] It has been suggested that NO· imbalance in the endothelium may be used as an early sign of vascular diseases such as atherosclerosis, hypertension, and myocardial ischemia.[41]

Nevertheless, many of the functions proposed for NO· remain controversial owing to the lack of direct evidence. The use of NO-reactive fluorescent indicators which allow bioimaging of NO· with high spatial and temporal resolution in conjunction with the fluorescence microscopy should overcome this problem. Some reactions that trap NO·

directly are known in the literature (*e.g.* interaction of NO· with heme/non heme groups).[42] However, the development of new flexible probes is essential. Unfortunately, in purely organic molecules a nitroso or nitro group will generally quench fluorescence, when dyes react with NO· generating these functional groups.

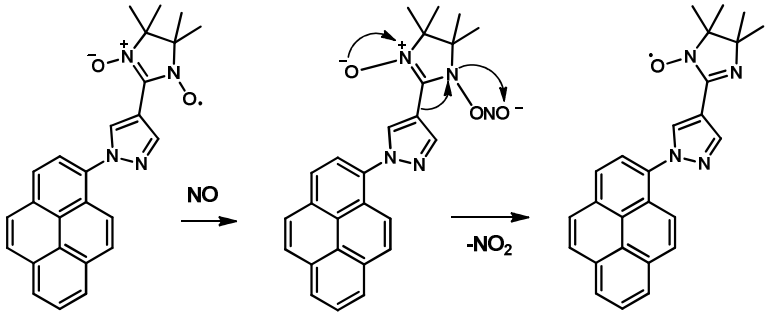

Scheme 2.10. Mechanism of the reduction of the nitronyl radical **57c** by nitric oxide.

Most of the procedures published during the last decades are based on electrochemical detection,[43,44] a few others exploit the oxidation or nitrosation of the fluorescent substrates.[45,46] The paramagnetic nature of the NO· should enable its detection by EPR spectroscopy; but this task was not easy to fulfill, due to the low stationary NO· concentration and high spin relaxation rate. Therefore, a great number of NO· donors and scavengers has been developed. Among these are nitronyl nitroxides, which specifically react with NO· to form imino nitroxides, with relatively high reaction constants of about ~10^4 $M^{-1}s^{-1}$.[47-49] Nitric oxide reduces nitronyl radicals according to the mechanism represented in *Scheme 2.10*.

This reaction causes drastic changes of the EPR spectra. The EPR envelope of the nitronyl radical **57c** in the initial stage of the reaction measured in DMSO is represented in *Figure 2.8 (1)*. DMSO is not a typical solvent for the EPR measurements, since as polar solvent it absorbs a lot of the microwave irradiation. Our choice was dictated by the necessity of utilizing cell-friendly solvent during NO-sensing experiments. Upon completion of the reaction the seven lines EPR spectrum corresponding to the imino species **57d** was expected. Accordingly, addition of excess NO· to 1 mM solution of **57c** resulted in the appearance of EPR peaks typical for the imino nitroxide. This difference in the EPR spectra of NN and IN radicals enables NO· quantification.

Similar changes in the spectrum occur when *N-(acetyloxy)-3-nitrosothiovaline (SNAP)*, a donor of NO·, is added to the nitronyl nitroxide **57c**. The liquid samples for the

analysis of SNAP were prepared shortly before the measurements. DMSO solution of the probe (1 mM solution) was purged with argon for ~10 min, and after addition of SNAP (its 1 mM solution was prepared by dilution in highly pure DMSO).

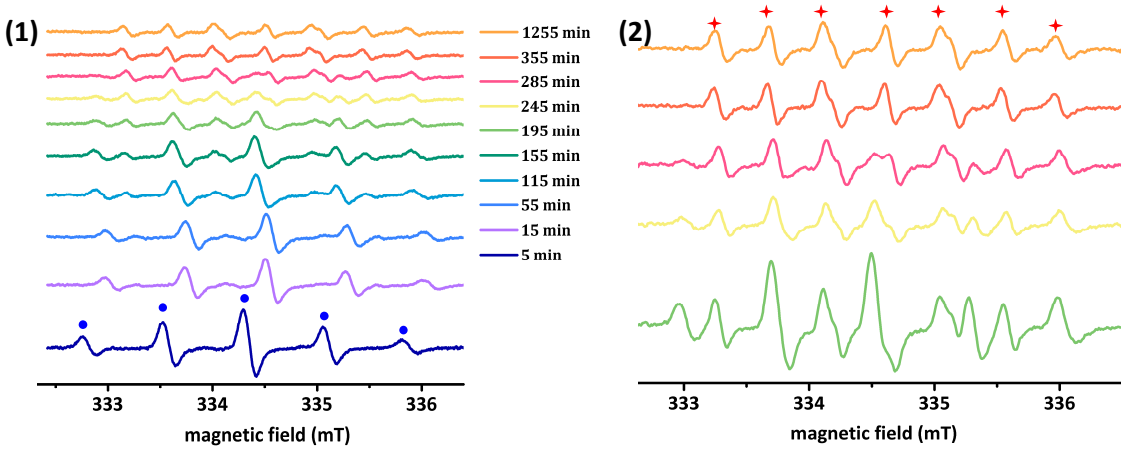

Figure 2.9. Evolution of the EPR envelope of **57c** probe (marked with the blue circles) after addition of the equivalent amount of SNAP to the oxygen-free DMSO solution of the radical at 298 K. Experimental parameters: 9.4 GHz frequency, 100 kHz modulation frequency, 0.64 mW nonsaturating microwave power, 0.2 mT modulation amplitude, (**1**) 3.2×10^4 receiver gain; (**2**) 2×10^5 receiver gain. The final state of the system (*i.e.* imino species) is marked with the red stars.

The evolution of the EPR spectrum of **57c** upon reaction with equivalent amount of SNAP is represented in *Figure 2.9*. It should be noted that the release of NO· from SNAP is a very slow process (half time is about 5 h) at pH 7.0 in the absence of catalytic metal ions.[50] It is, therefore, reasonable to assume that **57c** can also withdraw NO· directly from SNAP.

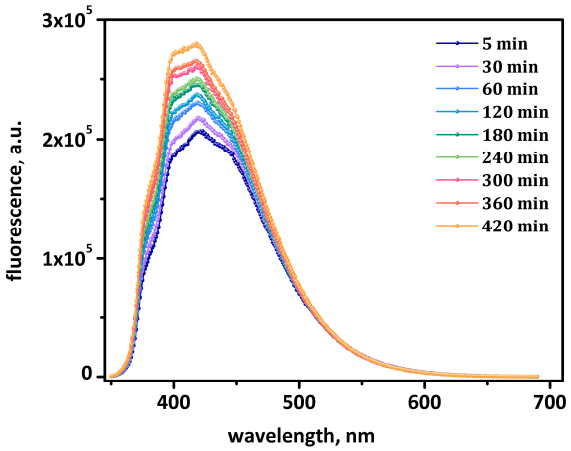

Figure 2.10. Evolution of the nitroxide **57c** fluorescence spectra after addition of an equivalent amount of SNAP at 298 K.

Likewise, to monitor the progress of the reaction the photoluminescence emission was measured. Fluorescence spectra of the sample containing DMSO solution of the nitronyl probe **57c** and equivalent amount of SNAP at different time intervals were recorded. The final measurement was carried out 7 h after the beginning of the experiment (marked as 420 min in *Fig. 2.10*). Initially, the fluorescence in nitroxide derivative **57c** is suppressed (see for more details *Subchapter 2.5.2*). However, the reaction of the radical **57c** with SNAP is accompanied by a drastic increase in the fluorescence intensity. This phenomenon is explained by the fact, that the nitronyl radical **57c** is a better fluorescence quencher, than the corresponding imino nitroxide **57d**. High fluorescence response of the system **57c** permits the detection of very low concentrations of NO already after 5 min of incubation with SNAP.

The applicability of the probe **57c** for detection of the nitric oxide *in vitro* by means of EPR and fluorescence techniques was demonstrated.

2.5. Photophysical properties

2.5.1. UV-Vis absorption spectra of the pyrene-pyrazole and perylene-pyrazole radicals in solution

The UV-Vis absorption spectra of the radical systems **57c**,**d** and **58c** were recorded in toluene solutions. Two distinctive set of absorption bands dominate the optical spectra of the nitronyl radicals **57c** and **58c** (*Fig. 2.11*). The first set of bands is characterized by differently enhanced vibronic components, and appeared at a longer wavenumber, around 600 nm. Those signals correspond to the n-π^* transitions of the aminoxyl oxide moieties. The second set of absorption values included π-π^* transitions and fell at much higher energy in the 300-380 nm wavelength range. That is another valuable fingerprint, which allows to distinguish different aromatic systems (*Fig. 2.11 (a)*).[14]

Interestingly, compound **57c** exhibited the characteristic deep blue colour, which is a typical feature for this class of radicals, while **58c** possessed emerald-green colour. The spectra of nitroxide **58c** in general was similar to the one of unsubstituted perylene, with a small red shift of the π-π^* absorption (~13 nm) relative to perylene.[51] Surprisingly low value of the molar extinction coefficient ε = 16651 $M^{-1}cm^{-1}$ (compared to 38500 M^{-}

$^{1}cm^{-1}$ of perylene[51]) was attributed to the low stability of the radical solutions at room temperature. Due to that reason the perylene-radical **58c** was not involved into further experiments.

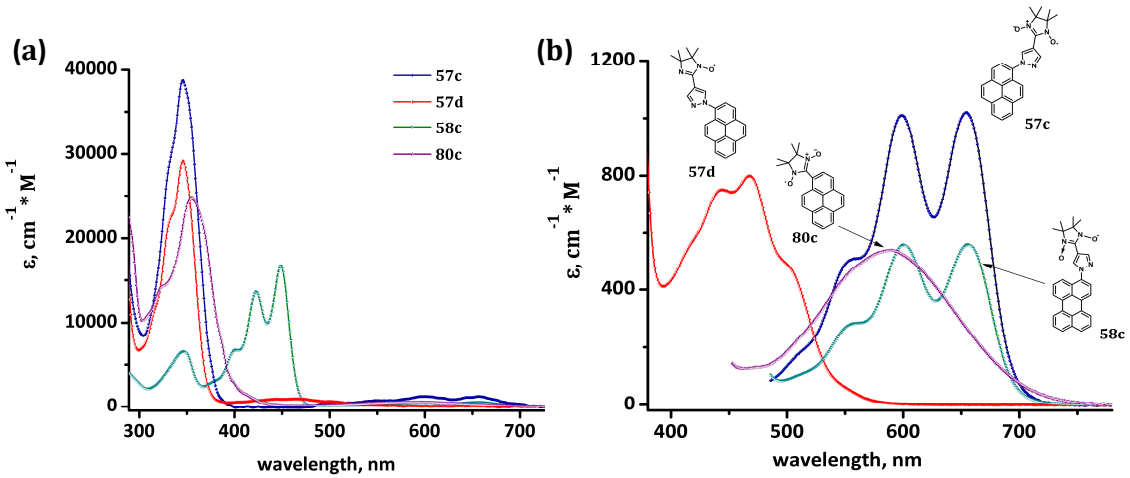

Figure 2.11. (a) UV-Vis spectra of nitronyl **57c**, **58c**, **80c** and imino **57d** nitroxide radicals recorded in toluene; (b) enlarged fragment of the spectra in the visible range.

The imino nitroxide **57d** radical featured a bright orange-red colour in solution, with a broad absorption band at 467 nm (n-π* transitions), as shown in *Figure 2.11 (b)*. Compound **80c** was synthesized[8,52] to compare the photophysical properties of the pyrazole-containing (**57c**) and pyrazole-free (**80c**) radicals. Enlarged fragment of the absorption envelopes in visible range is represented in *Figure 2.11 (b)*. Here, the pyrazole containing nitronyl **57c** and imino **57d** nitroxides exhibit similar absorption intensities, while pyrene radical **80c** features significantly less intense n-π* transitions.

2.5.2. Analysis of the analytes employing pyrene-based nitroxide radicals

Free radicals such as superoxide, hydroxyl and peroxyl radicals appear in the living systems as a result of redox processes. These short-living highly reactive species can attack biological molecules, including lipids, proteins and nucleic acids, causing damage in cell membranes, chromosomes and mitochondria. They play a crucial role in etiology (*i.e.* origination) of arteriosclerosis, virus infection, cell aging and cancer.[53,54] Ideally, natural and/or artificial antioxidants can suppress or prevent the oxidative damage, acting as scavengers of free radicals.[54,55] Namely, the antioxidants protecting cells from oxidative stress are: uric acid, ascorbate, tocopherol, *SH*-containing compounds (cysteine, serum

albumin, lipoic acid). Ascorbate is famous as one of the most efficient antioxidants in human blood. For example, it was proven, that decomposition of the lipids starts only after complete consumption of ascorbate.[53] Cysteine, or rather it's derivative *N-acetyl-L-cysteine (NAC)*, is another powerful antioxidant agent. NAC can help preventing side effects caused by drug reactions and toxic chemicals. It appears to have benefits in treating some respiratory conditions, such as bronchitis and chronic obstructive pulmonary disease. The direct reaction of an antioxidant with an indicator yields formation of a stable product, and could be employed to monitor the concentration of the studied compound in biological systems. The radicals **57c**,**d** can be used as such indicators.

The obtained nitroxide systems **57c**,**d** were found fairly well soluble in most of the organic solvents tested (e.g. MeOH, $CHCl_3$, THF, toluene). Nonetheless, during the early stage studies it appeared, that the employment of a protic medium was essential, since the solubility of the reagents (ascorbic acid, cysteine) in other solvents was negligible, and measurements in a two-phase system (such as toluene/methanol) provided us irreproducible results. Solvents rich with oxygen, from the other hand, could cause the reduction of the nitroxide radicals to the corresponding hydroxylamines, and inflict, therefore, the precision of the measurements.

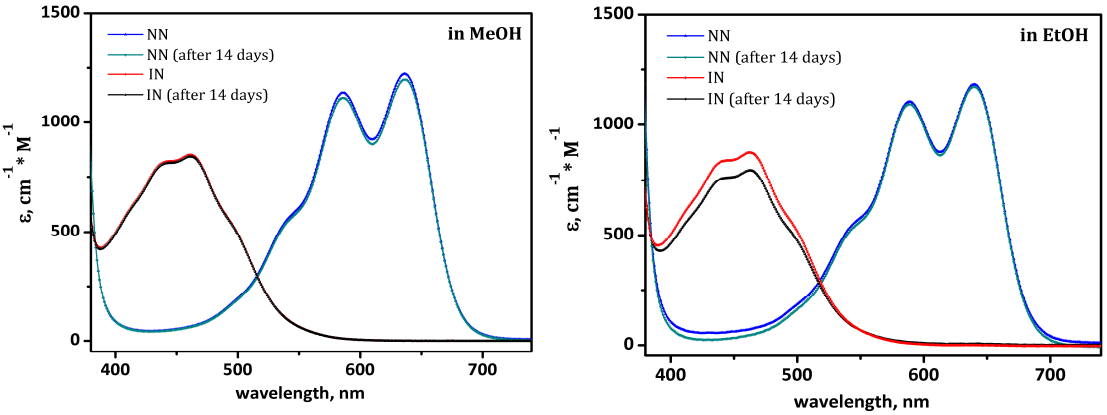

Figure 2.12. Stability of the probes **57c**,**d** in deaerated protic solvents.

To avoid inaccurate results, stability of the radicals upon standing in deaerated methanol and ethanol was studied. Thus, comparison of the initial absorption spectra and those repeated after 14 days of storage of the radicals **57c** and **57d** in protic solvents (*e.g.* methanol, ethanol) at 5°C is demonstrated in *Figure 2.12*. Although partial decomposition of the radicals was observed, as witnessed from the slight decrease of the radical signals

intensity in the UV-Vis absorption envelopes, stability of the molecules **57c** and **57d** in methanol was assumed appropriate. The radical signal decay in ethanol was stronger (*Fig. 2.12*), and this media was used only for qualitative studies (*Fig. 2.16*), while all the quantitative characteristics were recorded employing methanol.

Typical requirements for a new analytical system include high speed, simplicity and sensitivity of the method. The versatility of the technique can compliment itself. However, the pyrene derivatives are known to form excimers in concentrated solutions, due to the self-assembling of the polyaromatic hydrocarbon moieties.[56] This phenomena influences the emission spectra, leading to signals broadening and changes in the fluorescence intensities. Therefore, to study the probes detection limit and to confirm that pyrene-based radicals **57c,d** presented in solution in a non-aggregated state, experiments were done varying concentration of the radicals C_A ~2.5×10^{-4} M, C_B ~2.5×10^{-5} M, C_C ~2.5×10^{-6} M, while keeping the concentration of the reactants constant C_{Cys} ~5×10^{-4} M, C_{TFA} ~1.8×10^{-5} M; C_{vitC} ~5×10^{-4} M. Importantly, stock solutions of cysteine and ascorbate were prepared shortly before use, and were purged with argon immediately after solvent addition due to the sensitivity of the antioxidant agents. Afterwards, the solutions were mixed with freshly made nitroxide solution in methanol. In general, reaction of a nitroxide with an antioxidant reagent is shown to be fast (with a rate constant k in the range ~48 - 2×10^{-2} $M^{-1}s^{-1}$).[52,57] Therefore, after 15 min of incubation of the combined solutions, absorption and emission spectra were recorded.

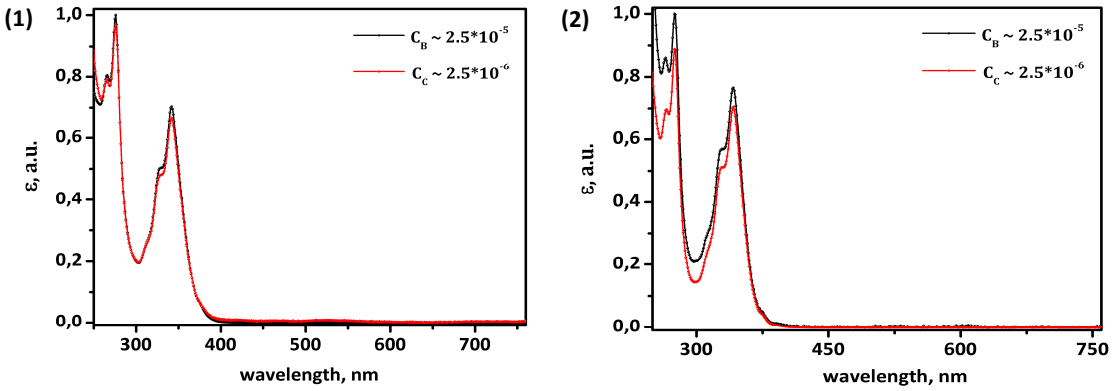

Figure 2.13. Comparison of the absorption spectra of the radicals (1) **57c**, (2) **57d** after 15 minutes of exposure to cysteine

The absorption spectra obtained for the series of experiments involving nitroxide radicals **57c** and **57d** are similar. As an example UV-Vis envelopes of the probes **57c,d**

after addition of cysteine are presented in *Figure 2.13*. No significant altering of the absorbance envelopes upon dilution of the radical solutions was registered. These experiments clearly showed, that the derivatives **57c**,**d** presented in solutions in unaggregated state.

To examine, whether (and how) the concentration of the radicals solutions could affect the sensing properties of the probes, PL measurements with various concentration of the nitroxides **57c**,**d** (2.5×10^{-4} M, 2.5×10^{-5} M, 2.5×10^{-6} M) were carried out. Qualitatively similar changes in the fluorescence spectra upon reaction with additives for all the samples were observed. As an illustration of such transformations, the emission spectra of the nitronyl **57c** and imino **57d** radicals with two concentrations (2.5×10^{-5} M, 2.5×10^{-6} M) are compared in *Figures 2.14* and *2.15*, respectively.

Here, the radicals **57c** and **57d** exhibited an emission band centered at ~450 nm. For the radical **57d** fluorescence of the highest intensity was registered for the most concentrated samples. Upon dilution of the nitroxide **57d** solutions the intensity tended to decrease linearly. Conversely, the derivative **57c** featured nearly constant PL intensity independently of the concentration used (~2-3 a.u.). This phenomenon was attributed to a more efficient self-quenching within the nitronyl nitroxide hybrid molecule **57c**, than in the corresponding imino analogue **57d**.

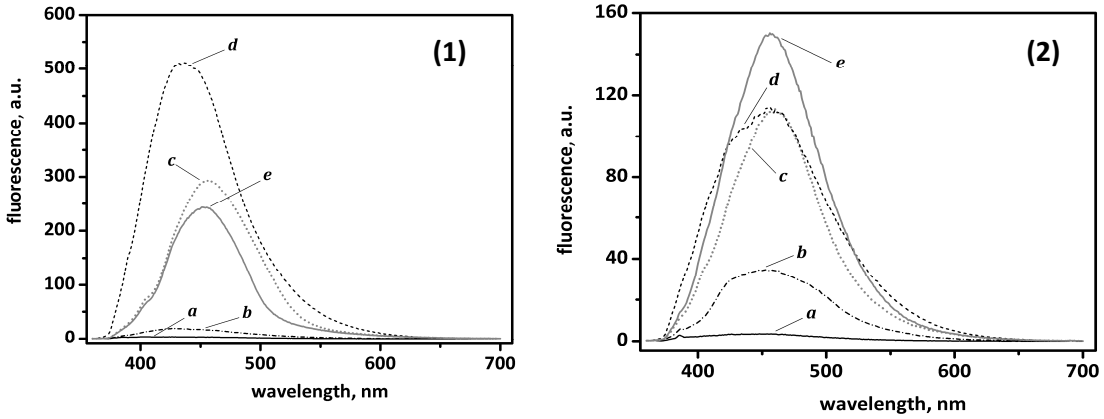

Figure 2.14. Fluorescence spectra of the nitronyl nitroxide **57c** in MeOH with the concentration (1) (2.5×10^{-5} M), (2) (2.5×10^{-6} M) and an excitation wavelength of 346 nm under different conditions: (*a*) pure solution of the radical; (*b*) after reaction with CF_3COOH (1.8×10^{-5} M); (*c*) after reaction with cysteine (5×10^{-4} M); (*d*) after reaction with ascorbic acid (5×10^{-4} M); (*e*) after sequential reactions with cysteine (5×10^{-4} M) and CF_3COOH (1.8×10^{-5}M).

Upon addition of an antioxidant (*i.e.* ascorbate or cysteine) to the radical solution, one-electron reduction effectively terminated the self-quenching within the probe, and, therefore, restored the fluorescence of the pyrene unit (the mechanism of the fluorescence quenching in fluorophore-nitroxide compounds is discussed in *Subchapter 2.5.4*). Here, for the nitronyl derivative **57c** samples with different concentration ascorbate demonstrated slightly higher scavenging activity than cysteine, while for the imino nitroxide **57d** at concentrations ≤ 2.5×10^{-5} M the reversed scenario was observed. Interestingly, that upon further dilution of the radical **57d** solutions (2.5×10^{-6} M) emission intensities of the samples treated with ascorbate and cysteine nearly matched each other (*Fig. 2.15 (2)*).

Nitroxides are often utilized as pH probes.[58] Moreover, acids reduce the electron donating ability of the imidazole moiety, and, therefore, suppress the quenching process.[58d] In this regard the behavior of the radical systems **57c** and **57d** after reaction with trifluoroacetic acid was studied. The release of the fluorescence was not that significant, as in the previous experiments involving reducing agents. However, the enhancement of the emission intensity was clearly observed (*Fig. 2.14, 2.15*).

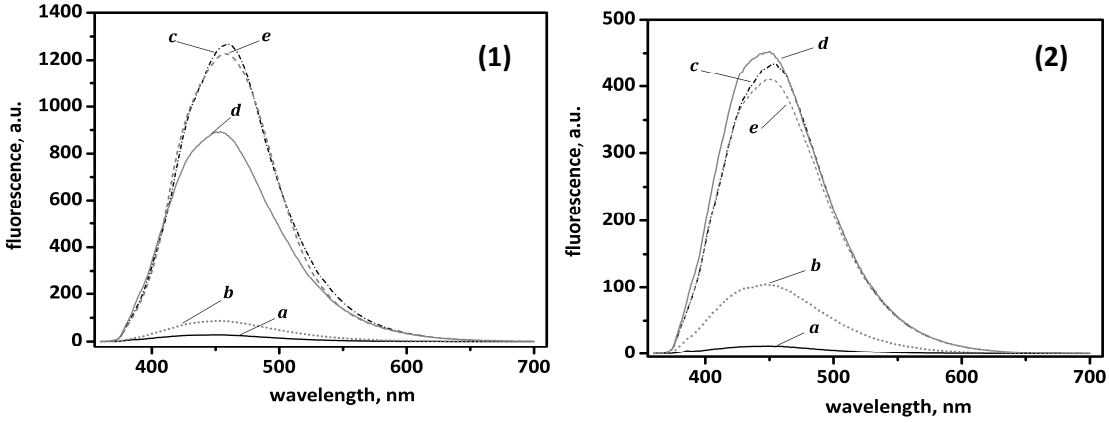

Figure 2.15. Fluorescence spectra of the imino nitroxide **57d** in MeOH with the concentration (1) (2.5×10^{-5} M), (2) (2.5×10^{-6} M) and an excitation wavelength of 346 nm under different conditions: (*a*) pure solution of the radical; (*b*) after reaction with CF_3COOH (1.8×10^{-5} M); (*c*) after reaction with cysteine (5×10^{-4} M); (*d*) after reaction with ascorbic acid (5×10^{-4} M); (*e*) after sequential reactions with cysteine (5×10^{-4} M) and CF_3COOH (1.8×10^{-5}M).

Recently it was reported in the literature,[8] that the sequential reactions of a fluorophore-nitroxide molecule with a scavenging agent (cysteine) and acid (TFA) induce significant PL enhancement of the probe. Therefore, series of experiments involving

nitroxides **57c** and **57d** were performed. Notably, the described method worked more efficient for the radicals at micromolar concentrations (*Fig. 2.14 (2), 2.15 (2)*). For the samples at higher concentrations (2.5×10^{-4} M, 2.5×10^{-5} M) the changes in the emission spectra, which appeared due to the simultaneous treatment of the probes with cysteine and trifluoroacetic acid, were in general less pronounced and comparable with the ones caused by net cysteine (*Fig. 2.14 (1), 2.15 (1)*).

To give more precise characterization of the radical systems **57c** and **57d**, the relative quantum yields (QY) of fluorescence with respect to 9,10-diphenylanthracene (6.8×10^{-6} M) in cyclohexane[59a,b] and anthracene (1.7×10^{-5} M) in ethanol[59c,d] were calculated, taking into account the refractive indexes of the solvents and using the equation (*12*):

$$\Phi_F = \Phi_{FR} \frac{n^2}{n_R^2} \frac{\int_0^\infty I_F(\lambda_E,\lambda_F)d\lambda F}{\int_0^\infty I_{FR}(\lambda_{ER},\lambda_F)d\lambda F} \frac{1-10^{-A_R(\lambda_{ER})}}{1-10^{-A(\lambda_E)}} \frac{I_0(\lambda_{ER})}{I_0(\lambda_E)} \qquad (\textbf{12})$$

where I_F, I_{FR} are corrected fluorescence spectra of sample and reference; n, n_R are the refractive indeces of the solvents; λ_E, λ_{ER} excitation wavelengths; $I_0(\lambda_E)$, $I_0(\lambda_{ER})$ excitation intensities at λ_E, λ_{ER}. The subscript Φ_{FR} refers to standard: Φ_{FR} is 0.90 for 9,10-diphenylanthracene, and is 0.27 for anthracene. For all spectra, appropriate instrument corrections were performed.

In general, imino nitroxide **57d** demonstrated a better response upon reaction with a chemical agent relative to the corresponding nitronyl radical **57c**. For instance, the quantum yield of **57d** after treatment with ascorbic acid reached 0.84, while the corresponding value obtained for compound **57c** was nearly two times lower (*Table 2.3*). From the other hand, the imino radical **57d** itself exhibited 2.6 times higher quantum yield (0.026) than the derivative **57c**. This confirms our assumption, that the imino nitroxide is a weaker quencher of the fluorescence. For an accurate comparison of the sensing properties the magnitude of the fluorescence enhancement relative to the parent radical species **57c** or **57d** was studied (Φ/Φ_o). The nitronyl nitroxide **57c** was found to be more sensitive towards reaction with analytes, with an exception in the case of treatment with trifluoroacetic acid. The later feature could be easily explained, since protonation affects foremost the imidazolidine ring, but not the radical function, as confirmed by UV-

Vis and EPR spectroscopy (see *Subchapter 2.5.4*). Consequently, the reaction of the samples with TFA led to 9-fold and 12-fold increase of the fluorescence intensity for nitronyl **57c** and imino **57d** derivatives, respectively (see *Table 2.3*).

Table 2.3. Quantum yields after reaction of **57c**, **57d** and **80c** with chemical reagents (according to anthracene and diphenylanthracene references).

	$QY^{[a]}$	$QY^{[b]}$	$\Phi/\Phi_o{}^{[c]}$
57c	0.01	0.01	1
ascorbic acid	0.46	0.42	46
Cys	0.51	0.44	**51**
CF_3COOH	0.09	0.08	9
Cys + CF_3COOH	0.32	0.27	32
57d	0.03	0.02	1
ascorbic acid	0.84	0.80	**28**
Cys	0.80	0.77	26
CF_3COOH	0.37	0.36	12
Cys + CF_3COOH	0.70	0.67	23
80c	0.01	0.01	1
ascorbic acid	0.05	0.06	5
Cys	0.20	0.23	20
CF_3COOH	0.01	0.01	1
Cys + CF_3COOH	0.27	0.30	27

[a] Quantum yields with respect to 9,10-diphenylanthracene;
[b] Quantum yields with respect to anthracene;
[c] Fluorescence enhancement calculated relative to the $QY_i{}^{[a]}$.

Sensing behaviour of the pyrene-pyrazole nitroxides **57c**, **57d** and pyrene nitronyl radical **80c** was compared (the evolution of the fluorescence spectra of compound **80c** upon reaction with chemical agents is shown in *Figure A1*, *Appendix*). The initial fluorescence in the probe **80c** was efficiently quenched (*Table 2.3*). However, the consequent changes in the quantitative parameters (QY and Φ/Φ_o values) caused by the treatment of the samples with the chemical agents were much less pronounced. Thus, upon sequential reaction of the radical **80c** with cysteine and TFA the relative quantum yield raised only till 0.27.

According to the literature,[58d] the probe's fluorescence response depends sometimes on the solvent media. To examine this possibility, some experiments in ethanol were carried out. Generally, the systems demonstrated analogous response to the analytes, as shown in *Figure 2.16*. Notable, when comparing the data obtained for the probes **57c**,**d** with similar concentrations (i.e. ~10^{-5} M) in different alcohols, the imino radical **57d** showed a better response towards cysteine/trifluoroacetic acid couple than to

ascorbic acid in both cases (*Fig. 2.14 (1), 2.15 (1), 2.16*). The nitronyl derivative **57c** dissolved in ethanol was likewise more sensitive to cysteine, whereas for the solutions of **57c** in methanol a higher response towards ascorbic acid was registered.

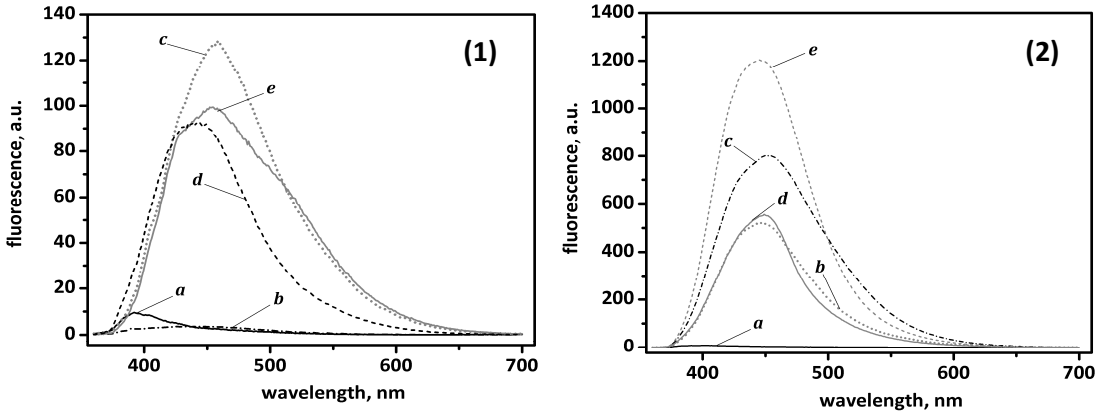

Figure 2.16. Fluorescence spectra of the probes (1) **57c**, (2) **57d** in EtOH with an excitation wavelength of 346 nm under different conditions: (*a*) pure solution of a radical (1.5×10^{-5} M); (*b*) after reaction with CF_3COOH (1.8×10^{-5} M); (*c*) after reaction with cysteine (5×10^{-4} M); (*d*) after reaction with ascorbic acid (5×10^{-4} M); (*e*) after sequential reactions with cysteine (5×10^{-4} M) and CF_3COOH (1.8×10^{-5}M).

Efforts to find a more cell-friendly solvent revealed that the probes were not soluble in water or water-containing media (such as phosphate buffer). Some trials with phosphate buffer/DMSO mixtures were done. Here, after addition of the buffer solution containing a reagent to DMSO solution of the radical, highly viscous suspension was formed, consequently, the measurements became unreliable and irreproducible. Therefore, pure DMSO as an alternative media with minimal citotoxicity was tested.

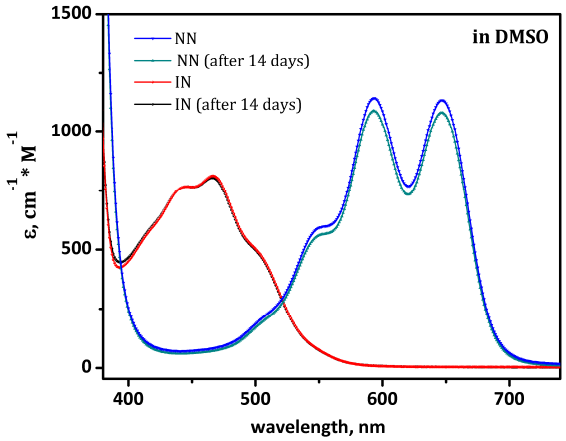

Figure 2.17. Stability of the probes **57c**,**d** in DMSO.

It was found, that upon standing in DMSO partial decomposition of compounds **57c**,**d** occurred, as witnessed from the decrease of the radical signal intensities in the absorption envelopes (*Fig. 2.17*). Nevertheless, some trials in freshly prepared deaerated DMSO/water solutions were performed.

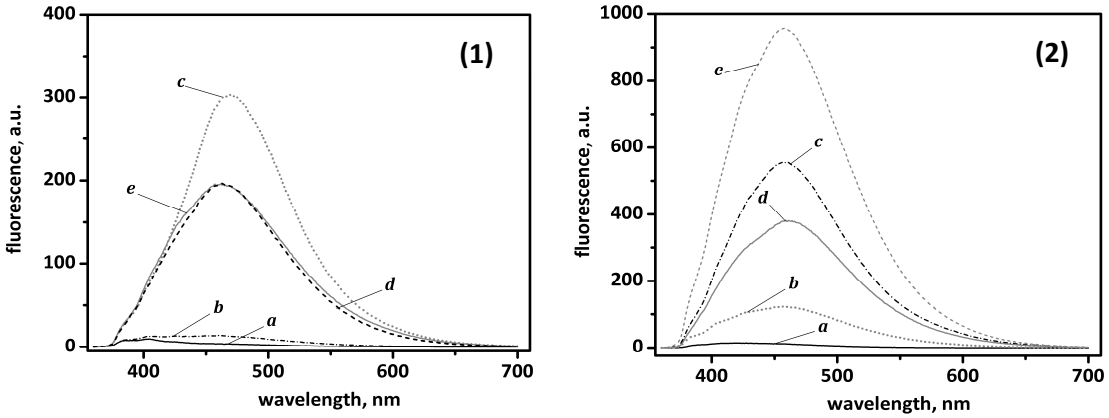

Figure 2.18. Fluorescence spectra of the probes (1) **57c**, (2) **57d** in DMSO with an excitation wavelength of 346 nm under different conditions: (*a*) pure solution of a radical (6×10^{-5} M); (*b*) after reaction with CF_3COOH (1.8×10^{-5} M); (*c*) after reaction with cysteine (5×10^{-4} M); (*d*) after reaction with ascorbic acid (5×10^{-4} M); (*e*) after sequential reactions with cysteine (5×10^{-4} M) and CF_3COOH (1.8×10^{-5}M).

Qualitatively, both probes **57c**,**d** featured a similar behaviour upon treatment with reagents as was witnessed earlier for the series of experiments in ethanol (*Fig. 2.18*). Thus, imino radical **57d** featured higher fluorescence than the derivative **57c**. In the presence of acid self-quenching within the molecules was reduced, leading to enhanced fluorescence of the samples treated with TFA. As can be clearly seen from *Figure 2.18 (1)* reaction of the nitronyl compound **57c** with cysteine resulted in a burst increase of in the fluorescence, whereas the employment of ascorbate or cysteine/TFA mixture led to a significantly smaller rise of the intensity. In case of the imino radical **57d** treatment of the samples with antioxidant agents (ascorbate, cysteine) led to a considerable increase in the fluorescence. However, the most intense fluorescence enhancement was observed upon simultaneous reaction of the probe **57d** solutions with cysteine/TFA pair.

In summary, the behaviour of the nitroxides **57c**,**d** in different solvents, at different concentrations and conditions was studied. It was found, that in the nitronyl radical **57c** the fluorescence self-quenching is stronger than in the imino derivative **57d**. The pyrene-pyrazole nitroxides **57c** and **57d** were found to be sensitive to acids. Thus, change of pH resulted in the fluorescence enhancement. Moreover, it was shown, that

the fluorescence quantum yield could be substantially increased by reactions of the probes with antioxidants (*Table 2.3*), *i.e.* reactions that lead to the loss of paramagnetism in the fluorophore-nitroxide compounds (see for more details *Subchapter 2.5.4*). Finally, the behaviour of the pyrene **80c** and pyrene-pyrazole **57c** nitronyl nitroxides upon treatment with various analytes was compared. Although initially in both radicals **57c**, **80c** the fluorescence was efficiently quenched, the release of the fluorescence in the second case was much weaker (*Table 2.3*). This demonstrates the feasibility of our strategy towards engineering of the radical systems with the desirable sensing properties, based on the absorption properties of compounds.

2.5.3. AFM studies, photophysical and sensing properties of the pyrene-based nitroxide radicals in film

Published studies concerning fluorophore-nitroxide compounds are usually limited to the solution phase.[5,8,47,52] It should be also mentioned that the effect of different solvents on the fluorescence of **57c**,**d** described in the previous section was examined considering their low water solubility. Thus, it appeared to be appealing to examine the applicability of the pyrene-pyrazole nitroxides (**57c** and **57d**) films for sensing in aqueous solutions.

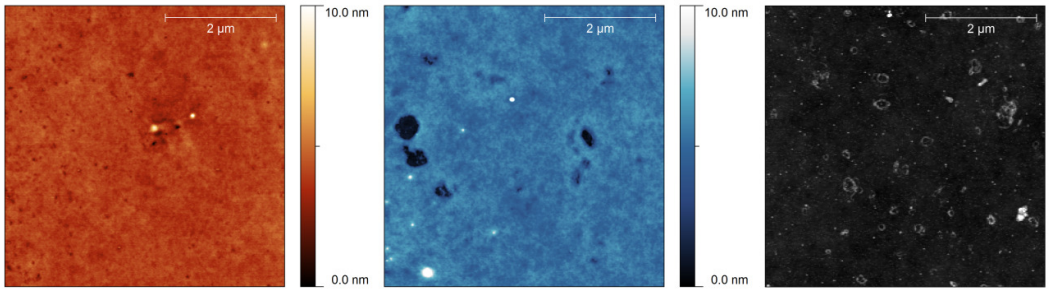

Figure 2.19. From left – **57d**, **57c**, glass substrate. AFM height images of 5µm×5µm of spin coated layers of materials and reference glass substrate. The roughness of surface for **57d** and **57c** is 0.27nm and 0.41nm (Ra) respectively.

The AFM height images[**] are presented in false colors gradients (orange, blue, grey) to demonstrate the properties of investigated material (**57d**, **57c** and uncoated glass slide, respectively). The prepared layers were of good quality, the roughness values are presented next to each figure according to the area that those values refer to. The

** AFM measurements were performed by PhD Marcin Makowski at MPI-P (Mainz).

roughness was calculated for the whole area with an exception of areas with height peaks that were clearly connected with impurities on the glass surface.

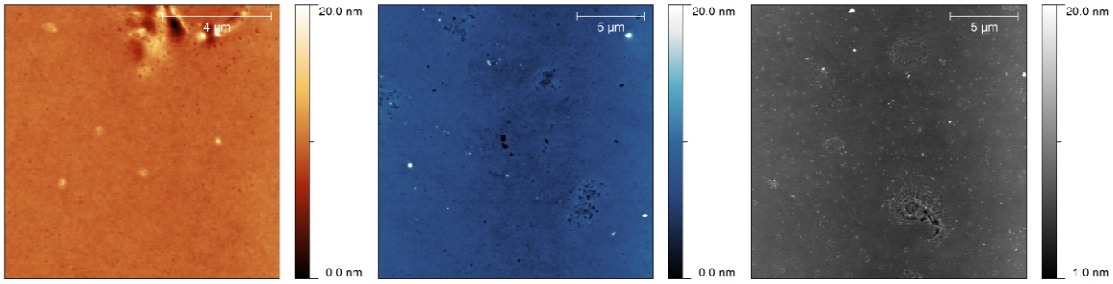

Figure 2.20. From left – **57d**, **57c**, glass substrate. AFM height images of 20µm×20µm of spin coated layers of materials and reference glass substrate. The roughness of surface for **57d** and **57c** is 0.27nm and 0.41nm (Ra) respectively.

The solid-state absorption spectra of the spin-coated films of the radicals **57c**,**d** demonstrated in *Figure 2.21 (1), (2)* exhibited nearly identical features as the spectra recorded from the toluene solutions (see *Fig. 2.11*), which implied the presence of weak *inter*molecular interaction. Thus, the n-π^* transitions of the aminoxyl oxide moieties appeared at 648 nm for nitronyl and at 470 nm for imino nitroxide radicals, but the emission intensity from the thin film was enhanced. The high energy peaks in the solid-state, on the contrary, were less pronounced (*Fig. 2.21 (1), (2)*).

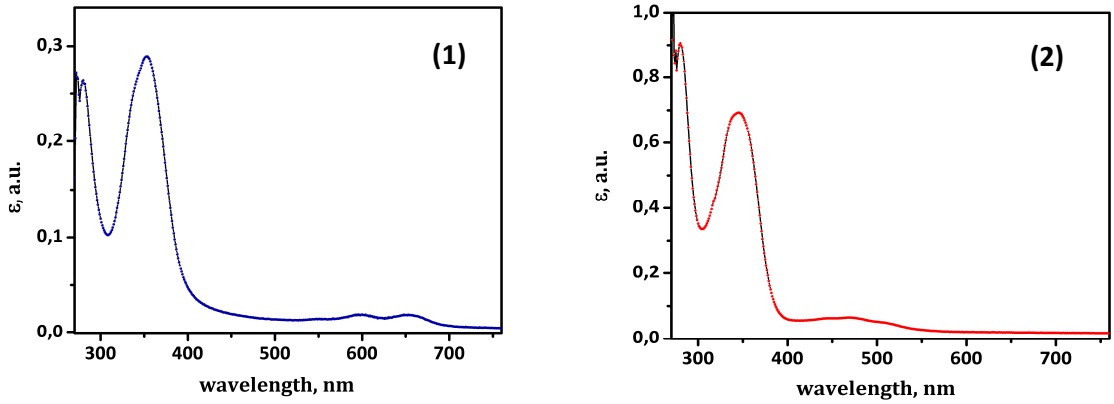

Figure 2.21. UV-Vis spectra of (1) nitronyl **57c** and (2) imino **57d** radicals recorded in films.

The thin films were treated with ascorbate (C ~6.5×10^{-3} M) and TFA (C ~8.2×10^{-3} M) water solutions during 40 min. After that the films were washed with water, dried with compressed air and the fluorescence spectra were recorded. The experiment was repeated to evaluate the approximate time interval required for the reaction between a reagent and the film surface to occur.

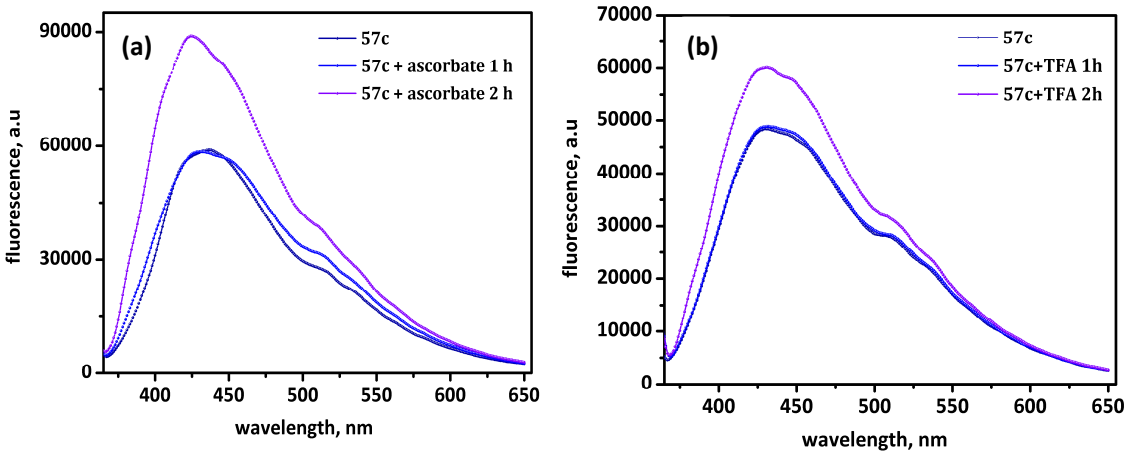

Figure 2.22. Fluorescence spectra of the nitronyl nitroxide **57c** before and after treatment of the films with (a) ascorbate and (b) TFA.

In parallel experiments stability of the films in water was examined. Thus, the films were placed in a water chamber and stored at room temperature for 2 h. Afterwards, the emission spectra were recorded (*Fig. A2*, *Appendix*). Alterations of the emission envelopes (such as enhancement of the fluorescence intensity, shifts of the signals, etc.) were not registered. Therefore, the observed spectral changes of the films treated with additives were attributed to the reaction of the analytes with nitroxide radicals **57c**,**d** on the film surface.

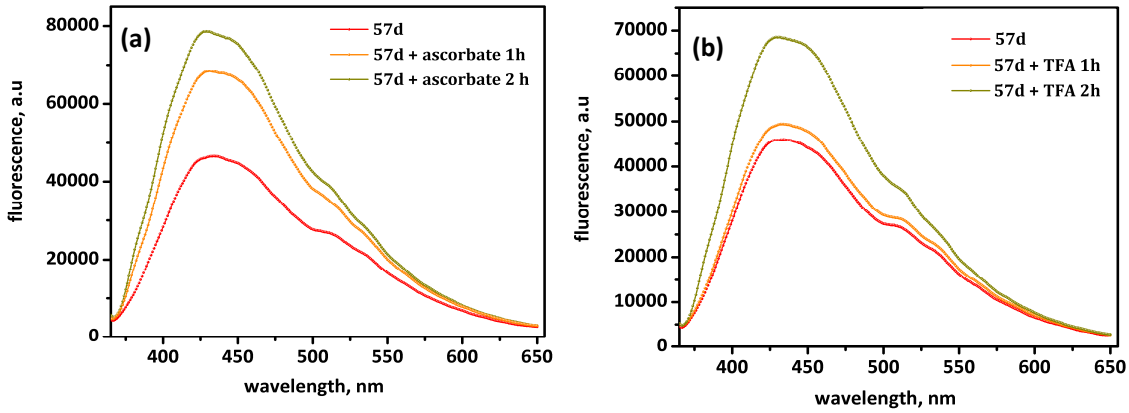

Figure 2.23. Fluorescence spectra of the imino nitroxide **57d** before and after treatment of the films with (a) ascorbate and (b) TFA.

Here, a qualitatively similar phenomenon of the fluorescence increase was observed as shown in *Figures 2.22*, *2.23*. Addition of a reducing agent (ascorbate) led to more pronounced changes for the radicals (*Fig. 2.22 (1)*, *2.23 (1)*). However, for the imino derivative **57d** significant increase in the emission intensity was registered already after 1

h of exposure to ascorbate aqueous solution, while in the case of the nitronyl nitroxide **57c** extension of the reaction time was required. In general, reaction of the spin-coated nitroxides with water solutions of the chemical reagents was shown to be much slower. Nevertheless, the ability to detect antioxidants (ascorbate) or acids (TFA) employing the pyrene-pyrazole nitroxides **57c**,**d** films in aqueous media was demonstrated.

2.5.4. The mechanism of the fluorescence quenching in fluorophore-nitroxide compounds

The quenching mechanism in fluorophore-nitroxide molecules originates from changes in the spin multiplicity of their electronic states. For example, the singlet ground (S_o) state and the lowest excited singlet (S_1) state of the fluorophore become the doublet (D_o and D_n, respectively) states, because of the unpaired electron spin of the doublet nitroxide radical.[60] On the other hand, the lowest excited doublet (D_1) and quartet (QA_1) states are generated by an interaction between the nitroxide and the triplet (T_1) of the fluorophore. Thus, the spin-forbidden transitions of the fluorophore, i.e. $S_1 \rightarrow T_1$ and $T_1 \rightarrow S_o$, partially change into the $D_n \rightarrow D_1$ and $D_1 \rightarrow D_o$ transitions, respectively. As these doublet states (D_n, D_1 and D_o) have the same spin multiplicity, the lifetimes of the excited state were believed to be very short as comparable to those of the $S_1 \rightarrow S_o$ transition.[61] Therefore, the mechanism of triplet quenching is interpreted by triplet-doublet energy transfer and enhanced intersystem crossing.[62,63]

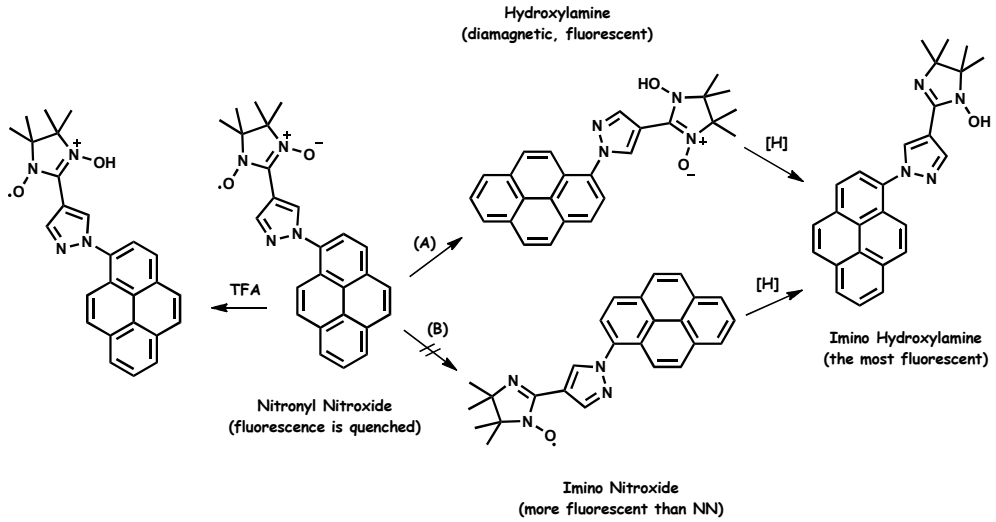

Scheme 2.11. Proposed mechanism of the reaction **57c** with chemical reagents.[64]

Reaction between the probe **57c** and reactive species can occur via two alternative mechanisms, i.e., *oxidation* (*A*) and *reduction* (*B*). Upon addition of a reducing agent (such as cysteine) nitronyl nitroxides are effectively reduced to hydroxylamine derivatives.[64] Therefore, we concluded that the reaction follows the reduction mechanism. The alternative mechanism of reduction to an imino-form can be excluded in our system either, since no EPR signal corresponding to the imino radical has been detected.[††]

Deep-blue solution of nitronyl nitroxide radical **57c** became colorless almost immediately after addition of cysteine, but the sample maintained the color when trifluoroacetic acid was used (even in 10^3 times larger excess). Analogous behavior was observed for the imino nitroxide **57d**, implying that upon reaction with an acid the radical function of the probe remained untapped. To confirm that suggestion, and to collect more information about the process, EPR and UV-Vis spectra of the probes **57c**,**d** after treatment with chemical agents were recorded.

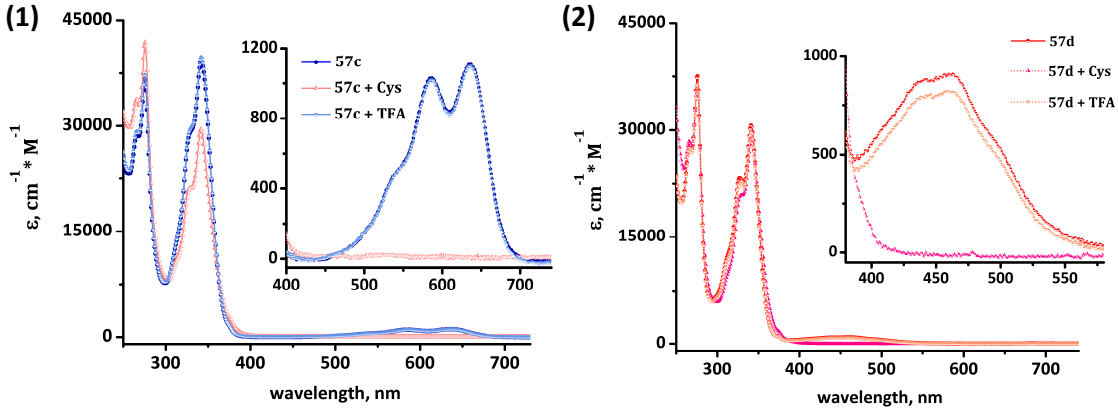

Figure 2.24. UV-Vis spectra of the radical after reaction with TFA (1) **57c** and (2) **57d**, respectively.

As could be clearly seen from the comparison of the UV-Vis envelopes of the radicals **57c** and **57d** before and after treatment with cysteine or TFA, addition of the acid had no sufficient effect on the absorption spectra (*Figure 2.24 (1), (2)*), while addition of the reductant (cysteine) led to the elimination of the characteristic signal of the aminoxyl moiety.[††] These observations supported by the analysis of EPR spectra led us to a conclusion that the reaction of a probe with an acid resulted into protonation of the imidazoline moiety (*Scheme 2.11*).

[††] Complementary to the UV-Vis envelopes, EPR spectra of the samples treated with acid contained characteristic for the nitroxide radicals signals, whereas the samples treated with cysteine remained EPR silence.

2.6. Synthesis of the anthracene-based nitroxide radicals

In order to study in more details the correlation between the sensitivity of a probe and the structure of a spacer attached to the fluorophore, 8 new targets shown in *Figure 2.25* were designed. The choice of anthracene as a fluorophore was dictated by the readily synthetic tunability, which granted the opportunity to modify the core according to our aims. Thus, an additional phenyl ring was introduced into the π-system, giving rise to the radicals **59c**,**d**. To exclude the torsion within the molecule, and to study the influence of the bridge extension, acetylene fragment was used in the monoradicals **60c**,**d**.

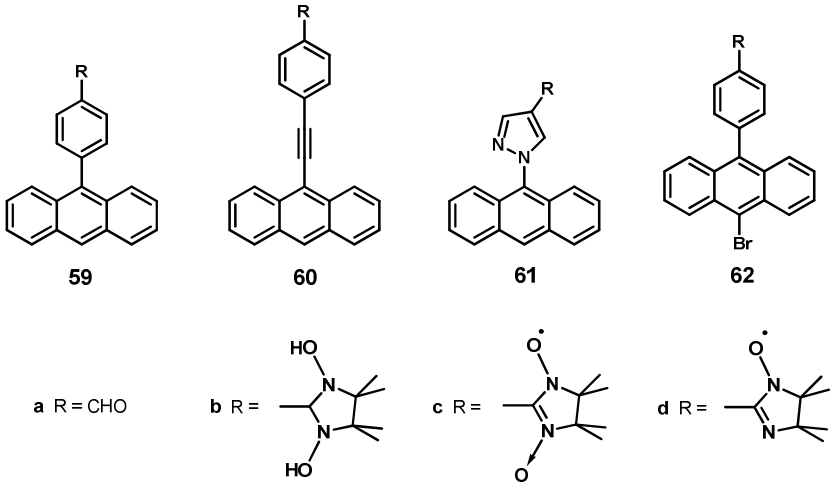

Figure 2.25. Anthrecene-based models.

As was demonstrated before, the attachment of the pyrazole to a fluorophore unit improved the efficiency of the pyrene probe **57c** greatly. To compare the influence of the pyrazole spacer with the other bridging units on the sensing properties, the radicals **61c**,**d** were engineered. To examine the influence of the acceptor substitution in the fluorophore core on the photophysical properties of the molecule, radicals **62c**,**d** were synthesized. Another consideration in their design was the potential ability to modify the framework by attachment to other molecules via organometallic coupling reactions.

The precursors to the target compounds, comprising anthracene nitroxide radicals, could be routinely prepared as illustrated in *Scheme 2.12*. The synthesis was based on functionalization of 9-bromoanthracene **81** at the most reactive sites (i.e. *9* and *10*). Suzuki coupling of 4-formylphenylboronic acid and derivative **81** provided after

purification on a chromatographic column 9-(4-formylphenyl)anthracene **59a** in 82% yield.[65] Attachment of 4-ethynylbenzaldehyde to 9-bromoanthracene **81** under microwave-assisted Sonogashira-Hagihara Pd(0)-catalyzed cross-coupling reaction afforded carbaldehyde **60a** in 32% yield. For the synthesis of the derivative **82** the same methodology as previously described for the pyrazole-pyrene **72** was employed. Thus, copper-catalyzed condensation provided compound **82** in high yield (83%), which was further involved into Vilsmeier–Haack reaction. Under strictly anhydrous conditions $POCl_3$ was added cautiously dropwise to dry DMF in a sealed flask at 5°C (ice bath). After 20 minutes of vigorous stirring at this temperature, the ice bath was removed. Pyrazole-anthracene **82** in dry DMF was than added to a clear solution of Vilsmayer-reagent, the flask was moved to an oil bath and heated up to 110°C for 18 h. After typical work-up carbaldehyde **61a** was obtained in 29% yield. Finally, selective bromination of the compound **59a** in *10* position with *N*-bromosuccinimide (NBS) in dry DMF gave 9-(4-formylphenyl)-10-bromoanthracene **62** in fairly high, almost quantitative yield (92%).

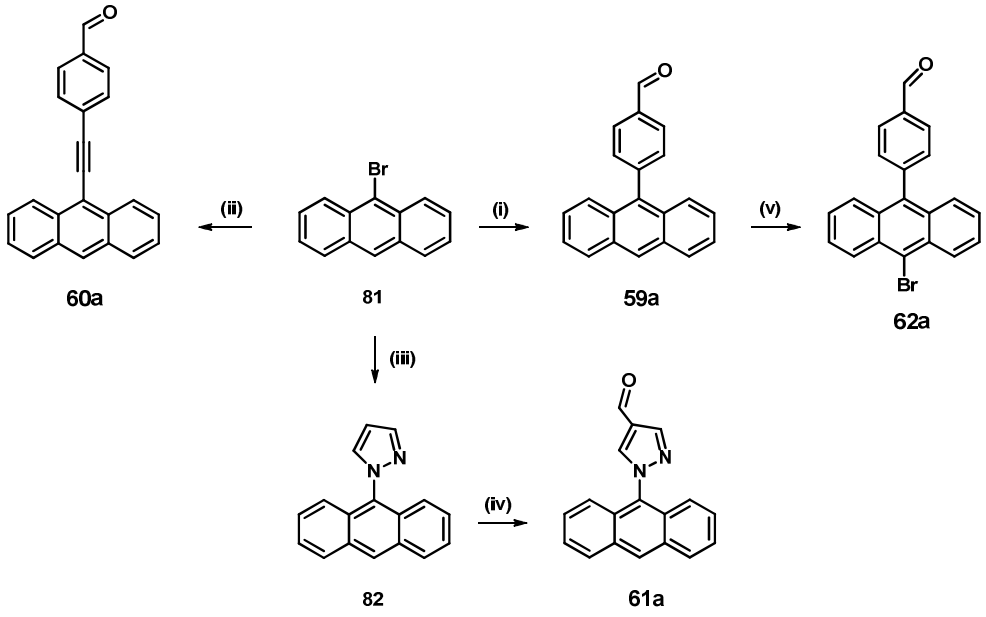

Scheme 2.12. Synthesis of the anthracene carbaldehydes **59-62a**. Key: (i) 4-formylboronic acid (1.3 eq.), $Pd(PPh_3)_4$ (3 mol%), K_2CO_3 (4 eq.), benzene/EtOH/H_2O (6:1:2); (ii) 4-ethynylbenzaldehyde (0.95 eq.), $Pd(PPh_3)_4$ (10 mol%), CuI (6 mol%), NEt_3/THF (1:2), 60°C, MW, 4h; (iii) pyrazole (1.5 eq.), Cs_2CO_3 (2 eq.), CuI (0.2 eq.), DMF, argon, 120°C,48h; (iv) DMF, $POCl_3$, 110°C, 20h; (v) NBS (1 eq.), DMF, rt, 18h.

Condensation between BHA and carbaldehyde **59a** was realized in deaerated toluene under argon at 110°C. The heating in 20 hours afforded the radical precursor – 9-

[4-(1,3-dihydroxy-4,4,-5,5-tetramethylimidazolidin-2-yl)phenyl]anthracene **59b** in quantitative yield. As for the other imidazolidine derivatives **60-62b**, reaction at room temperature in absolute methanol/toluene (1:1) mixture was preferred, while heating of the aldehydes **60**-**61a** in toluene caused partial decomposition of the products and significantly decreased the yields. Varying the oxidation conditions nitronyl **59-62c** and imino nitroxide radicals **59-62d** were obtained. Hence, oxidation of imidazolidine **59b** with sodium periodate in a two phase system (CH_2Cl_2/H_2O) gave after purification on a chromatographic column nitronyl nitroxide radical **59c** in 50% yield. For the preparation of **60-62c** excess of MnO_2 in methanol was employed. Oxidation of the precursors **59-62b** in CH_3NO_2 with excess of MnO_2 afforded the imino nitroxide radicals **59-62d** in 32-53% yield. A summary of the synthetic procedure is represented in *Scheme 2.13* on example of 9-(4-formylphenyl)-anthracene **59a** and 9-(4-formylphenyl)-10-bromoanthracene **62a** carbaldehydes.

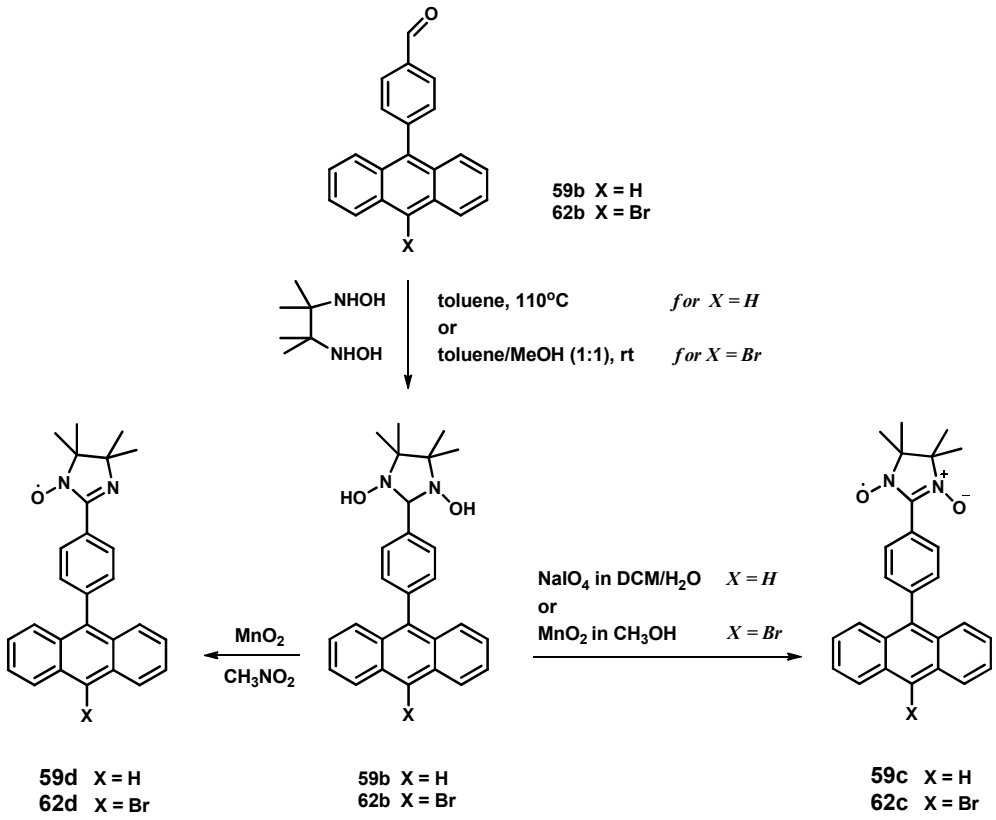

Scheme 2.13. Condensation of the aldehydes **59a**, **62a** with BHA followed by the oxidation of the imidazolidines **59b**, **62b** into nitronyl **59c**, **62c** and imino nitroxide radicals **59d**, **62d**.

2.7. Crystal structure analysis of the anthracene-based nitroxide radicals

The crystallization of the radicals was realized by diffusion of dichloromethane-hexane mixtures (1:3). Single crystals of nitronyl **59c**, **60c**, **62c** and imino **59d**, **62d** radicals were analyzed by X-ray diffraction and their ORTEP drawing are given in *Figures 2.26-2.30*. Pertinent crystallographic parameters and refinement data are listed in *Table 2.4*.

(a)

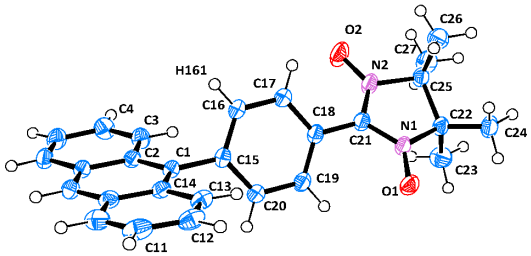

(b)

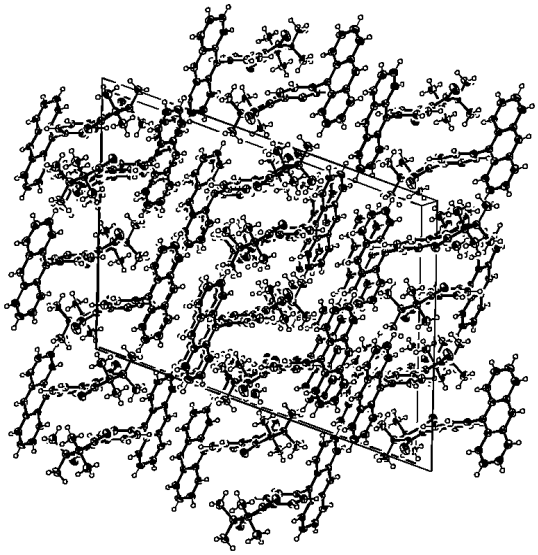

Figure 2.26. X-ray structure of **59c** with ORTEP drawn at the 50% of the probability level: (a) molecule (○ nitrogen, ● oxygen, ○ carbon); (b) crystal packing.

Single crystal X-ray diffraction study confirmed the molecular structure of the phenyl-anthracene nitronyl nitroxide **59c** (*Figure 2.26 (a)*). This compound belongs to the monoclinic class with $C2_1/c$ space group (*Table 2.4*). The molecule adopts propeller-shape conformation with torsion angles C(2)-C(1)-C(15)-C(16) 69.5° and C(14)-C(1)-C(15)-C(20) 73.3° between the mean plane of the anthracene and the aromatic ring, while the torsion between the radical fragment and the phenyl plane is about 33° (*Figure 2.26 (a)*).

Table 2.4. Crystallographic parameters of the nitronyl **59c**, **60c**, **62c** and imino **59d**, **62d** nitroxides.

	59c	**60c**	**62c**	**59d**	**62d**
Formula	$C_{27}H_{25}N_2O_2$	$C_{29}H_{25}N_2O_2$	$C_{27}H_{24}BrN_2O_2$	$C_{27}H_{25}N_2O$	$C_{27}H_{24}BrN_2O$
M	409.5	433.5	488	393.5	472
crystal system	monoclinic	monoclinic	monoclinic	orthorhombic	monoclinic
space group	$C2_1/c$	$C2_1/a$	$C2_1/c$	$Ccc2$	$C2_1/c$
$\boldsymbol{a}$, Å	26.3034(9)	9.8549(2)	26.5067(6)	19.0156(3)	25.9514(9)
$\boldsymbol{b}$, Å	8.7067(6)	28.6671(6)	8.7658(1)	25.2469(5)	8.7969(4)
$\boldsymbol{c}$, Å	19.8345(9)	16.1168(4)	19.6813(5)	8.9297(2)	19.8316(8)
$\boldsymbol{\beta}$, deg	108.644(4)	101.4712(12)	106.0276(10)	90	104.740(3)
$\boldsymbol{V}$, A^3	4304.0(4)	4462.23(17)	4395.24	4287.01(14)	4378.4(3)
$\boldsymbol{Z}$	8	8	8	8	8
$\boldsymbol{R_{factor}}(\%)$	5.1	4.56	3.59	3.68	3.67
$\boldsymbol{D_c}$, $g \times cm^{-3}$	1.264	1.291	1.476	1.219	1.433
$\boldsymbol{N_{ref}}$	5974	12324	6083	3338	5941
$\boldsymbol{N_{par}}$	280	595	289	271	280
S	1.092	1.103	1.083	1.007	1.171

The crystallographic data were collected on Nonius Kappa CCD (Mo kα, μ = 0.71073 Å) diffractometer equipped with a graphite monochromator.

The bond distances of the NO groups in the molecule **59c** are equivalent: N(1)-O(1) 1.280, N(2)-O(2) 1.284 Å. Interestingly, that O atom of the nitronyl moiety forms both ladder-like short contacts with another molecule in the same plane (O1···H161' 2.64 Å), and hydrogen bonds in a head-to-head fashion with the third nearly orthogonal molecule of the radical (O1···H243' 2.64 Å). The molecules are also related by the set of short intermolecular contacts (hydrogen bonds and π-π stacking) between the neighboring anthracene fragments: H41···H121' 2.38, C4···H121' 2.85, C13···H241' 2.85 Å, C11···C12' 3.4 Å.

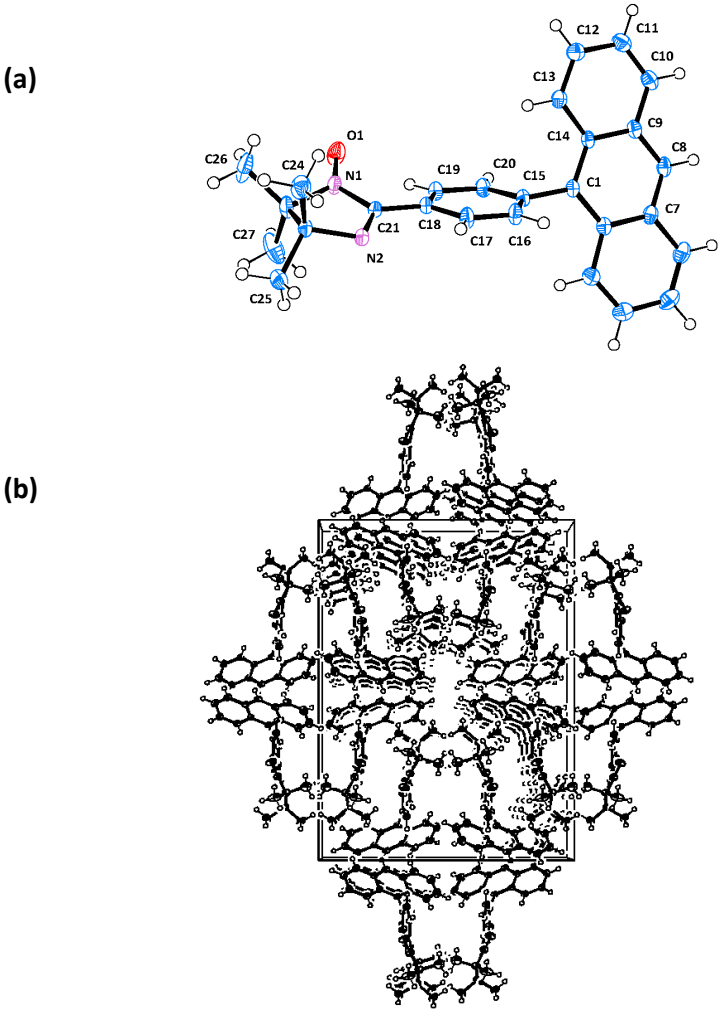

Figure 2.27. X-ray structure of **59d** with ORTEP drawn at the 50% of the probability level: (a) molecule; (b) crystal packing (view along the *c* axe).

The radical **59d** features *Ccc2* space group and possesses orthorhombic crystal arrangement. The molecule also adopt a propeller-shape conformation with torsion angles of 76.6° and -101.2° between the mean plane of the anthracene and the aromatic

ring (*Figure 2.27 (a)*), the radical fragment has an angle of ~20º with respect to the phenyl plane. Within the unit cell the molecules are related by weak hydrogen bonds between H atom of the methyl group and H atom of the phenyl ring (H161···H262' 2.18 Å), and short contacts formed by methylene proton of the nitroxide and the aromatic C atoms of the anthracene and phenyl moieties (C8···H241' 2.81 Å and C16···H262' 2.82 Å, respectively). These contacts connect the molecules together into distinct columns within *ab* plane. The columns are further connected by hydrogen bonds appearing between the anthracene fragment of one molecule and the phenyl ring (H41···C20' 2.87 Å) and anthracene core (H101···C12' 2.78, H81···C13' 2.9 and H81···C14' 2.81 Å) of the neighboring molecule.

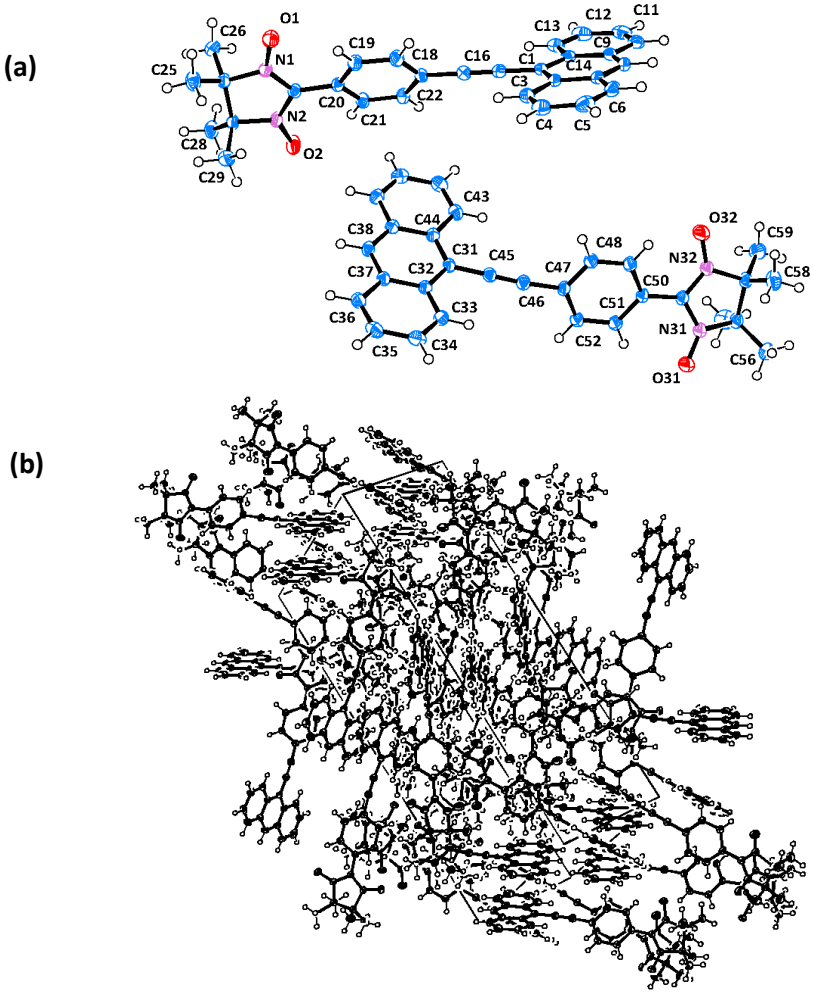

Figure 2.28. X-ray structure of **60c** with ORTEP drawn at the 50% of the probability level: (a) molecule; (b) crystal packing.

Compound **60c** exists in the crystal package as a combination of two independent half-molecules with nearly equal composition (*Fig. 2.28*). Consequently, the geometrical

parameters of each molecule have slight differences. For example, the aromatic rings are strongly twisted relative to the anthracene plane, and the corresponding torsion angles are: C(15)-C(16)-C(17)-C(18) 32.09º and C(45)-C(46)-C(47)-C(48) 37.24º.

The radical **60c** packs in $C2_1/a$ space group and features monoclinic arrangement. The O atoms of the imidazolidine ring form several short contacts with the surrounding molecules through bonding with the neighbouring anthracene sites (O1···H41' 2.7, O1···H411' 2.63, O2···H401' 2.68, O31···H361' 2.62 Å) and the C atom of the methyl group (O32···C58' 3.21 Å). Radical molecules of the first type are related via π–π stacking arising from parallel attached adjacent anthracene units (C11···C13' 3.35 Å). Conversely, the molecules of the second type are slightly twisted relative to the plane of the first ones, and form hydrogen bonding within neighboring anthracene fragments in a "herring-bone" fashion: H421···H121' 2.33, C11···H341' 2.84 Å.

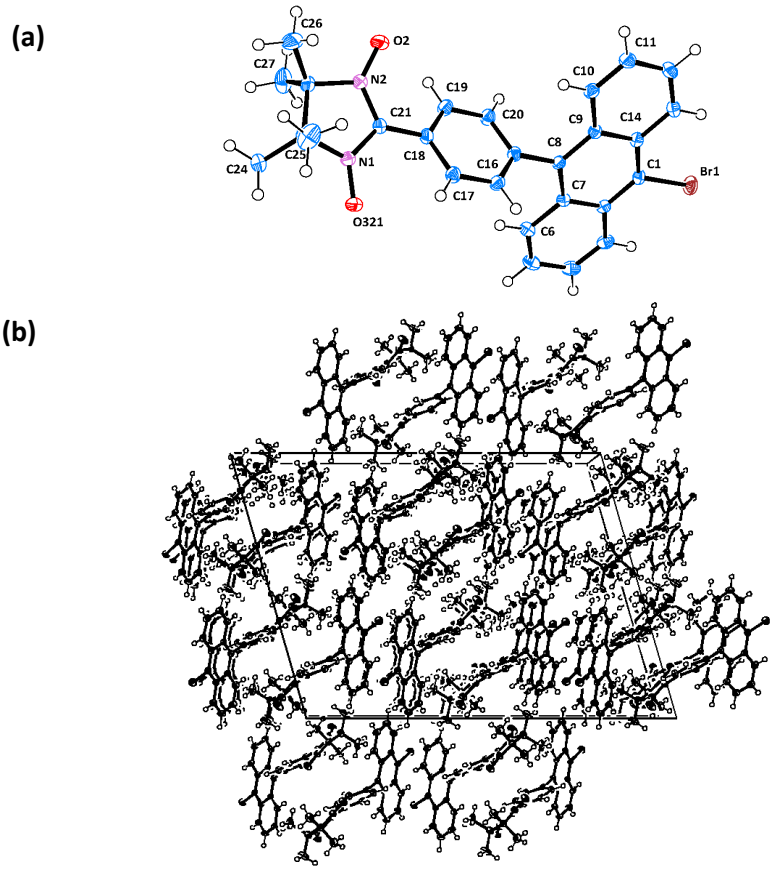

Figure 2.29. X-ray structure of **62c** with ORTEP drawn at the 50% of the probability level: (a) molecule; (b) crystal packing (view along the *b* axe).

The radical **62c** crystallizes in the $C2_1/c$ space group (*Table 2.4*). The molecule is twisted around the central symmetry axis with the torsion angles between the

anthracene core and the phenyl ring C(9)-C(8)-C(15)-C(20) 68.5° and C(9)-C(8)-C(15)-C(20) 70.3°, while the torsions between the phenyl plane and the radical moiety are C(17)-C(18)-C(21)-N(1) 31.3° and C(17)-C(18)-C(21)-N(2) 30.5° (*Figure 2.29 (a)*). The molecules are connected along the *c* axis by the set of weak intermolecular hydrogen bonds that involve an aromatic H atom of one molecule and the NO (O321···H201' 2.69 Å) of the neighboring molecule. Auxiliary intramolecular bonds between the molecules are formed by the bromide and carbon atoms of the anthracene units (Br1···C10' 3.46, Br1···C9' 3.51 Å). These various aromatic stacking interactions assure formation of a zig-zag like 2D hydrogen bonded network (*Figure 2.29 (b)*).

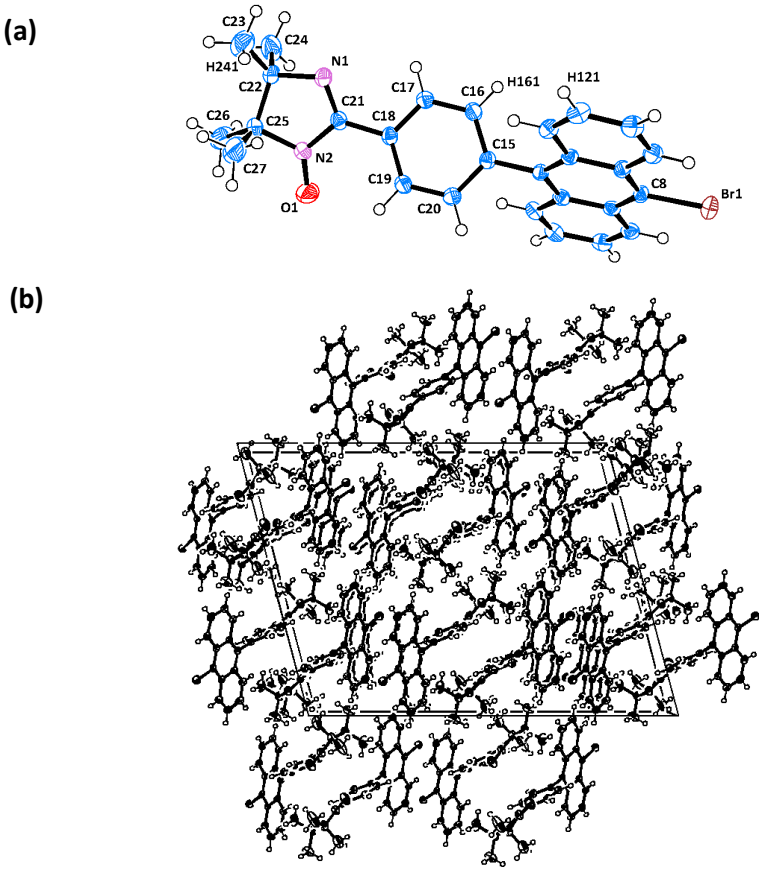

Figure 2.30. X-ray structure of **62d** with ORTEP drawn at the 50% of the probability level: (a) molecule; (b) crystal packing (view along the *b* axe).

Radical **62d** crystallized in the $C2_1/c$ space group (*Table 2.4*). The phenyl moiety is twisted out of the plane of the anthracene core by ~68° - a typical value for the series of the studied anthracene radicals. Meanwhile, the torsions formed by the phenyl plane with the radical fragment are ~ 25° (*Figure 2.30 (a)*), which is slightly less, when compared to the corresponding nitronyl nitroxide **62c**. Short contacts between neighboring

anthracene plates (H41···H121' 2.39, C4···H121' 2.88, C13···B1' 3.41, C4···C5' 3.4 Å) connect the radical molecules together into a "herring-bone" fashion within the crystal of **62d**. The interplanar distance between the phenyl rings is 3.4 Å, which together with the presence of additional short contacts (H161···H263' 2.29, C11···H263' 2.9, O1···H161' 2.69 Å) guarantees formation of intermolecular π–π interactions between the neighboring molecular units.

2.8. EPR studies of the anthracene-based nitroxide radicals

The X-band EPR measurements of the solutions of the anthracene-based radical systems in degassed toluene at room temperature were performed. In general, spectra were similar to the ones observed for the pyrene-nitroxides **57c**,**d**, confirming therefore, their radical nature. The g values and the hyperfine splitting constants (see *Table 2.5*) were coincident with those of nitroxides[65] within the experimental errors, meaning that the radical moiety was not disturbed by the attachment to the fluorophore.

Table 2.5. The g values and hyperfine coupling constants of the nitronyl nitroxide **59-62c** and imino nitroxide **59-62d** radicals.

Radical	g	Hyperfine coupling constants (mT)
59c	2.0066	0.744(1)
60c	2.0065	0.738(3)
61c	2.0066	0.75(0)
62c	2.0066	0.74(2)
59d	2.0059	A_1 = 0.40, A_2 =0.855
60d	2.0059	A_1 = 0.40, A_2 = 0.85
61d	2.0059	A_1 = 0.42, A_2 = 0.855
62d	2.0059	A_1 = 0.39, A_2 = 0.855

2.9. Photophysical properties of the anthracene-based nitroxides

2.9.1. UV-Vis absorption spectra of the anthracene-based nitroxide radicals

Absorption spectra recorded for the anthracene-based radicals in toluene at room temperature showed a rich mixture of transitions across the near-UV regions (*Fig. 2.31, 2.32*), and less intense transitions in the visible region, typical fingerprints of the nitronyl nitroxides. In each case, optical transitions associated with the nitronyl moiety could be recognized in the far-red region of the spectrum. Namely, the n-π^* transitions of the aminoxyl oxide fragment appeared at ~600-700 nm.

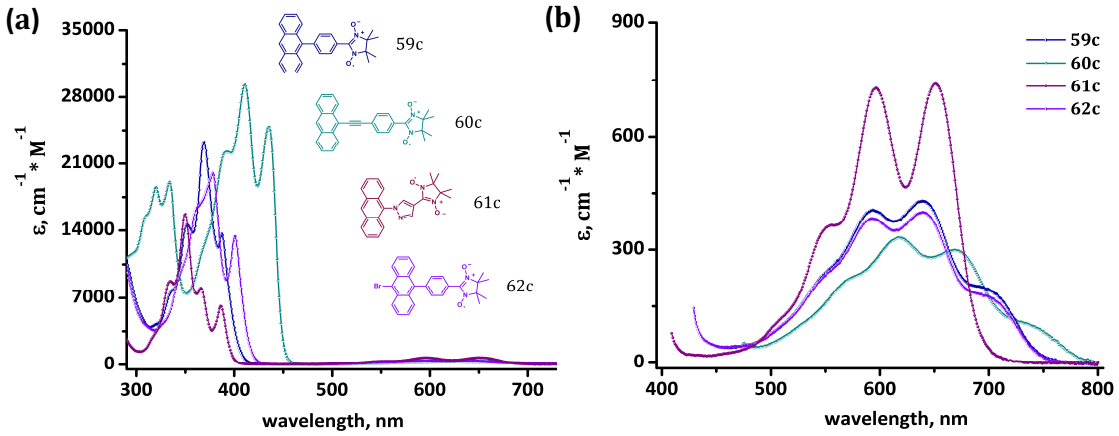

Figure 2.31. (a) UV-Vis spectra of nitronyl nitroxide radicals **57c**, **59-62c** recorded in toluene; (b) enlarged fragment of the spectra in the visible range.

Here, *Figure 2.31 (b)* is an important illustration of our concept, showing that the pyrazole-containing nitroxides (the radical **61c** in particular) feature n-π^* transition of the highest intensity within a series of structurally similar compounds. Thus, the extinction coefficient for the phenyl-bridged derivatives **59c**, **62c** is ~400 $M^{-1}cm^{-1}$, while this value is nearly twice larger (730 $M^{-1}cm^{-1}$) for the radical **61c** (see *Table 2.7*). Notably, the introduction of acetylenic function into the framework (compound **60c**) resulted in ~30 nm red-shift of the signal in comparison to the phenyl-anthracene radical **59c**.

A similar behaviour - 20 nm bathochromic shift - was observed for the imino derivative **60d**. Here, the n-π^* transition was seen as a weak shoulder at about 470 nm, which was obscured by the more intense π-π^* transitions of the aromatic core. Enlarged fragment of the absorption envelopes in visible range is shown in *Figure 2.32 (b)*. The

absorption bands at 400-460 nm represented characteristic signals of the anthracene fragment in the radicals **59c**,**d**, **61c**,**d** and **62c**,**d**, which were red-shifted by ~40 nm in the case of acetylene containing derivatives **60c**,**d** (*Fig. 2.31-2.32 (a)*).

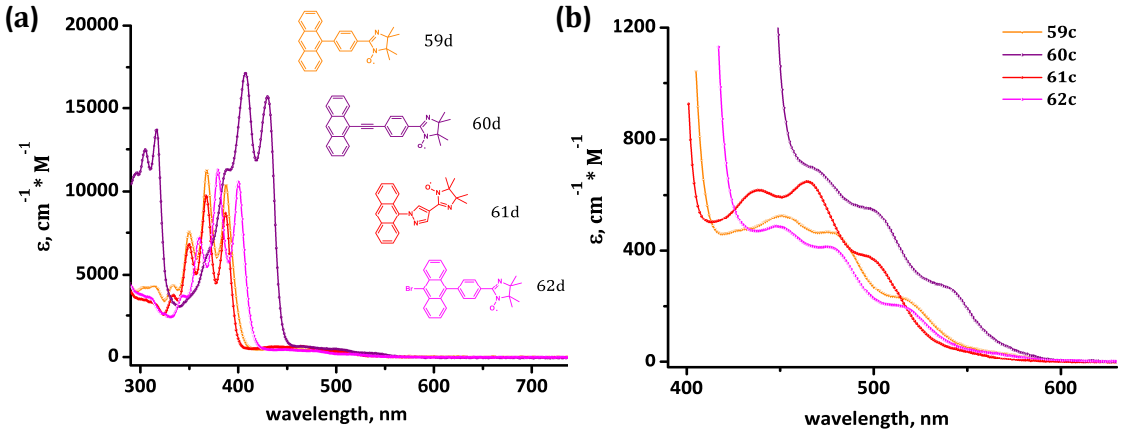

Figure 2.32. (a) UV-Vis spectra of imino nitroxide radicals **57d**, **59-62d** recorded in toluene; (b) enlarged fragment of the spectra in the visible range.

2.9.2. Analysis of the analytes employing anthracene-based nitroxide radicals

It has not, to date, been clearly determined whether the distance between the fluorophore and the nitroxide, the geometry of the system, the ring class employed (*i.e.* pyridine, pyrazole, etc.) or a combination of those, play the crucial role on the fluorescence release in a fluorophore-nitroxide molecule.[66] Therefore, the anthracene-derivatives **59-62c**,**d** were treated with chemical agents, to determine the correlation between the sensitivity of the probe and its structure. As an example, measurements performed for the nitronyl **59c**, **62c** and imino **60d**, **61d** derivatives are presented in *Figures 2.33* and *2.34*, respectively. The quantum yields of the samples were measured relative to the freshly prepared solution of 9,10-diphenyl-anthracene in cyclohexane, assuming value of a QY = 0.90 for the standard.[59a,b] The results are summarized in *Table 2.6*. In fact, for the anthracene-based fluorophore-nitroxide molecules **59-62c** and **59-62d** a similar trend, described earlier for the pyrene-based probes **57c**,**d** was observed. Primarily, the fluorescence intensity of the samples was negligible small due to the intramolecular self-quenching, although the extension of the π-conjugation in the radicals led to the less efficient fluorescence quenching (the molecules **60c**,**d**). Consequently,

ethynyl-anthracene nitroxides **60c** and **60d** featured the highest quantum yields (0.005 and 0.03, respectively) within the series of the anthracene radicals **59-62c**,**d**.

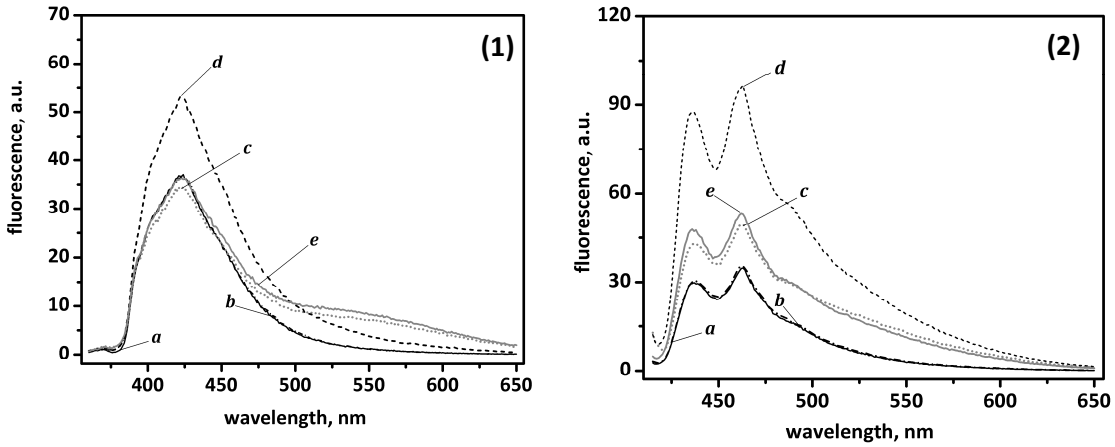

Figure 2.33. Fluorescence spectra of the nitronyl radicals (1) **59c** and (2) **60c** in MeOH with an excitation wavelength of (1) 350 nm and (2) 407 nm, respectively, under different conditions: (*a*) pure solution of a radical (2.6×10^{-6} M); (*b*) after reaction with CF_3COOH (5.1×10^{-5} M); (*c*) after reaction with cysteine (5.2×10^{-5} M); (*d*) after reaction with ascorbic acid (5×10^{-5} M); (*e*) after sequential reactions with cysteine (5.2×10^{-5} M) and CF_3COOH (5.1×10^{-5}M).

Addition of various chemical agents resulted in significant enhancement of the emission intensity (*Fig. 2.33, 2.34*). However, the quantum yields of the anthracene-based radicals **59-62c**,**d** were substantially smaller, than those of the pyrene derivatives **57c**,**d** (see *Table 2.3* for comparison).

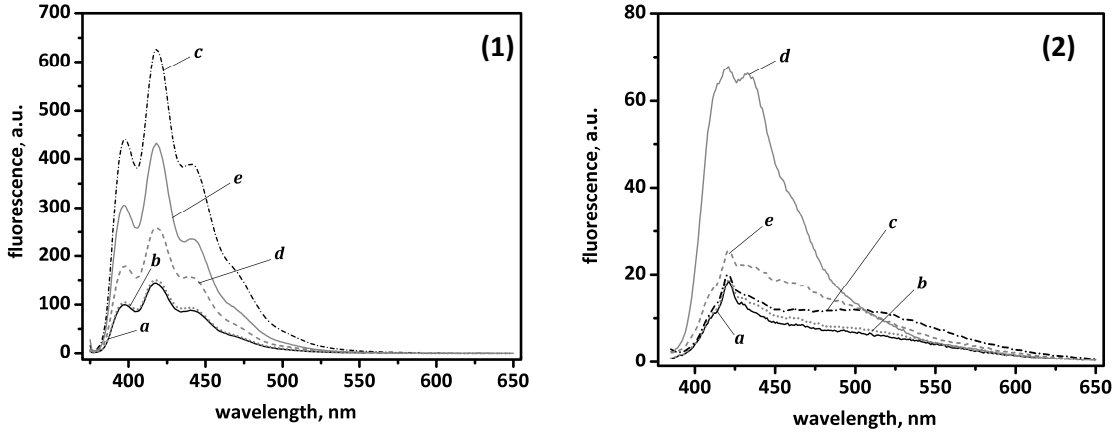

Figure 2.34. Fluorescence spectra of the imino radicals (1) **60d** and (2) **61d** in MeOH with an excitation wavelength of (1) 368 nm and (2) 374 nm, respectively, under different conditions: (*a*) pure solution of a radical (2.5×10^{-6} M); (*b*) after reaction with CF_3COOH (5.1×10^{-5} M); (*c*) after reaction with cysteine (5.2×10^{-5} M); (*d*) after reaction with ascorbic acid (5×10^{-5} M); (*e*) after sequential reactions with cysteine (5.2×10^{-5} M) and CF_3COOH (5.1×10^{-5}M).

Table 2.6. Quantum yields after reaction of the nitronyl **59-62c** and imino nitroxide **59-62d** radicals with chemical reagents (according to diphenylanthracene reference).

	$QY^{[a]}$	$\Phi/\Phi_0{}^{[b]}$		$QY^{[a]}$	$\Phi/\Phi_0{}^{[b]}$
59c	0.002	1	**59d**	0.002	1
ascorbic acid	0.005	2.5	ascorbic acid	0.004	2
Cys	0.006	3	Cys	0.004	2
CF_3COOH	0.002	1	CF_3COOH	0.002	1
Cys + CF_3COOH	0.007	3.5	Cys + CF_3COOH	0.005	2.5
60c	0.005	1	**60d**	0.030	1
ascorbic acid	0.020	4	ascorbic acid	0.050	1.7
Cys	0.020	4	Cys	0.050	1.7
CF_3COOH	0.005	1	CF_3COOH	0.040	1.3
Cys + CF_3COOH	0.030	**6**	Cys + CF_3COOH	0.070	2.5
61c	0.002	1	**61d**	0.004	1
ascorbic acid	0.006	3	ascorbic acid	0.010	2.5
Cys	0.010	**5**	Cys	0.050	**12.5**
CF_3COOH	0.002	1	CF_3COOH	0.004	1
Cys + CF_3COOH	0.012	**6**	Cys + CF_3COOH	0.060	**15**
62c	0.002	1	**62d**	0.003	1
ascorbic acid	0.005	2.5	ascorbic acid	0.010	3.3
Cys	0.002	1	Cys	0.005	1.7
CF_3COOH	0.002	1	CF_3COOH	0.004	1.3
Cys + CF_3COOH	0.002	1	Cys + CF_3COOH	0.006	2

[a] Quantum yields with respect to 9,10-diphenylanthracene;
[b] Fluorescence enhancement calculated relative to the QY_i[a].

Thus, ascorbate reduction of **59-62c**,**d** to the corresponding hydroxylamines resulted in ~2-4-fold increase in fluorescence yield, while for **57c** and **57d** this value was much greater (46- and 31-fold enhancement, respectively). Treatment of the samples **59-62c** and **59-62d** with cysteine led to ~1-7- and ~1-13-fold rise of the emission intensity, correspondingly. Here, the best results were obtained for the pyrazole containing nitroxides **61c** and **61d**. Unexpectedly, the imino radical **61d** demonstrated higher sensitivity towards net cysteine or cysteine/TFA couple, than its nitronyl analogue **61c**. To shed some light on this phenomenon, further studies are required.

After addition of trifluoroacetic acid to the anthracene-radicals solutions no tangible spectral changes occurred, as illustrated in *Figures 2.33*, *2.34*. Moreover, the usage of 100 times-excess of acid didn't help to improve the result, even in case of the imino derivatives **59-62d**. This suggests, that the synthesized anthracene-based radicals **59-62c**,**d** are much less sensitive proton receptors, than the pyrene nitroxides **57c**,**d**. Sequential reaction of the probes **59-62c**,**d** with cysteine/TFA led to significantly higher fluorescence release, especially for the ethynyl- **60c** (Φ/Φ_o = 6), pyrazole-anthracene nitronyl **61c** (Φ/Φ_o = 6) and imino **61d** (Φ/Φ_o = 15) derivatives. Importantly, that in the second case the enhancement of the fluorescence arise from the higher quenching efficiency of the fluorophore by the nitroxide, as the radicals **61c**,**d** possess the lowest quantum yields among the anthracene-nitroxides synthesized (*Table 2.6*).

Although the anthracene-based radicals **59-62c**,**d** demonstrated weaker sensing ability in comparison with the pyrene-pyrazole derivatives **57c**,**d**, the influence of the substituent character (**59**, **61**) and the length of the bridge between the radical center and the fluorophore (**60**) on response was studied. Furthermore, it was shown that the introduction of a strong acceptor (**62**) into the fluorophore unit resulted in a decreased sensitivity of the probe molecule.

Summarizing, on example of the radicals series **59-62c**,**d** the importance of the properly selected spacer between the fluorophore and the nitroxide was shown. The proposed method offers a logical strategy towards targeted design of novel probes with high sensing properties.

2.10. The IR absorption spectra of the pyrene-, perylene- and anthracene-based nitroxide radicals

The infrared spectroscopy (IR) carried out on the nitroxides (solid powders) revealed the appearance of strong bands at υ ~1350 cm^{-1} (*Table 2.7*), which were not present in either the carbaldehyde or imidazolidine precursors (for more detailed analysis see *Chapter 3*, *Subchapter 3.4.2*). The signal was attributed to the N-O stretching vibration of the imidazoline moiety, which was in harmony with comparable spectra, observed for several other NN systems described in the literature.[67] In the case of imino radicals novel signal, absent in **NN**, with relatively weaker intensity is shifted to the longer wave numbers (1365-1370 cm^{-1}), and is associated with the N-O stretching frequency of the aminoxyl fragment. For a better comparison, the infrared spectra of pyrazole-pyrene nitronyl nitroxide (**57c**) and corresponding imino radical (**57d**) are demonstrated in *Figure 2.35*.

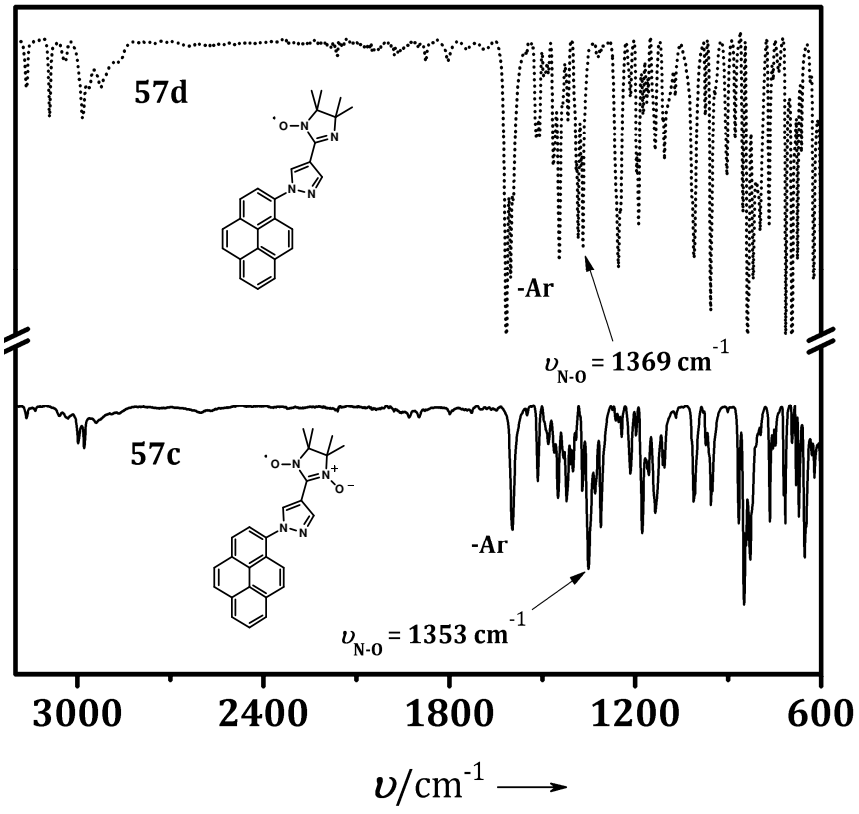

Figure 2.35. FT-IR spectra of pyrene-pyrazole nitronyl **57c** and imino **57d** nitroxides.

Signals originated from various vibrations of the aromatic rings were observed at around ~1480-1600 cm^{-1}.[68] These signals featured well-defined shape and high intensity due to the strong conjugation within the synthesized systems.[68] Stretching vibrations related to the pyrazole ring were observed at ~1420 and 1440 cm^{-1}.[69] Other strong signals appeared at around ~1550 cm^{-1}, but those are less characteristic since they belong to C=N stretching vibrations. Thus, UV-Vis and IR spectroscopy are the methods, which provide valuable information about the purity of the radical and its nature (imino or nitronyl species).The relevant UV-Vis and IR data of the studied systems **57c**,**d**, **59-62c**,**d** are listed in *Table 2.7*.

Table 2.7. Selected spectroscopic data for the nitronyl nitroxide **57c**, **59-62c** and imino nitroxide radicals **57d**, **59-62d**.

Radical	IR[a] ν_{NO}/cm^{-1}	UV-Vis[b] λ_{max}/nm ($\varepsilon/M^{-1}cm^{-1}$)
57c	1353	603 (1016)
58c	1354	600 (557)
59c	1358	593 (406)
60c	1356	617 (332)
61c	1359	597 (729)
62c	1358	593 (383)
57d	1369	467 (800)
59d	1362	451 (529)
60d	1366	469 (690)
61d	1365	464 (648)[c]
62d	1365	447 (487)[c]

[a] ν_{NO} measured in solid state;
[b] measured in toluene, unless otherwise specified;
[c] measured in dichloromethane.

2.11. Cyclic Voltammetry Measurements

The electrochemical behaviour of the pyrene-pyrazole nitroxides **57c**,**d**, as well as anthracene-based radicals **59c** and **62c**, in CH_2Cl_2 with 0.1 M tetrabutylammonium tetrafluoroborate ((*n*-C_4H_9)NPF_6) supporting electrolyte and ferrocene as internal standard at room temperature was studied. A platinum working electrode and Ag/AgCl as a reference were used. In general, the cyclic voltammogramms of the nitronyl nitroxide

derivatives containing electron-donating groups showed reversible oxidation in the investigated conventional timescale,[70,71] as shown in *Figures 2.36, 2.37* (the reduction part is specified with the black colour, and oxidation is specified with the red colour in the plot). Here, the nitroxide group was reversibly oxidized to the corresponding oxoammonium cation. The oxidation onset potential for the pyrene derivative **57c** was measured to be 0.29 V (all the reported potentials were calibrated against Fc/Fc^+ couple at 0.46 V). Typically, pyrene derivatives exhibit reduction potential at ~0.7-0.75 V, which was not observed during our experiments.[72]

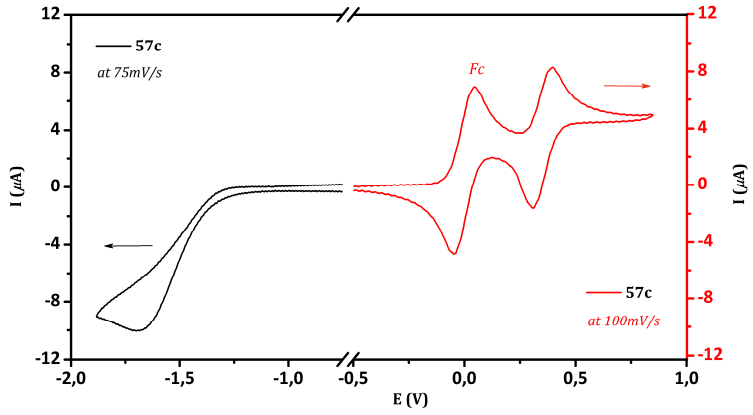

Figure 2.36. Cyclic voltammograms of the nitronyl radical **57c** registered at 75 mV/s and 100 mV/s in CH_2Cl_2 *vs*. Fc/Fc^+.

Conversely, the anthracene-based nitroxides **59c**, **62c** each displayed two reversible redox waves in the range ~0.34-0.36 and 0.81-0.90 V, specified in *Figure 2.37* with the red colour. The first oxidative wave corresponded to the oxidation of the radical unit (marked in *Fig. 2.37* with the red letter *(a)*).[73]

The further oxidation peak was assigned to successive oxidation of the anthracene fragment, specified in *Figure 2.37* with the red letter *(b)*. The values were consistent with those, observed for non-radical anthracene derivatives.[74]

That was another clear evidence, that the electronic communication in the studied radical systems remained weak, such that each unit of the molecule retained its own identity. As expected,[75] the imino derivative **57d** was oxidized irreversibly and at higher potentials (0.77 V).

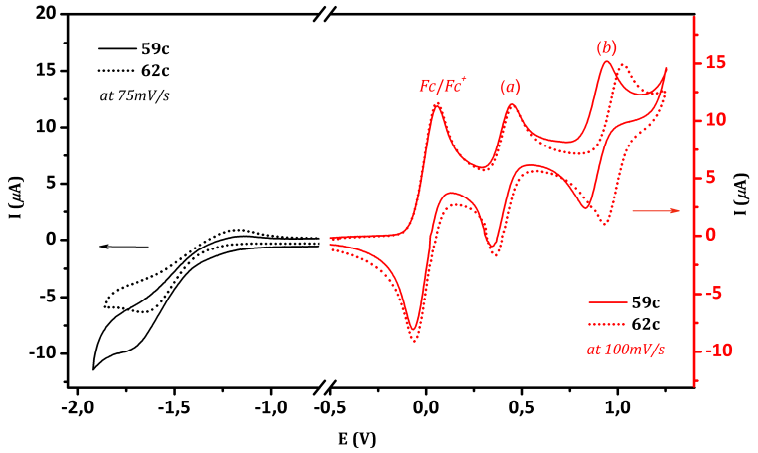

Figure 2.37. Cyclic voltammograms of **59c** and **62c** at 75 mV/s and 100 mV/s (reduction part is specified with the black colour and oxidation is specified with the red colour in the plot) registered in CH_2Cl_2 *vs*. Fc/Fc^+. Oxidation of the radical unit is marked with the red letter *(a)*, oxidation of the anthracene moiety with the letter *(b)*.

All the studied nitroxides exhibited irreversible reduction (*Fig. 2.36, 2.37*), with the exception in case of the reduction waves of the bromo-derivative **62c**. The radical moieties in NN and IN systems were reduced to the anions, which subsequently reacted with the traces of water presented in solvent, affording the corresponding bishydroxylamines.[75,76] The electrochemical-chemical mechanistic pathway for the reduction of these compounds could be exemplary described for **57c** (*Scheme 2.14*). Importantly, nitronyl nitroxide **62c** displayed quasi-reversible reduction, which was attributed to the electron-withdrawing character of the bromine substituent.

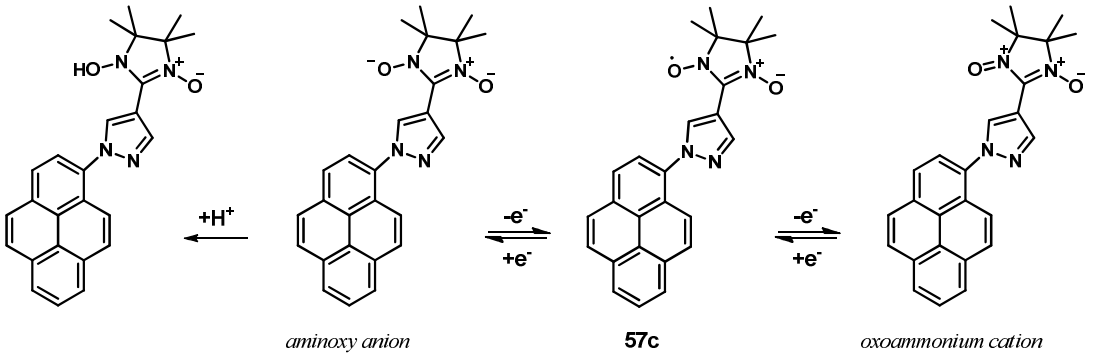

Scheme 2.14. Redox mechanism of a nitronyl nitroxide radical **57c**.

For the open-shell systems, such as neutral radicals, the singly occupied molecular orbitals (SOMOs) and the lowest unoccupied molecular orbitals (LUMOs) determine the redox properties of the compounds.[77] Therefore, the difference between the E_{Red} and E_{Ox}

(as well as the corresponding value of the E_{opt}) corresponds to the energy gap between the SOMO and the LUMO.[77c] Following the equations *(13), (14)*[78] calculations of the SOMO and the LUMO levels were carried out and listed in *Table 2.8*.

$$E_{SOMO} = -(E_{Ox,onset} - E^{(1/2)}_{Fc/Fc} + 4.8)\ eV \quad (\mathbf{13})$$

$$E_{LUMO} = -(E_{Red,onset} - E^{(1/2)}_{Fc/Fc} + 4.8)\ eV \quad (\mathbf{14})$$

In fact, studied nitronyl nitroxides **57c**, **58c**, **62c** featured similar LUMO levels (~ -3.45 eV), while the imino derivative **57d** possessed a slightly lower value (-3.57 eV). The highest SOMO levels were observed for the anthracene-based nitronyl nitroxides (~ -5.1 eV), due to the stronger donor character of the aromatic core.

Table 2.8. Electrochemical properties of the nitronyl nitroxide **57c**, **59**, **62c** and imino **57d** radicals (the potentials were calibrated against Fc/Fc^+ couple at 0.46 V).

Radical	E_{Ox}, V	E_{Red}, V	E_{SOMO}, eV	E_{LUMO}, eV	ΔE_g, eV	E_{opt}, eV
57c	0.286	-1.357	-5.09	-3.44	1.65	1.77
59c	0.337 0.813	-1.334	-5.14	-3.46	1.68	1.64
62c	0.361 0.897	-1.355	-5.16	-3.45	1.71	1.64
57d	0.771	-1.236	-5.57	-3.57	2.00	2.13

The lowest value of the SOMO level and, correspondingly, the biggest band gap (2.0 eV), was registered for the pyrene-pyrazole imino radical **57d**. Importantly, the ΔE_g values calculated from the SOMO-LUMO difference were in a good agreement with the E_{opt} obtained from the absorption spectra and coincident with the literature data for the other nitroxides.[79]

2.12. Conclusion

Recently it was shown, that covalently linked nitroxide-fluorophore hybrid molecules can be employed as sensitive optical probes of radical/redox reactions.[5,8,48,52,80] Until now, the attempts to improve the sensitivity of such hybrid molecules were focused on the fluorophore nature. In such cases the synthesis of a novel probe required each time more demanding synthetic sequences, which however, couldn't guarantee the high sensitivity of the probe.[66] Challenging, therefore, is the idea to be

able to tune the properties of already known fluorophores. The efficiency of the hybrid molecule could be significantly improved by introduction of an appropriate spacer into the radical-fluorophore system. The spacer could be selected based on the analysis of the corresponding absorption data. As an illustration of our approach, series of pyrene and anthracene-based nitronyl **57c**, **59-62c** and imino **57d**, **59-61d** nitroxides were synthesized and their potential as sensing probes in solution was studied. According to the spectroscopic data analysis it was concluded, that reaction of a probe with a chemical reagent follows reduction mechanism. It was demonstrated, that the sensitivity of the obtained radicals far surpassed the literature known analogues.[8] To overcome the problem of insolubility of the synthesized probes in water, some trials in films were carried out on example of pyrene derivatives **57c**,**d**. Furthermore, nitronyl radical **57c** was employed to monitor NO production in solution by EPR technique.

Summarizing, the importance of a properly selected building block for a targeted assembling of highly sensitive nitroxide-fluorophore complex systems was demonstrated. That finding opens new possibilities to design and construct better radical sensors.

References

[1] L. Stryer, H. O. Griffith, *Proc. Natl. Acad. Sci. U.S.A.*, **1965** (54), 1785-1791.

[2] G. I. Likhtenshtein, V. R. Bogatyarenko, A. V. Kulikov, K. Hideg, G. O. Hankovsy, N. V. Lukoyanov, B. S. Tanaseichuk, *Dokl. Akadem. Nauk SSSR*, **1980** (253), 481-484.

[3] I. M. Bystryak, G. I. Likhtenshtein, A. I. Kotelnikov, O. H. Hankovsky, K. Hideg, *J. Phys. Chem.*, **1986** (60), 1679-1983.

[4] (a) J. A. Green, L. A. Singer, J. H. Parks, *J. Chem. Phys.*, **1973** (58), 2690-2695; (b) J. A. Green, L. A. Singer, *J. Am. Chem. Soc.*, **1974** (96), 2730-2733; (c) A. R. Watkins, *Chem Phys. Lett.*, **1974** (29), 526-528.

[5] N. V. Blough, D. J. Simpson, *J. Am. Chem. Soc.*, **1988** (110), 1915.

[6] E. Szajdzinska-Pietek, M. Wolszczak, *Chem. Phys. Lett.*, **1997** (270), 527.

[7] (a) V. A. Kuzmin, A. S. Tatikolov, *Chem. Phys. Lett.*, **1977** (51), 45-47; (b) S. K. Chattopadhyay, P. K. Das, G. L. Hug, *J. Am. Chem. Soc.*, **1983** (105), 6205-6210.

[8] H. Wang, D. Zhang, X. Guo, L. Zhu, Z. Shuai, D. Zhu,*Chem. Commun.,* **2004**, 670–671.

[9] G. Zopellaro, *PhD Thesis*, **2004**, Mainz.

[10] R. D. Miller, C. R. Moylan, O. Reiser, C. A. Walsh, *Chem. Mater.*, **1993** (24), 625-632.

[11] M. Okazaki, N. Uchino, N. Nozaki, K. Kubo, *Bull. Chem. Soc. Japan*, **1995** (68), 1024-1029.

[12] S. Pu, T. Yang, J. Xu, B. Chen, *Tetrahedron Lett.*, **2006** (47), 6473-6477.

[13] S. Allen, T. D. McLean, P. F. Gordon, B. D. Bothwell, M. B. Hurthouse, S. A. Karaulov, *J. Appl. Phys.*, **1988** (5), 2583-2590.

[14] G. Zoppellaro, A. Geies, V. Enkelmann, M. Baumgarten, *Eur. J. Org. Chem.,* **2004**, 2367-2374.

[15] L. Catala, K. Wurst, D. B. Amabilino, J. Veciana, *J. Mater. Chem.*, **2006** (16), 2736-2745.

[16] P. Stanetty, H. Koller, M Mihovilovic, *J. Org. Chem.*, **1992** (57), 6833–6837.

[17] (a) S. F. Vasilevsky, S. V. Klyatskaya, E. V. Tretyakov, J. Elguero, *Heterocycles*, **2003** (60), 879; (b) M. I. Rodríguez-Franco, I. Dorronsoro, A. I Hernández-Higueras, G. Antequera, *Tetrahedron Lett.*, **2001** (42), 863–865.

[18] R. E. Sammelson, J. E. Casida, *J. Org. Chem.,* **2003** (68), 8075-8079.

[19] G. Zoppellaro, A. Geies, K. K. Andersson, V. Enkelmann, M. Baumgarten, *Eur. J. Org. Chem.*, **2008**, 1431–1440.

[20] A. Correa, C. Bolm, *Adv. Synth. Catal.,* **2007** (349), 2673 – 2676.

[21] L. Zhu, P.Guo, G. Li, J. Lan, R. Xie, J. You, *J. Org. Chem.,* **2007** (72), 8535-8538.

[22] N. Machinaga, C. Kibayashi, *Tetrahedron Lett.,* **1989** (30), 4165-4168.

[23] T. W. Greene, Peter G.M. Wuts, *Protective Groups in Organic Synthesis* (sec. ed.), **1991.**

[24] B. S. Ong, T. H. Chan, *Synth. Comm.***, 1977**, 7(4), 283-286.

[25] I. L. Finar, G. H. Lord, *J. Chem. Soc.*, **1959**, 1819.

[26] I. L. Finar, G. H. Lord, *J. Chem. Soc.*, **1959**, 3314.

[27] I. L. Finar, G. H. Lord, *J. Chem.Soc.,* **1957**, 3314.

[28] F. R.C. de Barros, L. F. C. C. Leite, J. M. Santos Filho, J. G. Lima, *Anais. Assoc. Bras. Quim*., **2001**, 50 (4), 162-165.

[29] F. Würthner, *Pure Appl. Chem.*, **2006** (78), 2341–2349.

[30] S. Takahashi, Y. Kuroyama, K. Sonogashira, N. Hagihara, *Synth.*, **1980**, 627-630.

[31] F. M. Romero, R. Ziessel, *Tetrahedron Lett.,* **1999** (40), 1895–1898.

[32] (a) C. Foces-Foces, F. H. Cano, J. Elguero, *Gazz. Chim. Ital*., **1993** (123), 477; (b) R. Goddard, R. M. Claramunt, C. Escolástico, J. Elguero, D. Schagen, H.-H. Limbach, *New J. Chem*., **1999** (23), 237; (c) I. Alkorta, J. Elguero, B. Donnadieu, M. Etienne, J. Jaffart, *New J. Chem*., **1999** (23), 1231.

[33] (a) S. Trofimenko, *Prog. Inorg. Chem*., **1986** (34), 115-210; (b) A. P. Sadimenko, S. S. Basson, *Coord. Chem. Rev.*, **2001** (222), 251; (c) R. Q. Zou, C. S. Liu, X. S. Shi, X. H. Bu, J. Ribas, *Cryst. Eng. Comm*., **2005** (7), 722.

[34] (a) L. A. Blumenfeld, A. N. Tichonov, *Soros Educational Journal*, **1997** (9); (b) D. Ingram, *EPR of Free Radicals* [Russian translation], IL, Moscow, **1951**; (c) D. J. E. Ingram, *Proc. Phys. Soc.*, **1949** (A 62), 664; (d) G. R. Eaton, S. S. Eaton, K. M. Salikhov, *Foundations of modern EPR*, World of Scientific Publishing Co, **1998**.

[35] (a) F. Gerson, W. Huber, *Electron Spin Resonance Spectroscopy of Organic Radicals*, **2004**, Wiley-VCH; (b) U. Barth, L. Hedin, *J. Phys. C: Solid State Phys.*, **1972** (5), 1629; (c) B. L. Bales, M. Peric, I. Dragutan, *J. Phys. Chem. A*, **2003** (107), 9086.

[36] (a) M. Baumgarten, *EPR of Free Radicals in Solids* (eds.: A. Lund, M. Shiotani), Kluwer Academics Publishers: Netherlands, **2003**; (b) J. E. Wertz, J. R. Bolton, Electron Spin Resonance, Chapman and Hall: New York, London, **1972** (Reprint); (c) J. E. Wertz, J. R. Bolton, *Electron Spin Resonance, Elementary Theory and Practical Applications*, Chapman & Hall, **1986**.

[37] L. Packer, Nitric oxide. In *Methods in Enzymology,* San Diego: Academic, **1994,** 739–749.

[38] D. J. Stuehr, S. Ghosh, *Handbook of Experimental Pharmacology*, **2000** (143), 33–70 (Nitric Oxide).

[39] (a) S. Moncada, R. M. J. Palmer, E. A. Higgs, *Pharmacol. Rev.*, **1991** (43), 109-142; (b) S. H. Snyder, D. S. Bredt, *Sci. Amer.*, **1992**, 266(5), 68-77.

[40] *Methods Enzymol.,* **1996**, 269 (the reference refers to the whole issue).

[41] E. Noack and M. Murphy, in *Oxidative Stress-Oxidants and Antioxidants* (ed.: H. Sies), Academic Press, **1991**, 445-489.

[42] P. L. Reddy, L. J. Bowie, S. Callistein, *Clin. Chem.*, **1997** (43), 1442-1447.

[43] S. Kudo, J. L. Bourassa, S. E. Boggs, *Ann. Biochem.*, **1997** (247), 193–202.

[44] T. Xiaorong, F. Cheng, Y. Bing, Z. Wuming, *Microchem. J.*, **1999** (62), 377–385.

[45] P. Meineke, U. Rauen, *Biol. Chem.*, **2000** (381), 575-582.

[46] A. M. Miles, Y. Chen, M. W. Owens, M. B. Grisham, *Methods,* **1995** (*7)*, 40–47.

[47] (a) S. I. Dikalov, I. A. Kirilyuk, M. A. Voinov, *Abstracts of Conference SPIN-2005*, **2005**, September 20-24, Novosibirsk, Russia, 58; (b) R. F. Haselhoff, S. Zollner, I. E. Blasig, *Free Radical Research*, **1997** (26), 7-17; (c) J. Joseph, B. Kalyanaraman, J. S. Hyde, *Biochem. Biophys. Res. Comm.*, **1993** (192), 926-934.

[48] E. M. Lozinsky, L. V. Martina, A. I. Shames, N. Uzlaner, A. Masarwa, G. I. Likhtenshtein, D. Meyerstein, V. V. Martin, Z. Priel, *Analytical Biochemistry*, **2004** (326), 139–145.

[49] (a) Y. Yu. Woldman, V. V. Khramtsov, I. A. Grigor'ev, I. A. Kiriljuk, D. I. Utepbergenov, *Biochem. Biophys. Res. Commun.*, **1994** (202), 195-203; (b) G. M. Rosen, S. Porasuphatana, P. Tsai, N. P. Ambulos, V. E. Galtsev, K. Ichikawa, H. J. Halpern, *Macromol.*, **2003** (36), 1021-1027.

[50] L. J. Ignarro, H. Lippton, J. C. Edwards, W. H. Baricos, A. L. Hyman, P. J. Kadowitz, C. A. Gruetter, *J. Pharmacol. Exp. Theor.*, **1981** (218), 739–749.

[51] I. B. Berlman, *Handbook of Fluorescence Spectra of Aromatic Molecules,* Academic Press, **1971**.

[52] E. M. Lozinsky, V. V. Martin, T. A. Berezina, A. I. Shames, A. L. Weis, G. I. Likhtenshtein, *J. Biochem. Biophys. Methods*, **1999** (38), 29–42.

[53] (a) M. K. Shigenaga, T. M. Hagen, B. N. Ames, *Proc. Natl. Acad. Sci. USA*, **1994** (91), 10771–8; (b) M. K. Shigenaga, B. N. Ames, *Basic Life Sci.*, **1993** (61), 419–36.

[54] B. Frey, L. England, B. N. Ames, *Proc. Natl. Acad. Sci. USA*, **1989** (86), 6377–81.

[55] (a) B. Halliwell, *Free Radic. Res. Commun*., **1990** (9), 1–32; (b) G. W. Burton, K. U. Ingold, *Acc. Chem. Res*., **1986** (19), 194–201; (c) L. Packer, E. H. Witt, H. J. Tritschler, *Free Radic. Biol. Med.*, **1995** (19), 227–50.

[56] S. Bernhardt, M. Kastler, V. Enkelmann, M. Baumgarten, K. Müllen, *Chem. Eur.J.*, **2006** (12), 6117-6128.

[57] N. Medvedeva, V. V. Martin, A. L. Weis, G. I. Likhtenshtein, *J. Photochem. Photobiol. A: Chemistry*, **2004** (163), 45–51.

[58] (a) V. V. Khramtsov, I. A. Grigor'ev, M. A. Foster, D. J. Lurie, I. Nicholson, *Cell and Molecular Biology* (Noisy-le-grand), **2000** (46), 1361-1374; (b) J. F. W. Keana, M. J. Acarregui, S. L. M. Boyle, *J. Am. Chem. Soc.*, **1982** (104), 887; (c) M. A. Voinov, J. F. Polienko, T. Schanding, A. A. Bobko, V. V. Khramtsov, Y. V. Gatilov, T. V. Rybalova, A. I. Smirnov, I. A. Grigor'ev, *J. Org. Chem.*, **2005** (70), 9702–9711; (d) J. Li, H. M. Wang, H. M. Ma, D. Q. Zhang, S. X. Xiong, *Chinese Chem. Lett*., **2005** (8), 1125-1128.

[59] (a) S. Hamai, F. Hirayama, *J. Phys. Chem.*, **1968** (72), 2680; (b) S. R. Meech, D. Phillis, *J. Photochem.*, **1983** (23), 193; (c) W. R. Dawson, M. W. Windsor, *J. Phys. Chem.*, **1968** (72), 3251; (d) W. H. Melhuish, *J. Phys. Chem.*, **1961** (65), 229.

[60] (a) M. Gouterman, *The Porphyrins*, Academic Press, New York (ed.: D. Dolphin), **1978** (3), 1–165; (b) K. Ishii, N. Kobayashi, *The Porphyrin Handbook*, Academic Press, New York (ed.: K. M. Kadish, R. M. Smith and R. Guilard), **2003** (16), 1–42; (c) M. Asano, Y. Kaizu, H. Kobayashi, *J. Chem. Phys.*, **1988** (89), 6567–6576.

[61] T. A. Fayed, G. Grampp, S. Landgraf, *Intern. J. Photoenergy*, **1999** (1), 1–4.

[62] T. Suzuki, K. Obi, *Chem. Phys. Lett.*, **1995** (246), 130.

[63] S. H. Herbelin, N. V. Blough, *J. Phys. Chem.*, **1998** (B:102), 8170.

[64] I. A. Volodarsky, S. A. Grigor'ev, V. A. Dikanov, *Nauka, Siberian Branch*, Novosibirsk, **1988**.

[65] Y. Teki, T. Toichi, S. Nakajima, *Chem. Eur. J.*, **2006** (12), 2329-2336.

[66] J. P. Blinco, K. E. Fairfull-Smith, B. J. Morrow, S. E. Bottle, *Aust. J. Chem.*, **2011** (64), 373-389.

[67] (a) L. Catala, J. L. Moigne, N. Gruber, J. J. Novoa, P. Rabu, E. Belorizky, P. Turek, *Chem. Eur. J.*, **2005** (11), 2440 – 2454; (b) O. N. Chupakhin, I. A. Utepova, M. V. Varaksin, E. V. Tretyakov, G. V. Romanenko, D. V. Stass, V. I. Ovcharenko, *J. Org. Chem.*, **2009** (74), 2870 – 2872; (c) S. V. Klyatskaya, E. V. Tretyakov, S. F. Vasilevsky, *Russ. Chem. Bull. Int.Ed.,* **2002** (51), 128-134; (d) J. H. Osiecki, E. F. Ullman, *J. Am. Chem. Soc*, **1968** (90), 1078.

[68] D. J. De Frees, M. D. Miller, D. Talbi, F. Pauzat, Y. Ellinger, *Astrophys. J*, **1993** (408), 530-538.

[69] V. S. Troitskaya, N. D. Konevskaya, V. G. Vinokurov, V. I. Tyulin, *Chem. Heteroc. Comp.*, **1975** (10), 471-476.

[70] T. Suga, Y. J. Pu, S. Kasatori, H. Nishide, *Macromol.*, **2007** (40), 3167.

[71] J. Lee, E. Lee, S. Kim, G. S. Bang, D. A. Shultz, R. D. Schmidt, M. D. E. Forbes, H. Lee, *Angew. Chem. Int. Ed.*, **2011** (50), 4414-4418.

[72] (a) X. Zhu, L. Xu, M. Wang, Z. Wang, R. Liu, J. Zhao, *Int. J. Electrochem. Sci.,* **2011** (6), 1730 – 1746; (b) E. Keskin, Y. Yardım, Z. Sentürk, *Electroanalysis*, **2010** (22), 1191 – 1199; (c) G. J. Bodwell, J. N. Bridson, M. K. Cyrañski, J. W. J. Kennedy, T. M. Krygowski, M. R. Mannion, D. O. Miller, *J. Org. Chem.*, **2003** (68), 2089-2098.

[73] R. Ziessel, S. Rihn, A. Harriman, *Chem. Eur. J.*, **2010** (16), 11942-11953.

[74] (a) Y. Takemoto, Y. Teki, *Chem. Phys. Chem*., **2011** (12), 104-108; (b) C.-W. Wan, A. Burghart, J. Chen, F. Bergström, R. M. Hochstrasser, L. B. A. Johansson, M. F. Wolford, T. G. Kim, M. R. Topp, K. Burgess, *Chem. Eur. J.*, **2003** (9), 4430-4441.

[75] R. Ziessel, G. Ulrich, R. C. Lawson, L. Echegoyen, *J. Mater. Chem.*, **1999** (9), 1435–1448.

[76] (a) T. Malinski, J. R. Fish, S. G. Swarts, M. D. Sevilla, *J. Phys. Chem.*, **1988** (92), 3745; (b) D. Serve, *Electrochim. Acta*, **1975** (20), 469.

[77] (a) K. Matsuda, M. Irie, *J. Am. Chem. Soc.*, **2000** (122), 7195–7201; (b) T. Yamasaki, F. Mito, Y. Ito, S. Pandian, Y. Kinoshita, K. Nakano, R. Murugesan, K. Sakai, H. Utsumi, K. Yamada, *J. Org. Chem.*, **2011** (76), 435–440; (c) Y. Morita, S. Nishida, J. Kawai, T. Takui, K. Nakasuji, *Pure. Appl. Chem.*, **2008** (80), 507–517.

[78] A. J. Bard, L. R. Faulkner, *Electrochemical Methods* (sec. ed.), J. Wiley & Sons Press, **2000**.

[79] Y. G. Budnikova, T. V. Gryaznova, M. K. Kadirov, E. V. Tret'yakov, K. V. Kholin, V. I. Ovcharenko, R. Z. Sagdeev, O. G. Sinyashin, *Russ. J. Phys. Chem.*, **2009** (83), 1976-1980.

[80] (a) D. J. Kieber, N. V. Blough, *Free Radical Res. Commun.*, **1990** (10), 109; (b) J. L. Gerlock, P. J. Zacmanidis, D. R. Bauer, D. J. Simpson, D. J. Blough, I. T. Salmeen, *Free Radical Res. Commun.*, **1990** (10), 119.

Chapter 3

Organic Based Magnetic Materials

3.1. State of the art

The design and synthesis of molecular-based quantum computers (QC) is one of the major subjects of material science,[1,2] as it ensures the further growth of the technological progress. Discovery of the Bose-Einstein condensate (BEC) in 1995[3,4] prompted the growth of new trends in fundamental research, especially in the field of molecular magnetism[5,6] due to their possible applications in information technology as a new generation of hard disks with an increased amount of storable data and read/write speed. BEC was long associated with the study of superfluid ^{4}He and ^{3}He-^{4}He mixtures.[7] In superfluid helium many features associated with BEC are masked by the strongly interacting character of the liquid.[7] This caused the rapid development of many other novel systems currently studied in the laboratory, and among them the model of weakly interacting boson gases holds a special place, since their momentum spectra and other properties can be more amenable to theoretical analysis. In this regard, molecular-based organic magnets are of particular high interest not only as perspective compounds for developing novel high-tech materials, but also for studying BEC. This could also provide scientists with the necessary materials suitable for investigation of the quantum information processing and computation in the fabricated test-devices.

From the experimental side, one of the main challenges is to create a matter suitable for large-scale quantum computation in the laboratory. Up-to-date, several approaches to construct QC have been reported.[8,9] Some promising results were achieved with cuprates[10,11] and silicon-based materials,[12] but still the task to fabricate a QC remains technically demanding. In this regard, organic-based magnetic materials may offer some advantages compared to the usual inorganic based supports. Organic compounds are transparent in many regions and could be obtained in optical active chiral

forms.[13] Hence, they might be used as magneto-optical switches and for the manipulation of polarized light in optical devices.[14] Lately they were extensively studied due to their potential application as radical-based batteries,[15,16] electric conductors[15a,17,18] and spintronic devices.[15a,17,19]

Nitronyl nitroxide (**NN**) radicals are one of the most often employed spin carries for the preparation of the molecular-based magnets due to their stability and bidentate character. The discovery of this class of compounds by Ullman in 1968 opened new horizons in pure organic magnetic materials quest. NNs possess weak basic properties, which allow them to form coordination bonds with acidic metal centers through the oxygen atoms of the O-N fragments, leading to a large variety of transition metal-radical complexes.[20,21] In nitronyl nitroxide radicals the spin density of the unpaired electron is delocalized over two sites of coordination, leaving open the possibility to arrange molecular units into a supramolecular network.

Importantly, synthetic chemistry permits to perform structural modifications in organic materials in order to control the *intra*- and *inter*-molecular exchange interactions between spin carriers.[22] Thus, the former can be designed and adjusted through synthesis of different conjugated bridges between the spin-containing sites, although the latter requires supramolecular approaches employing hydrogen bonding, π-stacking, and metal complexation. Such tunability is unprecedented in most of the traditional inorganic materials and is the key to obtain materials with unique magnetic properties.

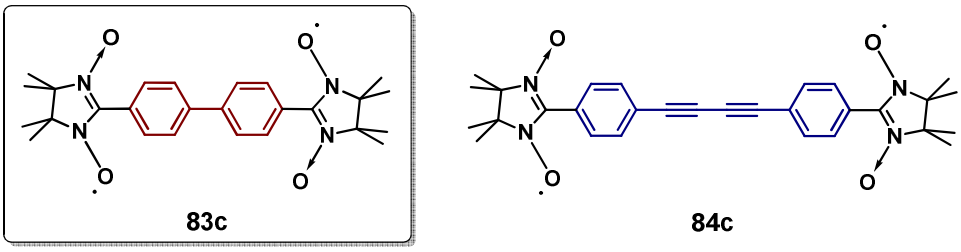

Figure 3.1. Biradical systems with different length of the π-bridge.

In our study we considered organic spin-dimer systems with singlet ground state and moderate *intra*-dimer interactions in the range of -2 to -8 K (the numbers refer to the exchange coupling defined in accordance with the Hamiltonian used in the DFT calculations).[23] In addition, the compounds should form interacting networks due to small *inter*-dimer interactions, giving rise to field-induced magnetic states, depending on

the dimensionality of the interactions, at fields below the saturation field.[24] The prediction of the magnitude of the *inter*molecular exchange interactions, based on coordination geometry and bond distances is not a trivial task. In this regard approximate primary model providing reliable information about magneto-structural correlations is of great value. The recently reported[25] synthesis of biphenyl bridged bisnitronyl nitroxide **83c** could be fairly called the milestone in our investigation. This biradical is depicted in *Figure 3.1* and features *intra*molecular exchange interaction J_{intra} of about -14 K (exp.), which is slightly too large for the laboratory magnet and for the expected *inter*molecular interactions to compete with. Therefore, several possible modifications of the bridging unit were considered to optimize the magnitude of the *intra*molecular coupling.

3.2. Synthesis of biradicals

3.2.1. Weakly coupled spin 1/2 dimers

In order to achieve fine tuning of the magnetic exchange interactions in biradical systems we used conjugation control of the bridging unit with topologically aligned radicals in *para*-position. Theoretical studies emphasized the importance of the mutual orientation and relative distances in the crystal packing for the unimpeded magnetic coupling propagation.[26] The diacetylene fragment was introduced as the spacer into the π-system, giving rise to the biradical **84c**. It is expected that **84c** should feature little or no torsion within the molecule, which is essential for the weak *intra*molecular coupling. The synthesis of nitronyl nitroxide radicals (NN) relied, in general, on the condensation between 2,3-bis(hydroxyamino)-2,3-dimethylbutane with carboxaldehyde group, followed by the oxidation reaction of the condensation products. The key precursor towards **84c** - formyl derivative **84a** - was synthesized following the approach outlined in *Scheme 3.1*.

One of the most efficient methods for the assembly of the molecules containing acetylene fragments relies on Glaser homo-coupling.[27] Regardless of the different coupling conditions tested, we could achieve only traces amounts of the dialdehyde **84a** employing direct Glaser coupling methodology to 4-ethynylbenzaldehyde **85**. Thus, another route was undertaken, where the aldehyde function was at first protected with

ethylene glycol affording the acetal precursor **86**.[28] The ^{1}H NMR spectrum of **86** showed characteristic signals of the dioxolane ring at 4.0 ppm (-CH_3, methylene groups) and at 6.7 ppm (-CH). The signal associated with the aldehyde group, on the contrary, was absent, hence ensuring the complete conversion into the aldehyde-protected intermediate. The dioxolane derivative **86** was subjected to Glaser coupling. The reaction required excess of copper (I) and (II) chlorides (7 eq. and 5 eq., respectively) in pyridine media, followed by acidic cleavage of the dioxolane ring in THF – water mixture (5:3). Here, appearance in the ^{1}H, ^{13}C NMR spectra of strong signals typical for the aldehyde fragments at 10.0 (^{1}H) and 191 (^{13}C) ppm, confirmed successful completion of the coupling reaction and formation of the desired diacetylene carbaldehyde **84a**.

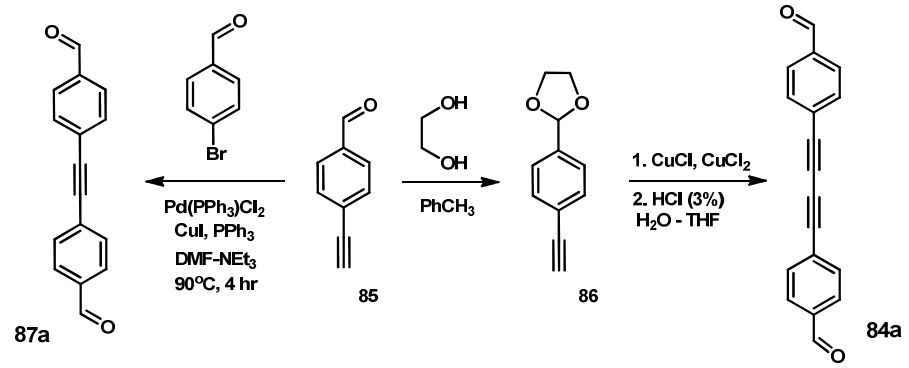

Scheme 3.1. Synthetic route employed for the assembly of the dialdehydes **84a**, **87a**.

To explore the potential of another closely associated derivative, the tolane dialdehyde **87a** was synthesized via Sonogashira-Hagihara cross-coupling reaction.[29] This system contains a shorter π-conjugated linker between the radical centres, hence the resulting through-bond exchange interaction is expected to be stronger in comparison to **84a**. The cross-coupling reaction between 4-bromobenzaldehyde and 4-ethynylbenzaldehyde **85** was carried out employing catalytic mixture of $Pd(PPh_3)_2Cl_2$, CuI, PPh_3 in the presence of base (Et_3N) and led to the formation of the dialdehyde **87a** in high yield (70%).

Among the most commonly used engineering tools for the rational design of molecular crystals are hydrogen bonding, π-π stacking formation, or strong dipolar interactions.[30] In this regard the diazatolane biradicals **88c** and **89c** were designed. It was anticipated, that additional contacts with heteroaromatic rings could offer a particularly attractive pathway for transmitting magnetic interaction.[31] Access to the family of the

diazatolane biradicals **88c**, **89c** required the synthesis of the key precursors **88a**, **89a**, which were prepared following Sonogashira-Hagihara methodology.[29] *Scheme 3.2* illustrates the synthetic sequence employed for the assembly of the 2,2'-diazatolane carbaldehyde **88a**.

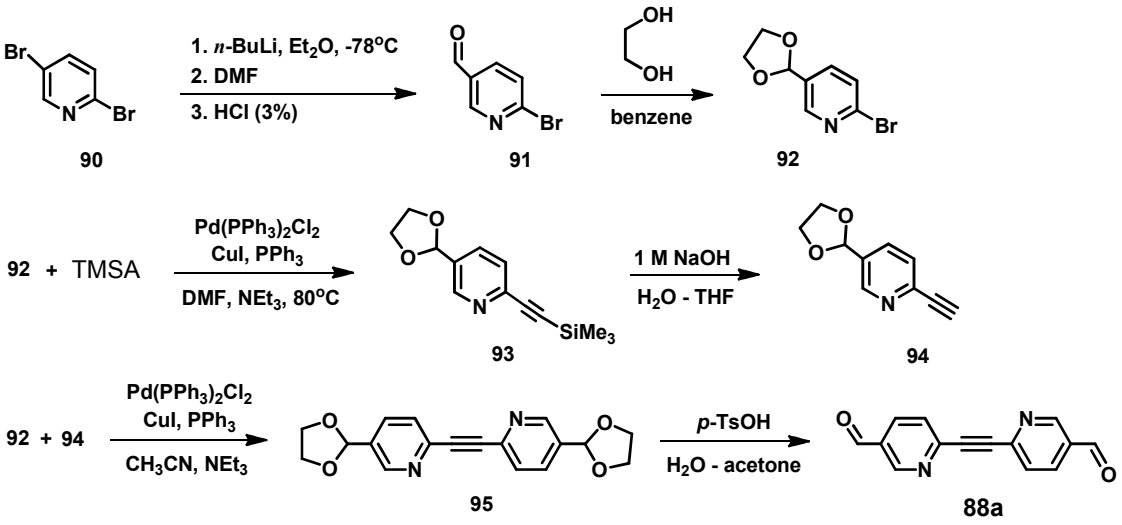

Scheme 3.2. Synthetic route employed for the assembly of the dialdehyde **88a**.

Interestingly, both structural isomers **88a**, **89a** could be achieved using reaction of commercially available 2,5-dibromopyridine **90** with *n*-BuLi, while the aldehyde function in **90** could be introduced selectively in *2* or *5* position according to necessity.[32-34] Reaction times and solvents play a crucial role on the direction of the electrophilic substitution, leading to the predominant formation of organolithium at the second or fifth position.[35,36] To drive the reaction in direction of the kinetically more stable 2-bromo-5-carbaldehyde-pyridine **91**, it was carried out in dry diethyl ether at -78°C, and DMF was added to the mixture 20 min after addition of *n*-BuLi was completed.

According to the preliminary results obtained in our group, 2-ethynyl-5-formyl-pyridine is unstable. Therefore, the aldehyde **91** was transformed into 2-bromo-5-[1,3]dioxolan-2-yl-pyridine **92** following the standard protocol,[28] which was obtained as a light-yellow oil. Intermediate **92** was involved into Pd-catalyzed Sonogashira-Hagihara coupling with trimethylsilyl acetylene (TMSA) giving derivative **93**. Hydrolysis of the trimethylsilyl group was realized in deaerated THF - water mixture (1:1) using 1N NaOH solution. The ethynyl derivative **94** was used further without additional purification.

Sonogashira coupling reactions were successfully carried out in various solvent mixtures. Among them the employment of the two combinations of the solvents was preferred - DMF/Et_3N (1:1) at 80°C and CH_3CN/Et_3N (1:1) at room temperature. It is worthy to note, that the use of CH_3CN/Et_3N showed some advantages compared to the former mixture. In fact, by preventing heating of the reaction, the products of the coupling were more easily isolated. Thus, the attachment of a 2-bromo-5-[1,3]-dioxolan-2-yl-pyridine **92** to the pre-organized 2-ethynyl-5-[1,3]-dioxolan-2-yl-pyridine **94** was carried out in the presence of $Pd(PPh_3)_2Cl_2$, CuI, PPh_3 catalysts and afforded the dioxolane derivative **95** in a fairly high yield (72%). Notably, attempts to remove the protective group in the presence of HCl (3%) led to the precipitation of the acid by the triple bond. Therefore, the final step towards **88a** was accomplished employing milder conditions. Here, to a solution of compound **95** in acetone-water mixture (7:1) a catalytic amount of *p*-TsOH acid (2 mol%) was added. Stirring the mixture for 3 days at room temperature granted the target 2,2'-diazatolane dialdehyde **88a** in high yield (81%).

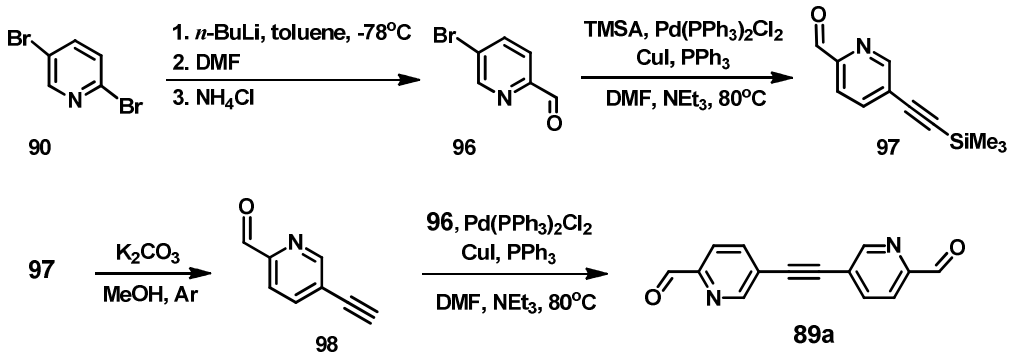

Scheme 3.3. Synthesis of the dialdehyde **89a**.

The isomeric 3,3'-diazatolane dialdehyde **89a** was obtained in a similar way. Thus, 2,5-dibromo-pyridine was selectively monolithiated in position *2* in toluene media. The time of the exchange reaction with *n*-BuLi was increased till 90 min to ensure the formation of the desired organolithium intermediate.[34] The mixture was quenched with stoichiometric amounts of DMF, and afforded carbaldehyde **96** using procedure described previously for 2-bromo-5-pyridine carbaldehyde **91**. The derivative **96** was isolated by chromatography on silica gel in a relatively good yield (49%). During the next steps standard Sonogashira-Hagihara methodology[29] was employed, and final separation on a

column with hexane/EtOAc eluent mixture (3:2) provided 5,5′-ethyne-1,2-diylbis(pyridine-2-carbaldehyde) **89a** in 69% yield.

Typically, imino nitroxides demonstrate decreasing of the J_{dimer} value. Taking this fact into account, already known bridges could be used, where otherwise the intramolecular exchange coupling was too large. Therefore, two bisimino nitroxides **99d**, **100d** were considered. There are several possible ways to obtain biphenyl-4,4'-dicarbaldehyde **99a**.[27] Inspired by the efficiency and simplicity of the approach sketched in *Scheme 3.4*, commercially available 4,4′-dibromobiphenyl **101** was treated with *n*-BuLi in the presence of catalytic amount of TMEDA in dry THF at -78°C. After addition of dry DMF the mixture was further stirred for 1 h at the same temperature, and than the temperature was slowly raised to ambient. The mixture was acidified with a saturated ammonium chloride solution and extracted with Et_2O. Purification via chromatographic column afforded biphenyl carbaldehyde **99a** in 58% yield.

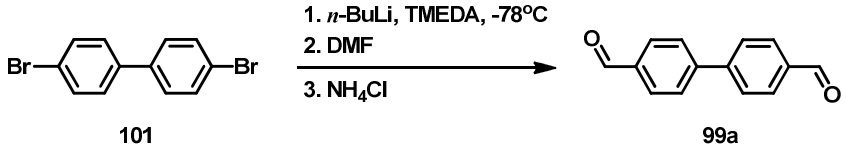

Scheme 3.4. Synthesis of dialdehyde **99a**.

Two- or ideally three dimensional structures able to demonstrate permanent magnetization based on metal complexes with organic spin carriers are of great interest. In this vein, imino radical **100d** bearing two nitroxide radicals moieties symmetrically attached to the chelating core was a promising candidate.

Bipyridine-4,4'-dicarbaldehyde **100a** was achieved following the synthetic sequence outlined in *Scheme 3.5*. (i) Formation of 5,5′-bis-(bromomethyl)-2,2′-bipyridin **103**, using a procedure described by F. Vögtle;[37] (ii) subsequent Sommelet reaction, consisting of a nucleophilic attack of the corresponding bromo derivative **103** with hexamethylenetetramine in ethanol - water mixture (1:1).[38]

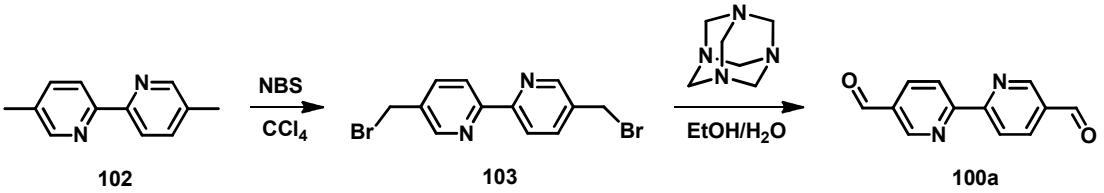

Scheme 3.5. Synthesis of dialdehyde **100a**.

The target nitronyl and imino nitroxide molecules could be routinely prepared as illustrated in *Scheme 3.6*. The condensation of the 2,3-diamino-*N,N'*-dihydroxy-2,3-dimethylbutane with carbaldehydes is an air-sensitive process and required, therefore, strict anaerobic conditions and degassed solvents. As a general rule, reaction with dialdehydes **84a**, **87a**, **88a**, **89a**, **99a**, **100a** was performed in deaerated toluene under argon at 110ºC, and afforded the corresponding *N,N'*-dihydroxyimidazolidines **84b**, **87b**, **88b**, **99b**, **100b** with quantitative yields. The condensation between compound **89a** with BHA was realized in absolute degassed methanol at room temperature.

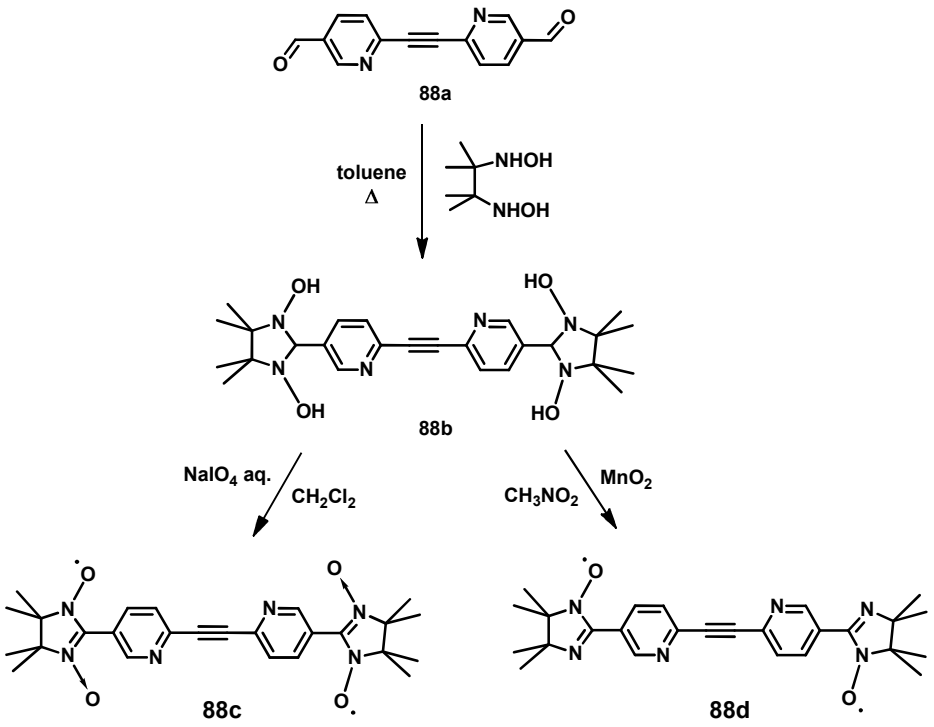

Scheme 3.6. Condensation of the dialdehyde **88a** with BHA followed by the oxidation of the imidazolidine **88b** into biradicals **88c**,**d**.

Once formed, the radical precursors (e.g. **88b** in *Scheme 3.6*) precipitated during the condensation step, and they were isolated by filtration as analytically pure (from ^{1}H-NMR spectra) white or yellowish powders. The ^{1}H-NMR spectra of these intermediates exhibited characteristic peaks of the hydroxy groups (~7.8-8.0 ppm, marked with the letter *a* in *Figure 3.2*) and the nodal proton located at the second position of the imidazolidine ring (~4.7 ppm, -CH group, labelled with the letter *d*). To illustrate this, the ^{1}H NMR spectrum of the condensation product **87b** is represented in *Figure 3.2*. Here, the remaining in the sample toluene is specified with the red asterisk.

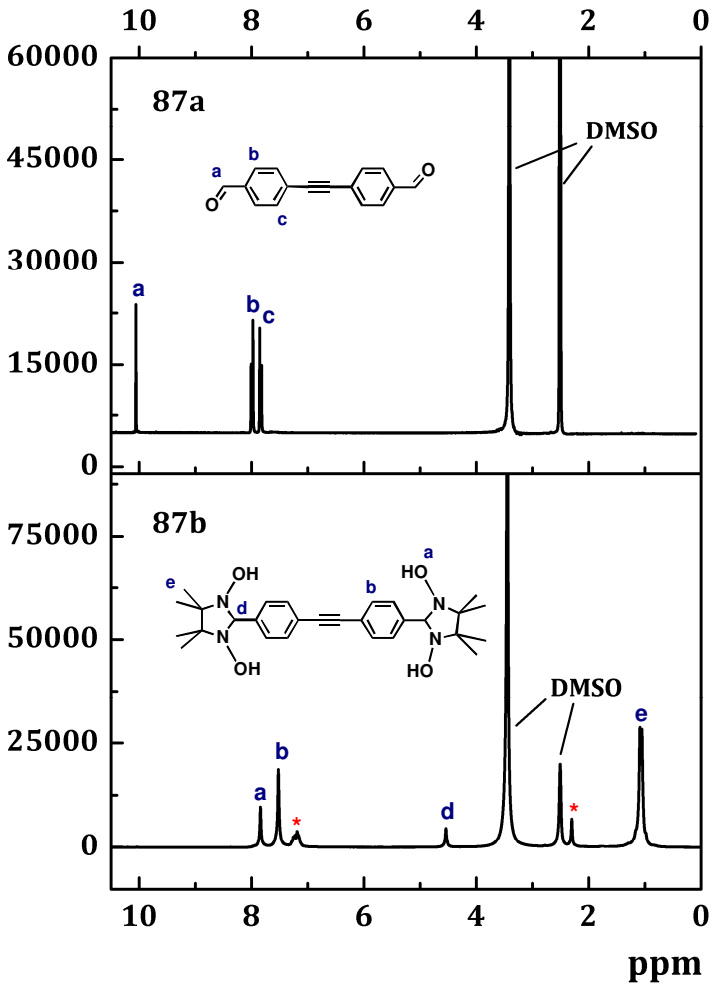

Figure 3.2. NMR spectrum of **87a**,**b** in DMSO at 250 MHz (128 and 105 scans correspondently). The intensities of the solvent signals differ so much due to the significantly lower solubility of the dialdehyde **87a** in DMSO. The red asterisk indicates toluene.

Oxidation of the *N,N'*-dihydroxyimidazolidines **84b**, **87b**, **88b**, **89b** with sodium periodate in a biphasic media of dichloromethane and water afforded nitronyl biradicals **84c**, **87c**, **88c**, **89c** (*Scheme 3.6*).[39] In order to avoid both further oxidation of the radicals to imino nitoxides, and to diminish the loss of the radical units, the reactions were carried out at T = 0-5°C using an ice bath. This method was preferred over the one, where solid metal oxides were applied as oxidizing agents,[40,41] because it allowed a better control of the oxidation reaction by using stoichiometric amounts of periodate in solution. The progress of the reaction was monitored by TLC of the reaction mixture aliquots. For the oxidation of imidazolidine **89b** excess of MnO_2 in methanol was found more appropriate.

To aid interpretation of the magnetic properties of isomeric NN **87c**, **88c** related **87d**, **88d** and two other IN biradicals **99d**, **100d** were also prepared. [42] Several methods for the preparation of the imino nitoxides from the precursors are reported in the literature.[43] Typically, the imino biradicals **87d**, **88d**, **99d**, **100d** were obtained using the procedure described by Tretyakov et al., since this method helped to avoid the usage of acids and to synthesize the target molecules in higher yields. Therefore, the transformation of *N,N'*-dihydroxyimidazolidine **88b** into the corresponding imino biradical **88d** depicted in *Scheme 3.6* was realized in CH_3NO_2 media with excess of MnO_2. All the biradicals were purified employing flesh-column chromatography on silica gel.

Systematic search and study of structurally similar compounds exhibiting different magnetic behaviour may be a rational approach to understand the correlation between the substituents in the aromatic ring and the intramolecular exchange constant J_{dimer}. In fact, modifications within the π-system often lead to various changes in the geometry of the molecule, caused by torsional demands. Therefore, some models with the functionalization in 2 and 2' positions of the tolane bridge were designed, as represented in *Figure 3.3*. These could be considered self complimentary as by combining two units in a 1:1 fashion (i.e. pyridine or NH_2 vs. OH), but also for larger self assembling units as through carboxyl groups forming strong hydrogen bonds, which could also be used for metal ion ligation (*Fig. 3.3*).

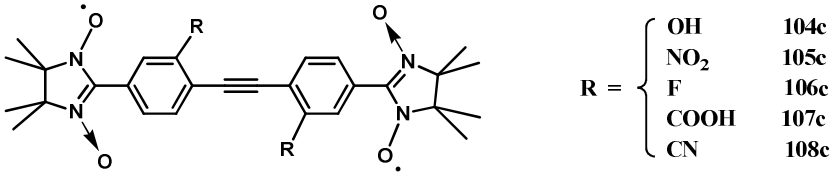

Figure 3.3. Promising for hydrogen-bonding targets.

The approach towards 4,4'-bis[2-(5-formyl-3-hydroxyphenyl)ethinyl]benzaldehyde **104a** was based on Sonogashira-Hagihara coupling reaction. Among several conditions described in the literature,[44,45] the one reported by Tamaru[46] was found to be the most appropriate, leading to the precursor **110** in high yield (75%). Treatment of the trimethylsilyl group in **110** with anhydrous K_2CO_3 in methanol resulted in a dark-red mixture of unidentified side-products. Hence, reaction was carried out in deaerated THF using 1M TBAF solution. Obtained after evaporation of the solvent residue was purified through a short column with silica, leading to the ethynyl derivative **111** in 69% yield.

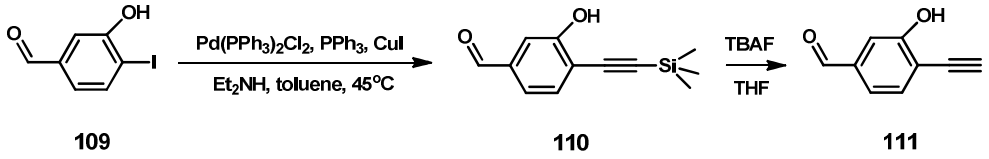

Scheme 3.7. Assembling the ethynyl precursor **111**.

Following the procedure described by Doye for the synthesis of diarylalkynes[47] Sonogashira-Hagihara cross coupling between the precursors **109** and **111** was realized. However, after chromatographic separation instead of the target hydroxy carbaldehyde **104a** the benzofuran derivative **112a** was collected as the major product in 23% yield (*Scheme 3.8 (a)*). In the next place conditions of the tandem synthesis were tested.[47] At first, Pd-catalyzed Sonogashira-Hagihara coupling of 3-hydroxy-4-iodobenzaldehyde **109** (1 eq.) with (trimethylsilyl)acetylene in dry *i*-Pr_2NH/ toluene media at room temperature under argon was realized in 18 h. Potassium hydroxide (2 eq.) in water - methanol solution (2:1) was added to the mixture in one portion, and 3 h later the starting benzaldehyde **109** (1 eq.) was inserted into the reaction flask. The stirring was continued for additional 16 h (*Scheme 3.8 (b)*). Here the procedure also led to the benzofuran dialdehyde **123a**, however, the titled compound was obtained in a higher yield (49%).

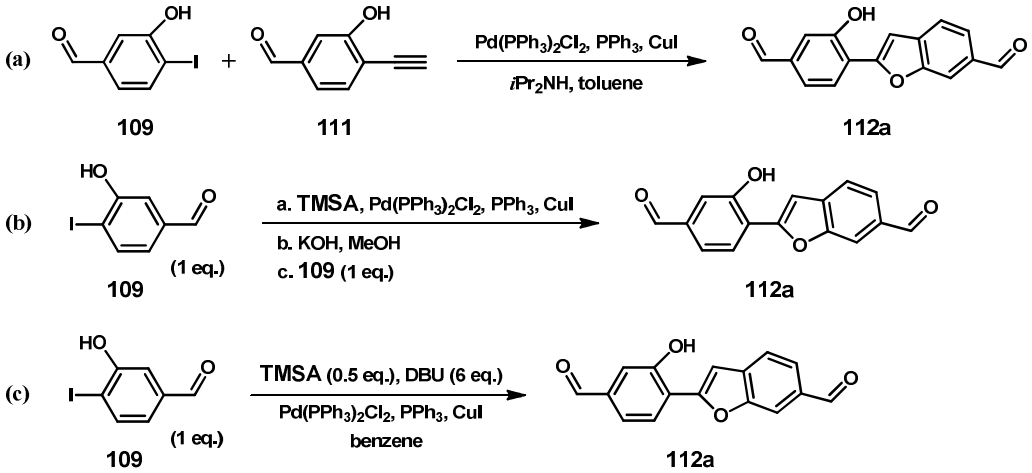

Scheme 3.8. Synthetic sequences leading to the dialdehyde **112a**.

Interestingly, the 'one-pot' preparation of differently substituted benzofuranes from hydroxylated halobenzenes described in the literature required large excess of potassium hydroxide (10 eq.) and heating (60-75°C).[48] Although the applied here

conditions were quite different,[47] the attraction of the triple bond towards the neighbouring hydroxyl function in the presence of potassium hydroxide was considered to be responsible for the formation of the derivative **112a**. In effort to avoid the ring closure, one-pot Sonogashira-Hagihara coupling reaction was carried out (*Scheme 3.8 (c)*).[49] Nevertheless, this attempt to obtain the hydroxy derivative **104a** led to the benzofuran carbaldehyde **112a** in high yield (78%). Hereby, it turned out, that for successful synthesis of the compound **104a** a prior protection of the hydroxy functional groups is essential. The work in this direction is in progress.

The condensation between the carbaldehyde **112a** and BHA was realized in deaerated methanol - toluene mixture (1:1). Although full conversion of the starting dialdehyde **112a** into the corresponding imidazolidine **112b** required 15 days stirring at the room temperature, our trials to carry out the reaction under the heating in toluene (110°C) or toluene/methanol mixtures (60°C) led to the decomposition of the condensation product (**112b**) and formation of unidentified side-products. Oxidation of the derivative **112b** with sodium periodate in DCM/water mixture (3:1) at ~0-5°C following the procedure described above (*Scheme 3.6*) granted the benzofuran biradical **112c** in 24% total yield.

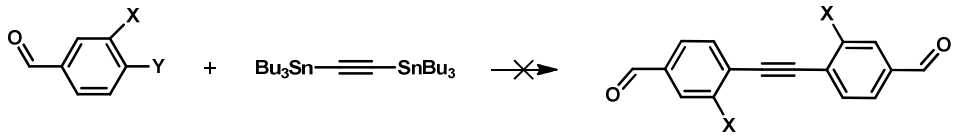

109 X = OH Y = I
113 X = NO_2 Y = Br
114 X = F Y = Cl

104a X = OH
105a X = NO_2
106a X = F

Scheme 3.9. Stille-based approach towards dialdehydes **104-106a**.

Beyond doubts Sonogashira-Hagihara cross-coupling reaction is the major approach applied for the assembly of alkyne derivatives nowadays. However, successful synthesis of the ethynyl-bridged compounds bearing strong electron-withdrawing (e.g. F, NO_2) substituents in ortho-position usually demands other methodology. In 1999 Fu first reported the general method of execution of Stille reaction for inactivated aryl chlorides.[50] The system employing palladium catalyst and P(*t*-Bu)$_3$ ligand in the presence of CsF worked effectively for electron-deficient, electron-rich and hindered aryl chlorides.[50] The work of Baldwin had significantly widened the scope of Stille reaction.[51] It was shown, that the use of copper (I) iodide and caesium fluoride combination allowed

the synthesis of sterically hindered systems and promoted electronically disfavored coupling reactions.[51] The conditions were mild and compatible with a variety of functional groups. Therefore, it was thought to synthesize the target carbaldehydes **104-106a** using the improved Stille coupling reaction,[51] but regardless of the conditions tested, the titled compounds could not be obtained via direct coupling of the formyl-arylhalides with bis(tributylstannyl)acetylene. According to FD-mass analysis of the trials homo-coupling derivatives were obtained as the major products. Conditions of all experiments are listed in *Table 3.1*.

Table 3.1. Conditions applied for Stille coupling of **109**, **113** and **114** with bis(tributylstannyl)acetylene.

Compound	Catalyst	Solvents	T	Time
109	$Pd(PPh_3)_2Cl_2$, CuI, PPh_3	DMF, NEt_3	40°C	48h
113	$Pd(PPh_3)_4$, CuI	toluene	90°C	96h
113	$Pd(PPh_3)_4$, CuI, CsF*	DMF	100°C	16h
113	$Pd(PPh_3)_2Cl_2$, CuI, PPh_3	DMF, NEt_3	40°C	48h
114	$Pd(PPh_3)_4$, CuI, CsF	DMF	100°C	48h
114	$PdCl_2$, $P(^tBu)_3$, CuI, PPh_3	DMF	80°C	48h
114	$PdCl_2$, $Pd[P(^tBu)_3]_2$, CuI, PPh_3	DMF	80°C	48h
114	$PdCl_2$, $Pd[P(^tBu)_3]_2$, CuI, PPh_3	dioxane	100°C	72h
114	$Pd(dba)_2$, $Pd[P(^tBu)_3]_2$, CuI, PPh_3	dioxane	100°C	72h

*CsF was additionally dried on high-vacuum line before use for 1,5h

Modification of the amino group opens a wide scope of possibilities to introduce various substituents into the aromatic system. Thus, 2-bromoaniline **116** was selectively transformed into 4-amino-3-bromobenzaldehyde **117** under mild conditions: a mixture of the aromatic amine in DMSO, conc. aqueous HCl and dried CuCl was heated at 90°C for ~ 5-6 hours.[52] The subsequent work-up of the reaction mixture afforded the aldehyde **117** in high yield (80%). Heating of the derivative **117** with CuCN in dry and deaerated DMF at 120°C during prolonged time slowly led to the formation of the cyano-derivative **118**, but

full conversion was not achieved even after 72 hours.[53] Metal-catalysed cyanation is not that common, since cyanide ions are poisonous for the catalytic cycle. However, cyanation of the benzaldehyde **117** was successfully realized in the presence of catalytic amount of $Zn(CN)_2$,[54] which facilitated the transmetallation of cyanide to the aryl palladium halide species, and provided the derivative **118** in 70% yield. The compound **118** was subjected to Sandmeyer reaction[55] leading to the one of the key pre-cursors for Sonogashira-Hagihara coupling - the iodo derivative **119** in high yield. The further work to optimize the synthetic procedure towards **108a** is currently on-going.

It appeares to be clear, that the idea first to assemble the functionalized tolane dialdehyde **115a** and further to substitute the bromide for cyano/nitro/etc group has certain advantages. This approach is outlined in *Scheme 3.10*. Moreover, the tolane framework in **115a** could be functionalized, employing for example mild conditions described above for the synthesis of the benzaldehyde **118**.

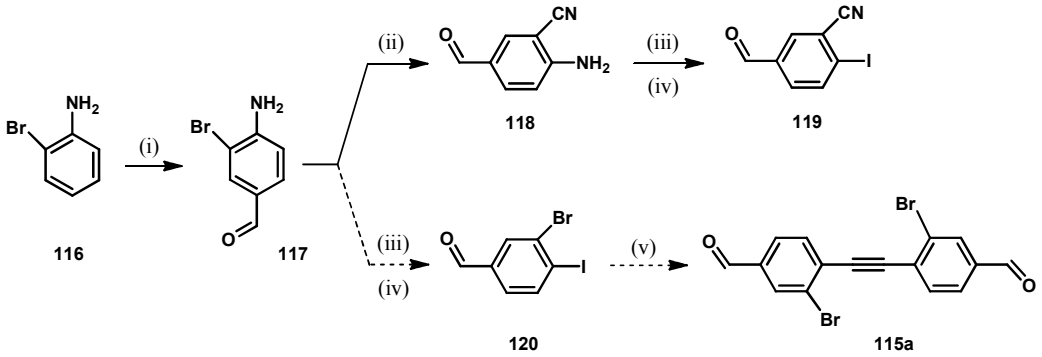

Scheme 3.10. Alternative pair for cross-coupling reaction. Conditions: (i) CuCl, DMSO, HCl; (ii) ZnCN, $Pd(PPh_3)_4$, 80°C; (iii) $NaNO_2$, HCl, 0°C; (iv) I_2, KI; (v) $Pd(PPh_3)_2Cl_2$, CuI, PPh_3.

The nitronyl **84c**, **87-89c**, **112c** and imino **87d**, **88d**, **99d**, **100d** nitroxides with various π-bridges between the radical centers were synthesized following the classical Ullman procedure.[56] These purely organic biradical systems can be used for studying the phenomenon of Bose-Einstein condensation (BEC) of magnetic excitations[23,24] under well-controlled conditions.[25] Their crystal structure characterization, photophysical properties and magnetic behaviour are discussed in detail later in the present chapter.

3.2.2. Ethynyl-bridged biradical systems – challenges and achievements

Continuing our interest in materials encoding spontaneous magnetization, which is one of the most challenging and demanding tasks nowadays,[57,58] compounds **121-123c** were designed. The organic based magnetic materials composed only of light elements such as carbon, hydrogen, nitrogen, and oxygen, are expected to provide properties that cannot be found in traditional inorganic metal based magnets, such as low density, transparency, low-temperature fabrication, and easy processability.[59]

The π-topology plays crucial role in spin manipulation of the π-conjugated organic spin systems. Therefore, structurally similar model compounds **121c** and **122c**, **123c** were expected to possess low- and high-spin ground states, respectively, in accordance with the valence bond theory of topological symmetry of alternant hydrocarbon π-systems (as outlined in the first chapter of this thesis), which predicted high-spin ground-state for compounds based on *m*-phenylene bridging block.[60,61] The key in obtaining magnetic ordering is the formation of high spin domains.[62] The sign of the molecular exchange interaction (J) can be either positive or negative depending on the coupling unit between the radical sites and their steric demands. It follows, that control of geometry and topology are essential for design of the molecules with the predictable spin states.[63] In fact, tailoring the structures in such a way, that the spin carrying units were attached to the aromatic ring through acetylene bridges, was thought to prohibit the twisting, and thus to guarantee the planar geometry of the molecules (*Fig. 3.4*).

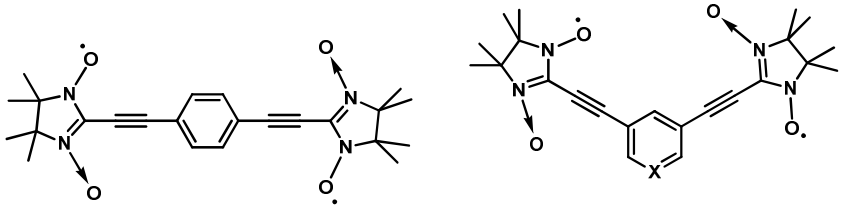

Figure 3.4. Target molecules.

Paying tribute to Sonogashira-Hagihara cross-coupling reaction, which is one of the most efficient and convenient methods, allowing to introduce the acetylene-moiety into the molecular structure,[29] scientists studied the applicability of this method for the assembly of the π-bridged nitroxide radicals. For example, Miura reported synthesis of

conjugated polymers with high spin density ~1.31×1021 spins/g.[64] To the best of our knowledge, such examples are rare, mainly due to the loss of the radical species on the coupling step. In this light the idea to synthesize target molecules **121c**, **122c** and **123c** employing Sonogashira methodology seemed to be a tempting and challenging task.

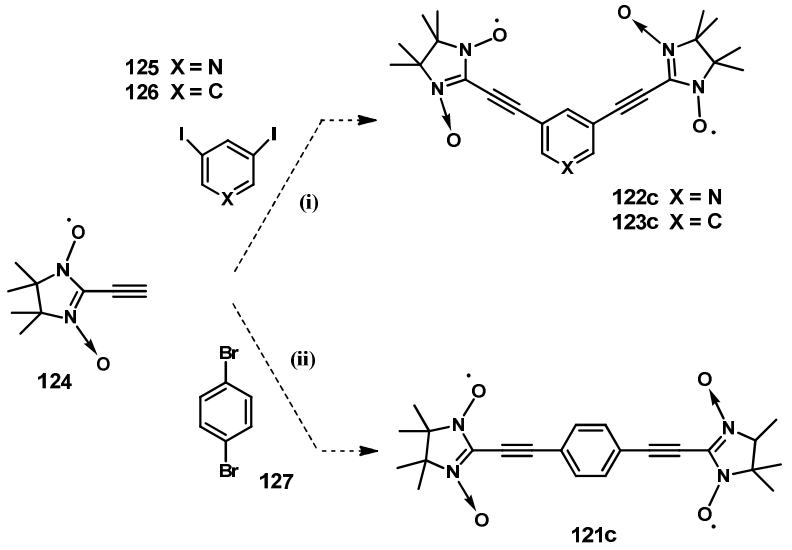

Scheme 3.11. Strategy based on Sonogashira-Hagihara cross coupling reaction. Conditions applied: (i) ethynyl-nitroxide **124** (2 eq.), diiodoaryl **125** or **126** (1 eq.), $(PPh_3)_2PdCl_2$ (5 mol%), CuI (2 mol%), NEt_3/pyridine (1:4); (ii) ethynyl-nitroxide **124** (2 eq.), dibromobenzene **127** (1 eq.), $Pd(OAc)_4$ (8 mol %), CuI (11 mol%), toluene/NEt_3 (1:10).

Ethynyl containing nitronyl radical **124** was obtained following the reported procedure.[65] When applying conditions described by Miura,[64] after 15 min the mixture turned dark brown, and 1 h later TLC showed the absence of the starting nitroxide radical **124**, although no traces of a new radical species were observed.

Nitronyl nitroxides are sensitive to the presence of triphenyl phosphine and can undergo competing reduction reaction. Accordingly, for the second set of experiments coupling conditions described by Tretyakov were examined (*Scheme 3.11*).[66] Here, the catalytic mixture of $Pd(OAc)_4$ and CuI was preferred, and in 1 h the starting nitroxide **124** was totally consumed. Formation of a minor bluish compound was detected by TLC, though no viable amounts of the desired biradical were isolated. It was assumed, that strong withdrawing effect of the NN fragment deactivated the terminal alkyne function and inhibited the catalytic processes. Therefore, nitronyl nitroxide **128** bearing iodine group was synthesized.[67] In addition to the procedures tested in our earlier trials conditions employing Pd(0)-catalysis were used,[68] as illustrated in *Scheme 3.12*.

However, in the first two sets of experiments the mixtures of unidentified products were formed. In the last case, unexpectedly, the mono-radical **128** underwent iodine-proton exchange reaction, yielding as a result bright pink nitronyl nitroxide **130**.[‡‡]

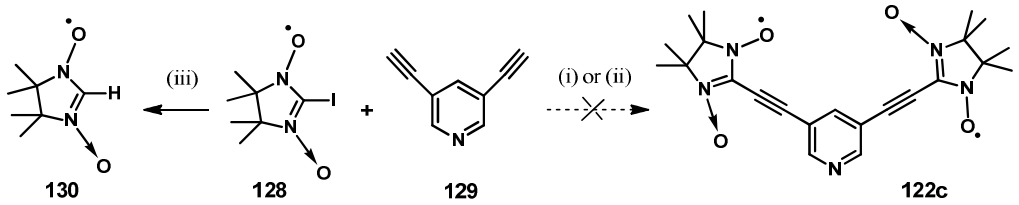

Scheme 3.12. Alternative pair for cross-coupling reaction. Conditions applied: (i) ethynyl-nitroxide **124** (2 eq.), diiodoaryl **125** or **126** (1 eq.), $(PPh_3)_2PdCl_2$ (5 mol%), CuI (2 mol%), NEt_3/pyridine (1:4); (ii) ethynyl-nitroxide **124** (2 eq.), dibromobenzene **127** (1 eq.), $Pd(OAc)_4$ (8 mol %), CuI (11 mol%), toluene/NEt_3 (1:10); (iii) iodo-nitroxide **85** (2 eq.), diiodpyridine **86** (1 eq.), $Pd(PPh_3)_4$ (10 mol%), CuI (8 mol%), *i*$PrNH_2$/benzene (1:3).

The strategy of the synthesis was reconsidered and our attention turned to the classical approach commonly employed for the synthesis of NN.[56] The key-precursor towards biradical **121c** could be obtained following the synthetic sequence suggested by our collaborator Naofumi Naga[§§] (*Scheme 3.13*), although this method contained a number of serious drawbacks and was found to be ineffective. For instances, the yield in the palladium-catalyzed reaction of 1,4-dibromobenzene **127** with propargyl alcohol **131** appeared to be initially good, but the crude contained only moderate amount of the target dialkohol derivative **132** (~25%). The mono-substituted species was isolated from the mixture as the main product.

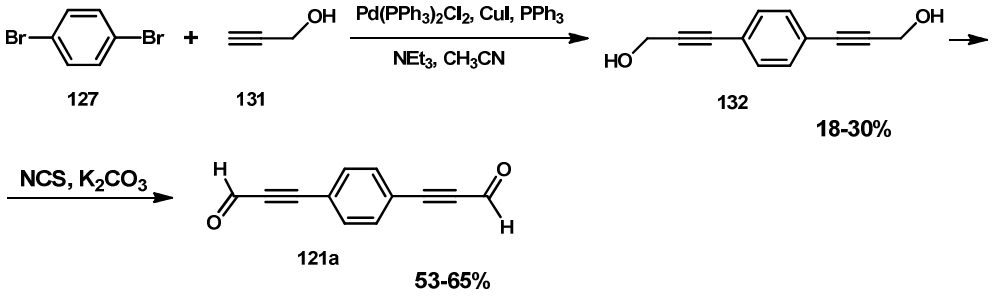

Scheme 3.13. Initial approach towards dialdehyde **121a**.

[‡‡] nitronyl nitroxide **130** possesses untypical for this class of compounds color.
[§§] Naofumi Naga, Shibaura Institute of Technology, 3-7-5 Toyosu, Koto-ku, Tokyo 195-8548, Japan.

An alternative route towards assembling the target dialdehyde **121a** was proposed and successfully realized. The 1,4-diethynylbenzene derivative **134** was synthesized applying standard Sonogashira-Hagihara coupling methodology in acetonitrile/triethylamine mixture in high yield. The intermediate phenylpropargyl dialdehyde diethyl diacetal **135** was then prepared,[69] following the literature procedure demonstrated in *Scheme 3.14*.

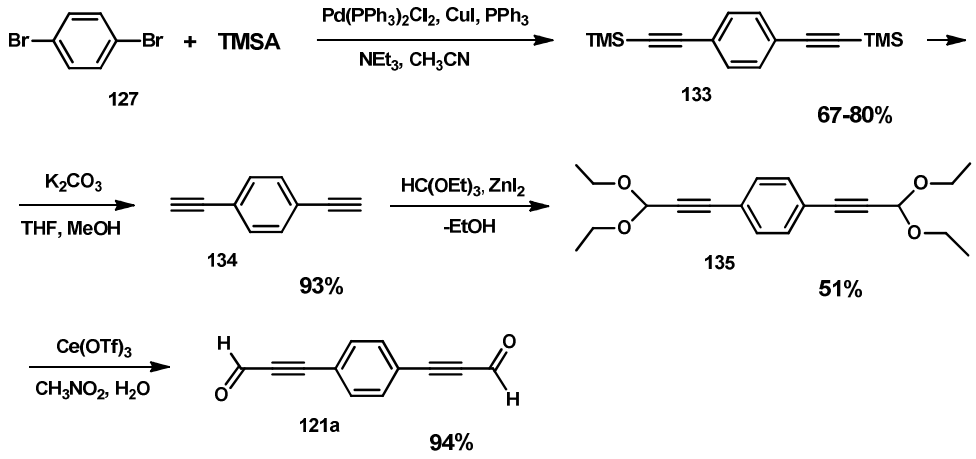

Scheme 3.14. Synthetic route employed for the dialdehyde **121a**.

The diethyl diacetal **135** was chemoselectivly cleaved using catalytic amounts of cerium(III) trifluoromethane sulfonate and water in nitromethane (*Scheme 3.14*). The so-obtained dialdehyde **121a** was used further without additional purification. Compound **121b** appeared to be not stable, and our attempts to realize the condensation of the corresponding dialdehyde **121a** with BHA each time led to a different product. Probably, the classical Ullman procedure towards α-ethynyl-substituted imidazolidine derivative **121b** didn't proceed smoothly due to the rearrangement reaction.[70]

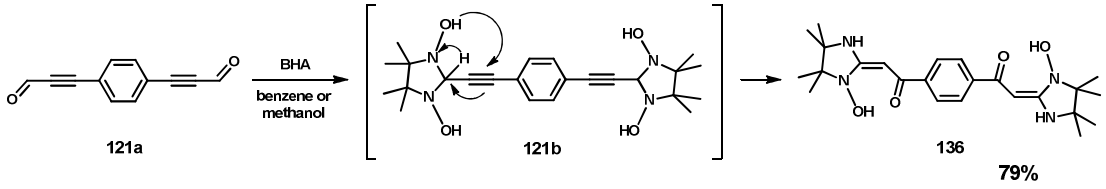

Scheme 3.15. Proposed mechanism of the competing reaction leading to a thermodynamically more stable keto vinyl derivative **136**.[70]

Thus, during the oxidation tests carried out on small amounts of the obtained yellowish precipitate no traces of nitronyl or imino radicals were observed. Moreover, the

absence of a signal in the visible range (~600 nm) characteristic for the n-π^* transition of the nitronyl moiety, as well as the absence of the typical absorption at ~470 nm[31] suggested formation of an alternative compound **136**.[70]

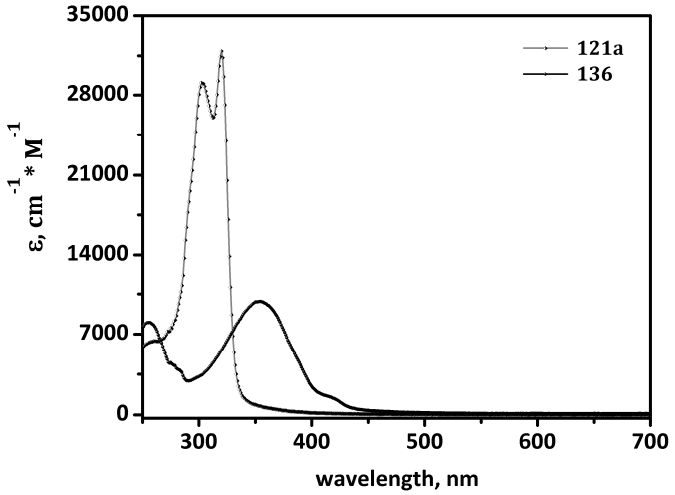

Figure 3.5. UV-Vis spectra of the derivatives **121a** and **136** recorded in THF.

From the other hand, the obtained UV-Vis spectra was found to be similar to the data reported for the (*R*)-2-(1-hydroxy-4,4,5,5-tetramethylimidazolidin-2-ylidene)ethanones (enaminones)[70,71] of general structure represented in *Figure 3.6*. Moreover, IR and ^{1}H NMR spectra were found to be consistent with the structure of the derivative **136**. Thus, proton NMR spectra featured significant broadening of the lines attributed to the –NH and –OH groups (9.01, 9.42 ppm) due to an exchange process and a singlet of doubled intensity corresponding to the =CH fragment (5.49 ppm). The proposed mechanism of this spontaneous rearrangement is represented in *Scheme 3.15.*

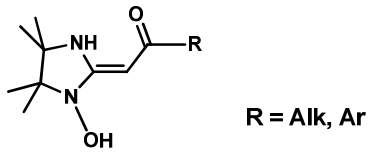

Figure 3.6. General structure of the enaminone derivatives.[70]

Comparison of the IR envelopes of the precursor **121a** and the product of the condensation **136**, revealed disappearance of a strong vibration band at ~2187 cm^{-1}, attributed to the stretching mode of the conjugated ≡C-C=O fragment in the starting dialdehyde **121a**, along with the loss of the corresponding to the aldehyde group signal at

1643 cm^{-1}. The newly arose broad signal at ~2792 cm^{-1} correlated with the literature reported data for the amino group in cyclic compounds.[72]

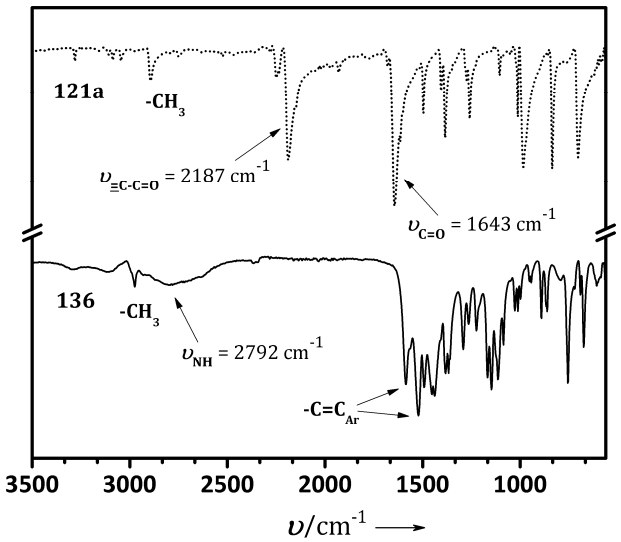

Figure 3.7 Comparison of FT-IR spectra of the starting dialdehyde **121a** with the condensation product **136**.

Summarizing, our attempts to obtain alkyne-substituted nitronyl nitroxides 121-123c included Pd-catalyzed Sonogashira-Hagihara coupling[64-68] and classical Ullman procedure.[56] However, the target radicals were not achieved using different coupling conditions[64-68] with ethynyl- 124 or iodo- 128 nitronyl derivatives as the starting compounds. Moreover, the reaction of the propargyl dialdehyde **121a** with 2,3-dihydroxylamino-2,3-dimethylbutane led to the formation of 1,4-di[2-(1-hydroxy-4,4,5,5-tetramethyl-2-ylidene)ethanone]-benzene **136**. One should admit that the task is rather challenging and deserves further consideration.

3.3. Crystal structure analysis of the biradicals

In this section the central point is devoted to the analysis of the structural factors that characterize five nitronyl nitroxide biradicals (namely **84c**, **87-89c**, **112c**). The structures of the four imino biradicals **87d**, **88d**, **99d**, **100d** are also reported. Single-crystals suitable for X-ray analysis were obtained by slow diffusion of dichloromethane-hexane mixture (1:4) for nitronyl **84c**, **87-89c**, **112c** and imino radicals **87d**, **88d**, **99d**, **100d** at room temperature. Deep-blue needle crystals of nitronyl nitroxides and red blocks of

imino nitroxides were analyzed by X-ray diffraction and their ORTEP drawings are given in *Figures 3.8-3.25*. Pertinent crystallographic parameters and refinement data are listed in *Table 3.3*; selected torsion angles are reported in *Table 3.2*. The synthesized nitroxides **84c**, **87c**, **88c**, **89c**, **87d**, **88d**, **99d**, **100d** possess a planar backbone, which is essential in propagating the weak *intra*molecular coupling. Furthermore, the torsion angles θ have a crucial influence on modulating further the magnetic exchange interactions in biradicals. Small differences in θ torsions (~ 25°), as witnessed in the derivatives **84c**, **87c**, **88c**, should give nearly identical degree of conjugation. Hence, similar spin polarization effects, and, consequently, very close values of the exchange integrals, should be present in these radical systems. Surprisingly though, in the nitronyl nitroxide **89c** the radical units are far more twisted (~ 53°). Thus, from its preliminary crystal structure analysis it was assumed, that the biradical **89c** would exhibit different intramolecular exchange energy with respect to the other bisnitronyl nitroxides (**84c**, **87c**, **88c**), and, consequently, a different magnetic behaviour should arise.

Table 3.2. Selected torsion angles and bond lengths for the nitroxide biradicals

	Radical	d, Å[a]	θ, deg[b]
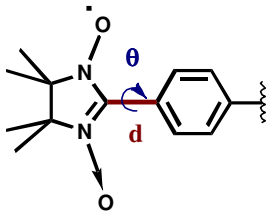	**84c**	1.460	25.0 ± 1
	87c	1.459	24.4 ± 1
	88c	1.454 ± 0.002	23.5 ± 1
	89c	1.472	52.5 ± 1
	87d	1.475	4.8 ± 1
	88d	1.473 ± 0.002	23.1 ± 1
	99d	1.471	17.5 ± 1
	100d	1.473	16.4 ± 1

[a] distance values were averaged (error within 0.002 Å);
[b] angle values were averaged (error within 1 degree).

Table 3.3. Selected spectroscopic data for the nitronyl **84c**, **87-89c**, **112c** and imino **87d**, **88d**, **99d**, **100d** nitroxide biradicals[i]

	84c	**87c**	**88c**	**89c**	**112c**	**87d**	**88d**	**99d**	**100d**
Formula	$C_{30}H_{32}N_4O_4$	$C_{28}H_{32}N_4O_4$	$C_{26}H_{30}N_6O_4$	$C_{26}H_{30}N_6O_4$	$C_{28}H_{32}N_4O_2$	$C_{28}H_{32}N_4O_2$	$C_{26}H_{30}N_6O_2$	$C_{26}H_{32}N_4O_2$	$C_{24}H_{30}N_6O_2$
M	512	488	490	490	520	456	458	432	434
crystal system	monoclinic	monoclinic	triclinic	monoclinic	monoclinic	monoclinic	triclinic	monoclinic	monoclinic
space group	$P2_1/c$	$P2_1/n$	*P1*(no.2)	$P2_1/c$	$P2_1/c$	$P2_1/n$	*P-1*	$P2_1/n$	$P2_1/n$
a, Å	8.1768(2)	6.0834(4)	7.3674(2)	10.0305(5)	7.1223(6)	6.6883(2)	7.0420(3)	6.2359(6)	6.3011(2)
b, Å	19.0191(8)	11.2581(5)	13.0178(4)	10.5040(7)	18.2337(8)	10.3043(4)	12.9582(9)	10.5265(7)	10.4759(5)
c, Å	11.4935(5)	19.1236(9)	13.7189(4)	12.3508(6)	20.0867(9)	18.2359(5)	14.2234(9)	17.6917(9)	17.1953(7)
β, deg	103.4(2)	90.832(3)	104.498(2)	102.582(3)	99.260(3)	93.231(2)	103.761(2)	94.553(4)	98.045
V, A^3	1315.89(8)	1309.59(12)	1230.61	1270.04	2574.7(3)	1254.79(7)	1217.41	1157.66	1123.89(8)
Z	4	4	4	4	8	4	4	4	4
$R_{factor}(\%)$	7.32	4.53	5.4	5.5	4.64	4.01	6.21	5.18	5.26
D_c, $g \times cm^{-3}$	1.294	1.239	1.324	1.283	1.343	1.208	1.251	1.241	1.284
N_{ref}	3687	3784	7176	3696	5834	3669	6769	2527	3217
N_{par}	173	163	325	163	370	154	334	154	154
S	0.985	1.081	0.986	1.073	0.957	1.112	0.978	1.025	1.091
CCDC	816633	816635	823716	816632	858604	810139	816630	823717	858078

The crystallographic data were collected on Nonius Kappa CCD (Mo kα, μ = 0.71073 Å) diffractometer equipped with a graphite monochromator.

[i] X-ray structure analysis was performed by Prof. Dr. Volker Enkelmann at MPI-P (Mainz).

A single crystal X-ray diffraction study confirmed the molecular structure of the diacethylene-bridged nitronyl nitroxide **84c**. The compound crystallized in a transoid arrangement with a center of symmetry located in the central C1-C1' bond (*Fig. 3.8 (a)*). The derivative **84c** is fairly planar and there is a dihedral angle between the mean plane of the C6 ring and the imidazolidine moiety of 25°. In the present structure the distances between the N-O and C-N atoms of the radical subunits are similar: N(16)-O(18) 1.276; N(17)-O(19) 1.281; N(16)-C(9) 1.36; N(17)-C(9) 1.345 Å. The symmetry is due to the complete delocalization of the odd electron in the non-bonding orbitals of the 'ONCNO' core.

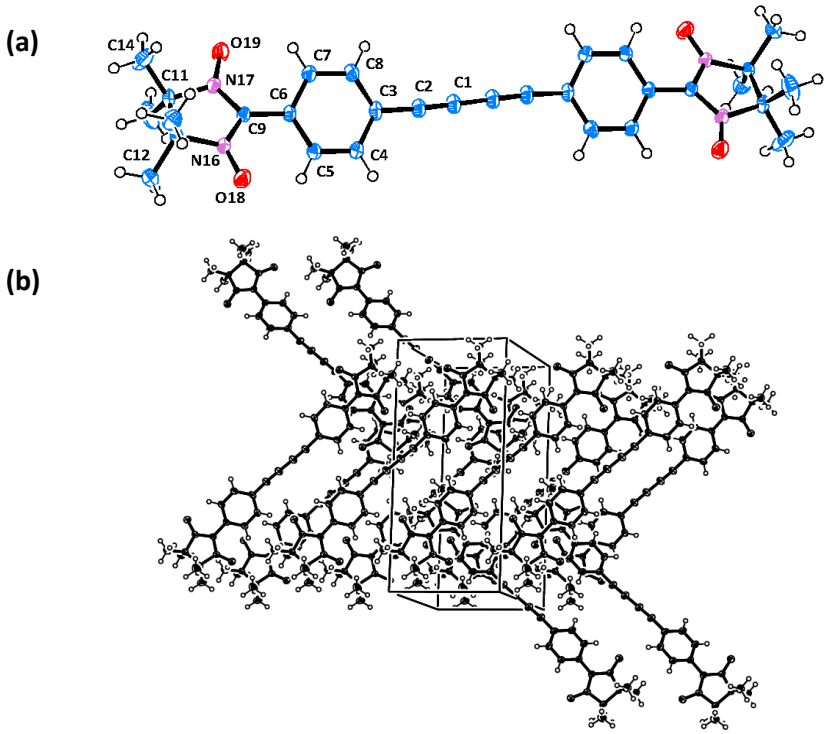

Figure 3.8. Crystal structure of **84c** with ORTEP drawn at the 50% of the probability level (as well as other pictures represented therein): (a) molecule; (b) crystal packing.

The N-O bonds and the C-N bonds distances are between the values of a single and a double bond. Closer examination of the crystal packing shows that the radicals are organized in a zig-zag fashion (O18 ···H133' 2.53 Å, *Fig.3.8 (b)*) with additional hydrogen bonds between the sheets formed by the C5 atom of the benzene ring with hydrogen atoms (C5 ···H71' 2.8, C5 ···H152' 2.86 Å, *Fig.3.9*).

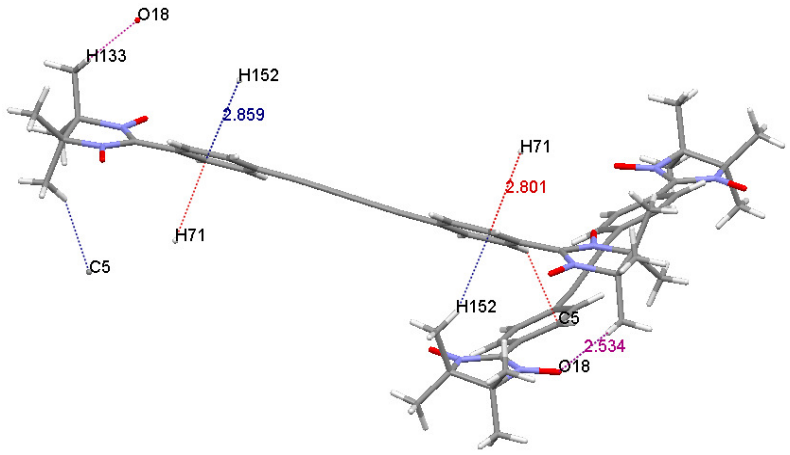

Figure 3.9. Fragment of the crystal packing of **84c** with emphasized short contacts and π-stacking**.**

The molecular structure of compound **87c** (*Fig. 3.10*) is similar to the previously reported biphenyl nitronyl nitroxide,[25] which has the same space group ($P2_1/n$). Probably, analogous cell organization can be explained by similar crystallization conditions. The torsion angle between the plane of the benzene ring and the radical moiety is around 25°.

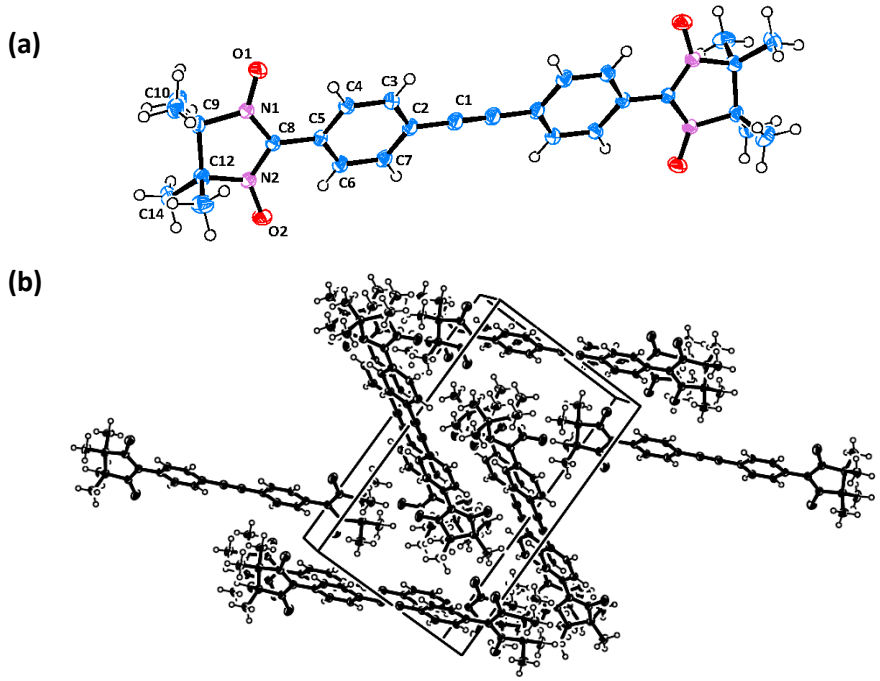

Figure 3.10. Crystal structure of **87c**: (a) molecule; (b) crystal packing.

Adjacent radicals are organized in a head-to-tail fashion forming *1D* network: the first N-O fragment of each radical unit is attached to C7, H71 atoms of the benzene ring, the second N-O group is joint to the methyl hydrogens of imidazolidine fragment. Geometrical parameters are: O2···H71' 2.52, O1···H141' 2.59, O2···C7' 3.16, C7···C13 3.40 Å; distance between H-bonded sheets is 2.36 Å (O1···H101').

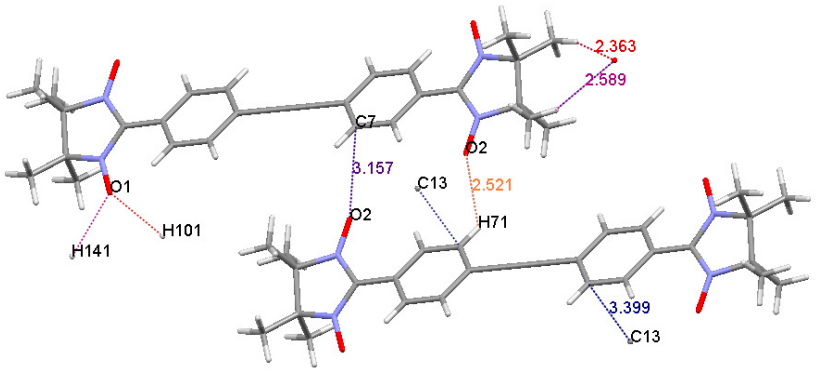

Figure 3.11. Fragment of the crystal packing of **87c** with emphasized short contacts**.**

Crystals of the imino nitroxide biradical **87d** have $P2_1/n$ group of symmetry. The structure of compound **87d** is shown in *Figure 3.12 (a)*. The θ angle (N1-C8-C5-C4) is around -5.50° and 4.0°, thus the overall tolane backbone is fairly planar. The N(2)-O(1) 1.271 Å bond distances are similar to previously described birdicals (for example, **84c**).

(a)

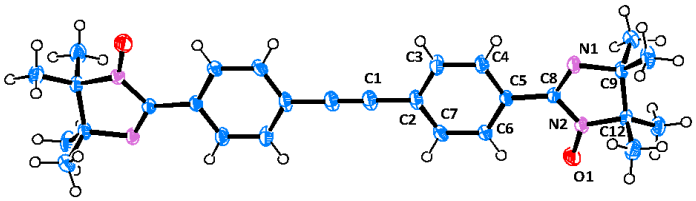

(b)

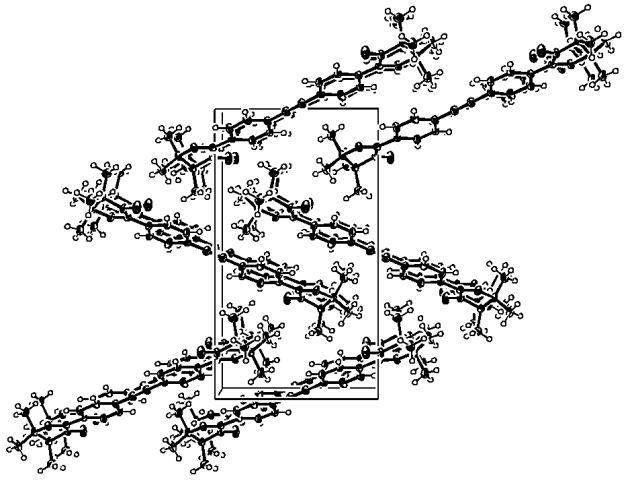

Figure 3.12. Crystal structure of **87d**: (a) molecule; (b) crystal packing.

Relevant intermolecular geometrical data are: O1···H141' 2.622, O1···H131' 2.654 Å - hydrogen bonds between NO group of the radical moiety and methyl groups; the angles within one molecule are nearly orthogonal ($\alpha \approx 90^\circ$ and $\beta \approx 93.2^\circ$) (*Fig. 3.13*). The radicals are organized in a zig-zag fashion (*Fig. 3.12 (b)*) with additional hydrogen bonding between the sheets formed by C atom of the benzene ring with C atom methyl group of the radical moiety: C7···C10' 3.387 Å. The shortest distance between the O(1) atoms of the N-O groups to the adjacement C(4) atoms of the benzene moieties is 3.31 Å (O1··· C4'). Consequently, the paramagnetic centers in the solid phase of imino nitroxide **87d** species are substantially spaced from each other (*Fig. 3.13*).

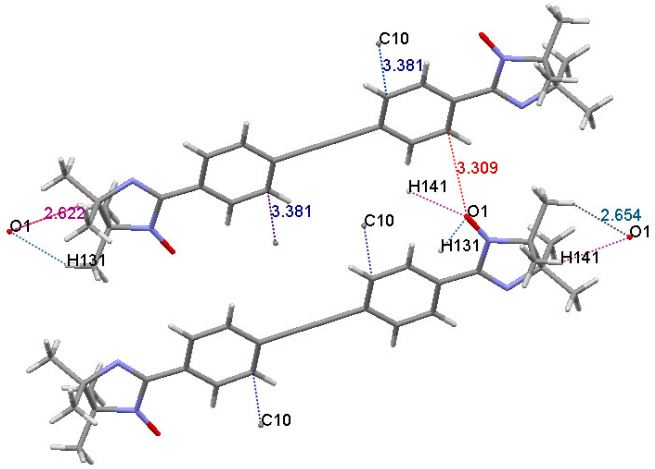

Figure 3.13. Fragment of the crystal packing of **87d** with emphasized short contacts and π-stacking**.**

Compound **88c** exists in the crystal package as the combination of the two independent half-molecules with nearly equal composition, and has an inversion center in the middle of the acetylene bridge (*Fig. 3.14*). The two pyridine rings are coplanar and form an angle of ≈ 20 and ≈ 24° with the mean plane of the imidazolidine subunit. The N(28)-O(33) 1.272, N(29)-O(34) 1.278; N(31)-O(35) 1.282, N(32)-O(36) 1.282; N(28)-C(7) 1.357, N(29)-C(7) 1.359; N(31)-C(20) 1.353, N(32)-C(20) 1.350 Å bond distances are similiar.

(a)

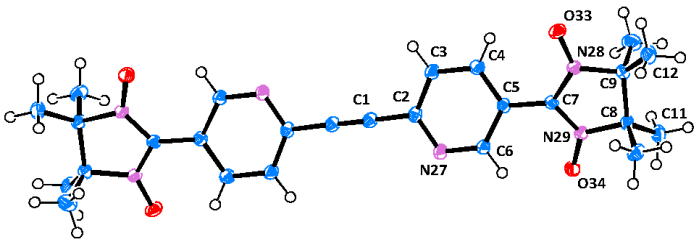

(b)

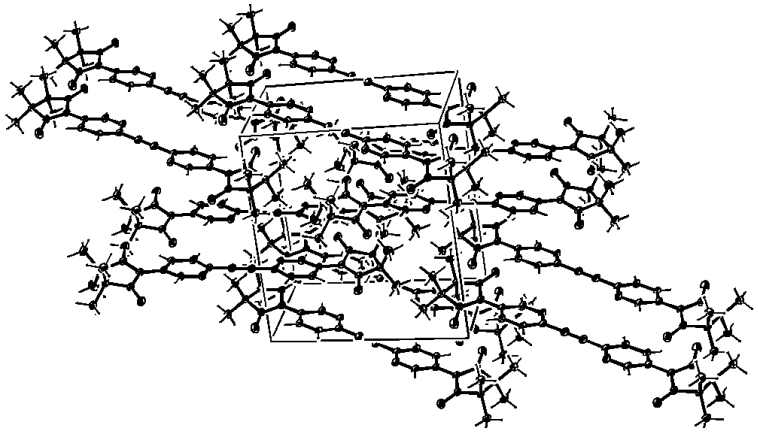

Figure 3.14. Crystal structure of **88c:**(a) molecule; (b) crystal packing (the hydrogen atoms are omitted for clarity).

Relevant intermolecular geometrical data are: O33···H10' 2.57, O33···H11' 2.69 Å - hydrogen bonds between NO group of the radical moiety and methyl group; O34··· H3' 2.62, O34···H4' 2.66, O33···C15' 3.13, O33···C14' 3.04 Å – short intersheet contacts of NO group with pyridine ring and carbon atom of acetylene fragment, correspondently; angles $\alpha \approx 90.95$ and $\beta \approx 104.5^{\circ}$. The shortest interchain distances between the π-bridges are: 2.6 Å (N27···H24') and 3.39 Å (C6···C18').

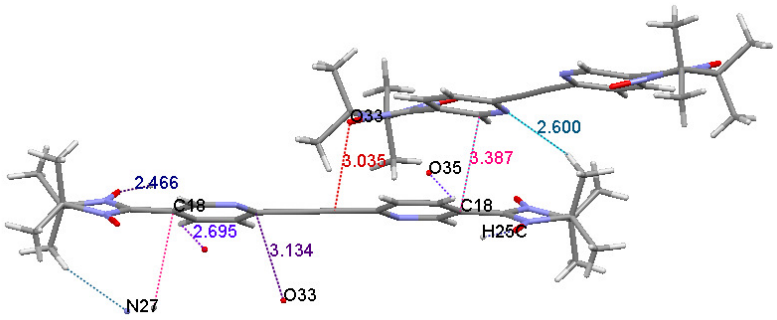

Figure 3.15. Fragment of the crystal packing of **88c** with emphasized short contacts and π-stacking**.**

Biradical **88d** has *P-1* group of symmetry, and exists in the crystal packing as the combination of the two independent half-molecules. Each half-molecule seats on a center of symmetry and one of them is in addition disordered (*Fig. 3.16*). The composition of the half-molecules is ~ 3:1.

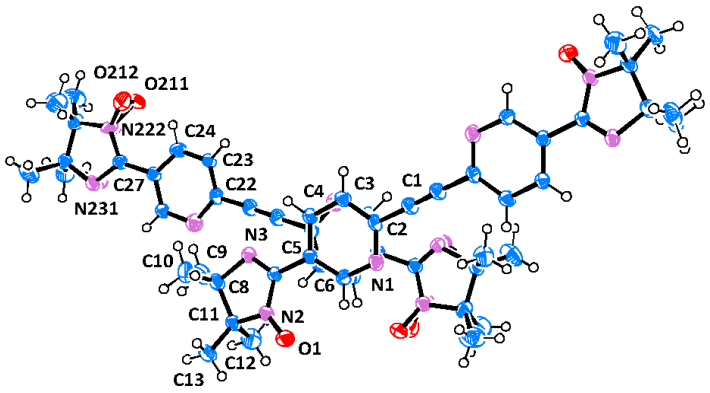

Figure 3.16. Crystal structure of **88d**.

Pyridine rings are coplanar and form angles θ ≈ 22.20° and θ ≈ 23.94° with the mean plane of the imidazolidine fragment. As a matter of fact, the crystal package parameters in the nitronyl **88c** *(Fig. 3.14-3.15)* and imino nitroxide biradical structure are similar, as can be seen for example from comparison of the bond distances within the molecules. Hence, the N(2)-O(1) 1.269, N(221)-O(211) 1.277; N(222)-O(212) 1.257 Å bond distances have inessential differences caused by disorder in the crystal packing. Relevant intermolecular geometrical data are: O211···H261' 2.456, O212···H261' 2.538 Å - hydrogen bonds formed NO group of the radical moiety and hydrogen atom pyridine ring; C23···H121' 2.758, C23···H123' 2.823, C25···H301' 2.831 Å - hydrogen bonds between carbon atoms of the pyridine ring and the hydrogens of the neighbouring methyl groups; intersheet contacts distances between a NO group and pyridine ring are: O1··· H31' 2.682, O1···H429' 2.66, O1···C4' 3.092 Å. The shortest interchain distances between two neighbouring diazatolane bridges are: 2.235 Å (H121···H123'), 2.255 Å (H121···H231') and 3.352 Å (C6···C25').

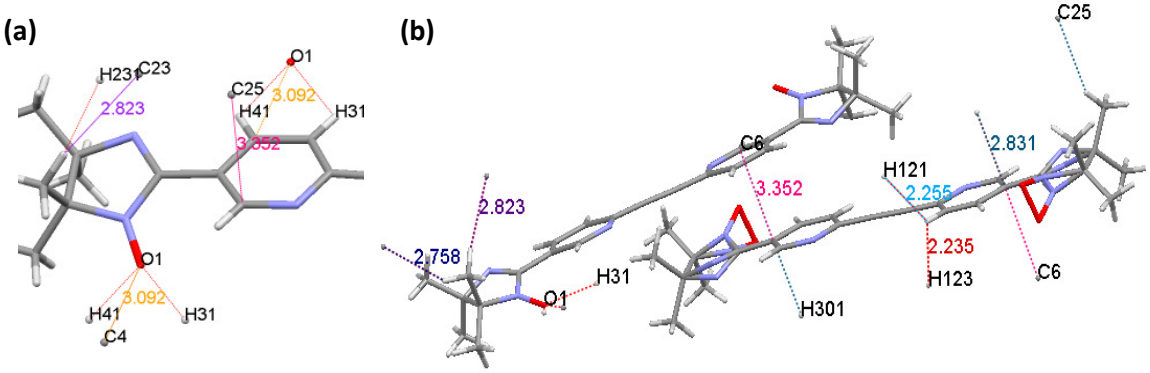

Figure 3.17. Short contacts and π-stacking in **88d** specified in a fragment of (a) molecule; (b) crystal packing.

Biradical **89c** crystallized in a transoid arrangement with an inversion center of symmetry located in the central C1-C1' bond, which is typical for acetylene bridged derivatives (*Fig. 3.18*). 3,3'-Diazatolane is planar, but the dihedral angle between the mean plane of the C5 ring and the imidazolidine moiety (N2-C7-C4-C5) is ~ 52°.

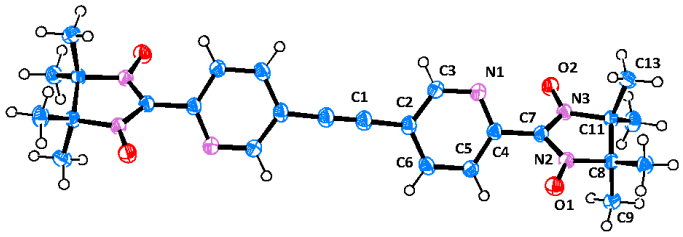

Figure 3.18. X-ray structure of **89c**.

Closer examination of the crystal packing shows that the N-O entities of neighboring molecules have contacts to the neighboring pyridine ring (O1···H61' 2.34, O1···C3' 3.03, O1···C6' 3.22 Å) and methyl group (O2···H93' 2.57, O2···H101' 2.55 Å). The shortest interchain distance is found between hydrogen atoms (methyl groups) of the neighboring molecules 2.38 Å (H93···H131').

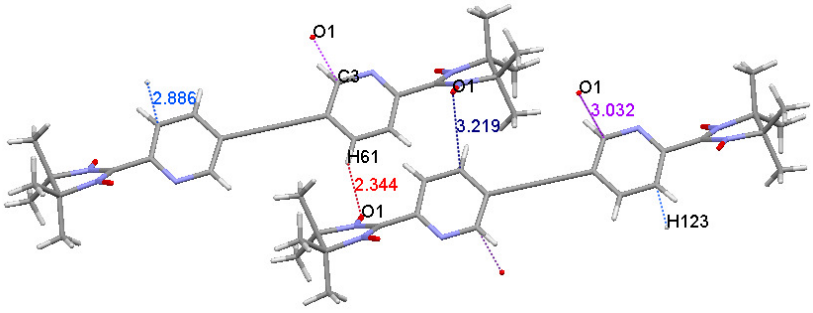

Figure 3.19. Fragment of the crystal packing of **89c** with emphasized short contacts and π-stacking**.**

Compound **99d** features $P2_1/n$ space group with a center of symmetry located in the middle of the biphenyl C-C bond, as demonstrated in *Figure 3.20*. The biphenyl is surprisingly planar, and the dihedral angle between the mean plane of the benzene ring and the imidazolidine moiety is only 18°. In the present structure the distances between the N-O subunits are similar for previously reported nitroxide compounds: N(1)-O(1) 1.226, N(2)-O(2) 1.213 Å, at the same time existence of two values can be explained by disordering in the crystal packing of the molecule **99d**, which is crystallized as a combination of the two forms with almost equal probability.

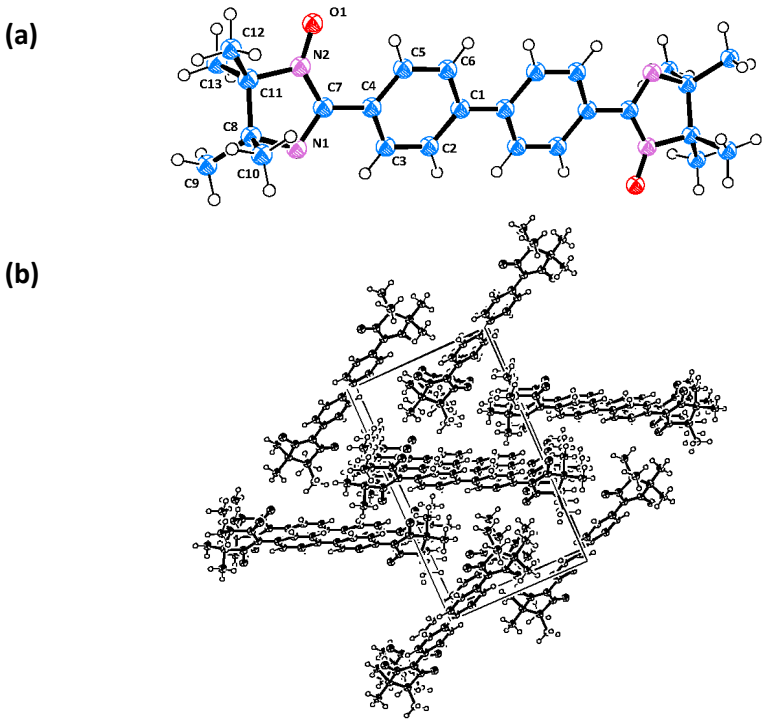

Figure 3.20. X-ray structure of **99d**: (a) molecule; (b) crystal packing.

Detailed investigation of the crystal packing shows that the N-O entities of neighboring molecules form hydrogen bonds with the hydrogen and carbon atoms of the phenyl moiety (C3 and H31, *Fig. 3.20*). Relevant intermolecular geometrical data are: O1 ···C3' 3.18, O1 ···H31' 2.58 Å, angles $\alpha \approx 90°$ and $\beta \approx 95°$. Therefore, the geometry of the molecule favors magnetic interactions.

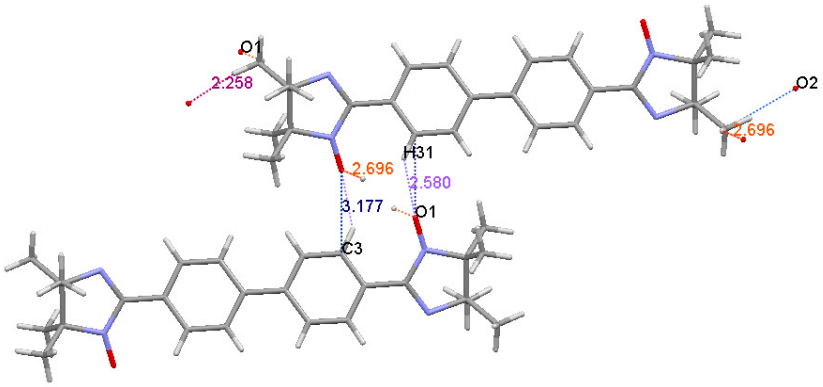

Figure 3.21. Fragment of the crystal packing of **99d** with emphasized short contacts and π-stacking**.**

The biradical **100d** crystallized in a monoclinic arrangement with a center of symmetry located on the central C1-C1' bond, as shown in the ORTEP diagram in *Figure*

3.22. Like the biphenyl analogues **100d** the studied compound **100d** is fairly planar and has $P2_1/n$ space group.

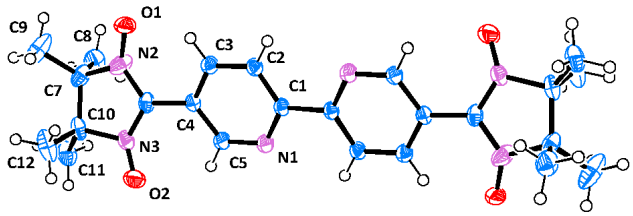

Figure 3.22. X-ray structure of **100d**.

Similar to the described above derivative **99d** the radical features orientation disorder in the crystal packing and exists in the crystal as a combination of two forms with the ratio ~ 38 : 62%. Thus, the dihedral angles between the aromatic rings and the radical plane are very similar: 16.66° (N2···C6···C4···C3) and 16.09° (N3···C6···C4···C5). The O-N-C-N-O moiety is planar, with nearly equivalent O-N bond lengths of 1.22 (O1···N2) and 1.17 (O2···N3) Å.

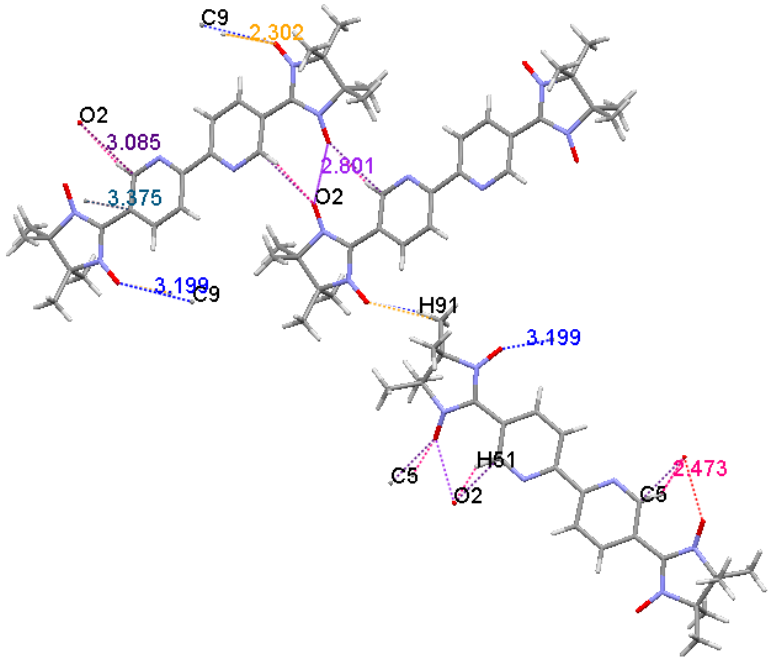

Figure 3.23. Fragment of the crystal packing of **100d** with emphasized short contacts and π-stacking**.**

Closer investigation of the crystal packing reveals that the N-O entities of the neighboring molecules form hydrogen bonds of three types. In the first place, the radical units are attached to the aromatic rings in a head-to-tail fashion with the following

contacts distances: O2···H51' 2.48, O2···C5' 3.09 Å. Secondly, the radical groups are involved into hydrogen bonding with the neighbouring methyls (O1···H91' 2.3, O1···C9' 3.2, O2···H93' 2.6 Å) leading to formation of a herringbone structure (*Fig. 3.23*). Finally, additional binding between the molecules is provided by the O1···O2' 3.09 Å contacts.

The nitroxide **112c** crystallized in the $P2_1/c$ space group (*Table 3.2*) with eight formula units in the unit cell. In the case of the benzofuran radical **112c** disorder is present on the methyl groups of the cycle 2 on the imidazoline ring and on the internal oxygen atoms O6 and O7 (*Fig. 3.24*).

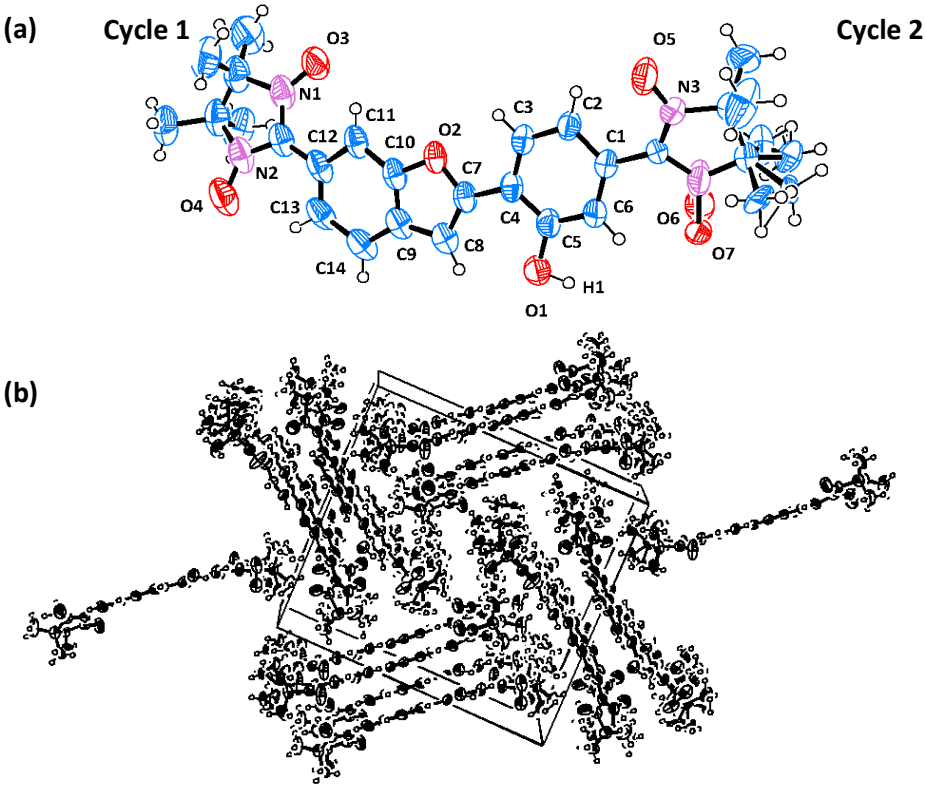

Figure 3.24. X-ray structure of **112c**: (a) molecule; (b) crystal packing.

Consequently, the geometrical parameters of the molecule have slight differences. For compound **112c** cycle 2 flips between two positions, which corresponds to the limits -40.24° and 30.40° for the dihedral angle between the phenyl ring and the plane of the ONCNO fragment. Furthermore, the length of the NO bond varies from 1.28 (N(1)-O(3), N(3)-O(5)), 1.29 (N(2)-O(4)) to 1.43 (N(4)-O(7)), 1.44 (N(4)-O(6)) Å. Within the unit cell the molecules are connected by weak hydrogen bonds as represented in *Figure 3.25*. The contacts along the *a* axes are governed by the linking of the O5 atoms to the aromatic

rings (O5···H1' 1.75, O5···H61' 2.51, O5···C6' 3.12 Å), and hydrogen bonding between phenyl fragments and the hydroxy groups (H1···H21' 2.19, O1···H21' 2.64 Å). The short intermolecular contacts between benzofuran units (H81···H141' 2.37 Å), as well as bonding between the oxygen atoms of the imidazoline moiety and the methyl groups (O4···H173' 2.61, O6···H262' 2.2, O6···C26' 3.05, O7···H253' 2.15, O7···C25' 3.02 Å) provide additional binding along this direction. Thus, the *primary pattern* of the crystal structure is made of the infinite wafer-like chains of molecules connected along the *a* axes.

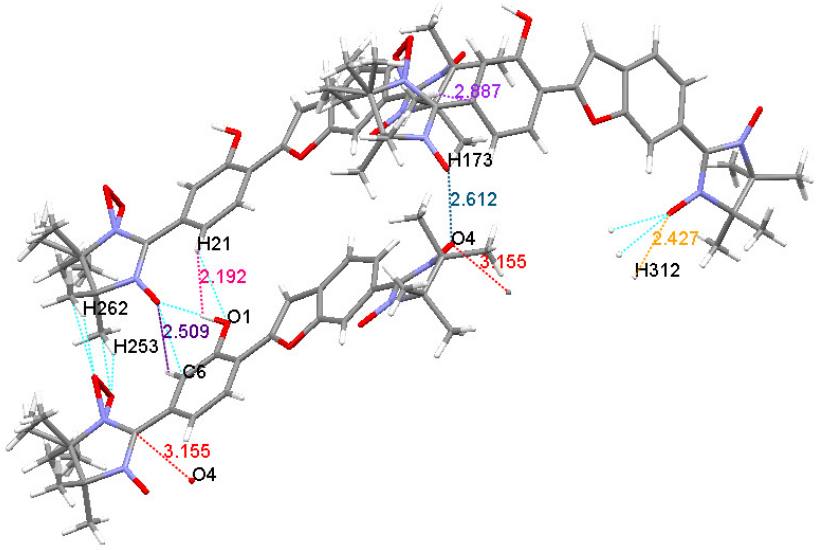

Figure 3.25. Fragment of the crystal packing of **112d** with emphasized short contacts and π-stacking**.**

The other six short contacts are formed by the methyl groups with the phenyl fragments (C1···H181' 2.89 Å) and the benzofuran moiety (C13···H302' 2.87, C14···H302' 2.88, C14···H322' 2.89, C13···C30' 3.28, C14···C30' 3.15 Å). These weak hydrogen bonds are oriented perpendicular to the chains of the primary pattern, and are responsible for appearing of the *secondary pattern*. Consequently, owing to the presence of various intramolecular bonding, the radical crystallized in a herringbone-type of architecture.

In order to rationalize the magnetic properties of molecular compounds, analysis of the molecular packing (so, as to find out the possible magneto-structural correlations) was carried out. The studied biradical NN and IN systems shared nearly planar arrangements of the coupling-core. Structural analyses revealed rather small torsions between the imidazolyl and the aromatic core (< 30°), with an exception in cases of biradicals **89c** (the torsion value is doubled in comparison to other compounds) and **87d**

(the torsion angle has significantly decreased till ~5°) facilitating, therefore, efficient conjugation between the radical moieties through the coupler. Additionally, the intersheet contacts are found to be short enough (2.38 - 2.6 Å) to favor magnetic interactions.

3.4. Optical properties of the biradicals

3.4.1. UV-Vis absorption spectra

The obtained nitroxide systems were found fairly well soluble in most of the organic solvents tested (e.g. MeOH, $CHCl_3$, THF). However, in aprotic media (e.g. toluene), longer stability of the radical molecules over the time was observed. In protic solvents (e.g. CH_2Cl_2 or $CHCl_3$), partial decomposition of the radicals into diamagnetic products occurred within a day, due to sequential release of water molecules (dehydratation), as witnessed from the decrease of the radical signal intensity in both UV-Vis absorption and in the EPR envelopes.

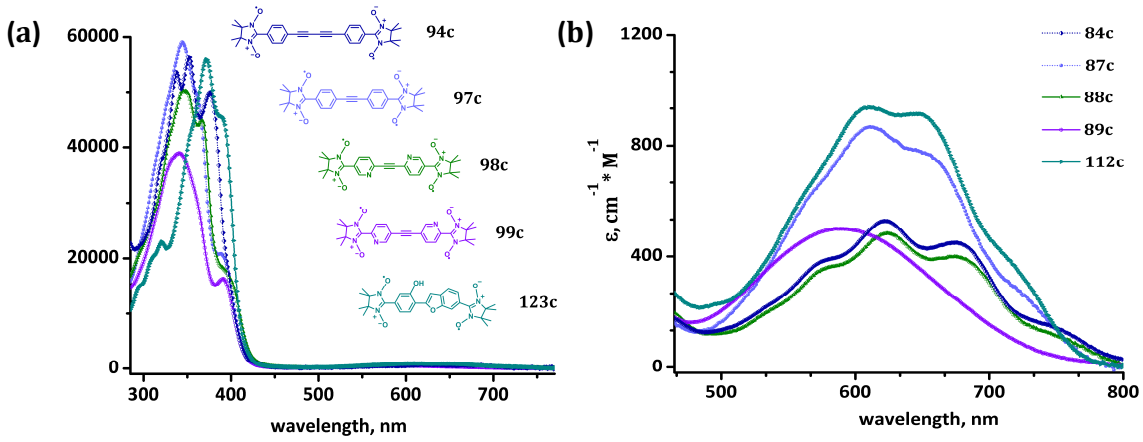

Figure 3.26. (a) UV-Vis spectra of nitronyl nitroxide radicals **84c**, **87c**, **88c**, **89c**, **112c** recorded in toluene; (b) enlarged fragment of the spectra in the visible range.

Nitronyl nitroxides solutions exhibit characteristic deep blue colour, which is typical for this class of the radicals. Since such radicals were shown to be stable in toluene solutions for month, toluene has been employed as the preferred solvent for nearly all the radicals studied in this work (except for the nitroxides **89c**, **100d**) in accordance to the statement above. Low solubility of the biradicals **89c**, **100d** in toluene forced us to use

chloroform in that case. Two distinctive set of absorption bands dominate the optical spectra (*Fig. 3.26, 3.27 (a), (b)*). The first set of bands is characterized by differently enhanced vibronic components, and takes place at a longer wavelength, around 600 nm (*Fig. 3.26 (b)*). Those signals correspond to the n-π^* transitions of the aminoxyl oxide moieties. The second set of absorption values includes the π-π^* transitions and falls at much higher energy in the 300-380 nm wavelength range (*Fig. 3.26 (a)*).[73]

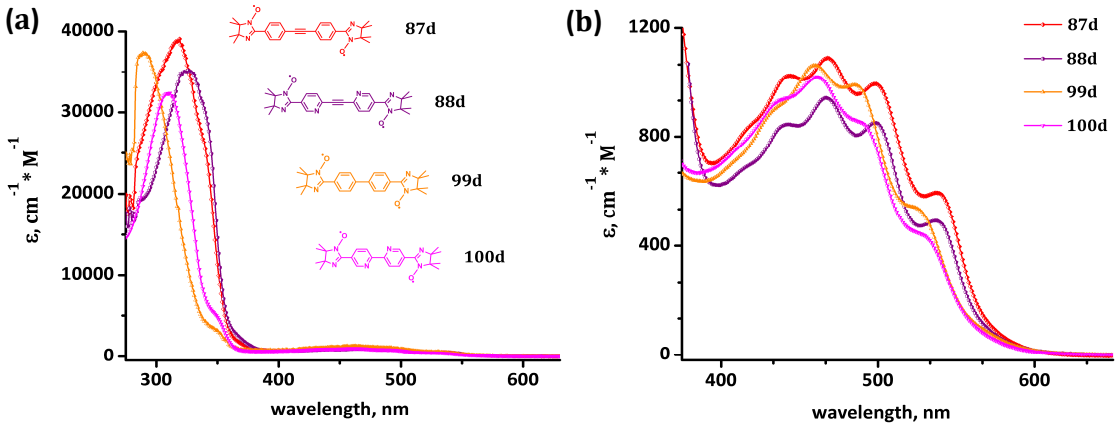

Figure 3.27. (a) UV-Vis spectra of imino nitroxide radicals **87d**, **88d**, **99d**, **100d** recorded in toluene; (b) enlarged fragment of the spectra in the visible range.

The imino nitroxide derivatives featured a bright orange-red colour in solution, with a broad absorption band around ~470 nm (n-π^* transitions).[31,74] Enlarged fragment of the UV-Vis envelope represented in *Figure 3.27 (b)* illustrates this statement.

3.4.2. The IR absorption spectra of the radicals

IR spectroscopy is a valuable method, which helps to ensure quality of the nitroxide radicals purification, confirming the absence of some possible contaminants, namely, the aldehyde precursors, or other radical species (such as imino nitroxide radicals). As a general rule, the carbaldehyde moiety shows a strong signal at ~1680 cm^{-1} (-C=O), which is not found in the studied biradical powders. This band disappeared upon the completion of the reaction between the aldehyde function with BHA, and a new broad signal attributed to the –N-OH stretching mode at ~3250 cm^{-1} was observed. Such structural transformation into a part of imidazolidine heterocycle is accompanied by distinguished changes in the IR envelopes. To illustrate this statement the IR spectra of both derivatives **87a**,**b** are shown in *Figure 3.28*.

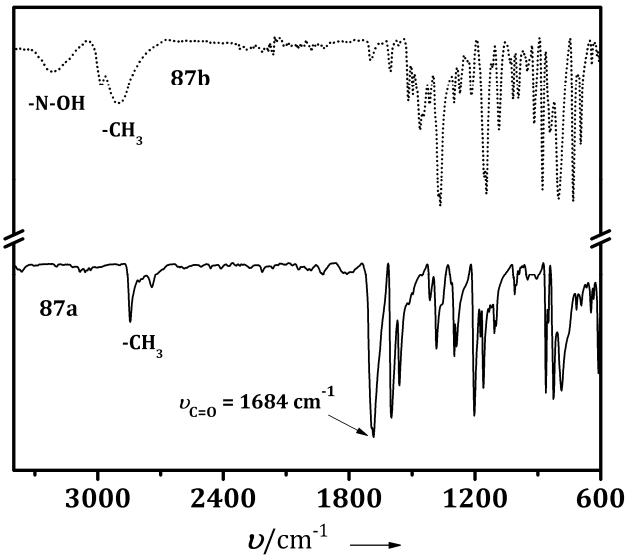

Figure 3.28. Comparison of the FT-IR spectra of the starting dialdehyde **87a** with the corresponding condensation product **87b**.

Therefore, the appearance of a novel signal after oxidation of the imidazolidine derivatives at around $\upsilon \sim 1350$ cm^{-1} (*Table 3.4*) was assumed to arise from the N-O stretching vibration of the imidazoline moiety, which was in harmony with comparable signals observed for several other NN systems described in the literature.[74-77]

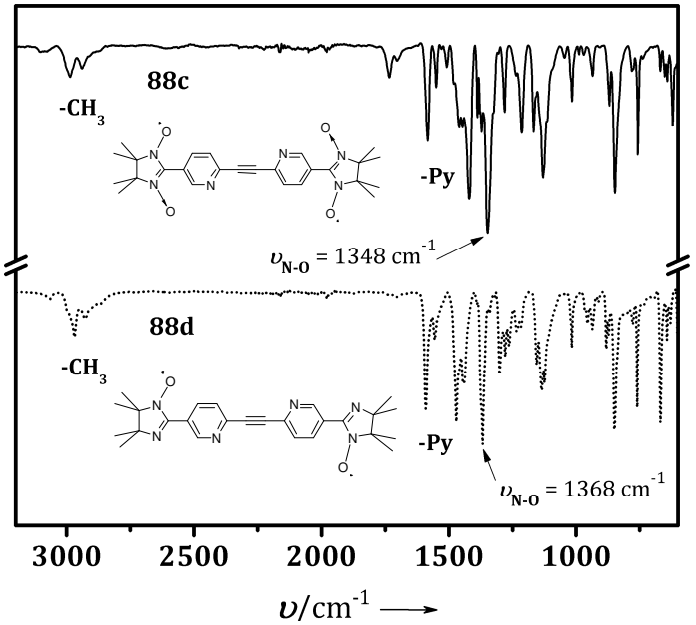

Figure 3.29. FT-IR spectra of nitronyl **88c** and imino nitroxide **88d** biradials.

In the case of imino derivatives the signal attributed to the N-O stretching frequency of the radical fragment with relatively weaker intensity was shifted to the longer wave numbers (1365 - 1370 cm^{-1}). For a better comparison, spectra of nitronyl nitroxide biradical **88c** and the corresponding imino derivative **88d** are demonstrated in *Figure 3.29*. Vibrations related to the pyridine rings were observed at ~1420, 1470 and 1580 cm^{-1}.[78] Other strong signals appeared in the region at ~ 1550 cm^{-1}, and those originated from the -C=N stretching vibrations.[74] The relevant UV-Vis and IR data are summarized in *Table 3.4*.

Table 3.4. Selected spectroscopic data for the nitronyl **84c**, **87-89c**, **112c** and imino nitroxide radicals **87d**, **88d**, **99d**, **100d**

Radical	IR[a] ν_{NO}/cm^{-1}	UV-Vis[b] λ_{max}/nm ($\varepsilon/M^{-1}cm^{-1}$)
84c	1365	622 (578)
87c	1356	615 (442)
88c	1348	627 (557)
89c	1360	589 (502)
112c	1357	610 (938)
87d	1365	468 (1091)
88d	1368	467 (944)
99d	1364	461 (1090)
100d	1366	462 (1021)

[a] ν_{NO} measured in solid state;
[b] measured in toluene except compounds **89c**, **100d** recorded in $CHCl_3$ solution.

3.5. Cyclic voltammetry measurements

Evaluation of the potential applications of the stable radicals in the design of molecule-based magnets[79,80], magnetic imaging and magneto-optics[81] is based on the physicochemical characteristics of these compounds, including estimation of the redox properties of the radicals. Since nitronyl **84c**, **87-89c** and imino **87d**, **88d**, **99d**, **100d** nitroxide biradicals are compounds with open-shell electron structure lying between the corresponding hydroxylamines (strong reducing agents) and oxoammonium salts (strong

oxidants) on the Latimer[†††] diagram,[82] electrochemical certification is especially important for them.

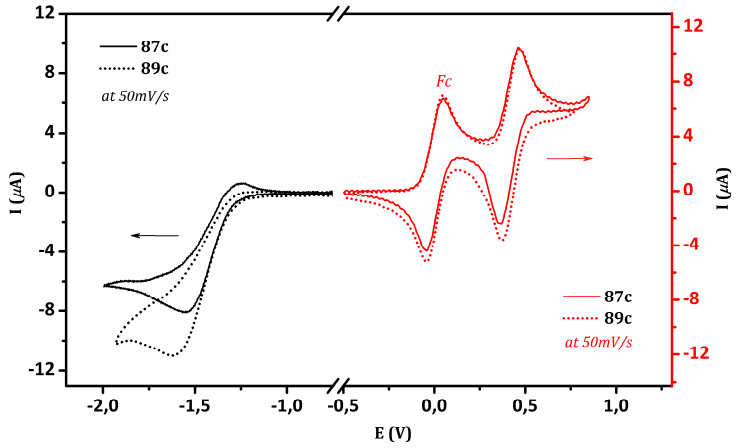

Figure 3.30. Cyclic voltammograms of **87c** and **89c** at 50 mV/s registered in CH_2Cl_2 with 0.1M (n-C_4H_9)NPF_6, Pt electrode (reduction part is specified with the black colour and the oxidation is specified with the red colour in the plot).

In nitroxide radicals the singly occupied molecular orbitals (SOMOs) and the lowest unoccupied molecular orbitals (LUMOs) determine the redox properties of the compounds.[83] So, the relative SOMO and LUMO levels of the nitronyl **84c**, **87-89c** and imino **87d**, **88d**, **99d**, **100d** nitroxide radicals were determined by cyclic voltemmetry in CH_2Cl_2 with 0.1 M tetrabutylammonium tetrafluoroborate ((n-C_4H_9)NPF_6) supporting electrolyte and ferrocene as internal standard (shown in the reduction part of the spectrum). A platinum working electrode and Ag/AgCl as a reference were utilized. For a better representation of the data the reduction and oxidation parts demonstrated in *Figure 3.30* are displayed with different colors – black and red, respectively.

Similar to the electrochemical oxidation of the mono nitronyl species (which was discussed previously in *Subchapter 2.11*), the oxidation of the nitronyl biradicals **84c**, **87-89c** was found to be reversible in the investigated conventional timescale. Most probably, two essentially independent nitroxide groups were simultaneously oxidized to the nitrosonium dications in a two-electron quasi-reversible process.[84] On example of tolane derivative **87c** *Scheme 3.16* illustrates formation of dication **87e**.

[†††] Latimer or reduction potential diagrams show the standard reduction potentials connecting various oxidation states of an element.

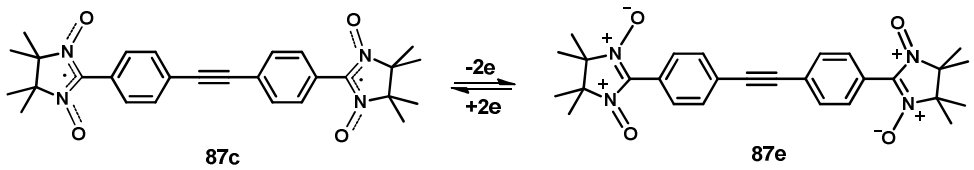

Scheme 3.16. Formation of the nitrosonium dication **87e.**

Nitronyl nitroxide biradical systems **84c**, **87-89c** featured irreversible reduction. Most probably, the two independent radical moieties were simultaneously reduced to the corresponding anions, which subsequently reacted with traces of water presented in the solvent media affording bishydroxylamines.[84a,85] The electrochemical-chemical mechanistic pathway for the reduction of these compounds could be described using the derivative **87c** as an example (*Scheme 3.17*).

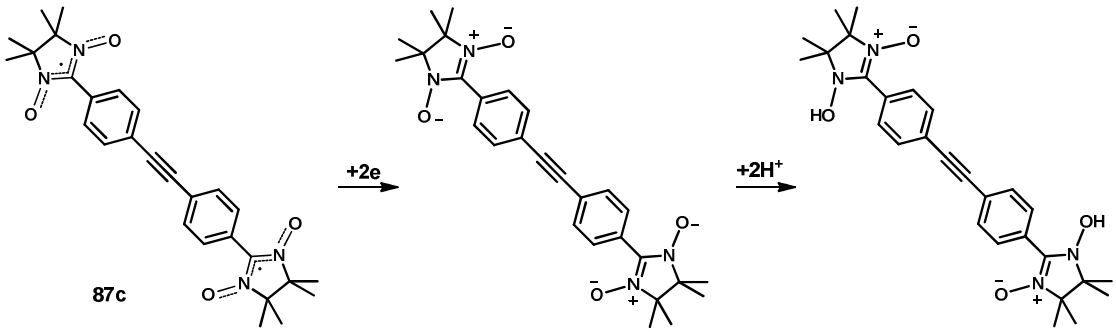

Scheme 3.17. Electrochemical reduction of the nitronyl biradical **87c**.

Following the equations *(13), (14)*[86] calculations of the SOMO and the LUMO levels for the studied nitroxide systems were carried out and listed in *Table 3.5*.

$$E_{SOMO} = -(E_{Ox,onset} - E^{(1/2)}_{Fc/Fc} + 4.8)\ eV \qquad (\mathbf{13})$$

$$E_{LUMO} = -(E_{Red,onset} - E^{(1/2)}_{Fc/Fc} + 4.8)\ eV \qquad (\mathbf{14})$$

In contrast to the nitronyl radicals all the imino nitroxides were oxidized irreversibly and at higher potentials. Furthermore, the voltammogramms of the studied imino compounds demonstrated irreversible reduction. Imino nitroxides featured similar E_{Red} (*Table 3.5*), while the 2,2'-diazatolane imino derivative **88d** exhibited the maximum value of E_{Red} = -1.15 V (the potentials were calibrated against Fc/Fc^+ couple at 0.46 V).

Table 3.5. Electrochemical properties of the nitronyl nitroxide **84c**, **87-89c** and imino **87d**, **88d**, **99d**, **100d** biradicals (the potentials were calibrated against Fc/Fc^+ couple at 0.46 V).

Radical	E_{Ox}, V	E_{Red}, V	E_{SOMO}, eV	E_{LUMO}, eV	ΔE_g, eV	E_{opt}, eV
84c	0.360	-1.291	-5.16	-3.51	1.65	1.55
87c	0.331	-1.301	-5.13	-3.50	1.63	1.61
88c	0.414	-1.193	-5.21	-3.61	1.60	1.57
89c	0.348	-1.310	-5.15	-3.49	1.66	1.60
87d	0.777	-1.260	-5.58	-3.54	2.04	2.08
88d	0.760	-1.146	-5.56	-3.65	1.91	2.07
99d	0.670	-1.247	-5.47	-3.55	1.92	2.02

It's generally known, that the redox properties of the nitroxides are structurally dependent.[87] Among the main influencing factors are the ring size and substituent inductive and electrostatic effects.[87a,88] From the other hand, analysis of the voltammograms revealed that the two nitroxide groups in the studied biradical systems are equivalent and independent from each other. Similar situation was observed by Ziessel for a series of oligopyridine bis(nitronyl nitroxides).[85a] One way or another, the logic suggests that the structural modifications in the π-bridge combining two nitroxide fragments shouldn't severely affect the electrochemical properties of the biradicals, and therefore SOMO-LUMO levels should exhibit similar values within the series **84c**,**d 87-89c**,**d**. Indeed, for the majority of the nitronyl nitroxides under study the electrochemical gap ΔE_g (the difference between the SOMO and LUMO energies)[83] is ~1.6 eV. This value is slightly higher for the imino derivatives, where the gap of ~2.0 - 2.1 eV was found.

3.6. EPR properties

3.6.1. EPR spectra of the systems with S > 1/2

For a paramagnetic species in the absence of magnetic field the energy levels are degenerated, and the system remains at the lowest level. In the presence of an applied magnetic field the degeneracy is removed, resulting into level splitting. For a two electron spin system (the simplest example of a system with S > 1/2), the four orientation

dependent configurations are possible (*Fig. 3.31*), which can be divided into a singlet state ($S = 0$, $M_S = 0$, $2S + 1 = 1$) and a triplet state ($S = 1$, $M_S = \pm 1$ or $M_S = 0$, $2S + 1 = 3$). The spin Hamiltonian for a two-spin system is given by the formula (*15*):

$$\hat{H} = g\,\beta\,B_o\,\hat{S} - 2\,J\,\hat{S}_1\,\hat{S}_2 + A(\hat{S}_1\,\hat{I}_1 + \hat{S}_2\,\hat{I}_2) \qquad (\mathbf{15})$$

The term $2J\hat{S}_1\hat{S}_2 = \hat{H}_{exch}$ describes the electron-exchange interaction in the system and is called Heisenberg-Dirac-van Vleck Hamiltonian (HDVV).[89]

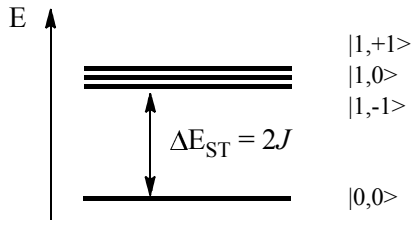

Figure 3.31. Singlet-triplet energy gap for a system with S = 1, when $2J < 0$.

The singlet and triplet states are the eigenfunctions of the HDVV Hamiltonian with the energies (3/2) J and (-1/2) J.[90,91] Therefore, the magnetic coupling constant is given by the energy difference between |S>-|T> = $2J$ corresponding to the singlet-triplet energy gap (ΔE_{ST}). Notably, the signal intensity for the species with triplet ground state or triplet-singlet nearly degenerate states follows Curie law [$\chi_{ESR} = C/T$].

3.6.2. The exchange interactions

The correlation between the relative size of J and A_N constants strongly influences the spectral shape, i.e. number of the lines. Thus, when the exchange interaction is much smaller than the hyperfine coupling constant ($2J/k_B < 3\times10^{-4}$ K), each radical centre behaves independently, and can be treated as uncorrelated spin-system. It follows, that the total spread in the magnetic field of the observed EPR spectrum exactly matches the one of a monoradical with the doubled intensity compared to the later (see for comparison *Fig. 2.7* in *Subchapter 2.4.2*).

In the case that the exchange interaction is much larger than the hyperfine coupling constant ($2J/k_B > 0.04$ K), for n equivalent nuclei one would expect $2nI + 1$ lines pattern. Namely, (2×4×1 + 1) = 9 for the nitronyl nitroxide and (2×2×1 + 1) × (2×2×1 + 1) = 25 lines for the imino biradical, with the observed A_N half of that featured by the related monoradical. However, some of the transition lines in the imino nitroxide species overlap

each other, leading to the reduced - 13 lines - pattern. The total width of the observed EPR spectrum remains, however, the same as that observed in the monoradical case.

For the intermediate cases ($J \sim A$ or $J < A$) the total spectral width changes and a number of additional lines with different intensities appears. Importantly, increasing of the exchange constant value leads to a larger splitting between the states, and consequently to the enlargement of the gap between the singlet and triplet states. In that case the EPR analyses studies could provide only the relative value of the exchange magnitude.

3.6.3. Zero field splitting (*zfs*)

Zero field splitting (*zfs*) is the effect of removal spin microstates degeneracy for systems with two or more unpaired electrons in the absence of an applied field. That is, the degeneracy is removed as a consequence of molecular electronic structure and/or spin density distribution. *Figure 3.32* illustrates this phenomenon, where D is the dipolar tensor and represents the *zfs*. Zero field splitting causes magnetic anisotropy.

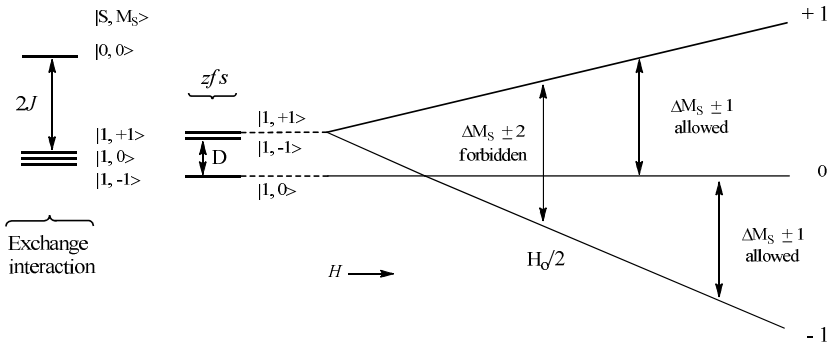

Figure 3.32. Triplet state zero splitting for a ferromagnetic system ($J > 0$) with two S = ½ (for a system with antiferromagnetic interactions the singlet level lies below triplet).

In frozen solution or in a powder the relevant spin-Hamiltonian describing the EPR transitions for biradical systems is reported in equation (*16*):

$$\hat{H} = g\,\beta\,B_0\,\hat{S}_{1,2} - 2\,J\,\hat{S}_1\,\hat{S}_2 + S\,A\,I + S\,D\,S \qquad (\mathbf{16})$$

Where g and A are the tensors with different space components (anisotropy) such as $g = (g_{xx} + g_{yy} + g_{zz})/3$, and $A = (A_{xx} + A_{yy} + A_{zz})/3$ (as described in *Subchapters 2.4.1, 2.4.2*).[91b,92]

In $S \geq 1$ systems the equation (*16*) can be transformed into (*17*), assuming that the $\boldsymbol{D}$- and g-tensors have the same principal axis:

$$\hat{H} = g\,\beta\,B_0\,\hat{S}_{1,2} - 2\,J\,\hat{S}_1\,\hat{S}_2 + D(S^2_z - S(S+1)/3) + E(S^2_x - S^2_y) + S\,A\,I \qquad (\mathbf{17})$$

$\boldsymbol{D}$ and $\boldsymbol{E}$ depend on which axis is chosen as Z, and are related to the principal values of the D-tensor through $D = 3\,D_{zz}/2$ and $E = |D_{xx} - D_{yy}|/2$. They represent the fine structure parameters (axial and rhombic) also called zero-field–splitting parameters. $\boldsymbol{D}$, $\boldsymbol{E}$ parameters originate from the electron-spin-electron-spin dipole interaction,[93] which causes the three fold degeneracy of the triplet state to be removed even in zero magnetic fields.

The *zfs* parameter of the fine structure (D) gives information about the dipolar interaction of the unpaired electrons in a molecule and is related to the *intra*radical distance (r) as $1/r^3$. In the absence of *zfs* the two allowed EPR transitions ($\Delta M_S = \pm 1$) occur at the same magnetic field, but in the presence of *zfs* these transitions are no longer degenerated and could be observed separately (i.e. fine structure of the spectra). The separation depends on the magnitude of the *zfs* parameter D. Here, the dipolar coupling constant is related to the radical separation r as $D \sim 1/r^3$. According to Anderson's theory,[94a,b] the contribution of the through-space interactions to the exchange energy term J is described by the equation (*18*):

$$J = J_0 \exp\,[-\alpha\,(r - d)] \qquad (\mathbf{18})$$

where d represents the minimum distance-approach, J_0 and α are the empirical values.[94c] Therefore, at small J values D is negligible and fine structure could not be observed.

3.6.4. The observed EPR spectra of the π- conjugated biradicals in solution

The EPR spectra of the biradical systems **84c**, **87-89c** were recorded in oxygen-free toluene solutions. *Figure 3.33 (1)* shows as an example, the EPR resonance envelope obtained for the acetylene derivative **84c** at room temperature (T = 298 K). The nine lines splitting pattern witnessed in the system highlights the efficient through-bond coupling of the two nitronyl nitroxide residues *via* π-spacer. Regardless of the different distances between radical centers as well as the molecular identity of the coupling units employed, the same property was observed for the compounds **87c**, **88c** and **89c**, and thus, within the limit of X-band EPR spectroscopy, the attainment of strong exchange interactions

$|J/A_N|$ >>1 between the spin carriers was experimentally verified for all studied biradical systems.

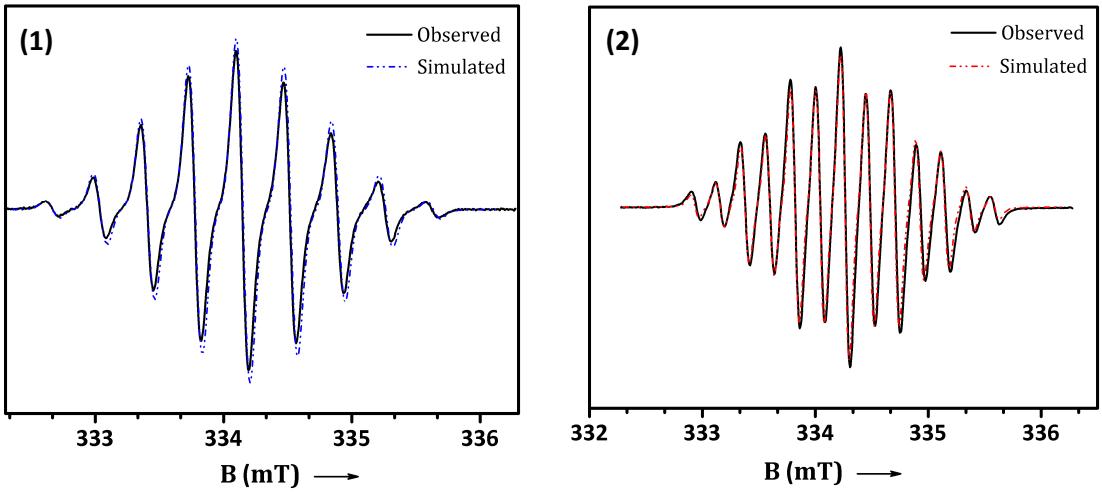

Figure 3.33. EPR spectrum recorded in dilute and oxygen-free toluene solution at 298 K of diacetylene biradical **84c** (1) with following experimental parameters: 9.4 GHz, 100 kHz modulation frequency, 5.1 mW power, 41 msec time constant, 42 sec sweep time, 2×10^4 gain, 0.012 mT modulation amplitude; 2,2'-diazatolane biradical **88d** (2) with experimental parameters: 9.4 GHz, 100 kHz modulation frequency, 10 mW power, 20.5 msec time constant, 10.5 sec sweep time, 1×10^4 gain, 0.052 mT modulation amplitude. The dash-dotted lines represented the computer simulations with the following parameters: (1) A_N = 0.744 mT, g_{iso} = 2.0065, ΔB_{pp} = 0.108 mT; (2) A_{N1} = 0.430, A_{N2} = 0.853, g_{iso} = 2.0057, ΔB_{pp} = 0.145 mT.

The spin -concentrations for **84c**, **87-89c** at T = 298 K were consistent with two spin centers, where singlet and triplet states are thermally populated and statistically distributed according to the Boltzmann law. The calculated values of the hyperfine coupling constant (A_N) for **84c**, **87-89c** are given in *Table 3.6* and fall between 0.7 and 0.75 mT ($g_{iso} \approx 2.0063$). These values were in a good agreement with the comparable data for the nitronyl nitroxide radicals found in the literature.[95] The best fitting to the experimentally obtained curve was obtained with the Lorentzian/Gaussian line-width ratio = 1/3 (shown with the dash-dotted line in the *Figure 3.33 (1)*). The EPR envelope typical for the imino biradicals is shown in *Figure 3.33 (2)*. The EPR spectra obtained for **88d** is split into 13 lines with the following parameters: $A_{N1} \approx 4.30$ G, $A_{N2} \approx 8.85$ G, $g \approx 2.0061$.

Table 3.6. The g values and hyperfine coupling constants of nitronyl nitroxide **84c**, **87-89c** and imino nitroxide **87d**, **88d**, **99d**, **100d** biradicals.

Radical	g	Hyperfine coupling constants (mT)
84c	2.0065	0.744
87c	2.0065	0.762
88c	2.0062	0.738
89c	2.0064	0.752
112c	2.0063	0.750
87d	2.0059	A_1 = 0.430, A_2 =0.849
88d	2.0057	A_1 = 0.430, A_2 = 0.853
99d	2.0060	A_1 = 0.430, A_2 = 0.870
100d	2.0060	A_1 = 0.430, A_2 = 0.849

The solution EPR spectra of the biradical systems **84c**, **87c**, **88c**,**d** and **89c** featured a very small increase in the peak-to-peak line-width upon cooling. The variable temperature EPR spectra of **88c**,**d** compounds are shown in *Figure 3.34 (1),(2)* demonstrating the temperature effect on the exchange interactions in the biradicals along with the related Curie-behaviour for **87c** and **88c** (*Figure 3.35 (1),(2)*). The typical increase of the signal intensities was registered with lowering the temperature.[96]

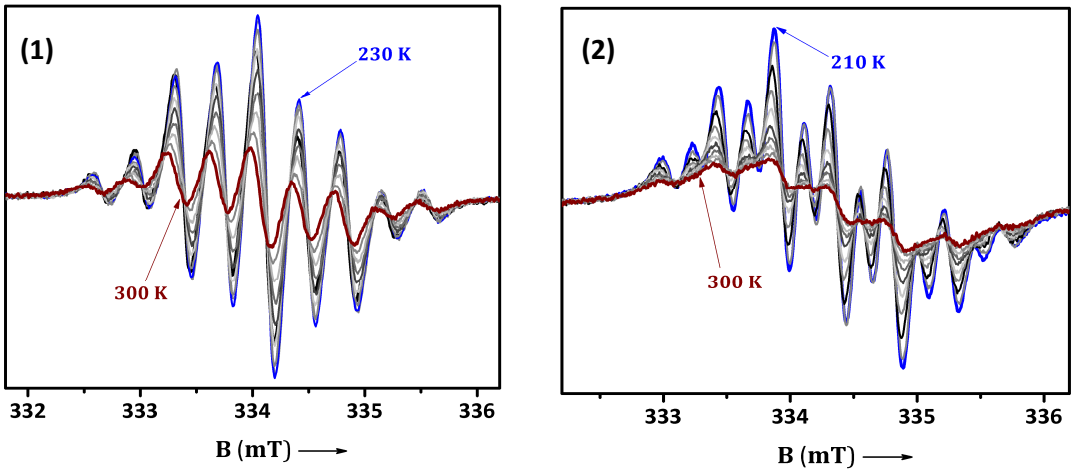

Figure 3.34. X-band EPR spectra of the nitroxide biradicals **88c** (1) and **88d** (2) in toluene recorded at different temperatures. The samples were allowed to equilibrate in the cavity-cell at the fixed temperature for over 15 min.

Nitronyl nitroxide and imino nitroxide biradicals in solution followed nicely Curie-law with the linear increase of the signal intensities (**I**) upon lowering the temperature in the range 300-235 K (*Figure 3.35*). Further cooling of the solutions after 230 K led to

anisotropic broadening of the signals (*Figure 3.34*) together with significant deviations from the Curie-linear behaviour.

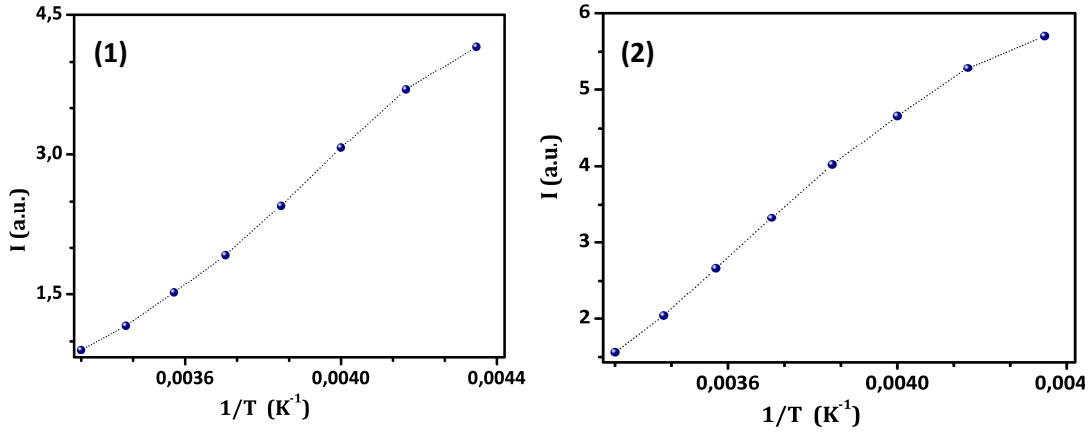

Figure 3.35. Curie plot of the nitroxide biradicals **87c** (1) and **88c** (2) recorded in diluted (1×10^{-4}) toluene solutions. **I** represents the signal intensity.

This process corresponds to the out of phase internal rotation of the two radical moieties, which is able to modulate the exchange interaction J.[77] It seems that in solution biradicals may exist in different conformations with different J values. At room temperature interconversion between these conformations is obviously too fast on the EPR timescale, but slow enough for the detection at lower temperatures.

3.6.5. The observed EPR spectra of the radicals in frozen solutions

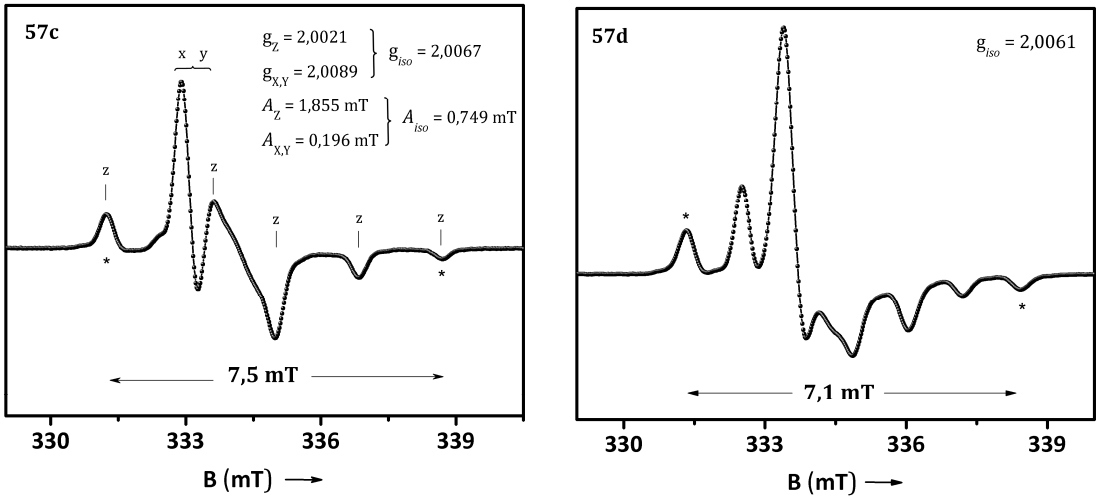

Figure 3.36. The EPR powder spectra of the monoradical systems **57c** and **57d** in dilute toluene solutions recorded with the following experimental parameters: 9.4 GHz, 100 kHz modulation frequency, 2.5 mW power, 82 msec time constant, 42 sec sweep time, 1×10^{4} gain, 0.05 mT modulation amplitude at 145 K.

The monoradical spectra for the nitronyl- (**57c**) (g_{iso} = 2.0067) and imino nitroxide (**57d**) (g_{iso} = 2.0061) recorded in diluted frozen solutions [10^{-4} M] are shown in *Figure 3.36*. The anisotropic constants g_Z, A_Z were obtained from the experimentally received data and $g_{X,Y}$, $A_{X,Y}$ were calculated following the equations described earlier in *Subchapter 3.6.3*. The monoradicals could be used as spin-standards for the biradical systems. The EPR spectrum of the imino nitroxide biradical **100d** recorded in toluene glass is demonstrated in *Figure 3.37*.

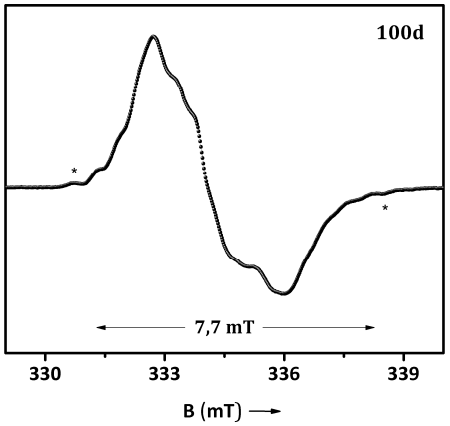

Figure 3.37. The EPR powder spectra of the imino biradical system **100d**, recorded with following experimental parameters: 9.4 GHz, 100 kHz modulation frequency, 10 mW power, 82 msec time constant, 42 sec sweep time, 1×10^4 gain, 0.05 mT modulation amplitude at 145 K. The arrows indicate the estimated $|2D|$ range.

Although the fine structure spectra of the derivative **100d** still possessed some hyperfine interactions, the envelope was nearly symmetric and the total width of the spectra was different in comparison to the monoradical species (*Fig. 3.36*). Several attempts to record EPR spectra with good resolution for the biphenyl biradical **99d** at different temperature and microwave power were made, but most of the hyperfine couplings were not resolved. According to the point-dipole approximation[77] (*Eq. 19*) the $|D|$ value in axial systems is related with the averaged radical distances as:

$$|D| \text{ (MHz)} = 77924\ (g_{obs} / g_e) / r^3 \qquad (\mathbf{19})$$

with r (in Angstrom, Å) considered as their averaged through-space separation. From the expression (*15*) the inverse correlation between the intramolecular radical distance and the magnitude of *zfs* component is clearly observed, leading to the conclusion that the increase of r causes decreasing of the D value. Therefore, increase of the intramolecular

radical distances (in biradicals **94c**, **97c**,**d**, **98c**,**d**, **99c** and, unexpectedly, **99d**) causes rapid decrease of the *zfs* component.[77]

The evaluated value of $|2D|$ accounted for **100d** was ~ 7,7 mT. Notably, the acquired average distance between the radical units - 12.7 Å – was in a good agreement with the size of the distance obtained from X-ray crystal structure analysis (~ 12 Å).

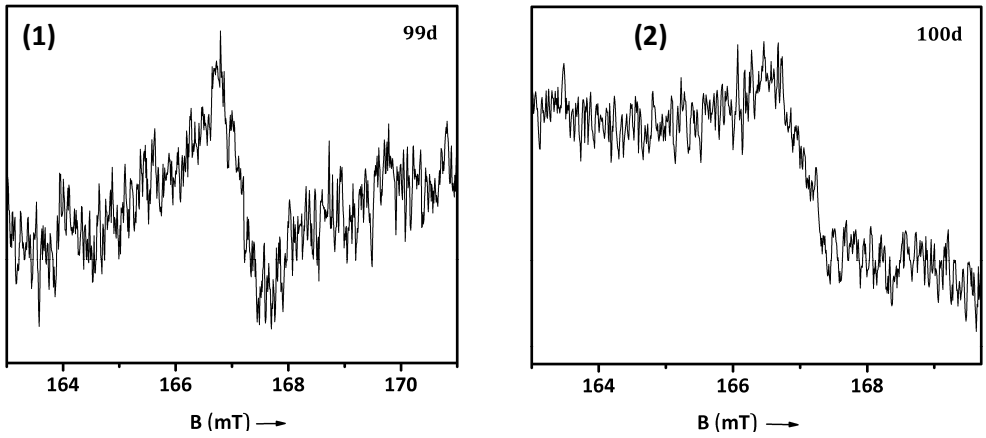

Figure 3.38. The EPR spectra of the imino biradical systems (1) **99d** (40 scans), (2) **100d** (60 scans), with the following experimental parameters: 9.4 GHz, 100 kHz modulation frequency, 82 msec time constant, 42 sec sweep time, 5×10 gain, 0.411 mT modulation amplitude, recorded at 120 K.

Both imino biradical systems **99d** and **100d** (C ~ 1×10^{-4}M) showed the forbidden (ΔM_S = 2) half-field transition at g ~ 4.01 down to liquid helium temperature, thereby supporting their biradical nature (*Fig. 3.38*). The measurements were repeated at different microwave powers (5 and 40 mW) to ensure that the signals were not saturated.

3.7. DFT calculations and magnetic properties of the biradical systems

In order to understand the influence of the bridging unit on the electronic properties and especially on the exchange coupling, DFT calculations were performed. We thus carried out geometry optimization with the B3LYP hybrid function and 6-31G* basis set and we then applied the broken symmetry approach (BS) for the singlet and triplet states with BLYP (to avoid Hartree-Fock contamination) and 6-31G* basis set according to an approximate projection technique as suggested by Yamaguchi.[97] For the simplest case

of two spins S = ½ this form of the spin Hamiltonian ($H = -2J_{12}S_1S_2$, here the exchange parameter J will be negative in the case of antiferromagnetic interaction) gives the exchange interaction as $J = (E(BS) - E(T))/(S^2(T)-S^2(BS))$, where $E(BS)$ is the energy of the broken symmetry approach, $E(T)$ is the energy of the triplet state and S^2 are the eigenvalues of the spin operator for these states. In case of weak interaction without spin contamination $S^2(T)$ = 2 and $S^2(BS)$ = 1 the direct exchange yields $J = E(BS) - E(T)$. The obtained theoretical exchange coupling constants J are listed in *Table 3.7* together with the experimental values for a better comparison.

The magnetic properties of the samples **84c**, **87-89c**, **87d**, **88d**, **99d**, **100d** were determined in the temperature range 2 K ≤ T ≤ 270 K and in magnetic fields $B \leq 5$ T using a Quantum Design SQUID magnetometer.[23] All the data were corrected for the temperature-independent diamagnetic core contribution of the constituents[98] and the magnetic contribution of the sample holder.[‡‡‡] For the temperatures below 2 K the AC-susceptibility shown in *Figure 3.43* was recorded using an ultra-high resolution AC-susceptometer adapted to a ^{3}He-^{4}He top-loading dilution refrigerator. The compensated-coil susceptometer was optimized for measuring small single crystals in the mg range. The system was equipped with a 12 T superconducting magnet.

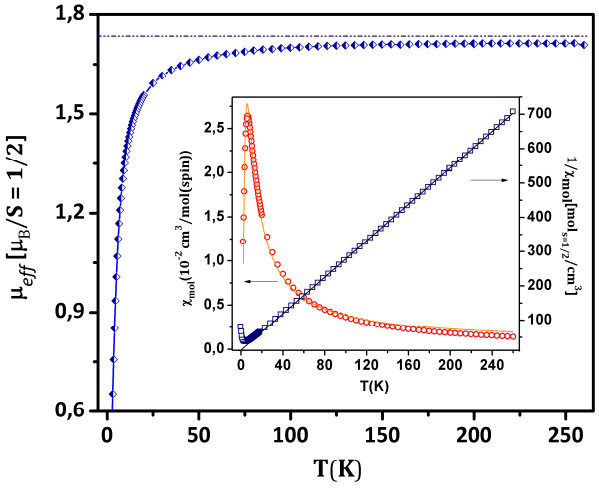

Figure 3.39. Effective magnetic moment $\mu_{eff} = \chi \cdot T$ per S = ½ spin of **87c**. The broken line indicates exactly the theoretical value of 1.73 μ_B of a spin S = 1/2 system. Inset: molar susceptibility χ_{mol} (left scale) and invers (right scale) of molar susceptibility as a function of temperature in the range 2 K < T < 270 together with fitting calculation (Thick solid line refers to the Curie-Weiss fit and broken line for Bleany-Bowers fit).

[‡‡‡] Magnetic measurements were performed by PhD student Pham Thanh Cong and Prof. Dr. Bernd Wolf at Physikalisches Institut, J.W. Goethe-Universität (Frankfurt).

Generally, all the biradicals under investigation (**84c**, **87-89c**, **87d**, **88d**, **99d**, **100d**) featured a similar magnetic behaviour in the studied temperature range. As an example, the effective magnetic moment per spin (μ_{eff}) of the biradical **87c** is shown in *Figure 3.39*. The observed μ_{eff} is nearly temperature independent in the range of 100-270 K, and with 1.71 μ_B matches almost exactly the theoretical value of 1.73 μ_B, (broken line in *Fig. 3.39*) expected for a single, uncoupled spin $S = ½$ at high temperatures. That is a clear indicator of the high quality of the synthesized single crystalline material. For the biradicals **84c**, **88c**, **89c**, **87d**, **88d**, **99d** and **100d** values of 1.71 ± 0.02 μ_B of μ_{eff} were found.

On cooling the magnetic susceptibility reaches a maximum and then tends to fall to zero (*i.e.* $J < 0$, as shown in *Figure 3.40*). That means that only the diamagnetic ground state is thermally populated, which is a clear evidence of dominant antiferromagnetic through-bond interactions between the radical centers (*intra*-dimer coupling). The temperature T_{max} where the maximum is located is related to J as: $/J/ / k_B T_{max}$ = 1.599 (*Table 3.7*).

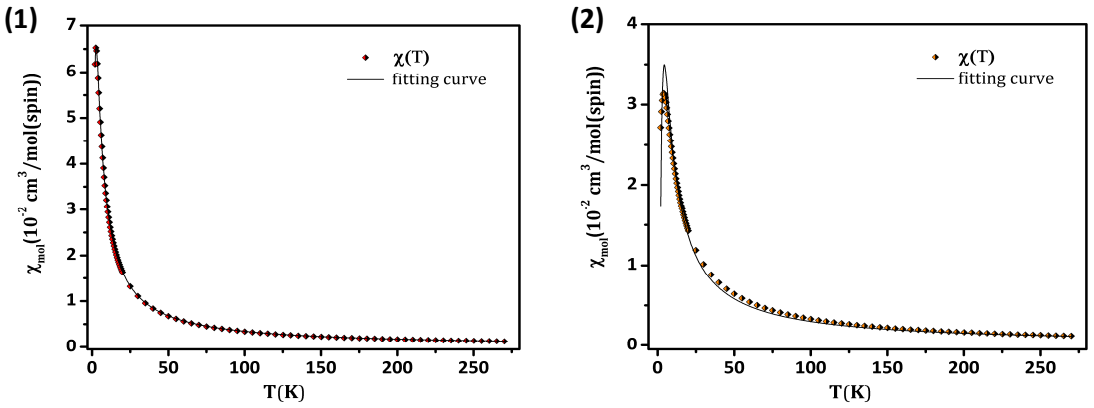

Figure 3.40. Molar susceptibility χ_{mol} of the imino biradicals (1) **87d** and (2) **100d** as a function of temperature in the range 2 K < T < 270 together with the fitting calculation

An estimate of the mean value for the magnetic exchange coupling in the high-temperature regime can be obtained by fitting the inverse magnetic susceptibility $1/\chi_{mol}$ by a Curie-Weiss model in the temperature range 70 K ≤ *T* ≤ 270 K, cf. straight line in the inset of *Figure 3.39*. The fit yields antiferromagnetic Weiss temperature θ = - (8.2 ± 0.5) K.

For a more precise determination of the dominant magnetic interactions, the temperature dependence of the molar magnetic susceptibility over the whole temperature range 2 K ≤ *T* ≤ 270 K was fitted using the Bleaney-Bowers equation (*20*) for the isolated dimers:[99]

$$\chi_{dimer} = \frac{2N(\mu_B g)^2}{k_B T(3+\exp(\frac{J}{k_B T}))} + \chi_c \qquad (20)$$

where N is Avogadro's number, χ_c is the temperature-independent term (due to the impurity of the sample), J is the *intra*molecular interaction. The *intra*-dimer magnetic exchange coupling constant J_{intra} between two S = ½ spins used in this expression refers to a Hamiltonian of the form $H = -2JS_1S_2$, which was taken also for the DFT calculations.

Table 3.7. The *intra*-dimer magnetic exchange coupling calculated J_{calc} and experimental constant J_{exp} values. T_{max} denotes the position of the maximum in $\chi_{mol}(T)$

Radical	T_{max} [K]	J_{calc}[K] [a]	J_{calc}[K] [b]	J_{calc}[K] [c]	J_{exp}[K]
84c	3.2	-14.4	-5.8	-2.6	-2.4
87c	6.3	-16.8	-8.3	-5.0	-4.8
88c	7.0	-19.6	-9.8	-5.6	-5.3 - 5.6
89c	57.0	-2.4	-3.1	-45.6	-45.5(!)
87d	2.5	-2.6	-1.6	-2.2	-2.2
99d	4.0	-4.7	-5.0	-3.2	-3.5
100d	4.0	-3.2	-3.6	-3.2	-3.2

[a] Optimized geometries were obtained from DFT calculations (B3LYP, 6-31 G*), then the broken symmetry approach was applied (BLYP, 6-31 G* for the evaluation of *J*).

[b] The exchange interactions were evaluated for X-ray crystal structures applying the broken symmetry approach with BLYP functionals and 6-31G* basis set.

[c] Expected from the isolated dimer model, where $2J/k_B T_{max} = 1.599$.

The biradicals **84c**, **88c**, **87d**, **88d**, **99d** and **100d** exhibited similar behaviour, in accordance with the theoretical prediction, and their $\chi_{mol}(T)$ data were analyzed by an analogous procedure. Their *intra*-dimer exchange constants are listed in *Table 3.7*. Remarkably, the imino nitroxide **88d** showed a paramagnetic susceptibility down to 2K – the lowest value of the temperature, which can be reached using a conventional bulk susceptibility apparatus (SQUID). In other words, the magnetic couplings in the derivative **88d** are less than 1.5K. However, closer examination of the low-temperature ($T < J_{intra}/k_B$) susceptibility data for the studied biradicals revealed significant deviations from the isolated-dimer model. These deviations were attributed to the small magnetic *inter*molecular interactions between the neighbouring biradicals mediated via hydrogen

bonds (**84c**, **88c**). The strength of these interactions depends on the distance and relative orientation of the radicals.[100,101]

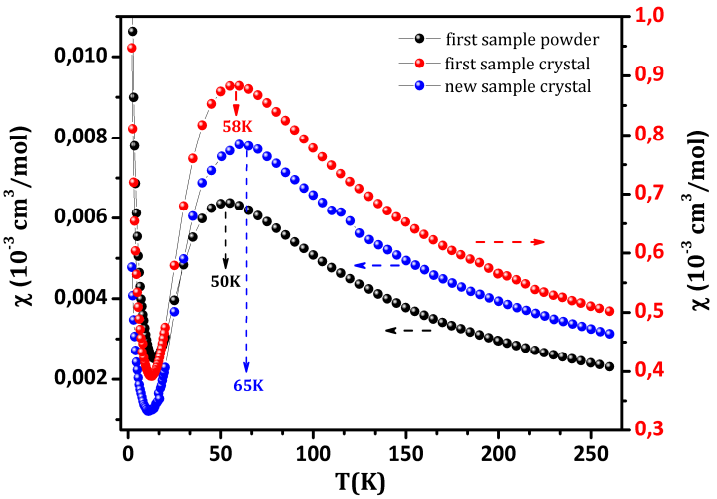

Figure 3.41. Susceptibility χ_{mol} of the nitronyl biradical **89c** as a function of temperature in the range 2 K < T < 270 (red scale corresponds to the measurements carried out for the first crystalline sample).

Important to note, that the magnetic behaviour of the derivative **89c** strongly contrasted with the other studied biradical systems (*Fig. 3.41*). Moreover, considerable deviations from the theoretically predicted values were observed (cf. *Table 3.7*). This might be the result of the magneto-structural correlation influence and/or strong *inter*molecular exchange interactions existing in the material. This phenomenon was reproducible and independent of the samples of 3,3-diazatolane nitronyl nitroxide **89c**, as illustrated in *Figure 3.41.* Here, the magnetic behaviour of the powder sample and the crystalline materials obtained under different crystallization conditions was compared (titled as the 'first sample' and the 'new sample' in *Figure 3.41*, respectively). The temperature dependences of the $\chi_{mol}(T)$ values was analyzed to give the best fit value J_{intra} = -45.5 K (*Table 3.7*).

A single energy calculation for the triplet and the singlet states of the crystal structure geometry provided us the value J_{inter}/k_B ~ -3.2 K for the biradical **89c**. Upon further analysis of the X-ray data short antiferromagnetic contacts of ~3.5 Å between the two NO fragments in 3,3'-diazatolane nitronyl nitroxide shown in *Figure 3.42* were found. These linkages were considered to be responsible for the unexpectedly strong exchange interactions within the molecule. Hence, taking into account these *inter*molecular

interactions the value J_{intra}/k_B ~ -87.3 K was calculated, which is very close to the experimentally obtained one.

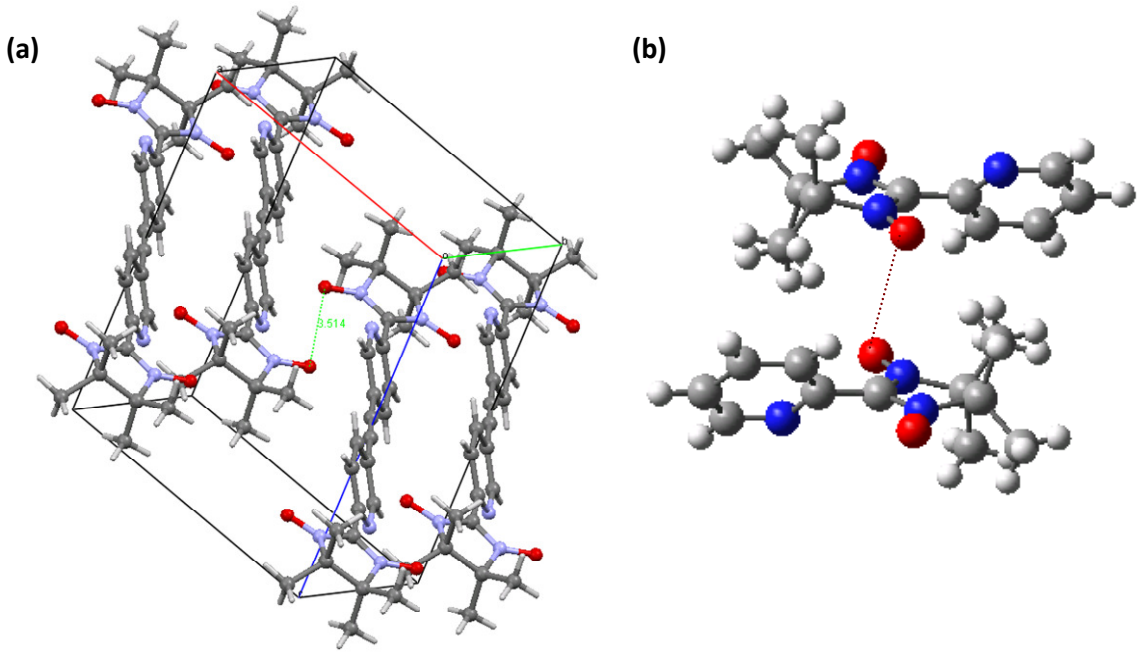

Figure 3.42. Crystal structure of the nitronyl biradical **89c**: (a) the unit cell; (b) fragment of the structure with emphasized short antiferromagnetic contacts.

The magnetic interactions based on structural peculiarities are difficult to predict. The strength of these interactions strongly depends on the relative geometry between the interacting magnetic orbitals, which is also determined by the crystal packing. As a matter of fact, the torsion angles θ (see *Table 3.2*) play a crucial role in transmission of the effective π-conjugation between the spin carriers through the spacer. A rapid increase of the torsion hindered the conjugation within the system **89c**, decreasing the *intra*molecular exchange interactions within the molecule, and, conversely, enhancing the *inter*molecular coupling. As a result in **89c** unprecedentedly high value of the coupling constant was observed. Per contra, for the structurally similar biradicals **84c**, **87c**, **88c**, **87d**, **88d**, **99d** and **100d** weak through-space antiferromagnetic *intra*molecular interactions are predominant. This demonstrates the difficulties in the design and prediction of a target structure and the need for the experimental proof.

To study in more depth magnetic properties of the tolane bis(nitronyl nitroxide) **87c** the AC-susceptibility (shown in *Fig. 3.43*) at very low temperatures was measured. The rounded double-peak structure in the AC-susceptibility between the lower critical

field B_{c1} and the saturation field B_s of about 9.2 T indicates a field-induced magnetic transition. While a rounded double-peak structure is expected when the *inter*-dimer couplings are quasi two-dimensional, sharp peaks reflect three-dimensional interactions.

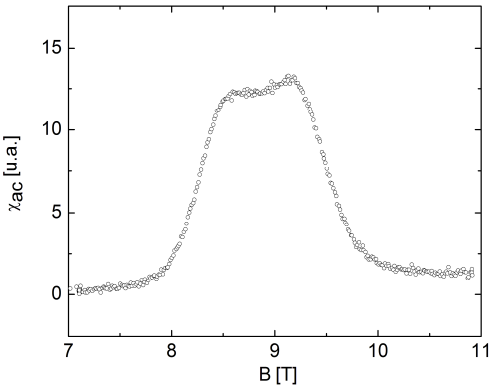

Figure 3.43. AC-susceptibility of the biradical **87c** at T = 191 mK. The data feature rounded peaks at $B_{c1} \approx 8.5$ T and $B_s \approx 9.2$ T.

In fact, a quasi two-dimensional magnetic behaviour for the biradical **87c** is also suggested by its crystal structure. From the difference of B_{c1} and B_s in the AC-susceptibility data, J_{inter} is estimated to be of the order of -1 to -2 K, a typical value for magnetic interactions mediated by hydrogen bridges. Thus, according to the magnetic characterization, the nitronyl biradical **87c** is a promising candidate for a purely organic low-dimensional quantum magnet.

3.8 Conclusion

In this study a family of novel nitronyl and imino nitroxide biradicals coupled via modified tolane linkers was synthesized and their magnetic behavior was studied.[26] The tolane bridge seemed to perfectly suite the requirements of *intra*dimer exchange coupling with $J \sim 10$ K. The structural analyses showed that the small torsions between the radical moieties (with exception in the case of derivative **89c**) and the modified diacetylene bridging subunit assist unimpeded through-bond exchange, as well as small intersheet distances (π-stacking) favor efficient magnetic interactions. Magnetic measurements and their interpretation revealed that the biradical **89c** exhibit surprisingly

strong antiferromagnetic interactions, owing to strong *inter*dimer interaction. In all other cases weak through-space antiferromagnetic interactions are predominant.

Summarizing, we found promising candidates for the quest to synthesize a purely organic molecular magnet. Efforts toward preparation of extended networks through the formation of complexes with different metal ions coordinated to the radical unit and/or π-bridge are presently on-going. It would be of interest to extend these studies to other series of tolane-bridged biradicals, in particular the idea to introduce additional chelating sites within the core is considered.

References

[1] D. A. Dougherty, *Mol. Cryst. Liq. Cryst.,* **1993** (232), 289 - 304.

[2] Y. Miura, K. Nakai, *Die Makromolekulare Chemie,* **1973** (172), 233-236.

[3] A. Griffin, D. W. Snoke, S. Stringari, *Bose-Einstein Condensation*, Cambridge University Press, Cambridge, **1995**.

[4] M. H. Anderson, J. R. Ensher, M. R. Matthews, C. E. Wieman, E. A. Cornell, *Science,* **1995** (269), 198.

[5] V. Barone, I. Cacelli, A. Ferretti, S. Monti, G. Prampolini, *Phys. Chem. Chem. Phys.*, **2011** (13), 4709-4714.

[6] (a) V. A. Ivanov, T. G. Aminov, V. M. Novotvortsev, V. T. Kalinnikov, *Izv. Akad. Nauk, Ser. Khim.,* **2004**, 2255; (b) C. Felser, G. H. Fecher, B. Balke, *Angew. Chem., Int. Ed.,* **2007** (46), 668.

[7] C. H. Bennett, D. P. DiVincenzo, *Nature,* **2000** (404), 247-255.

[8] H. P. Specht, C. Nölleke, A. Reiserer, M. Uphoff, G. Rempe, *Nature,* **2011** (473), 190-193.

[9] A. Galindo, M. A. Martin-Delgadot, *Rev. Mod. Phys.*, **2002** (74), 347.

[10] J. Zaanen, S. Chakravarty, T. Senthil, P. Anderson, P. A. Lee, J. Schmalian, M. Imada, D. Pines, M. Randeria, C. M. Varma, M. Vojta und T. M. Rice, *Nat. Phys*. **2006** (2), 138-143.

[11] M. Greiter, *Nat. Phys*., **2010** (6), 5-6.

[12] H.-S. Goan, *Int. J. Quantum Information,* **2005** (3), 27-40.

[13] C. Hirel, J. Pécaut, S. Choua, P. Turek, D. B. Amabilino, J. Veciana, P. Rey, *Eur. J. Org. Chem.,* **2005**, 348-359.

[14] J. Veciana, J. Cirujeda, C. Rovira, E. Molins, J. J. Novoa, *J. Phys. I France,* **1996** (6), 1967-1986.

[15] (a) In *Stable Radicals: Fundamentals and Applied Aspects of Odd-Electron Compounds* (ed.: R. G. Hicks), Wiley: Chichester, **2010**; (b) H. Nishide, K. Oyaizu, *Science,* **2008** (319), 737-738.

[16] (a) S. Nishida, Y. Morita, K. Fukui, K. Sato, D. Shiomi, T. Takui, K. Nakasuji, *Angew. Chem.,* **2005** (117), 7443-7446; *Angew. Chem. Int. Ed.,* **2005** (44), 7277-7280; (b) K. Sato, S. Nakazawa, R. Rahimi, T. Ise, S. Nishida, T. Yoshino, N. Mori, K. Toyota, D. Shiomi, Y. Yakiyama, Y. Morita, M. Kitagawa, K. Nakasuji, M. Nakahara, H. Hara, P. Carl, P. Höfer, T. Takui, *J. Mater. Chem.,* **2009**, (19), 3739-3754; (c) Y. Morita, S. Suzuki, K. Sato, T. Takui, *Nat. Chem.,* **2011** (3), 197-204.

[17] T. Sugawara, H. Komatsu, K. Suzuki, *Chem. Soc. Rev.,* **2011** (40), 3105-3118.

[18] (a) S. K. Pal, M. E. Itkis, F. S. Tham, R. W. Reed, R. T. Oakley, R. C. Haddon, *Science,* **2005** (309), 281-284; (b) A. Iwasaki, L. Hu, R. Suizu, K. Nomura, H. Yoshikawa, K. Awaga, Y. Noda, K. Kanai, Y. Ouchi, K. Seki, H. Ito, *Angew. Chem.,* **2009** (121), 4082-4084.

[19] (a) E. Coronado, A. J. Epstein, *J. Mater. Chem.,* **2009** (19), 1670-1671; (b) E. Coronado, P. Day, *Chem. Rev.,* **2004** (104), 5419-5448.

[20] (a) A. Caneschi, D. Gatteschi, R. Sessoli, P. Rey, *Acc. Chem. Chem. Res*., **1989** (22), 392; (b) K. Fegy, D. Luneau, T. Ohm, C. Paulsen, P. Rey, *Angew. Chem., Int. Ed. Engl.,* **1998** (37), 1270.

[21] Y. Wang, L. Wang, L. Ma, *J. Mol. Struct.*, **2008** (877), 138–144.

[22] M. Tamura, Y. Nakazawa, D. Shiomi, K. Nozawa, Y. Hosokoshi, M. Ishikawa, M. Takahashi, M. Kinoshita, *Chem. Phys. Lett.,* **1991** (186), 401.

[23] B. Wolf, C. T. Pham, Y. B. Borozdina, E Mostovich, M. Baumgarten, M Lang, *J. Phys.: Conf. Ser. 200*, **2010**, 1-4.

[24] (a) Ch. Rüegg, K. Kiefer, B. Thielemann, D. F. McMorrow, V. Zapf, B. Normand, M. B. Zvonarev, P. Bouillot, C. Kollath, T. Giamarchi, S. Capponi, D. Poilblanc, D. Biner, K. W. Krämer, *Phys. Rev. Lett.,* **2008**, (101), 247202; (b) V. Gurarie, J. T. Chalker, *Phys. Rev. Lett.,* **2002** (89), 136801; (c) T. Giamarchi, Ch. Rüegg, O. Tchernyshyov, *Nat. Phys.,* **2008** (4), 198 – 204.

[25] E. Mostovich, Y. Borozdina, V. Enkelmann, K. Remović-Langer, B. Wolf, M. Lang, M. Baumgarten, *Cryst. Growth Des.*, **2012** (12), 54–59.

[26] K. Yamaguchi, M. Okumura, J. Maki, T. Noro, H. Namimoto, M. Nakano, T. Fueno, K. Nakasuji, *Chem. Phys. Lett.,* **1992** (190), 353.

[27] P. Siemsen, R. C. Livingston**, F. Diedrich,** *Angew. Chem. Int. Ed.*, **2000** (39), 2632-2657.

[28] T. W. Greene, P. G. M. Wuts, *Protective Groups in Organic Synthesis* (sec. ed.), **1991**.

[29] S. Takahashi, Y. Kuroyama, K. Sonogashira, N. Hagihara, *Commun.*, **1980**, 627-630.

[30] F. M. Romero, R. Ziessel, M. Bonnet, Y. Pontillon, E. Ressouche, J. Schweizer, B. Delley, A. Grand, C. Paulsen, *J. Am. Chem. Soc.,* **2000** (122), 1298-1309.

[31] G. Zoppellaro, A. Geies, V. Enkelmann, M. Baumgarten, *Eur. J. Org. Chem.*, **2004**, 2367–2374.

[32] C. Bolm, M. Ewald, M. Felder, G. Schlinglo., *Chem. Ber.*, **1992** (125), 1169.

[33] (a) F. C. Alderweireldt, I. Vrijens, E. L. Esmans, E. De Clercq, *Nucleosides Nucleotides*, **1989** (8), 891; (b) J. Wicha, M. Masnyl, *Heterocycles*, **1981** (16), 521; (c) F. J. Romero-Salguero, J.-M. Lehn, *Tet. Lett*., **1999** (40), 859.

[34] X. Wang, P. Rabbat, P. O'Shea, R. Tillyer, E. J. J Grabowski, P. J. Reider, *Tetrahedron Lett.*, **2000** (41), 4335-4338.

[35] A. Landa, A. Minkkila, G. Blay, K. A. Jørgensen, *Chem. Eur. J.*, **2006**, (12), 3472 – 3483.

[36] M. A. Peterson, J. Mitchell, *J. Org. Chem.*, **1997** (62), 8237.

[37] F. Ebmeyer, F. Vögtle, *Chem. Ber.*, **1989** (122), 1725–1727.

[38] I. Karamé, M. Jahjah, A. Messaoudi, M. L. Tommasino, M. Lemaire, *Tetrahedron Asymm.*, **2004** (15), 1569-1581.

[39] R. Ziessel, G. Ulrich, R. C. Lawson, L. Echegoyen, *J. Mater. Chem.*, **1999** (9), 1435-1448.

[40] T. Kalai, J. Jeko, Z. Szabo, L. Parkanyi, K. Hideg, *Synthesis*, **1997**, 1049-1055.

[41] V. A. Reznikov, L. B. Volodarsky, *Tetrahedron*, **1993** (49), 10669.

[42] E. Tretyakov, S. Tolstikov, A. Mareev, A. Medvedeva, G. Romanenko, D. Stass, A. Bogomyakov, V. Ovcharenko, *Eur. J.Org. Chem.,* **2009**, 2548-2561.

[43] E.V. Tretyakov, V.I. Ovcharenko, *Russ. Chem. Rev.,* **2009** (78*)*, 971-1012.

[44] B. J. Graham, M. W. Justin, G. Hynd, J. K. Wyatt, P. M. Warner, R. S. Huber, A. Li, M. W. Kilgore, R. P. Sticca, R. S. Pollenz, *J. Org. Chem.*, **2002** (67), 5727-5732.

[45] (a) M. W. Khan, M. J. Alam, M. A. Rashid, R. Chowdhury, *Bioorg*. *Med. Chem*., **2005** (13), 4796–4805; (b) C. Ma, A. Lo, A. Abdolmaleki, M. J. MacLachlan, *Org*. *Lett.*, **2004** (6), 3841-3844.

[46] M. Kimura, A. Ezoe, M. Mori, Y. Tamaru, *J. Am. Chem. Soc*., **2005** (127), 201-209.

[47] R. Severin, J. Reimer, S. Doye, *J. Org. Chem*., **2010** (75), 3518–3521.

[48] (a) Z. Novák, G. Timári, A. Kotschy, *Tetrahedron*, **2003** (59), 7509; (b) M. Csékei, Z. Novák, G. Timári, A. Kotschy, *Arkivoc*, **2004** (vii), 285-291.

[49] M. J. Mio, L. C. Kopel, J. B. Braun, T. L. Gadzikwa, K. L. Hull, R. G. Brisbois, C. J. Markworth, P. A. Grieco, *Org. Lett.,* **2002** (4), 3199-3202.

[50] A. F. Littke, C. G. Fu, *Angew. Chem. Int. Ed.*, **1999** (38), 2411-2413.

[51] S. P. H. Mee, V. Lee, J. E. Baldwin, *Angew. Chem. Int. Ed*., **2004** (43), 1132 –1132.

[52] B. Liedholm, *J. Chem. Soc. Perkin Trans*., **1992** (1), 2235-2237.

[53] (a) J. R. Dalton, S. L. Regen, *J. Org. Chem*, **1979** (44), 4443; (b) K. Takagi, K. Sasaki, Y. Sakakibara, *Bull. Chem. Soc. Jpn.*, **1991** (64), 1118; (c) D. M. Tschaen, R. Desmond, A.O. King, M. C. Fortin, B. Pipik, S. King, T.R. Verhoeven, *Synth. Commun.*, **1994** (24), 887-890.

[54] E. Negishi, N. Okukado, A. O. King, D. E. Van Horn, B. I. Spiegel, *J. Am. Chem. Soc.*, **1978** (100), 2254.

[55] (a) J. Zhang, J. Wang, H. Wu, G. Zhu, X. Cui, L. Tang, *Bioorg. Med. Chem. Lett*., **2009** (19), 3324–3327; (b) G. Mao, A. Orita, D. Matsuo, T. Hirate, T. Iwanaga, S. Toyota, J. Otera, *Tet. Lett.*, **2009** (50), 2860–2864; (c) W.-W. Mao, T.-T. Wang, H.-P. Zeng, Z.-Y. Wang, J.-G. Shen, *Bioorg. Med. Chem. Lett.*, **2009** (19), 4570–4573; (d) P. A. Brough, X. Barril, J. Borgognoni, P. Chene, N. G. M. Davies, B. Davis, M. J. Drysdale, B. Dymock, S. A. Eccles, C. Garcia-Echeverria, C. Fromont, A. Hayes, R. E. Hubbard, A. M. Jordan, M. R. Jensen, A. Massey, A. Merrett, A. Padfield, R. Parsons, T. Radimerski, F. I. Raynaud, A. Robertson, S. D. Roughley, J. Schoepfer, H. Simmonite, S. Y. Sharp, A. Surgenor, M. Valenti, S. Walls, P. Webb, M. Wood, P. L. Workman, L. Wright, *J. Med. Chem*., **2009** (52), 4794–4809.

[56] J. H. Osiecki, E. F. Ullman, *J. Am. Chem. Soc.,* **1968** (90), 1078.

[57] (a) P. M. Lahti, *Magnetic Properties of Organic Materials* (ed.: Marcel Dekker), New York, **1999**; (b) J. A. Crayston, J. N. Devine, J. C. Walton, *Tetrahedron,* **2000** (56), 7829-7857.

[58] (a) D. A. Dougherty, *Acc. Chem. Res*., **1991**, (24), 88-94; (b) C. Rajadurai, A. Ivanova, V. Enkelmann, M. Baumgarten, *J. Org. Chem.,* **2003** (68), 9907-9915.

[59] J. Luzón, J. Campo, F. Palacio, G. J. McIntyre, A. E. Goeta, C. M. Pask, J. M. Rawson, *Polyhedron*, **2003** (22), 2301.

[60] (a) T. Ishida, H. Iwamura, *J. Am. Chem. Soc.,* **1991** (113), 4238; (b) K. Inoue, H. Iwamura, *J. Am. Chem. Soc.,* **1994** (116), 3173.

[61] F. Kanno, K. Inoue, N. Koga, H. Iwamura, *J. Phys. Chem*., **1997** (97), 13267.

[62] M. Baumgarten, *Acta Chem. Scan.,* **1997** (51), 193.

[63] W. M. Nau, *Angew. Chem. Int. Ed. Engl*., **1997** (36), 2445.

[64] Y. Miura, Y. Ushitani, K. Inui, Y. Teki, T. Takui, K. Itoh, *Macromol*., **1993** (232), 135-142.

[65] E. Tretyakov, G. Romanenko, V. Ikorskii, D. Stass, V. Vasiliev, M. Demina, A. Mareev, A. Medvedeva, E. Gorelik, V. Ovcharenko, *Eur. J. Org. Chem.*, **2007**, 3639–3647.

[66] S. V. Klyatskaya, E. V. Tretyakov, S. F. Vasilevsky, *Russ. Chem. Bull. Int. Ed.,* **2002** (51), 128-134.

[67] Y. Hosokoshi, M. Tamura, K. Nozawa, S. Suzuki, M. Kinoshita., H. Sawa, R. Kato, *Synth. Metals*, **1995** (71), 1795-1796.

[68] F. M. Romero, R. Ziessel, *Tetrahedron Lett.,* **1999** (40), 1895–1898.

[69] B. W. Howk, J. C. Sauer, *Org. Synth.*, **1963** (4), 801; **1959** (39), 59.

[70] E. Tretyakov, G. Romanenko, A. Podoplelov, V. Ovcharenko *Eur. J. Org. Chem.*, **2006**, 2695–2702.

[71] V. A. Reznikov, G. I. Roshchupkina, D. G. Mazukin, P. A. Petrov, S. A. Popov, S. V. Fokin, G. V. Romanenko, T. V. Rybalova, Y. V. Gatilov, Y. G. Shvedenkov, I. G. Irtegova, L. A. Shundrin, V. I. Ovcharenko, *Eur. J. Org. Chem.,* **2004***,* 749-765.

[72] E. V. Tretyakov, A. V. Tkachev, T. V. Rybalova, Y. V. Gatilov, D. W. Knight, S. F. Vasilevsky, *Tetrahedron*, **2000** (56), 10075 – 10080.

[73] G. Zoppellaro, *PhD Thesis*, **2004**, Mainz.

[74] T. Yoshida, S. Kaizaki, *Inorg. Chem.,* **1999** (38)*,* 1054-1058.

[75] (a) L. Catala, J. L. Moigne, N. Gruber, J. J. Novoa, P. Rabu, E. Belorizky, P. Turek, *Chem. Eur. J.*, **2005** (11), 2440 – 2454; (b) O. N. Chupakhin, I. A. Utepova, M. V. Varaksin, E. V. Tretyakov, G. V. Romanenko, D. V. Stass, V. I. Ovcharenko, *J. Org. Chem.*, **2009** (74), 2870 – 2872; (c) S. V. Klyatskaya, E. V. Tretyakov, S. F. Vasilevsky, *Russ. Chem. Bull. Int.Ed.,* **2002** (51), 128-134; (d) J. H. Osiecki, E. F. Ullman, *J. Am. Chem. Soc*, **1968** (90), 1078.

[76] (a) I. A. Grigor'ev, M. M. Mitasov, G. I. Shichikin, L. B. Volodarskii, *Seriya Khimicheskaya*, **1979** (11), 2606, *Russ. Chem. Bull.,* **1979** (28), 2421-2424; (b) L. Rintoul, A. S. Micallef, S. E. Bottle, *Specrtochimica Acta Part A*, **2008** (70), 713–717.

[77] G. Zoppellaro, A. Ivanova, V. Enkelmann, A. Geies, M. Baumgarten, *Polyhedron*, **2003** (22), 2099-2110.

[78] (a) K. N. Wong, S. T. Colson, *J. Mol. Spectr.*, **1984** (104), 129-151; (b) K. N. Wong, S. T. Colson, *J. Phys. Chem.*, **1957** (61), 458–462.

[79] V. Ovcharenko, E. Fursova, G. Romanenko, I. Eremenko, E. Tretyakov, V. Ikorskii, *Inorg. Chem.*, **2006** (45), 5338.

[80] (a) A. Caneschi, D. Gatteschi, P. Rey, *Prog. Inorg. Chem.*, **1991** (39), 331; (b) A. Caneschi, P. Chiesi, L. David, F. Ferraro, D. Gatteschi, R. Sessoli, *Inorg. Chem.*, **1993** (32), 1445-1453.

[81] K. Itoh, M. Kinoshita, *Molecular Magnetism. New Magnetic Materials*, Gordon and Breach Science: Amsterdam, **2000**.

[82] (a) P. H. Rieger, *Electrochemistry* (sec. ed.), Springer, **1994**; (b) P. Atkins, T. Overton, J. Rourke, M. Weller, F. Armstrong, *Inorganic Chemistry* (fourth ed.), OUP, **2006**.

[83] Y. Morita, S. Nishida, J. Kawai, T. Takui, K. Nakasuji, *Pure. Appl. Chem.*, **2008** (80), 507–517.

[84] (a) R. Ziessel, G. Ulrich, R. C. Lawson, L. Echegoyen, *J. Mater. Chem.*, **1999** (9), 1435–1448; (b) L. Bugnon, C. J. H. Morton, P. Novak, J. Vetter, P. Nesvadba, *Chem. Mater.*, **2007** (19), 2910–2914.

[85] (a) T. Malinski, J. R. Fish, S. G. Swarts, M. D. Sevilla, *J. Phys. Chem.*, **1988** (92), 3745; (b) D. Serve, *Electrochim. Acta*, **1975** (20), 469.

[86] A. J. Bard, L. R. Faulkner, *Electrochemical Methods* (sec. ed.), J. Wiley & Sons Press, **2000**.

[87] (a) L. Marx, B. Schöllhorn, *New J. Chem.*, **2006** (30), 430-434; (b) M. Castillo, E. Brillas, C. Rillo, M. D. Kuzmin, L. Juliá, *Tetrahedron*, **2007** (63), 708-716.

[88] (a) G. Morris, G. Sosnovsky, B. Hui, C. O. Huber, N. U. M. Rao, H. M. Swartz, *J. Pharm. Sci.*, **1991** (80), 149; (b) P. H. Krzyczmonik, H. Scholl, *J. Electroanal. Chem.*, **1992** (335), 233-251.

[89] (a) W. Heisenberg, *Z. Phys*., **1928** (49), 168; (b) P. A. M. Dirac, *The principles of Quantum Mechanics* (3rd ed.), Clarendon, Oxford.

[90] W. J. Casper, *Spin Systems*, World Scientific, Singapore, **1989**.

[91] (a) K. Yoshida, *Theory of Magnetism*, Springer, Berlin-Heidelberg-New York, **1998**; (b) F. E. Mabbs, D. Collins, *Electron Paramagnetic resonance of Transition Metal Compounds*, Elsevier, **1992**; (c) M. S. De Groot, J. H. van dr Waals, *Physica*, **1963** (29), 1128; (d) J.-Ph. Grivet, J. Mispelter, *Mol. Phys.*, **1974** (27), 15.

[92] J. E. Wertz, J. R. Bolton, *Electron Spin Resonance, Elementary Theory and Practical Applications*, Chapman & Hall, **1986**.

[93] O. Kahn, *Magnetism: A Supramolecular Function* (ed.: Kluwer), Dordrecht, **1996**.

[94] (a) P. W. Anderson, *Phys. Rev.*, **1959** (115), 2-13; (b) J. E. Wertz, J. R. Bolton, *Electron Spin Resonance, Elementary Theory and Practical Applications*, Chapman & Hall, **1986**, 153-154; (c) Y. Kobori , K. Takeda, K. Tsuji, A. Kawai, K. Obi, *J. Phys. Chem. A*, **1998** (102), 5160.

[95] L. Catala, J. L. Moigne, N. Kyrisakas, P. Rey, J. J. Novoa, P. Turek, *Chem. Eur. J.*, **2001** (7), 2466–2480.

[96] G. R. Luckhurst, A. Hudson, *Mol. Phys.*, **1967** (13), 409.

[97] (a) M. Shoji, K. Koizumi, Y. Kitagawa, T. Kawakami, S. Yamanaka, M. Okumura, K. Yamaguchi, *Chem. Phys. Lett.*, **2006** (432), 343–347; (b) T. Soda, Y. Kitagawa, T. Onishi, Y. Takano, Y. Shigeta, H. Nagao, Y. Yoshioka, K. Yamaguchi, *Chem. Phys. Lett.*, **2000** (319), 223–230; (c) K. Yamaguchi, F. Jensen, A. Dorigo, K. N. Houk, *Chem. Phys. Lett.*, **1988** (149), 537–542.

[98] C. T. Pham, B. Wolf, M. Lang, Y. B. Borozdina, M. Baumgarten, manuscript in preparation.

[99] A. Zheludev, V. Barone, M. Bonnet, B. Delley, A. Grand, E. Ressouche, P. Rey, R. Subra, J. Schweitzer, *J. Am. Chem. Soc.*, **1994** (116), 2019.

[100] (a) T. Mitsumori, K. Lnoue, N. Koga, H. Iwamura, *J. Am. Chem. Soc.*, **1995** (117), 2467; (b) R. Akabane, M. Tanaka, K. Matsuo, N. Koga, K. Matsuda, H. Iwamura, *J. Org. Chem.*, **1997** (62), 8854.

[101] B. Bleaney, D. K. Bowers, *Proc. R. Soc. London, Ser. A.*, **1952** (214), 451.

Chapter 4

Summary and Outlook

The main objectives of this work were the design, synthesis and characterization of novel π-conjugated spin systems. As the spin carriers, *nitroxide radicals* were chosen due to their stability and bidentate character. Nitroxides find applications in a wide variety of fields, including free radical polymerization, EPR imaging, spin probing and magnetic materials. This research work is focused on the last two aspects.

1. Hybrid fluorophore-nitroxide molecules

It has recently been shown that covalently linked nitroxide-fluorophore hybrid molecules can be employed as sensitive optical probes of radical and redox reactions. The high interest in such hybrid molecules is based on their potential application as a versatile analytical tool in physicochemistry, biochemistry, medicine and even environmental chemistry. It was suggested that the efficiency of such hybrid molecules in sensing applications could be significantly improved by the introduction of an appropriate spacer into the radical-fluorophore system. The spacer can be selected based on the analysis of the corresponding absorption data.

In this project three probes, containing nitronyl or imino nitroxide radical covalently linked to a fluorophore (pyrene or perylene), have been designed. The synthesis of the nitroxide radicals relies, in general, on the condensation between 2,3-bis(hydroxyamino)-2,3-dimethylbutane with the corresponding aldehyde, followed by the oxidation of the condensation products under well-controlled conditions into the nitronyl (NN) or imino (IN) nitroxide species. In order to assemble the aldehyde precursors **57-58a** bromination, copper-catalyzed condensation of pyrazole with bromo-pyrene and Vilsmeier–Haack reactions were employed. Furthermore, to expand our knowledge about the correlation between the structure of a spacer attached to the radical unit and the probe sensitivity, eight anthracene-based nitroxides were synthesized. Here, Suzuki and

Sonogashira-Hagihara coupling methodologies were applied to assemble the carbaldehyde derivatives **59-62a**.

The X-band EPR spectra recorded for monoradicals **57-62c** at room temperature in fluid (non-viscous) solutions exhibit a pattern of five lines, while the imino species **57**,**59-62d** feature seven line spectra, typical fingerprints of nitroxides. X-ray diffraction studies performed on dark-blue needle-like crystals of the pyrazole-pyrene **57c**, phenyl-anthracene **59c,** phenyl-ethynylanthracene **60c** and phenyl-bromoanthracene **62c** and red blocks of the pyrazole-pyrene **57d**, phenyl-anthracene **59d** and phenyl-bromoanthracene **62d** confirm the molecular structure of the derivatives. Despite numerous attempts no suitable crystals of NN **58c** were achieved. In fact, storage of the radical **58c** solutions at room temperature led to decomposition of the compound. Absorption data analysis reveals that 3-[4-(1-oxyl-3-oxo-4,4,5,5-tetramethylimidazolidin-2-yl)-pyrazole]perylene **58c** possesses an unexpectedly low molar extinction coefficient (in comparison to other perylene derivatives), which was attributed to the low stability of the radical solutions at room temperature. To avoid inaccurate results, perylene NN **58c** was not involved in further sensing experiments.

UV-Vis spectra of the nitronyl nitroxides show two specific absorption bands. The first corresponds to the n-π^* transitions of the aminoxyl oxide moieties, and appears at ~ 600 nm. The second absorption band includes π-π^* transitions and occurs at a much higher energy, in the 300-380 nm wavelength range. It was noted that both the position and intensity of the bands could be tuned by varying the structure of the substituent to which the radical unit is attached. Thus, pyrene nitronyl nitroxide **80c** shows rather weak n-π^* absorption in the visible range (~ 500 $M^{-1}cm^{-1}$), while introduction of the pyrazole hetero ring into the radical-fluorophore π-system **57c** significantly enhanced the transition intensity (~ 1000 $M^{-1}cm^{-1}$). Additionally for NN **57c** a ~10 nm blue-shift of the π-π^* absorption was observed. The imino nitroxide **57d** radical has a bright orange-red colour in solution, with a broad absorption band at 467 nm (n-π^* transitions). The π-π^* transition appears at a similar wavelength as in the spectra of the nitronyl analogue (345 nm), although the absorption intensity is slightly lower.

The UV-Vis studies of the anthracene series **59-62c**,**d** show that the pyrazole containing nitronyl radical **61c** exhibits the highest intensity n-π^* transition, as for the pyrene derivative **57c**. Extension of the conjugation in the compounds **60c** and **60d** results

in a bathochromic shift of the n-π^* absorption of ~20 and 30 nm, respectively (relative to the phenyl-anthracene radical **59c**), but with a lower extinction coefficient.

Photophysical studies of the radicals **57c** and **57d** in solution reveal that for IN **57d**, emission intensity tends to decrease linearly upon dilution, while in the case of the NN derivative **57c** the fluorescence is efficiently quenched over a broad range of concentrations (~ 10^{-4} - 10^{-6} M). This additional evidence confirms that the NN fragment more efficiently suppresses fluorescence in hybrid molecules. Owing to this property of the radical system **57c**, this nitronyl nitroxide has been successfully employed to monitor NO production in solution.

Moreover, it was demonstrated that the fluorescence quantum yield (QY) of the probes **57c** and **57d** could be substantially increased by subjecting the radicals to reactions leading to the loss of paramagnetism (*e.g.* treatment with antioxidants). Initially IN **57d** demonstrated a better response towards chemical agents. However, an accurate comparison of the fluorescence intensity changes over the parent radical (**57c** or **57d**) emission spectra (Φ/Φ_o) shows that nitronyl species **57c** exhibited higher sensitivity than the corresponding imino derivative **57d**. Furthermore, despite the general structural similarity of NNs **57c** and **80c**, introduction of the pyrazole spacer into the fluorophore-radical framework leads to a considerable enhancement of the molecules' sensitivity. For example, the QY (Φ/Φ_o) value for NN **57c** samples treated with cysteine was 2.55 (1.55) times higher than for the corresponding derivative without pyrazole, **80c**.

In efforts to find cell-friendly media, several solvents and solvent mixtures were tested. The probes **57c** and **57d** demonstrate qualitatively similar behaviour upon treatment with reagents in methanol, ethanol and DMSO. Furthermore, the applicability of the pyrene-pyrazole nitroxide (**57c** and **57d**) films for sensing in aqueous solutions was shown, although the reaction of the nitroxides with the additives was found to be much slower in the spin-coated films.

Notably, the π-bridge extension between the radical center and fluorophore (**60**) leads to a weaker intramolecular self-quenching, as seen in the emission spectra of the nitroxide radicals **60c**,**d**. Within the anthracene series **59-62c**,**d**, the most efficient fluorescence suppression, and, consequently, the highest fluorescence increase upon reaction with additives, is observed for derivatives **61c**,**d**. Although the anthracene-based radicals **59-62c**,**d** demonstrate weaker sensing ability relative to the pyrene-pyrazole

derivatives **57c**,**d**, the influence of the substituent character (**59**, **61**, **62**) and the length of the bridge between the radical center and the fluorophore (**60**) on the response was studied.

The findings presented in this work demonstrate a logical strategy for the engineering of novel radical systems with desirable sensing properties. This strategy is based upon the absorption properties of the fluorophore-nitroxide compounds. It is demonstrated, that the sensitivity of the synthesized radicals far surpasses literature known analogues.

2. Weakly-coupled spin ½ dimers

To obtain purely organic low-dimensional quantum magnets suitable for studying the phenomenon of Bose-Einstein condensation (BEC) of magnetic excitations, a family of novel nitronyl **84c**, **87-89c**, **112c** and imino **87d**, **88d**, **99d**, **100d** nitroxides with various π-bridges between the radical centers was synthesized, following a classical Ullman procedure. The appropriate molecular design of the coupling unit is crucial, since it provides control over the *intra*- and *inter*-molecular exchange interactions between spin carriers. The obtained π-conjugated systems **84c**, **87c** were made by rigid and planar molecules. It was suggested that additional contacts with heteroaromatic rings could offer a particularly attractive pathway for transmitting magnetic interaction. To this end, the diazatolane biradicals **88c** and **89c** were designed. Finally, the bis(imino nitroxides) **87d**, **88d**, **99d**, **100d** were considered for studying the influence of the radical unit on the ordering and exchange interaction.

EPR spectra of the nitronyl and imino nitroxide biradical systems recorded at room temperature show patterns of nine and thirteen lines, respectively, regardless of the different distances between radical centers, as well as the molecular identity of the coupling units employed. Thus, within the limit of X-band EPR spectroscopy, for the studied biradical systems strong exchange interactions $|J/A_N|$ >>1 between the spin carriers were experimentally verified. The NN biradicals exhibit the observed g_{iso} at ~2.0062 – 2.0065, while for IN the g values fall in a slightly lower range ~2.0057 – 2.0060. The solution EPR spectra of the biradical systems **84c**, **87c**, **88c**,**d** and **89c** show a very small increase in the peak-to-peak line-width upon cooling. In solution, NN and IN biradicals follow Curie-law behavior, with a linear increase of the signal intensities upon lowering the temperature down to ~ 230 K. Further cooling of the solutions leads to

anisotropic broadening of the signals. This process corresponds to the out of phase internal rotation of the two radical moieties, which is able to modulate the exchange interaction J. The EPR spectra of the monoradical systems recorded in toluene glass show patterns typical for axial systems, while for the imino biradical **100d** zero field splitting (*zfs*) is observed. In other cases (biradicals **94c**, **97c**,**d**, **98c**,**d**, **99c** and, unexpectedly, **99d**) most of the hyperfine couplings were not resolved. This is a direct consequence of the correlation between the *zfs* value and the relative intramolecular radical distance r. Thus, the increase of r causes a decrease in the *zfs* magnitude. The evaluated value of the radical distance in **100d** is ~ 12.7 Å, in good agreement with the value obtained from X-ray crystal structure analysis (~ 12 Å). For dilute solutions of the imino biradicals **99d** and **100d** the forbidden (ΔM_S = 2) half-field transition at g ~ 4.01 down to low temperatures is observed, thus supporting their biradical nature.

Crystal structure analysis shows that the synthesized biradicals are planar, with a relatively small twist around the radical fragments. These are essential prerequisites for obtaining weak intramolecular coupling. Additionally, short intersheet contacts (2.38 - 2.6 Å) are found to be favorable for magnetic interactions. Indeed, magnetic measurements carried out on crystalline samples confirm that for the biradicals **84c**, **87c**, **88c**, **87d**, **88d**, **99d** and **100d**, weak antiferromagnetic *intra*molecular interactions are predominant. According to the magnetic characterization these π-bridged nitroxides possess moderate *intra*-dimer coupling in the range -3 - 6 K.

2,2'-(5,5'-(Ethyne-1,2-diyl)bis(pyridine-2,5-diyl))bis(4,4,5,5-tetramethyl-4H,5H-imidazoline-1-oxyl-3-oxo) **89c** exhibits rather exceptional magnetic behavior, with unexpectedly high J/k_B (~-50 K). In fact, the magnetic interactions based on structural peculiarities are difficult to predict. The strength of these interactions strongly depends on the relative geometry between the interacting magnetic orbitals, which is also determined by the crystal packing. The detailed X-ray structure analysis, supported by theoretical calculations, reveals that a rapid increase of the dihedral angle between the radical entities and the pyridine rings from 25° to 51° hinders the conjugation, therefore decreasing *intra*molecular exchange interactions in 3,3'-diazatolane nitronyl nitroxide **89c**. However, for **89c**, additional short antiferromagnetic contacts (~3.5 Å) between two NO sites were found. These linkages are considered to be responsible for the unexpectedly strong *inter*molecular exchange interactions within the molecule. Taking

into account these *inter*molecular interactions the value J_{intra}/k_B ~ -87.3 K was calculated and found to be consistent with the experimentally obtained value. This demonstrates the difficulties in the design and prediction of a target structure and the need for an experimental proof.

The idea behind this investigation was to show how, by using a set of structural units, the *intra*molecular exchange interactions in π-conjugated spin systems can be adjusted to obtain molecules with the desired magnetic properties. Research on preparation of the extended networks through formation of complexes with different metal ions coordinated to the radical unit and/or π-bridge is presently ongoing (some encouraging results were recently obtained, *e.g.* silver complex with 2,2'-(bipyridine-1,1'-diyl)bis(4,4,5,5-tetramethylimidazolidine-1-oxyl) **100d**).

It is strongly believed that this study will stimulate further investigations in the field of nitroxide-based sensing and magnetic materials.

Chapter 5

Experimental Section

General Remarks. All chemicals and reagents were used as received from commercial sources (Acros Organics, Aldrich, Fluka, Lancaster, Merck and Strem) without additional purification. Solvents for synthesis were used as received, unless otherwise mentioned. ESR spectra were recorded in dilute, oxygen-free solutions in toluene, concentration ~10^{-4} mol×L, using a Bruker X-band spectrometer ESP300 E, equipped with an NMR gaussmeter (Bruker ER035), a frequency counter (Bruker ER041XK) and a variable temperature control continuous flow N_2 cryostat (Bruker B-VT 2000). The g-factor corrections were obtained using the DPPH (g = 2.0037) as standard. UV-Vis spectra were recorded in toluene solutions with a Perkin-Elmer spectrometer (UV/Vis/NIR Lambda 900) using a 1-cm optical path quartz cell at room temperature, unless otherwise specified. ^{1}H and ^{13}C NMR spectra were recorded on a Bruker DPX 250, Bruker DMX 300 spectrometer. Solid powders were pressed and IR spectra of the samples were recorded as they were (Nicolet 730 FT-IR spectrometer). Mass spectra were obtained on FDMS, VG Instruments ZAB-2 mass spectrometer. Elemental analyses were performed at the University of Mainz, Faculty of Chemistry and Pharmacy on a Foss Heraeus Varieo EL. The melting points were measured on a Büchi B-545 apparatus (uncorrected) by using open-ended capillaries. Atomic force microscopy (AFM) was performed by using a Nanoscope IIIa MultiMode scanning probe microscope; Digital Instruments, Santa Barbara, CA. The dynamic mode of AFM (Dimension 3100, Veeco Instruments, CA) was used to characterize structure and quality of the layers. OLYMPUS OMCL-AC240TS cantilevers were employed for imaging.

Theoretical calculations: all geometry calculations presented in this work were done with the B3LYP[§§§] non-local exchange-correlation density functional,[****] using the 6-

[§§§] B3LYP is a density functional obtained by taking the three parameter non-local exchange functional of Becke and the non-local correlation functional of Lee–Yang–Parr (a) A. D. Becke, *J. Chem. Phys.*, **1993** (98), 5648 – 5652; (b) C. Lee, W. Yang, R. G. Parr, *Phys. Rev. B*, **1988** (37), 785 –789.

[****] R. Parr, W. Yang, In *Density Functional Theory of Atoms and Molecules*; Oxford University Press: New York, **1998**.

31G* basis Gaussian set.[††††] The broken symmetry approach with BLYP functionals and 6-31G* basis set was applied for evaluation of exchange couplings, in order to avoid the overestimation brought about by Hartree-Fock contaminations. The tight option was used to obtain enough accuracy in computing the integrals and energy.

2,3-Dimethyl-2,3-bis(hydroxylamino)butane (BHA)

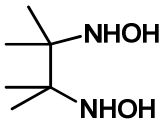

A mixture of 17.6 g 2,3-dimethyl-2,3-dinitrobutane and 27.0 g of Zn (dust) in 300 mL THF and 50 mL H_2O was cooled down to 0-5^oC in an ice bath. Keeping this temperature constant solution of 43 g NH_4Cl in 150 mL H_2O was added dropwise under vigorous (mechanical) stirring. After addition was completed (ca. 2.5 h) the reaction was stirred for 1.5 h at the same temperature, and an additional 0.5 h at room temperature. The white-gray precipitate of Zn slurry was filtered off, and was washed with THF (4×20 mL). Filtrate was evaporated to viscous residue, cooled to -15^oC (the mixture was kept in the freezer for 1 h). After that the flask was filled with argon and a mixture of 50 g Na_2CO_3 and 30 g NaCl salts was added at once. The flask was shaken for 15 min, and after homogenization the white solid was charged into a Soxhlet apparatus, protected from air (argon balloon) and extracted with 300 mL of dichloromethane (72 h). White precipitate was filtered off, washed with dichloromethane (2×15 mL), hexane (2×10 mL) and dried on air. Yield is 6.1 g (42%). **M.p.**: 160-161°C. **FT-IR** (powder, v/cm^{-1}): 3257 (vs and broad, ν_{OH}), 2987 (vs, ν_{C-H}), 1479-1374 (vs, several bands), 1261 (s), 1178 (vs), 1145 (vs), 1080 (s), 1035 (vs), 989 (m), 952 (vs), 904 (vs), 852 (m), 790 (m), 690 (m).

4-Iodo-pyrazole (66)

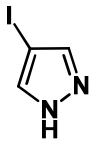

Pyrazole **65** (2.33 g, 34 mmol) was dissolved in acetonitrile (35 mL). Iodine (5.21 g, 20.5 mmol) was added to the solution followed by ceric ammonium nitrate (11.27 g, 20.5 mmol) portionwise over 10 min. The mixture was stirred at room temperature for 3 h, and the solvent was removed. Ethyl acetate (250 mL) and chilled 5% aqueous sodium bisulfite (100 mL) were added to the white residue. The organic layer was washed with

[††††] J. S. Binkley, J. A. Pople, W. J. Hehre, *J. Am. Chem. Soc.*, **1980** (102), 939 – 947.

brine, dried with sodium sulfate, and concentrated in *vacuo* to give 4-iodopyrazole **66** (6.25 g, 94%). **^{1}H NMR** (THF-d^{8}, 250 MHz, 298 K, 16 scan), δ (ppm): 7.61 (s, asymmetric, 2H, 2-CH), 11.64 (s, broad, 1H, -NH). **^{13}C NMR** ($CDCl_3$, 63 MHz, 256 scan), δ (ppm): 56.5 (C-I), 138.7 (C=C), 143.8 (C=C). **FD-MS** (70 kV, CH_2Cl_2) m/z: 194.4 (100%), MW calculated $C_9H_7BrN_3O$ (MW^+) 193.97.

1-(1-Ethoxyethyl)-4-iodo-pyrazole (67)

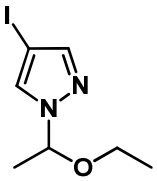

To a solution of 4-iodo-pyrazole **66** (6.25 g, 32 mmol, 1 eq.) in benzene (50 mL) 6 drops of HCl (33%, v/v) were added, followed by ethoxyethene (4.2 mL, d = 0.754 g/mL, 43.5 mmol, 1.4 eq.), and left under stirring for 6 h at 45-50°C. Bright yellow-orange solution was formed. Solution was cooled to ambient temperature and neutralized with $NaHCO_3$ saturated aqueous solution. The organic phase was separated, and the water phase was extracted with portions of benzene (3×10 mL). The combined organic extracts were dried over $MgSO_4$ and reduced to a small volume on rotary. The crude mixture was purified on Al_2O_3 column using a mixture of hexane/$CHCl_3$/ethyl acetate (2:4:1) to give 1-(1-ethoxyethyl)-4-iodo-pyrazole **67** as a pale yellowish oil in quantitative yield (92%). **^{1}H NMR** ($CDCl_3$, 250 MHz, 298 K, 16 scan), δ (ppm): 1.08 (t, ^{3}J = 7 Hz, 3H, -CH_3), 1.57 (d, ^{3}J = 6 Hz, 3H, -CH_3), 3.22-3.42 (m, 2H, -CH_2), 5.39-5.47 (q, ^{3}J = 6 Hz, 2H, -CH), 7.44 (s, 1H, -CH), 7.57 (s, 1H, -CH). **^{13}C NMR** ($CDCl_3$, 63 MHz, 298 K, 256 scan), δ (ppm): 14.7 (CH_2-$\underline{CH_3}$), 22.1 (CH-$\underline{CH_3}$), 57.3 (C-I), 64.2 ($\underline{CH_2}$-CH_3), 87.9 (-$\underline{CH}$-CH_3), 130.6 (C=C), 143.7 (C=C). **MS-FD** (70 eV, CH_2Cl_2) m/z: 266.1 (100%), MW calculated $C_7H_{11}IN_2O$ (MW^+) 266.08.

4-Formyl-1(*H*)-pyrazole (64)

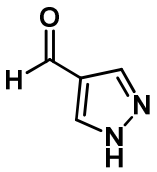

Route A. Tert-butyllithium (36 mL, 1.7 M hexane solution, 60 mmol) was charged into a flame-dried flask filled with argon and cooled to -78°C. Solution of 4-bromo-pyrazole **63** (3 g, 20 mmol) dissolved in 20 mL of THF was then added dropwise. A white precipitate appeared in the mixture when approximately half of *t*-BuLi was added. The temperature

was maintained for half an hour, and then allowed to increase slowly to -70°C. The mixture was stirred for 3 h at this temperature. The mixture was again cooled to -78°C (the precipitate reappeared) and dimethylformamide (2 mL, *d* = 0.944 g/mL, 25.9 mmol) was introduced with a syringe dropwise. The temperature was allowed to rise slowly. After stirring at room temperature for 1 h, the mixture was decomposed with ammonium chloride saturated solution. The reaction mixture was extracted with dichloromethane (4×40 mL), and combined organic extracts were dried over $MgSO_4$. Solvents were evaporated on rotary. Crude product was purified using flesh chromatography on silica gel with petroleum ether/ethyl acetate eluent (4:1 gradually to 2:1), to give compound **64** as slightly brownish solid (0.8 g, 41% yield).

Route B. 1-(1-Ethoxyethyl)-4-iodo-pyrazole **67** (1.5 mL, 5.2 mmol) and THF (6 mL) were placed into a flame-dried flask filled with argon. The resulting solution was cooled in an ice bath (0-4°C), and the solution of Grignard reagent EtMgBr (1.9 mL, 5.7 mmol) was added dropwise within 15 min. A milky suspension was slowly formed due to the low solubility of the pyrazolyl-magnesiate derivative. The mixture was left stirring for 2 h. Dry DMF (0.5 mL, 6.5 mmol) was added dropwise, while keeping the temperature constantly at around ~2°C. Solution was left under stirring overnight. Afterwards the mixture was decomposed with NH_4Cl saturated solution (25 mL). The organic layer was collected, and the water phase was extracted with portions of chloroform (3×15 mL). The combined organic extracts were dried over $MgSO_4$, and the solvents were evaporated in *vacuo*.

The residual pale yellowish oil contained the aldehyde still protected with the ethoxyethyl-group. Therefore, the oil was transferred into a flask together with HCl (10 mL, 20% in water) and dioxane (10 mL), and left stirring at 60°C overnight. The resulted solution was neutralized with K_2CO_3 saturated aqueous solution, and the water phase was extracted with ethyl acetate (5×10 mL). The organic phases were collected, reduced to a small volume and chromatographed over a SiO_2 column (ethyl acetate/ hexane, 1:2). 4-Formyl-1(*H*)-pyrazole **64** was collected as a yellowish powder (0.45 g, yield 90%). **^{1}H NMR** ($CDCl_3$, 250 MHz, 298 K, 16 scan), δ (ppm): 8.07 (d, 2H, -CH), 9.85 (s, 1H, -CHO), 12.05 (s, broad, 1H, -NH). **^{13}C NMR** ($CDCl_3$, 63 MHz, 298 K, 256 scan), δ (ppm): 123.9 (C-C-C), 136.5 (C=C), 184.9 (-CHO).

1-Pyrazole-pyrene (72)

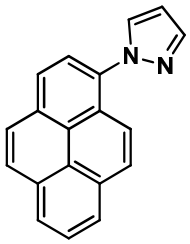

Solids - CuI (0.2 mmol), Cs_2CO_3 (2.0 mmol), pyrazole (1.4 mmol) and 1-bromo-pyrene **68** (1.0 mmol) - were transferred into a flame-dried flask. Dry dimethylformamide (6 mL) was added, and the resulting viscous mixture was deaerated using argon bubbles for 25 minutes. The mixture was heated at 120°C for 40 h under argon. After the reaction was completed (monitored by TLC on Al_2O_3), the mixture was cooled to ambient temperature, diluted with 2-3 mL of ethyl acetate, filtered through a plug of silica gel, and washed with 20 mL of ethyl acetate. The combined organic extracts were concentrated on rotary to a small volume, and the resulting residue was purified on silica gel using hexane/ethyl acetate gradient solvent mixture (100:0, 95:5, 90:10). Pyrene-pyrazole **72** was collected as light yellow solid in 75% yield. **M.p.**: 96-97°C. **^{1}H-NMR** ($CDCl_3$, 250 MHz, 298K, 16 scan), δ ppm: 6.61 (t, 1H, $H_{pyrazole}$), 7.91 (d, 1H, $H_{pyrazole}$), 8.0-8.24 (m, 9H, Ar-H), 9.0 (s, 1H, ArH). **^{13}C-NMR** ($CDCl_3$, 63 MHz, 298K, 256 scan), δ ppm: 106.8, 122.1, 123.6, 124.4, 124.8, 125.3, 125.6, 125.9, 126.2, 126.5, 127.1, 128.2, 128.88, 128.9, 131.2, 131.3, 132.1, 141.1.). **FT-IR** (powder, ν/cm^{-1}) 3141, 3123, 3095 (w, ν_{C-H}, aromatic), 3043, 2954, 2920, 2847 (m, ν_{C-H}), 1598 (m, ν_{Ar}), 1516 (vs), 1488 (m), 1460 (m), 1394 (vs, ν_{methyl}), 1336, 1307 (m, pyrazolyl- moiety), 835 (vs, ν_{Ar}). **MS-FD** (70 eV, CH_2Cl_2) 267.9 (100%), MW calculated $C_{19}H_{12}N_2$ (MW^+) 267.7.

3-Pyrazole-perylene (74)

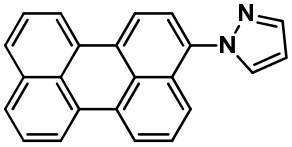

Following the method described above for the pyrene derivative **72** perylene derivative **74** was obtained. The reaction required an increased amount of dimethylformamide (15 mL) due to the low solubility of 3-bromoperylene **73** in this solvent. Flesh column on Al_2O_3 with hexane/dichloromethane gradient solvent mixture (6:1, 3:1) afforded **74** as orange solid in 63% yield. **M.p.**: 195-198°C. **^{1}H-NMR** (THF-d^8, 250 MHz, 298K, 16 scan), δ ppm:

6.41 (t, 1H, $H_{pyrazole}$), 7.36-7.46, 7.62-7.66, 8.21-8.28 (m, 12H, Ar-H), 7.86-7.87 (dd, 1H, $H_{pyrazole}$). **MS-FD** (70 eV, CH_2Cl_2) 317.9 (100%), MW calculated $C_{23}H_{14}N_2$ (MW^+) 318.37. **^{13}C-NMR** (THF-d^8, 63 MHz, 298K, 256 scan), δ ppm: 105.7, 119.2, 120.35, 120.4, 122.9, 123.2, 126.7, 127.6, 127.8, 128.0, 131.1, 134.4, 136.8, 140.0. **FT-IR** (powder, ν/cm^{-1}) 3101, 3048 (w, ν_{C-H}, aromatic), 3007, 2954, 2921 (m, ν_{C-H}), 1589 (m, ν_{Ar}), 1502 (vs), 1479 (m),1458 (m), 1396 (vs, ν_{methyl}), 1326 (m, pyrazolyl- moiety), 807 (vs, ν_{Ar}). **MS-FD** (70 eV, CH_2Cl_2) 317.9 (100%), MW calculated $C_{19}H_{12}N_2$ (MW^+) 318.12.

1-(4-Formyl-pyrazole)-pyrene (57a)

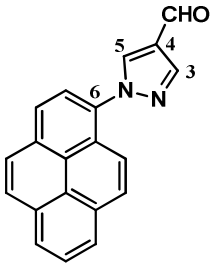

Vilsmeier-Haack reaction. Phosphorus oxychloride (1.4 mL, d = 1.645 g/mL, 15 mmol, 0.7 eq.) was added dropwise under vigorous stirring to dry dimethylformamide (1.6 mL, 20.7 mmol, 1 eq.) in a flame-dried flask equipped with a rubber septum, and the temperature being kept at ~0-5°C using an ice bath. 1-Pyrenepyrazole **72** (0.55 g, 2.07 mmol, 0.1 eq.) in dimethylformamide (2.6 mL) was then slowly added under stirring, and the temperature was maintained at 20-30°C. The resulting mixture was heated at 110°C for 3.5 h, cooled down to room temperature and then poured on a crashed ice. The solution was treated with 20% sodium hydroxide. The yellow precipitate was filtered off, washed with water and dried. The described procedure afforded pyrene aldehyde **57a** in 63% yield. **^{1}H-NMR** ($(CD_3)_2SO$, 250 MHz, 298 K, 16 scan), δ ppm: 7.98 (d, 1H, $H_{pyrazole}$), 8.16-8.5 (m, 9H, Ar-H), 9.14 (s, 1H, $H_{pyrazole}$), 10.05 (s, 1H, -CHO). **^{13}C-NMR** ($(CD_3)_2SO$, 63 MHz, 298 K, 8690 scan), δ ppm: 121.5, 123.9, 124.1, 125, 125.1, 125.3, 126, 126.4, 128.6, 129.2, 130.1, 130.7, 137.9, 141. **UV-Vis** ($CHCl_3$) λ/nm (ε, mol^{-1}×cm^{-1}): 345 (8247). **MS-FD** (70 eV, CH_2Cl_2) 295.9 (100%), MW calculated $C_{20}H_{12}N_2O$ (MW^+) 296.32.

3-(4-Formyl-pyrazole)-perylene (58a)

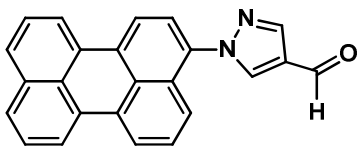

The method described previously for the carbaldehyde **57a** was applied towards perylene derivative **74**. Here, after the work-up and purification on a short column (Al_2O_3) with dichloromethane/ethyl acetate gradient solvent mixture (100:0, 99:1, 98.5:1.5), the product **58a** was obtained as a gaudy orange solid in 23% yield. **^{1}H-NMR** (THF-d^8, 250 MHz, 298 K, 145 scan), δ ppm: 7.84 (d, 1H, $H_{pyrazole}$), 7.6-8.27 (m, 11H, Ar-H), 8.52 (s, 1H, $H_{pyrazole}$), 9.88 (s, 1H, -CHO). **UV-Vis** ($CHCl_3$) λ/nm (ε, $mol^{-1}\times cm^{-1}$): 422 (4593), 447 (5817). **MS-FD** (70 eV, CH_2Cl_2) 346.1 (100%), MW calculated $C_{23}H_{14}N_2$ (MW^+) 346.38.

A1. General procedure of the condensation between 2,3-dimethyl-2,3-bis(hydroxylamino)butane and an aldehyde carried out in toluene. A suspension of BHA (1.1 eq. for each aldehyde group) and an aldehyde (1.0 eq.) in toluene (5 mL/1 mmol) was carefully deaerated using argon bubbling for ~20-25 minutes. The flask was provided with a condenser equipped with an argon balloon, and moved into an oil bath. The mixture was heated under argon near reflux for 2-18 h. The progress of the reaction was monitored by TLC (SiO_2, hexane/ethyl acetate or dichloromethane with 5% of methanol). After the process was completed and the flask was cooled down to room temperature, the precipitate (white or yellowish) was filtered off, washed with toluene (2×10 mL), heptane (1×10 mL) and dried on air. The so-obtained derivatives were used for the next step without additional purification.

A2. General procedure of the condensation between 2,3-dimethyl-2,3-bis(hydroxylamino)butane and an aldehyde carried out in absolute methanol. The solution containing BHA (1.3 eq. for each aldehyde group) and an aldehyde (1.0 eq.) in absolute deaerated methanol (10 mL/1 mmol) was stirred at room temperature for 12-72 h. Formed precipitate was filtered off, washed with cold (~5°C) methanol and dried on air. The product was used for the next step without additional purification.

B. General procedure for the oxidation of 4,4,5,5-tetramethylimidazolidine-1,3-diol derivatives to nitronyl nitroxides. A suspension of 4,4,5,5-tetramethylimidazolidine-1,3-diol (1 mmol) in H_2O/CH_2Cl_2 (1:2) mixture (~50 mL) was cooled down to 0-5°C (to avoid overoxidation and formation of the imino nitroxide species) using an ice bath. To that mixture $NaIO_4$ 5% aqueous solution (0.8 eq.) was added dropwise. The progress of the reaction was monitored by TLC (SiO_2, hexane/ethyl acetate or dichloromethane with 5% of mathanol). After reaction was complete (0.5-3 h), dark-blue organic layer was

separated. The water phase was extracted with dichloromethane (3×25 mL). The combined organic extracts were additionally washed with water (2×30 mL), brine (1×50 mL), and dried over $MgSO_4$ (in some cases - Na_2SO_4). The residue after filtration was reduced to a small volume, and purified on a chromatographic column (SiO_2, hexane/ethyl acetate or CH_2Cl_2/MeOH).

C. General procedure of the oxidation of 4,4,5,5-tetramethylimidazolidine-1,3-diol derivatives to imino nitroxides. To a magnetically stirred solution of the imidazolidine (1 mmol) in nitromethane (12 mL) MnO_2 (14 mmol) was added. After ~35 minutes stirring at room temperature the oxidant was filtered and washed carefully with small portions of ethyl acetate on filter. The filtrate was diluted with toluene (12 mL) and concentrated to a volume of ca. 2 mL in *vacuo*. The residue was placed on a column wetted with toluene, and eluted with ethyl acetate/hexane mixture.

1-[4-(1-Oxyl-3-oxo-4,4,5,5-tetramethylimidazolidin-2-yl)-pyrazole]-pyrene (57c)

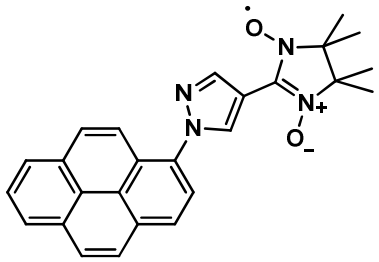

The condensation of 4-formyl-1-pyrenepyrazole **57a** (0.19g, 0.63 mmol) with BHA (0.125g, 0.84 mmol) in 13 mL of toluene was carried out following the methodology **A1**. The so-obtained imidazolidine **57b** was further involved into oxidation reaction with sodium periodate in H_2O/CH_2Cl_2 two-phase mixture, as described in detail in the previous paragraph (general procedure **B**). Purification on silica (hexane/ ethyl acetate, 1:1) afforded the dark-blue crystals of the radical **57c** in 26% (70 mg) overall yield. **M.p.**: 212-213°C. **UV-Vis** (toluene) λ/nm (ε, $mol^{-1}\times cm^{-1}$): 654 (1020), 598 (1010), 346 (38700). **FT-IR** (powder; ν/cm^{-1}): 3120, 3055 (m, $\nu_{C\text{-}H}$, aromatic), 2998, 2978, 2939 (m, $\nu_{C\text{-}H}$), 1596 (s, ν_{Ar}), 1515 (s), 1480 (m), 1461 (m), 1449 (s), 1422 (s), 1370 (s, ν_{methyl}), 1353 (vs, ν_{NO}), 1330 (m), 1311 (s) (pyrazolyl- moiety), 1212 (s), 1177 (s), 848 (vs, ν_{Ar}). **MS-FD** (70 eV, CH_2Cl_2) 421.9 (100%), MW calculated $C_{26}H_{23}N_4O_2$ (MW^+) 423.18. **Elemental analysis:** C 73.5; H 5.38; N 13.04; calculated for $C_{26}H_{23}N_4O_2$: C 73.74; H 5.47; N 13.23.

1-[4-(1-Oxyl-4,4,5,5-tetramethylimidazolidin-2-yl)-pyrazole]-pyrene (57d)

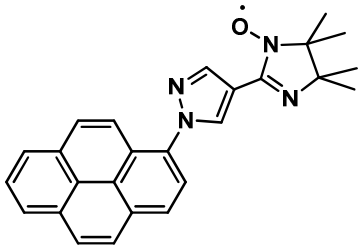

Pyrene-pyrazole imino nitroxide radical **57d** was synthesized from the imidazolidine **57b** following the general procedure **C**. Purification on silica (hexane/ethyl acetate, 1:1) gave the red needle crystals of the radical **57d** in 35% (0.180 g) overall yield. **M.p.**: 230-232°C. **UV-Vis** (toluene) λ/nm (ε, $mol^{-1}\times cm^{-1}$): 467 (800), 444 (751), 345 (29153). **FT-IR** (powder; ν/cm^{-1}): 3164, 3090, 3040 (m, ν_{C-H}, aromatic), 2984, 2960, 2921 (m, ν_{C-H}), 1616, 1602 (s, ν_{Ar}), 1519 (s), 1509 (m), 1464 (m), 1445 (s), 1417 (m), 1369 (s, ν_{NO}), 1330 (m), 1254 (s), 1189 (s), 1010 (s), 957 (s), 838 (vs, ν_{Ar}). **MS-FD** (70 eV, CH_2Cl_2) 406.3 (100%), MW calculated $C_{26}H_{23}N_4O$ (MW^+) 407.19. **Elemental analysis:** C 76.42; H 5.47; N 14.01; calculated for $C_{26}H_{23}N_4O$: C 76.64; H 5.69; N 13.75.

3-[4-(1-Oxyl-3-oxo-4,4,5,5-tetramethylimidazolidin-2-yl)-pyrazole]perylene (58c)

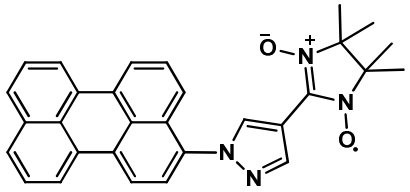

The condensation of the pyrene-pyrazole carbaldehyde **58a** was carried out in dearated methanol/toluene mixture (1:1) in accordance to the methodology **A2** (28% yield). The nitronyl nitroxide **58c** was obtained following standard procedure **B** described above. The radical was purified using flesh-column chromatography with neutralized (1% Et_3N) silica gel in 3% overall yield. **M.p.**: compound started to decompose above 235°C. **UV-Vis** (toluene) λ/nm (ε, $mol^{-1}\times cm^{-1}$): 656 (559), 600 (557), 449 (16656), 423 (13637), 347 (6558). **FT-IR** (powder; ν/cm^{-1}): 3126, 3052 (m, ν_{C-H}, aromatic), 2957, 2926, 2853 (m, ν_{C-H}), 1730 (m), 1690 (m), 1601 (s, ν_{Ar}), 1504 (s), 1460 (m), 1443 (s), 1419 (s), 1401 (m), 1384 (s, ν_{methyl}), 1354 (vs, ν_{NO}), 1330 (m), 1326 (m), 1314 (s) (pyrazolyl- moiety), 1260 (s), 1180 (s), 1133 (s), 1016 (s), 944 (s), 807, 765 (vs, ν_{Ar}). **Elemental analysis:** C 75.8; H 5.26; N 11.75; calculated for $C_{30}H_{25}N_4O_2$: C 76.09; H 5.32; N 11.83.

9-[2-(4-Formylphenyl)ethynyl]-N-(2,6-di-iso-propylphenyl)-perylene-3,4-dicarboxiimide (76a)

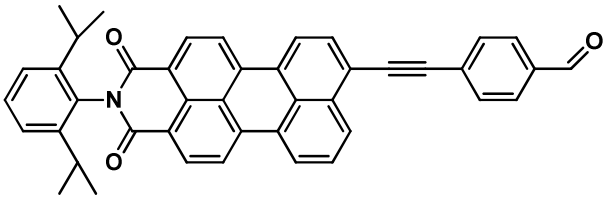

9-Bromo-N-(2,6-di-iso-propylphenyl)-perylene-3,4-dicarboxiimide **75** (0.1 g, 0.18 mmol, 1 eq.) together with 4-ethynylbenzaldehyde (0.03 g, 0.208 mmol, 1.2 eq.) were charged into a microwave vessel. Dry solvents - THF (6 mL) and *i*Pr_2NH (1.5 mL) - were added, and the mixture was carefully dearated with argon bubbling. After that the catalytic mixture of $Pd(PPh_3)_2Cl_2$ (0.07 g, 0.1 mmol, 0.05 eq.), PPh_3 (0.052 g, 0.2 mmol, 0.1 eq.), CuI (0.019 g, 0.1 mmol, 0.05 eq.) was charged into the vessel, which was then moved into the microwave. The reaction mixture was heated to 60°C for 105 min under the maximum microwave irradiation. The solvents were evaporated on rotary with silica, and the residue was purified using column chromatography (SiO_2) with hexane/dichloromethane gradient solvent mixture (3:1, 0:1). The title compound **76a** was obtained as a violet solid in 86% yield (0.09 g). **^{1}H-NMR** ($CDCl_3$, 250 MHz, 298 K, 32 scan), δ ppm: 1.12-1.15 (d, 12H, CH_3), 2.67-2.78 (p, 2H, ^3J = 6.8 Hz), 7.27-7.30 (d, 2H, ^3J = 7.6 Hz), 7.40-7.46 (t, 1H, ^3J = 8.3 Hz), 7.58-7.64 (t, 1H, ^3J = 7.9 Hz), 7.72-7.80 (t, 3H, ^3J = 8.6 Hz), 7.87-7.91 (d, 2H, ^3J = 8.2 Hz), 8.20-8.36 (m, 5H, Ar-H), 8.55-8.59 (dd, 2H, $^3J_1$ = 8.0 Hz, $^3J_2$ = 2.8 Hz, Ar-H), 10.00 (s, 1H, -CHO). **^{13}C-NMR** ($CDCl_3$, 63 MHz, 298 K, 256 scan), δ ppm: 23.0, 28.2 (-CH_3); 119.5, 119.8, 121.9, 123.0, 123.2, 126.7, 127.8, 128.5, 128.8, 130.5, 130.9, 131.0, 131.3 - aromatic core; 190.3 (-CHO). **MS-FD** (70 eV, CH_2Cl_2) 608.9 (100%), MW calculated $C_{43}H_{31}NO_3$ (MW^+) 609.23.

9-(4-Formylphenyl)anthracene (59a)

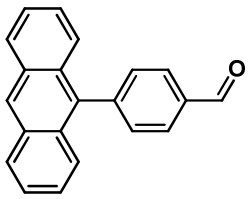

A mixture of 9-bromoanthracene **81** (1.07 g, 4.2 mmol, 1 eq.), 4-formylphenylboronic acid (0.81 g, 5.4 mmol, 1.3), $Pd(PPh_3)_4$ (0.15 g, 0.13 mmol, 0.03 eq.), and K_2CO_3 (2.3 g, 16.7 mmol, 4 eq.) in benzene /EtOH/H_2O (24:4:8 mL) was refluxed for 24 h under argon. The organic layer was separated, water was extracted with dichloromethane (3×30 mL),

and washed with brine. The combined organic extracts were dried under $MgSO_4$. The solvents were evaporated with silica. Column chromatography (silica gel, hexane/1% ethyl acetate) gave **59a** in 82% yield (0.92 g) as slightly yellow solid. **^{1}H-NMR** ($CDCl_3$, 250 MHz, 298 K, 16 scan), δ ppm: 7.25–7.31 (m, 2H, ArH), 7.36-7.42 (m, 2H, ArH), 7.46-7.55 (m, 4H, ArH), 7.96–8.03 (m, 4H, ArH), 8.45 (s, 1H, ArH), 10.12 (s, 1H, -CHO). **^{13}C-NMR** ($CDCl_3$, 63 MHz, 298 K, 256 scan), δ ppm: 126.1, 126.7, 127.1, 128.1, 129.9, 130.2, 130.5, 132.0, 135.9, 136.0, 145.3 - signals of the aromatic core; 192.0 (-CHO). **MS-FD** (70 eV, CH_2Cl_2) 281.9 (100%), MW calculated $C_{21}H_{14}O$ (MW^+) 282.10.

9-(4-(4,4,5,5-Tetramethyl-1,3-dihydroxyimidazolidin-2-yl)phenyl]-anthracene (59b)

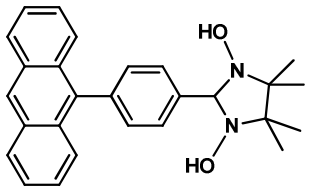

The titled imidazolidine **59b** was prepared following the general method **A1**. Thus, anthracene aldehyde **59a** (0.17 g, 0.59 mmol, 1 eq.) together with BHA (0.11 g, 0.76 mmol, 1.3 eq.) were heated near reflux for 37 h under argon in toluene. Yield: 93% (0.22 g). **^{1}H-NMR** ($(CD_3)_2SO$, 250 MHz, 298K, 64 scan), δ ppm: 1.14-1.15 (d, 12H, $-CH_3$), 4.70 (s, 1H), 7.36-7.60 (m, 8H, ArH), 7.73-7.76 (d, 2H, ^3J = 8 Hz, ArH), 8.14-8.17 (d, 2H, ^3J = 8.2 Hz, ArH), 8.67 (s, 1H, ArH).

9-(4-(1-Oxyl-3-oxo-4,4,5,5-tetramethylimidazolidin-2-yl)phenyl]-anthracene (59c)

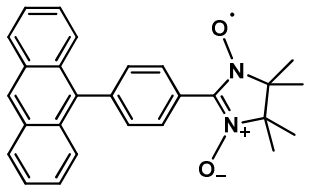

Oxidation of the imidazolidine **59b** was realized in accordance to the procedure **B**. Purification using silica chromatography with hexane/ethyl acetate/dichloromethane (20:5:1) eluent mixture gave the target nitronyl nitroxide **59c** in 34% yield as blue needles. **M.p.**: 212-213°C. **UV-Vis** (toluene) λ/nm (ε, $mol^{-1}\times cm^{-1}$): 593 (406), 387 (13662), 369 (23281). **FT-IR** (powder; ν/cm^{-1}): 2987, 2972 (w, ν_{C-H}), 1442 (w), 1416 (s), 1386 (s, ν_{methyl}), 1358 (s, ν_{NO}), 1310 (m), 1220 (m), 1142 (m), 1014 (m), 935 (m), 884, 871, 844 (s, ν_{Ar}). **Elemental analysis:** C 78.93; H 6.22; N 7.15; calculated for $C_{27}H_{25}N_2O_2$: C 79.19; H 6.15; N 6.84.

9-(4-(1-Oxyl-4,4,5,5-tetramethylimidazolidin-2-yl)phenyl]-anthracene (59d)

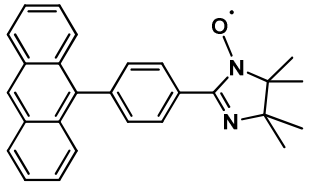

Anthracene imino nitroxide radical **59d** was synthesized from the imidazolidine **59b** in 32% overall yield applying conditions **C**. Separation on a chromatographic column with silica (hexane/ethyl acetate/dichloromethane, 20:1:1) afforded red prisms of the radical **59d** with 52% overall yield. **M.p.**: 195-196°C. **UV-Vis** (toluene) λ/nm (ε, $mol^{-1}\times cm^{-1}$): 451 (529), 387 (10390), 368 (11264). **FT-IR** (powder; ν/cm^{-1}): 3052 (w, ν_{C-H}, aromatic), 2989 (w, ν_{C-H}), 1611 (m, ν_{Ar}), 1503 (w), 1478 (m), 1442 (m), 1400 (m), 1387 (m, ν_{methyl}), 1361 (s, ν_{NO}), 1315 (m), 1292 (m), 1267 (m), 1156 (m), 1134 (m), 1100 (m), 1011 (m), 955 (m), 935 (m). **Elemental analysis:** C 82.17; H 6.46; N 7.01; calculated for $C_{27}H_{25}N_2O$: C 82.41; H 6.40; N 7.12.

9-[2-(4-Formylphenyl)ethynyl]anthracene (60a)

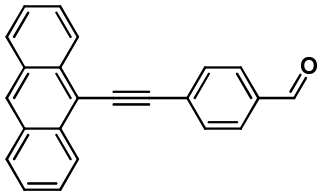

9-Bromoanthracene **81** (0.257 g, 1 mmol, 1 eq.), 4-ethynylbenzaldehyde (0.17 g, 1.3 mmol, 1.3 eq.), $Pd(PPh_3)_4$ (0.074 g, 0.06 mmol, 0.06 eq.) and CuI (0.013 g, 0.07 mmol, 0.07 eq.) in dry deaerated toluene (8 mL) *i*Pr_2NH (5mL) solvents mixture were heated to 80°C for 1 h under the maximum microwave irradiation. The solvents were evaporated with silica, and the residue was purified using column chromatography (SiO_2) with hexane/ethyl acetate solvent mixture (3:1). The aldehyde **60a** was obtained in 43% yield (0.13 g). **^{1}H-NMR** ($CDCl_3$, 250 MHz, 298 K, 16 scan), δ ppm: 7.39–7.54 (m, 4H, ArH), 7.73-7.82 (q, 4H, $^3J_1$ = 8.3 Hz, $^3J_2$ = 5.03 Hz, ArH), 7.89-7.92 (d, 2H, ^3J = 8.3 Hz, ArH), 8.34 (s, 1H, ArH), 8.48-8.51 (d, 2H, ^3J = 8.6 Hz, ArH), 9.93 (s, 1H, -CHO). **^{13}C-NMR** ($CDCl_3$, 63 MHz, 298 K, 256 scan), δ ppm: 90.6, 99.8 (-C≡C-), 116.3, 125.8, 126.5, 127.0, 128.8, 128.9, 129.7, 129.8, 131.2, 132.1, 132.8, 135.5 – aromatic signals; 191.4 (-CHO). **MS-FD** (70 eV, CH_2Cl_2) 306.4 (100%), MW calculated $C_{23}H_{14}O$ (MW^+) 306.1.

9-{2-[4-(4,4,5,5-Tetramethyl-1,3-dihydroxyimidazolidin-2-yl)phenyl]ethynyl}anthracene (60b)

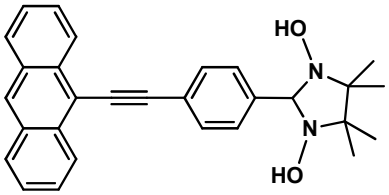

The solution containing BHA (0.25 g, 1.68 mmol, 3 eq.) and the anthracene carbaldehyde **60a** (0.17g, 0.56 mmol, 1.0 eq.) in deaerated absolute methanol/toluene (15:7 mL) solvent mixture was stirred at room temperature for 7 days. The solvents were evaporated in *vacuo*. To the residue methanol (5mL) and water (10 mL) were added. The white precipitate was filtered off, washed with water (1×10 mL), methanol (1×10 mL), and dried on air, affording the target imidazolidine **60b** in 70% yield (0.17 g). **^{1}H-NMR** ($(CD_3)_2SO$, 250 MHz, 298K, 64 scan), δ ppm: 1.09-1.12 (d, 12H, -CH_3), 4.61 (s, 1H), 7.60-7.66 (m, 4H, ArH), 7.81-7.85 (d, 2H, ^{3}J = 8.03 Hz, ArH), 8.17-8.21 (d, 2H, ^{3}J = 8.3 Hz, ArH), 8.60-8.63 (d, 2H, ^{3}J = 8.5 Hz, ArH), 8.71 (s, 1H, ArH). **^{13}C-NMR** ($CDCl_3$, 63 MHz, 298 K, 256 scan), δ ppm: 17.2, 20.8, 66.3, 125.97, 126.05, 127.4, 128.9, 128.92, 130.7, 130.9, 131.7, 135.2, 143.2, 147.8.

9-{2-[4-(1-Oxyl-3-oxo-4,4,5,5-tetramethylimidazolidin-2-yl)phenyl]ethynyl}anthracene (60c)

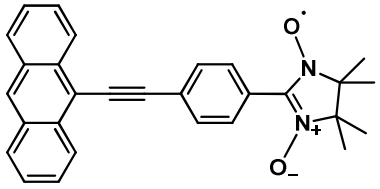

The imidazolidine **60b** (0.17 g, 0.39 mmol) was dissolved in methanol/dichloromethane (30:8 mL) mixture, and MnO_2 (0.5 g, 5.75 mmol) was added under vigorous stirring. The mixture was filtered, and the residue was concentrated in *vacuo* till a small volume (ca. 2-3 mL). Purification on a chromatographic column with silica and hexane/ethyl acetate/dichloromethane (100:5:2) eluent mixture afforded the target nitronyl nitroxide **60c** as greenish powder in 50% (0.12 g) overall yield. **M.p.**: 207-208°C. **UV-Vis** (toluene) λ/nm (ε, $mol^{-1}×cm^{-1}$): 617 (332), 435 (24847), 411 (29269). **FT-IR** (powder; ν/cm^{-1}): 3084, 3051 (m, ν_{C-H}, aromatic), 2998, 2985 (w, ν_{C-H}), 1620, 1601 (m, ν_{Ar}), 1520 (w), 1445 (m), 1419 (m), 1385 (m, ν_{methyl}), 1356 (s, ν_{NO}), 1299 (m), 1201 (m), 1163 (m), 1129 (m), 1098

(m), 1011 (m), 839 (s). **Elemental analysis:** C 80.08; H 5.54; N 6.41; calculated for $C_{29}H_{25}N_2O_2$: C 80.34; H 5.81; N 6.46.

9-{2-[4-(1-Oxyl-4,4,5,5-tetramethylimidazolidin-2-yl)phenyl]ethynyl}anthracene (60d)

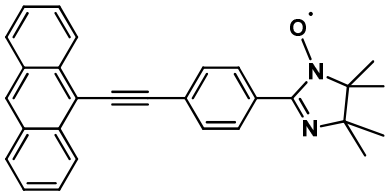

The oxidation of the precursor **60b** (0.11 g, 0.25 mmol) was realized using an excess of MnO_2 (0.4 g, 4.6 mmol) in nitromethane/dichloromethane (20:10 mL) solvent mixture. After reaction was complete the inorganic salt was filtered off, washed on filter with dichloromethane (3×15 mL) and ethyl acetate (3×15 mL). The filtrate was evaporated, and separation on a chromatographic column with silica (hexane/ethyl acetate/dichloromethane, 100:2:5) afforded the red crystals of the radical **60d** in 30% overall yield. **M.p.**: 76-78°C. **UV-Vis** (toluene) λ/nm (ε, $mol^{-1}\times cm^{-1}$): 469 (690), 430 (15688), 407 (17126). **FT-IR** (powder, ν/cm^{-1}): 3052(m, ν_{C-H}, aromatic), 2976, 2927, 2856 (m, ν_{C-H}), 1606 (s, ν_{Ar}), 1501 (s), 1441 (s), 1403 (s), 1388 (m, ν_{methyl}), 1366 (s, ν_{NO}), 1307 (m), 1291 (m), 1262 (m), 1222 (m), 1155 (s), 1139 (s), 1102 (m), 1015 (s), 954 (m), 882 (s), 841 (s). **Elemental analysis:** C 83.72; H 5.91; N 6.68; calculated for $C_{29}H_{25}N_2O$: C 83.42; H 6.04; N 6.71.

9-Pyrazole-anthracene (82)

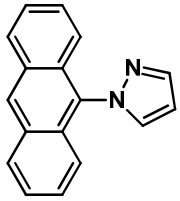

The titled compound **82** was routinely synthesized following the procedure described for the pyrazole-pyrene derivative **72**. Thus, copper-catalyzed coupling between 9-bromoanthracene **81** (2g, 7.8 mmol, 1 eq.) and pyrazole (0.8 g, 11.8 mmol, 1.5 eq.) led after purification on a silica column with hexane/toluene gradient mixture (3:1, 1:1, 7:13) to the product **82** in 83% yield (1.57 g). **^{1}H-NMR** ($CDCl_3$, 250 MHz, 298K, 16 scan), δ ppm: 6.59-6.61 (t, 1H, ^3J = 2.1 Hz, $H_{pyrazole}$), 7.35-7.23 (m, 5H, ArH), 7.73-7.74 (d, 1H, ^3J = 2.25 Hz, Ar-H), 7.90 (d, 1H, ^3J = 1.65 Hz, $H_{pyrazole}$), 7.98 (s, 1H, ArH), 8.0 (d, 1H, ^3J = 2.23 Hz, Ar-H), 8.52 (s, 1H, $H_{pyrazole}$). **^{13}C-NMR** ($CDCl_3$, 63 MHz, 298K, 256 scan), δ ppm: 122.9, 125.7,

127.3, 128.2, 128.5, 129.2 – anthracene core; 106.4, 133.5, 140.9 – pyrazole ring. **MS-FD** (70 eV, CH_2Cl_2) 243.8 (100%), MW calculated $C_{17}H_{12}N_2$ (MW^+) 244.10.

9-(4-Formylpyrazole)-anthracene (61a)

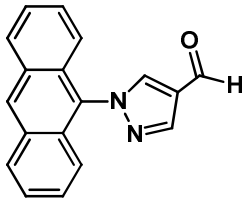

The Vilsmeier-Haack reaction conditions were applied similar to that reported for the compound **57a**. The carbaldehyde **61a** was obtained after isolation from the reaction mixture using a chromatographic column with silica (toluene/ethyl acetate/dichloromethane, 100:1:5) as slightly yellowish solid (0.36 g, 0.66% yield).**^{1}H-NMR** ($CDCl_3$, 250 MHz, 298 K, 64 scan), δ ppm: 7.28–7.32 (m, 2H, ArH), 7.41-7.49 (m, 4H, ArH), 8.0 (m, 2H, ArH), 8.25 (s, 1H, $H_{pyrazole}$), 8.35 (s, 1H, ArH), 8.58 (s, 1H, $H_{pyrazole}$), 10.03 (s, 1H, -CHO). **^{13}C-NMR** ($CDCl_3$, 63 MHz, 298 K, 204 scan), δ ppm: 122.1, 125.1, 126.0, 128.0, 128.5, 128.6, 129.6, 131.3, 137.3, 141.7, 184.2. **MS-FD** (70 eV, CH_2Cl_2) 272.1 (100%), MW calculated $C_{18}H_{12}N_2O$ (MW^+) 272.09.

9-[4-(1-Oxyl-3-oxo-4,4,5,5-tetramethylimidazolidin-2-yl)-pyrazole]-anthracene (61c)

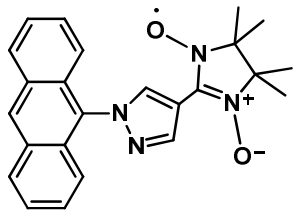

The radical precursor - imidazolidine **61b** - was synthesized in 80% yield following the protocol reported previously for the ethynyl-anthracene derivative **60b**. The oxidation of the derivative **60b** was carried out under mild conditions. Hence, solution of the compound **60b** (0.19 g, 0.47 mmol) in toluene/dichloromethane (20:2 mL) mixture was cooled to 5°C using an ice bath, and excess of PbO_2 (0.5 g, 5.75 mmol) was added under vigorous stirring. The inorganic salt was filtered, and washed twice on filter with dichloromethane (2×15 mL) and ethyl acetate (2×15 mL). The filtrate was concentrated in *vacuo*. Purification on a chromatographic column with silica and toluene/ethyl acetate (4:1, 3:1) gradient mixture afforded the target nitronyl nitroxide **61c** as the dark-blue needles in 47% (0.11 g) total yield. **M.p.**: 216-218°C. **UV-Vis** (toluene) λ/nm (ε, $mol^{-1}\times cm^{-1}$): 597 (729), 386 (6146), 350 (15712). **FT-IR** (powder, ν/cm^{-1}): 3155, 3120, 3055 (m, ν_{C-H},

aromatic), 2984, 2933 (m, ν_{C-H}), 1595 (s, ν_{Ar}), 1480 (m), 1445, 1422 (vs, Pyrazole$_{C=N}$ stretching), 1359 (s, ν_{NO}), 1336 (s), 1304 (m), 1218 (s), 1176 (s), 1138 (s), 1100 (s), 1012 (s), 983 (s), 914 (s), 890 (s). **Elemental analysis:** C 70.08; H 5.56; N 13.95; calculated for $C_{24}H_{23}N_4O_2$: C 72.16; H 5.80; N 14.03.

9-[4-(1-Oxyl-4,4,5,5-tetramethylimidazolidin-2-yl)-pyrazole]-anthracene (61d)

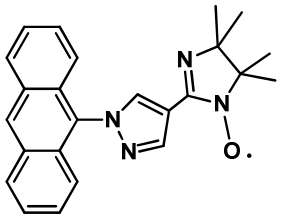

Oxidation of the imidazolidine **61b** into imino nitroxide species **61d** was realized following the general procedure **C**. Separation on a chromatographic column with silica (toluene/ethyl acetate, 5:1) led to the red prisms of the radical **61d** in 56% overall yield. **M.p.**: 192-193°C. **UV-Vis** (toluene) λ/nm (ε, $mol^{-1}\times cm^{-1}$): 464 (648), 387 (8706), 367 (9743). **FT-IR** (powder, ν/cm^{-1}): 3158, 3052 (m, ν_{C-H}, aromatic), 2977, 2924 (m, ν_{C-H}), 1611 (s, ν_{Ar}), 1515 (m), 1480 (m), 1439(vs, Pyrazole$_{C=N}$ stretching), 1376 (s, ν_{methyl}), 1365 (s, ν_{NO}), 1326 (m), 1253 (s), 1221 (m), 1200 (m), 1157 (s), 1107 (s), 1014 (s), 982 (s), 951 (m), 915 (s), 893 (s), 874 (s). **Elemental analysis:** C 74.88; H 5.86; N 14.47; calculated for $C_{24}H_{23}N_4O$: C 75.17; H 6.05; N 14.61.

9-(4-Formylphenyl)-10-bromoanthracene (62a)

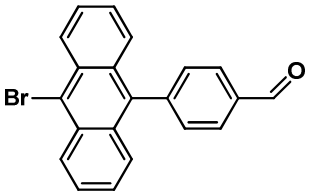

A mixture of **81** (0.406 g, 1.44 mmol) and N-bromosuccinimide (NBS, 0.256 g, 1.44 mmol) in anhydrous DMF (17 mL) was stirred at room temperature for 48 h under argon. Water (100 mL) was than added to the solution. The precipitate was filtered, washed twice with water and dried in *vacuo*, giving 0.48 g (92%) of the crystalline product **62a**. **^{1}H-NMR** ($CDCl_3$, 250 MHz, 298 K, 16 scan), δ ppm: 7.29–7.35 (m, 2H, ArH), 7.46 (s, 1H, ArH), 7.49-7.57 (m, 5H, ArH), 8.03–8.06 (d, 2H, ^3J = 8.2 Hz, ArH), 8.54-8.58 (d, 2H, ^3J = 8.85 Hz, ArH), 10.13 (s, 1H, -CHO). **^{13}C-NMR** ($CDCl_3$, 63 MHz, 298 K, 256 scan), δ ppm: 122.1, 125.1, 126.0, 128.0, 128.5, 128.6, 129.6, 131.3, 137.3, 141.7- signals of the aromatic core; 184.2 (-CHO). **MS-FD** (70 eV, CH_2Cl_2) 359.9 (100%), MW calculated $C_{21}H_{13}BrO$ (MW^+) 360.09.

9-(4-(4,4,5,5-Tetramethyl-1,3-dihydroxyimidazolidin-2-yl)phenyl)-10-bromoanthracene (62b)

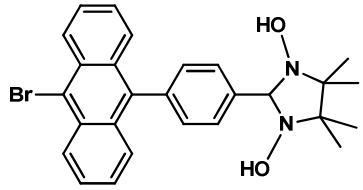

The titled imidazolidine **62b** was prepared following the described above for the ethynyl-anthracene derivative **60b** method. Thus, 10-bromoanthracene carbaldehyde **62a** (0.24 g, 0.67 mmol, 1 eq.), BHA (0.25 g, 1.7 mmol, 2.5 eq.) were stirred in deaerated absolute methanol/toluene (20 mL, 1:1 v/v) mixture at room temperature during 7 days. The solvents were evaporated in *vacuo*. Water (10 mL) was added to the residue. The light-yellow precipitate was filtered off, washed with water (1×10 mL), methanol (1×10 mL), and dried on air, giving the imidazolidine derivative **62b** in 83% yield (0.27 g). **^{1}H-NMR** ($(CD_3)_2SO$, 250 MHz, 298K, 64 scan), δ ppm: 1.13-1.15 (d, 12H, $-CH_3$), 4.70 (s, 1H), 7.37-7.40 (m, 2H, ^{3}J = 8 Hz, ArH), 7.51-7.63 (m, 4H, ArH), 7.70-7.77 (m, 4H, ArH), 8.52-8.56 (d, 2H, ^{3}J = 8.8 Hz, ArH). **^{13}C-NMR** ($(CD_3)_2SO$, 250 MHz, 298K, 64 scan), δ ppm: 17.2, 24.5, 66.2, 126.1, 126.9, 127.2, 127.8, 128.7, 129.5, 130.1, 130.4, 132.3, 141.8.

9-(4-(1-Oxyl-3-oxo-4,4,5,5-tetramethylimidazolidin-2-yl)phenyl)-10-bromoanthracene (62c)

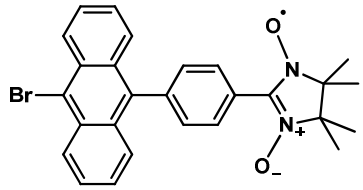

Oxidation of the imidazolidine **62b** with excess of MnO_2 in methanol/toluene mixture after purification on a silica column with toluene/ethyl acetate (100:3) afforded target nitronyl nitroxide **62c** in 53% overall yield as blue needles. **M.p.**: 247-249°C. **UV-Vis** (toluene) λ/nm (ε, $mol^{-1}\times cm^{-1}$): 593 (383), 400 (13382), 378 (20012). **FT-IR** (powder, ν/cm^{-1}): 3069, 3034 (m, ν_{C-H}, aromatic), 2980, 2936 (m, ν_{C-H}), 1620, 1607 (s, ν_{Ar}), 1520 (m), 1480 (m), 1439 (s), 1424 (s), 1386 (s, ν_{methyl}), 1358 (vs, ν_{NO}), 1310 (s), 1260 (s), 1220 (s), 1164 (s), 1143 (s), 1132 (s), 1103 (m), 1027 (s), 935 (s), 880 (s). **Elemental analysis:** C 65.98; H 4.76; N 5.51; calculated for $C_{27}H_{24}BrN_2O_2$: C 66.40; H 4.95; N 5.74.

9-(4-(1-Oxyl-4,4,5,5-tetramethylimidazolidin-2-yl)phenyl)-10-bromoanthracene (62d)

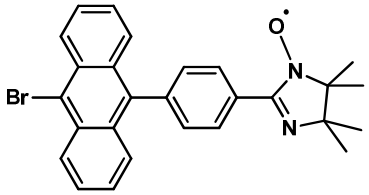

The imino derivative **62d** was obtained as a site-product upon oxidation of the imidazolidine **62c** in 7% yield. **M.p.**: compound decomposed above 232°C. **UV-Vis** (toluene) λ/nm (ε, $mol^{-1}\times cm^{-1}$): 447 (487), 400 (10557), 379 (11273). **FT-IR** (powder, ν/cm^{-1}): 3084, 3040 (m, ν_{C-H}, aromatic), 2978, 2930 (s, ν_{C-H}), 1613 (s, ν_{Ar}), 1546 (m), 1521 (m), 1506 (m), 1477 (m), 1440 (s), 1403 (m), 1386 (m, ν_{methyl}), 1365 (vs, ν_{NO}), 1348 (s), 1315 (m), 1295 (m), 1260 (s), 1222 (m), 1155 (s), 1136 (s), 1103 (m), 1026 (s), 956 (m), 936 (s), 882 (s). **Elemental analysis:** C 69.02; H 5.26; N 6.11; calculated for $C_{27}H_{24}BrN_2O$: C 68.65; H 5.12; N 5.93.

2-(4-Ethynylphenyl)-1,3-dioxolane (86)

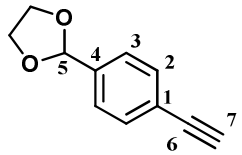

4-Ethynylbenzaldehyde **85** (1.76 g, 13.53 mmol) was charged into a flask together with toluene (60 mL), ethyleneglycol (1.4 mL, 25.15 mmol) and para-toluene-sulfonic acid as catalyst (0.2 g, 1 mmol). The solution was heated to reflux with Deane-Stark for one day. Then it was neutralized with $NaHCO_3$ aqueous solution, and the phases were separated. The aqueous layer was extracted with small portions of toluene (3×10 mL). The combined organic layers were dried over $MgSO_4$ and filtrated. Toluene solution was evaporated under reduced pressure. Crude orange oil was purified using column chromatography (SiO_2, dichloromethane). Compound **86** was obtained as slightly yellow oil in 85% yield. **^{1}H-NMR** ($CDCl_3$, 250 MHz, 298K, 16 scan), δ ppm: 3.02 (s, 1H, H-7), 3.99 (m, 4H, $-CH_2$), 6.73 (s, 1H, H-5), 7.91 (dd, 4H, ^3J = 8 Hz, Ar-H). **^{13}C-NMR** ($CDCl_3$, 63 MHz, 298K, 256 scan), δ ppm: 67.2 ($-CH_2$), 82.4 (C-7), 84.2 (C-6), 103.9 (C-5), 123.2 (C-1), 127.2 (C-3), 134.5 (C-2), 137.8 (C-4). **MS-FD** (70 eV, CH_2Cl_2) m/z: 173.0 (M^+), MW calculated $C_{11}H_{10}O_2$ (MW^+) 174.20.

4,4′-(Buta-1,3-diyne-1,4-diyl)dibenzaldehyde (84a)

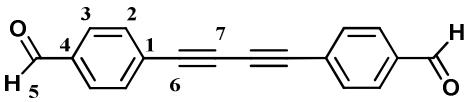

Glaser coupling. A mixture of 2-(4-ethynylphenyl)-1,3-dioxolane **86** (3.57 g, 20.52 mmol), CuCl (14 g, 141.4 mmol), $CuCl_2$ (14.3 g, 106.3 mmol) and dry pyridine (120 mL) was stirred at room temperature for 24 h; then it was washed with 10% HCl and extracted with Et_2O. The combined organic extracts were washed with NH_4Cl saturated aqueous solution (to remove excess of copper from the solution), and dried over $MgSO_4$. 1,4-Bis(4-(1,3-dioxolan-2-yl)phenyl)buta-1,3-diyne was isolated from the reaction mixture as the main product in 60% yield using column chromatography (SiO_2, dichloromethane). **^{1}H-NMR** ($CDCl_3$, 250 MHz, 298K, 16 scan), δ ppm: 3.95 (m, 8H, -CH_2), 5.77 (s, 2H, H-5), 7.38 (d, 4H, ^3J = 8 Hz, H-3), 7.45 (d, 4H, ^3J = 8 Hz, H-2). **^{13}C-NMR** ($CDCl_3$, 63 MHz, 298K, 256 scan), δ ppm: 66.5 (-CH_2), 73.3 (C-7), 82.4 (C-6), 103.1 (C-5), 122.6 (C-1), 126.8 (C-3), 133.1 (C-2), 138.9 (C-4). **MS-FD** (70 eV, CH_2Cl_2) m/z: 346.2 (M^+), MW calculated $C_{22}H_{18}O_4$ (MW^+) 346.38.

In the so-obtained yellowish solid the aldehyde function was still protected with the acetal-groups. Therefore, solution of the dioxolane precursor (1.78g, 5.14 mmol) in THF (50 mL) was treated with 3% HCl (30 mL) at 5°C (ice bath). The mixture was kept for further 45 min in the ice bath, and an additional 1 h at ambient temperature. After that THF was evaporated in *vacuo*. The residue was diluted with Et_2O (60 mL), washed with water (3×35 mL) and dried over $MgSO_4$. The solvent was concentrated under reduced pressure. Dialdehyde **84a** was obtained as light yellow solid in 86% yield. **^{1}H-NMR** ($(CD_3)_2SO$, 250 MHz, 298 K, 16 scan), δ ppm: 7.91 (d, 4H, ^3J = 8 Hz, H-2), 8.03 (d, 4H, ^3J = 8 Hz, H-3), 10.12 δ (s, 2H, H-5). **^{13}C-NMR** ($(CD_3)_2SO$, 75 MHz, 353 K, 1801 scan), δ ppm: 75.8 (C-7), 82.1 (C-6), 125.5 (C-1), 129.1 (C-3), 132.7 (C-2), 136.3 (C-4), 191.7 (-CHO). **MS-FD** (70 eV, CH_2Cl_2) m/z: 258.0 (M^+), MW calculated $C_{18}H_{10}O_2$ (MW^+) 258.27.

2-(4-{4-[4-(1,3-Dihydroxy-4,4,5,5-tetramethyl-imidazolidine-2-yl)phenyl]buta-1,3-diyn-1-yl}phenyl)-4,4,5,5-tetramethyl-imidazolidine-1,3-diol (84b)

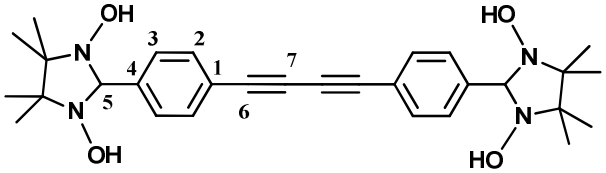

Following protocol **A1** dibenzaldehyde **84a** (0.3g, 1.19 mmol) was converted into imidazolidine **84b** after 3 h of heating near reflux with BHA in toluene. Yield: 97% (0.58 g). **^{1}H-NMR** ($(CD_3)_2SO$, 250 MHz, 298K, 128 scan), δ ppm: 1.28 (d, 24H, CH_3), 4.84 (s, 2H, H-5), 7.92 (d, 4H, ^3J = 8 Hz, H-3), 8.11 (d, 4H, ^3J = 8 Hz, H-2). **^{13}C-NMR** ($(CD_3)_2SO$, 63 MHz, 298 K, 256 scan), δ ppm: 23 (CH_3), 69.7 ($\underline{C}$-CH_3), 74.9 (C-7), 82.3 (C-6), 103.1 (C-5), 123.6 (C-1), 130.1 (C-3), 134.0 (C-2), 138.6 (C-4).

2-(4-{4-[4-(1-Oxyl-3-oxo-4,4,5,5-tetramethylimidazolin-2-yl)-phenyl]buta-1,3-diyn-1-yl}phenyl)-4,4,5,5-tetramethyl-imidazoline-1-oxyl-3-oxo (84c)

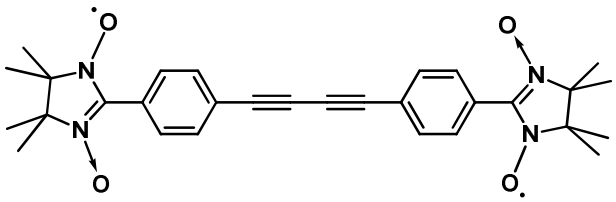

Following the typical procedure **B** the biradical **84c** was obtained in 24% total yield (0.140 g). **M.p.**: 220-221°C. **UV-Vis** ($CHCl_3$) λ/nm (ε, $mol^{-1}\times cm^{-1}$): 607 (912), 349 (33844); (toluene) λ/nm (ε, $mol^{-1}\times cm^{-1}$): 622 (578), 352 (71875). **FT-IR** (powder, ν/cm^{-1}): 3099, 3049 (w, $\nu_{C\text{-}H}$, aromatic), 2991, 2940 (m, $\nu_{C\text{-}H}$), 1602 (m, ν_{Ph}), 1543 (w), 1522 (m), 1481 (w), 1447 (m), 1428 (s), 1427(s), 1418 (vs), 1386 (vs, ν_{methyl}), 1365 (vs, ν_{NO}), 1302 (vs), 1212 (s), 1164 (s), 1141 (s), 1130 (vs), 831 (vs, $\nu_{p\text{-sub-}Ph}$). **Elemental analysis:** C 70.30; H 6.25; N 10.90; calculated for $C_{30}H_{32}N_4O_4$: C 70.29; H 6.29; N 10.93.

General procedure for Sonogashira coupling reaction of aryl halides with terminal alkyne. (I) Starting aryl bromide (21.7 mmol, 1 eq.) was transferred into a flame-dried flask in argon stream. Dry solvents mixture – DMF/NEt_3 (50 mL, 1:1) - was added through the rubber septum. Solution was deaerated using argon bubbling during 20 min, and the catalytic mixture of $Pd(PPh_3)_2Cl_2$ (1.1 mmol, 0.05 eq.), PPh_3 (2.2 mmol, 0.1 eq.), CuI (1.1 mmol, 0.05 eq.) was added at once. The reaction mixture was slightly heated (to 45^{o}C) and ethynyl-trimethyl-silan (32.6 mmol, 1.5 eq.) was added through the septum. After that the heating was increased to 80^{o}C. A white precipitate began to form after ~15 min of heating. After reported time, the mixture was cooled to ambient temperature, and the crystalline white solid of triethylamine hydrobromide was isolated by filtration. The orange-brown filtrate was concentrated, mixed with NH_4Cl saturated aqueous solution (50 mL), and extracted with dichloromethane or diethyl ether (3×40 mL). The organic

fractions were combined, dried over magnesium sulfate, and concentrated with silica gel in *vacuo*. The residue was purified using column chromatography.

(II). The set-up and the catalyst/reagents ratio remained the same; yet a mixture of dry NEt_3/CH_3CN (1:1) was preferred as the reaction media. Here, already after 5 minutes of stirring at room temperature formation of triethylamine hydrobromide salt was observed. Light yellow reaction mixture was stirred at room temperature for 17-19 h. The work-up of the mixture was done in accordance with the procedure **(I)**.

4-[2-(4-Formylphenyl)ethynyl]benzaldehyde (87a)

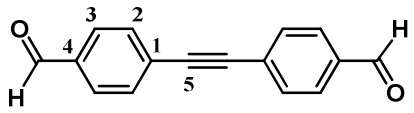

Following the procedure **(I)** coupling reaction of 4-ethynylbenzaldehyde **85** (0.2 g, 1.54 mmol) with 4-bromobenzaldehyde (0.284 g, 1.54 mmol) was complete after 12 h of heating under argon at 70°C. Separation on a chromatographic column (SiO_2, dichloromethane) afforded compound **87a** in 92% yield (0.33 g). **^{1}H-NMR** ($CDCl_3$, 250 MHz, 298 K, 64 scan), δ ppm: 7.71, 7.90 (both dd 2H, Ar-H, ^3J = 8.2 Hz), 10.04 (s, 2H, -CHO). **^{13}C-NMR** (THF-d^8, 75 MHz, 298 K, 1725 scan), δ ppm: 92.4 (C-5), 129.0 (C-1), 130.1 (C-3), 132.9 (C-2), 137.5 (C-4), 191.3 (-CHO). **MS-FD** (70 eV, CH_2Cl_2) m/z: 234.063 (M^+), MW calculated $C_{16}H_{10}O_2$ (MW^+) 234.068.

2-(4-{2-[4-(1,3-Dihydroxy4,4,5,5-tetramethyl-imidazolidine-2-yl)phenyl]ethynyl}phenyl)-4,4,5,5-tetramethyl-imidazolidine-1,3-diol (87b)

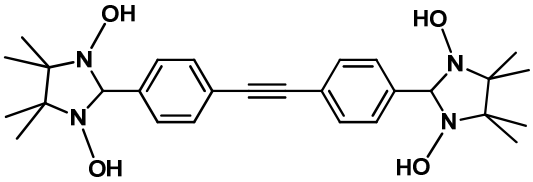

Following the general method **A1** from 0.45 g (1.94 mmol) of the tolane dialdehyde **87a** 0.94 g of yellowish bisimidazolidine **87b** was synthesized (98% yield). **^{1}H-NMR** ($(CD_3)_2SO$, 250 MHz, 298K, 105 scan), δ ppm: 1.05, 1.09 (both s 12 H, $-CH_3$), 4.54 (s, 2H, C_{imid}-2), 7.53 (w. s, 8H, Ar-H), 7.84 (w. s, 4H, -N-OH). **^{13}C-NMR** ($(CD_3)_2SO$, 63 MHz, 298K, 256 scan), δ ppm: 17.4, 24.5 ($-CH_3$), 66.4 (C_{imid}-4, C_{imid}-5), 88.2 (-C≡C-), 90.1 (C_{imid}-2), 121.6 (Ar-C), 128.2, 131.0 (ArC-H), 143.5 (Ar-C). **MS-FD** (70 eV, $(CD_3)_2SO$) m/z: 494.293 (M^+), MW calculated $C_{28}H_{38}N_4O_4$ (MW^+) 494.291.

2-(4-{2-[4-(1-Oxyl-3-oxo-4,4,5,5-tetramethyl-4H,5H-imidazolin-2-yl)phenyl]-ethynyl}phenyl)-4,4,5,5-tetramethyl-imidazoline-1-oxyl-3-oxo (87c)

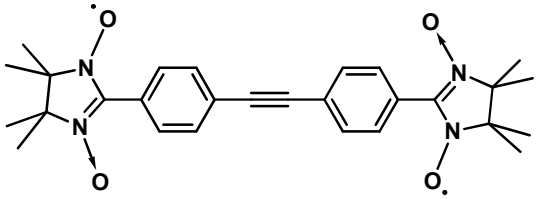

Oxidation of the bisimidazolidine **87b** (0.94 g, 1.9 mmol) using method **B** afforded 0.47 g (50%) dark-blue crystals of the biradical **87c**. **M.p**.: 225-227°C. **UV-Vis** (toluene) λ/nm (ε, $mol^{-1}\times cm^{-1}$): 611 (868), 342 (59101). **FT-IR** (powder, ν/cm^{-1}): 3100 (w, $\nu_{C\text{-}H}$, aromatic), 2989, 2943 (m, $\nu_{C\text{-}H}$), 1677 (m), 1606 (s, ν_{Ph}), 1530 (w), 1484 (w), 1447 (m), 1422 (s), 1390(s, ν_{methyl}), 1365, 1356 (vs, ν_{NO}), 1301 (vs), 1211 (s), 1166 (s), 1131 (vs), 833 (vs, $\nu_{p\text{-}sub\text{-}Ph}$). **Elemental analysis:** C 68.67; H 6.56; N 11.37; calculated for $C_{28}H_{32}N_4O_4$: C 68.83; H 6.60; N 11.47.

2-(4-{2-[4-(1-Oxyl-4,4,5,5-tetramethyl-4H,5H-imidazolin-2-yl)phenyl]-ethynyl}phenyl)-4,4,5,5-tetramethyl-imidazoline-1-oxyl-3-oxo (87d)

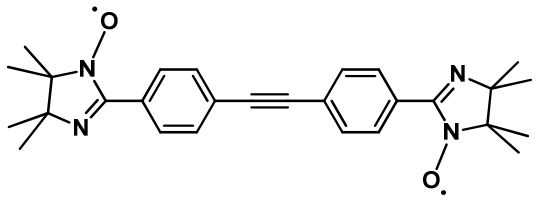

Compound **87d** was synthesized from the precursor **87b** (0.27g, 0.55 mmol) employing excess of MnO_2 (0.7 g, 8.05 mmol) as described in more details in the general procedure **C**. Isolation of the product **87d** using a chromatographic column with silica gel and hexane/ethyl acetate (3:2) eluent mixture afforded the red crystalline **87d** in 58% total yield. **M.p**.: compound decomposed above 195°C. **UV-Vis** (toluene) λ/nm (ε, $mol^{-1}\times cm^{-1}$): 467 (944), 326 (35207). **FT-IR** (powder, ν/cm^{-1}): 3067, 2969, 2924 (s, $Py_{\text{-}C\text{-}H}$ stretching), 2136 (w, C≡C), 1591 (s, $Py_{C=C}$ stretching), 1555 (s, $C=N_{imid}$), 1368 (m, N-O). **Elemental analysis:** C 73.15; H 6.76; N 12.11; calculated for $C_{28}H_{32}N_4O_2$: C 73.66; H 7.06; N 12.27.

2-Bromo-5-pyridinecarbaldehyde (91)

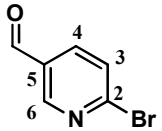

2,5-Dibromopyridine **90** (10 g, 42.2 mmol) was charged into a flask, evacuated and kept under argon. Dry diethylether (250 mL) was added from a syringe and the resulting

solution was cooled to -78°C in dry ice/acetone bath. Then *n*-BuLi (34 mL, 1.6 M in hexane, 53.8 mmol) was added dropwise through the septum. Upon addition of *n*-BuLi the solution turned red. The temperature was kept constant for further 45 min, and then dry dimethylformamide (4.7 mL, d = 0.94 g ml^{-1}, 60.3 mmol) was added dropwise within 15 min. The solution turned deep red. The temperature (-78°C) was maintained for further 90 min, and then slowly raised. Diethyether was evaporated under the reduced pressure. After that 3% HCl (100 mL) and THF (100 mL) were added. The resulted mixture was stirred for 20 min. THF was concentrated in *vacuo*. The oily mixture was neutralized with $NaHCO_3$, and extracted with dichloromethane (4×60 mL). The combined organic layers were dried over $MgSO_4$, and the solvent was evaporated. Crystals were filtrated and washed carefully with hexane (3×20 mL). The filtrate was reduced to a small volume (ca. 2 mL), and was purified on a flash column (SiO_2, dichloromethane). The aldehyde **91** was obtained in 72% total yield. **^{1}H-NMR** ($CDCl_3$, 250 MHz, 298K, 16 scan), δ ppm: 7.66 (d, 1H, ^3J = 8 Hz, H-3), 8.01 (dd, 1H, ^3J = 8 Hz, H-4), 8.82 (s, 1H, H-6), 10.08 (s, 1H, -CHO). **^{13}C-NMR** ($CDCl_3$, 63 MHz, 298K, 256 scan) δ ppm: 129.4 (C-3), 131 (C-5), 137.9 (C-4), 148.7 (C-2), 152.9 (C-6), 189.9 (-CHO). **MS-FD** (70 eV, CH_2Cl_2) m/z: 187.3 (M^+), MW calculated C_6H_4BrNO (MW^+) 186.01.

2-Bromo-5-[1,3]-dioxolan-2-yl-pyridine (92)

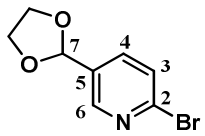

Starting compound **91** (5g, 26.85 mmol) was charged into a flask together with benzene (100 mL), ethyleneglycol (2.7 mL, 48.5 mmol) and catalytic amount of para-toluene-sulfonic acid (0.4 g, 2.1 mmol). The solution was heated to reflux with Deane-Stark for 20 h. Then cold reaction mixture was neutralized with $NaHCO_3$ aqueous solution, and the phases were separated. The aqueous layer was extracted with small portions of benzene (3×15 mL). The combined organic layers were collected, dried over $MgSO_4$ and filtrated. Toluene solution was evaporated under the reduced pressure. Compound **92** was obtained as yellowish oil in 85% yield (5.4g). **^{1}H-NMR** ($CDCl_3$, 250 MHz, 298K, 16 scan), δ ppm: 3.92 (m, 4H, -CH_2), 5.71 (s, 1H, H-7), 7.34 (d, 1H, ^3J = 8 Hz, H-3), 7.62 (dd, 1H, ^3J = 8 Hz, H-4), 8.47 (s, 1H, H-6). **^{13}C-NMR** ($CDCl_3$, 63 MHz, 298K, 256 scan), δ ppm: 64.4 (-CH_2),

100.2 (C-7), 126.9 (C-3), 132.4 (C-5), 135.9 (C-4), 142 (C-2), 147.9 (C-6). **MS-FD** (70 eV, CH_2Cl_2) m/z: 231.2 (M^+), MW calculated $C_8H_8BrNO_2$ (MW^+) 230.06.

2-Ethynyl-trimethyl-silyl-5-[1,3]-dioxolan-2-yl-pyridine (93)

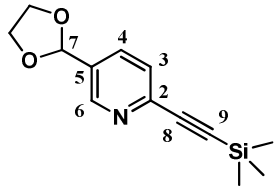

The derivative **93** was synthesized according to the synthetic procedure **(I)**. Purification through a column (SiO_2) with dichloromethane/hexane eluent (3:2) afforded the precursor **93** in 89% yield. **^{1}H-NMR** ($CDCl_3$, 250 MHz, 298K, 16 scan), δ ppm: 0.28 (s, 9H, -CH_3), 4.09 (m, 4H, -CH_2), 5.85 (s, 1H, H-7), 7.47 (d, 1H, ^3J = 8 Hz, H-3), 7.74 (dd, 1H, ^3J = 8 Hz, H-4), 8.65 (s, 1H, H-6). **^{13}C-NMR** ($CDCl_3$, 63 MHz, 298K, 256 scan), δ ppm: 0 (-CH_3), 67.1 (-CH_2), 94.8 (C-9), 102.2 (C-7), 104.1 (C-8), 126.7 (C-3), 132.6 (C-5), 134.9 (C-4), 143.4 (C-2), 148.6 (C-6). **MS-FD** (70 eV, CH_2Cl_2) m/z: 247.1 (M^+), MW calculated $C_{13}H_{17}NO_2Si$ (MW^+) 247.37.

2-Ethynyl-5-[1,3]-dioxolan-2-yl-pyridine (94)

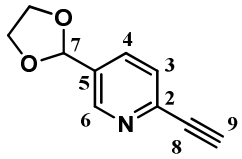

Solution of 2-ethynyl-trimethyl-silyl-5-[1,3]-dioxolan-2-yl-pyridine **93** (0.33 g, 1.3 mmol) in THF (25 mL) was treated under argon with 1N NaOH (50 mL) at 5°C (ice/water bath). After 35 min the reaction was complete (according to TLC analysis of the reaction mixture aliquots). The solvent was evaporated under the reduced pressure, and brine (50 mL) was added to the residue. The aqueous layer was extracted with dichloromethane (3×60 mL). The combined organic fractions were dried over $MgSO_4$ and concentrated in *vacuo*. The so-obtained compound **94** (89% yield) was used for the next step without additional purification. **^{1}H-NMR** ($CDCl_3$, 250 MHz, 298K, 16 scan), δ ppm: 3.2 (s, 1H, H-9), 4.11 (m, 4H, -CH_2), 5.88 (s, 1H, H-7), 7.51 (d, 1H, ^3J = 8 Hz, H-3), 7.78 (dd, 1H, ^3J = 8 Hz, H-4), 8.69 (s, 1H, H-6). **^{13}C-NMR** ($CDCl_3$, 63 MHz, 298K, 256 scan), δ ppm: 65.4 (-CH_2), 72.8 (C-9), 81.4 (C-8), 101.8 (C-7), 127.4 (C-3), 134.2 (C-5), 134.7 (C-4), 142.5 (C-2), 149.4 (C-6). **MS-FD** (70 eV, CH_2Cl_2) m/z: 175.3 (M^+), MW calculated $C_{10}H_9NO_2$ (MW^+) 175.18.

1,2-Bis(5-(1,3-dioxolan-2-yl)pyridine-2-yl)ethyne (95)

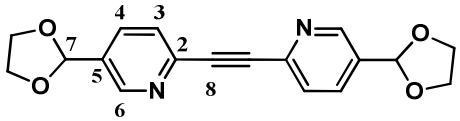

Sonogashira cross-coupling of components **92** and **94** was realized using methodology **(II)**. As the major product 1,2-bis(5-(1,3-dioxolan-2-yl)pyridine-2-yl)ethyne **95** was isolated in 72% yield using flash chromatography (SiO_2, dichloromethane). **^{1}H-NMR** ($CDCl_3$, 250 MHz, 298K, 16 scan), δ ppm: 4.01 (m, 8H, -CH_2), 5.8 (s, 2H, H-7), 7.56 (d, 2H, ^3J = 8 Hz, H-3), 7.72 (dd, 2H, ^3J = 8 Hz, H-4), 8.65 (s, 2H, H-6). **^{13}C-NMR** ($CDCl_3$, 63 MHz, 298K, 256 scan), δ ppm: 65.8 (-CH_2), 88.5 (C-8), 101.9 (C-7), 127.8 (C-3), 133.9 (C-5), 134.9 (C-4), 143.5 (C-2), 149.1 (C-6). **MS-FD** (70 eV, CH_2Cl_2) m/z: 324.5 (M^+), MW calculated $C_{18}H_{16}N_2O_4$ (MW^+) 324.33.

2,2′-Ethyne-1,2-diylbis(pyridine-5-carbaldehyde) (88a)

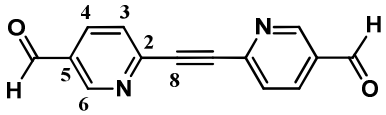

To a solution of **95** (0.38 g, 1.35 mmol) in acetone-water mixture (7:1, 40 mL) para-toluene-sulfonic acid (52 mg, 0.027 mmol, 2 mol%) was added. The progress of the reaction was monitored by TLC (SiO_2, hexane/ethyl acetate, 3:1). After 84 h of stirring at room temperature the reaction was complete. Acetone was evaporated, and the residue was diluted with dichloromethane (30 mL). The organic layer was separated, and the water phase was extracted with dichloromethane (3×30 mL). The combined organic extracts were dried over $MgSO_4$. The solvent was removed in *vacuo* giving 0.26 g (81%) of the dialdehyde **88a** as yellow solid. **^{1}H-NMR** ($(CD_3)_2SO$, 250 MHz, 298K, 16 scan), δ ppm: 8.01 (d, 2H, ^3J = 8 Hz, H-2), 8.37 (dd, 2H, ^3J = 8 Hz, H-3), 9.19 (s, 2H, H-6), 10.20 (s, 2H, -CHO). **^{13}C-NMR** ($(CD_3)_2SO$, 63 MHz, 298K, 256 scan), δ ppm: 90.1 (C-8), 128.8 (C-3), 131.1 (C-5), 137.3 (C-4), 145.7 (C-2), 152.2 (C-6), 192.2 (-CHO). **MS-FD** (70 eV, CH_2Cl_2) m/z: 236.3 (M^+), MW calculated $C_{14}H_8N_2O_2$ (MW^+) 236.23.

2,2'-(2,2'-(Ethyne-1,2-diyl)bis(pyridine-2,5-diyl))bis(4,4,5,5-tetramethylimidazolidine-1,3-diol) (88b)

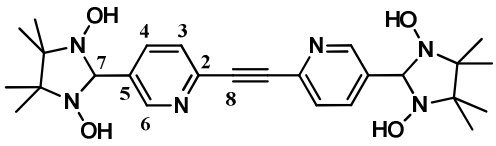

Following the protocol **A1** starting dipyridinedialdehyde **88a** (0.25g, 1.1 mmol) was converted into the corresponding imidazolidine derivative **88b** after 4 h of heating near reflux. The product **88b** was obtained as pale-yellow powder in 80% yield (0.42 g). **^{1}H-NMR** ($(CD_3)_2SO$, 250 MHz, 298K, 128 scan), δ ppm: 1.08 (d, 24H, CH_3), 4.62 (s, H-7), 7.72 (d, 2H, ^3J = 8 Hz, H-3), 7.92 (dd, 2H, ^3J = 8 Hz, H-4), 8.69 (s, 2H, H-6). **^{13}C-NMR** ($(CD_3)_2SO$, 75 MHz, 298K, 18904 scan), δ ppm: 17.6, 24.5 (CH_3), 66.7 ($\underline{C}$-CH_3), 88.1 (C-7), 127.2 (C-3), 136.8 (C-4), 137.9 (C-5), 140.9 (C-2), 150.7 (C-6). **MS-FD** (70 eV, CH_2Cl_2) m/z: 496.4 (M^+), MW calculated $C_{26}H_{36}N_6O_4$ (MW^+) 496.60.

2,2'-(2,2'-(Ethyne-1,2-diyl)bis(pyridine-2,5-diyl))bis(4,4,5,5-tetramethyl-4H,5H-imidazoline-1-oxyl-3-oxo) (88c)

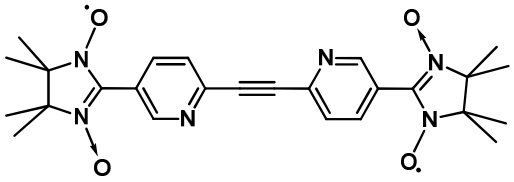

Procedure **B** and subsequent purification through a short flesh-column (SiO_2, hexane/ethyl acetate, 1:3) afforded 54 mg of the bluish crystals of **88c** (13% total yield). **M.p**.: 219-220°C. **UV-Vis** ($CHCl_3$) λ/nm (ε, $mol^{-1}\times cm^{-1}$): 612 (808), 344 (55554); (toluene) λ/nm (ε, $mol^{-1}\times cm^{-1}$) 623 (483), 345 (50402). **FT-IR** (solid; ν in cm^{-1}): 3108, 3072, 2986, 2939 (s, $Py_{\text{-C-H}}$ stretching), 2144 (w, C≡C), 1734 (m, C=O), 1583 (s, $Py_{C=C}$ stretching), 1549 (s, $C=N_{imid}$), 1347 (s, N-O). **Elemental analysis:** C 62.7; H 5.96; N 17.02; calculated for $C_{26}H_{30}N_6O_4$: C 63.66; H 6.16; N 17.13.

2,2'-(2,2'-(Ethyne-1,2-diyl)bis(pyridine-2,5-diyl))bis(4,4,5,5-tetramethyl-4H,5H-imidazoline-1-oxyl) (88d)

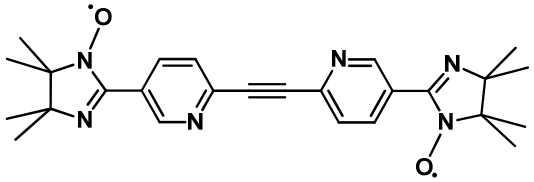

Compound **88d** was synthesized from the imidazolidine **88b** (0.47g, 0.95 mmol) using MnO_2 (1.23 g, 14.1 mmol) as described in the general procedure **C**. The yield of the crystalline **88d** was 250 mg (61%). **M.p**.: compound decomposed at 195°C. **UV-Vis** (toluene) λ/nm (ε, $mol^{-1}\times cm^{-1}$): 467 (944), 326 (35207). **FT-IR** (powder, ν/cm^{-1}): 3067, 2969, 2924 (s, $Py_{\text{-C-H}}$ stretching), 2136 (w, C≡C), 1591 (s, $Py_{C=C}$ stretching), 1555 (s,

C=N_{imid}), 1368 (m, N-O). **Elemental analysis:** C 67.6; H 6.43; N 18.07; calculated for $C_{26}H_{30}N_6O_2$: C 68.10; H 6.59; N 18.30.

5-Bromo-2-pyridinecarbaldehyde (96)

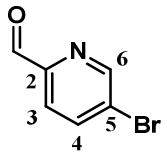

n-BuLi (48 mL, 1.6 M solution in hexane, 76.8 mmol) and 50 mL of dry toluene were transferred into a flame-dried flask filled with argon through the rubber septum. Solution was cooled to -78ºC in dry ice/acetone bath, and solution of 2,5-dibromopyridine **90** (15 g, 63 mmol) in dry toluene (300 mL) was added dropwise within 1.5 h. Upon addition of the starting compound to the mixture the color changed from colorless to yellow. The mixture was stirred for 30 min, and the temperature was allowed to rise to -65°C. Afterwards the solution was cooled again to -78°C, and dry dimethylformamide (5.89 mL, *d* = 0.94 g/mL, 75.8 mmol) was added slowly dropwise. The mixture was left stirring for overnight, and then decomposed with 3% HCl (100 mL). The organic layer was separated, and the water was extracted with dichloromethane (4×50 mL). The combined organic extracts were washed with $NaHCO_3$, dried over $MgSO_4$ and the solvent was evaporated in *vacuo*. The oily residue was purified through a flash column (SiO_2, petroleum ether/ethyl acetate, 100:3). 5-Bromo-2-pyridinecarbaldehyde **96** was obtained in 49% yield. **^{1}H-NMR** ($CDCl_3$, 250 MHz, 298K, 16 scan), δ (ppm): 7.8 (d, 1H, H-6), 7.9 (dd, 1H, ^3J = 8 Hz, H-4), 8.78 (d, 1H, H-3), 9.97 (s, 1H, -C=O). **^{13}C-NMR** ($CDCl_3$, 63 MHz, 298K, 256 scan), δ ppm: 122.7 (C-5), 126.2 (C-3), 139.9 (C-4), 151.1 (C-2), 151.5 (C-6), 192.3 (-CHO). **MS-FD** (70 eV, CH_2Cl_2) m/z: 187.3 (M^+), MW calculated C_6H_4BrNO (MW^+) 186.01.

5-Ethynyl-trimethyl-silyl-2-formylyl-pyridine (97)

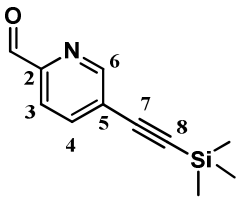

The procedure **(I)** afforded after purification on a chromatographic column with silica and ethyl acetate/hexane (3: 100) eluent mixture derivative **97** in 87% yield (2.37 g). **^{1}H-NMR** ($CDCl_3$, 250 MHz, 298K, 16 scan), δ ppm: 0.26 (s, 9H, $-CH_3$), 7.86 (d, 2H, ^3J = 2 Hz, H-3, H-4), 8.77 (s, 1H, H-4), 8.65 (s, 1H, H-6), 10.02 (s, 1H, -C=O). **^{13}C-NMR** ($CDCl_3$, 63 MHz,

298K, 256 scan), δ ppm: 0 (-CH_3), 98.8 (C-8), 101.9 (C-7), 121.1 (C-3), 122.4 (C-5), 140.4 (C-4), 150.8 (C-2), 151.7 (C-6), 192.7 (C=O). **MS-FD** (70 eV, CH_2Cl_2) m/z: 202.7 (M^+), MW calculated $C_{11}H_{13}NOSi$ (MW^+) 203.31.

5-Ethynyl-2-formyl-pyridine (98)

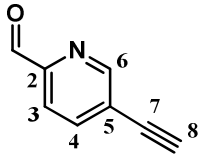

Solution of **97** (1.43 g, 7 mmol) and K_2CO_3 (0.46 g, 3.33 mmol) in deaerated THF/water mixture (80 mL, 1:1 v/v) was stirred at rt for 1.5 h. Brine was added to the mixture, organic layer was separated, and the water phase was extracted with THF (4×30 mL). Combined organic extracts were dried over Na_2SO_4, and the solvent was evaporated under reduced pressure. Light-brown solid was washed with hot hexane/acetone mixture (~20:1) to give pale yellow precipitate in 51% yield (0.47 g). **^{1}H-NMR** ($CDCl_3$, 250 MHz, 298K, 16 scan), δ ppm: 3.36 (s, 1H, H-8), 4 7.87 (d, 2H, ^3J = 8 Hz, H-3, H-4), 8.79 (t, 1H, ^3J = 8 Hz, H-6), 10.0 (s, 1H, -C=O). **^{13}C-NMR** ($CDCl_3$, 63 MHz, 298K, 256 scan), δ ppm: 78.7 (C-7), 83.6 (C-8), 119.9 (C-3), 122.7 (C-5), 139.2 (C-4), 150.4 (C-2), 152.0 (C-6), 191.4 (-CHO). **MS-FD** (70 eV, CH_2Cl_2) m/z: 130.3 (M^+), MW calculated C_8H_5NO (MW^+) 131.13.

5,5′-Ethyne-1,2-diylbis(pyridine-2-carbaldehyde) (89a)

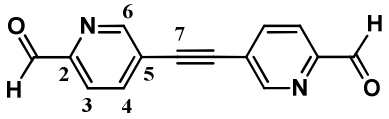

Compound **89a** was synthesized applying Sonogashira-Hagihara coupling methodology **(I)** towards components **96** and **98**. After solvents were evaporated, the residue was diluted with chloroform (40 mL), and washed with NH_4Cl saturated aqueous solution. The solvent was evaporated in *vacuo*. The product was isolated from the reaction mixture using flash chromatography (SiO_2, hexane/chloroform/ethyl acetate, 2:4:1), and recrystallized from hexane/acetone/THF mixture (2:1:1) to give 1,2-bis(2-formyl-5-yl)pyridinel)ethyne **89a** as yellow solid in 62% yield. **^{1}H-NMR** ($CDCl_3$, 250 MHz, 298K, 64 scan), δ ppm: 8.04 (d, 2H, ^3J = 8 Hz, H-4), 8.33 (d, 2H, ^3J = 8 Hz, H-3), 9.09 (s, 2H, H-6), 10.03 (s, 2H, -CHO). **^{13}C-NMR** ($CDCl_3$, 63 MHz, 298K, 256 scan), δ ppm: 59.3 (C-7), 121.6 (C-4), 125.1 (C-5), 138.8 (C-3), 150.2 (C-2), 150.5 (C-6), 191.2 (-CHO). **MS-FD** (70 eV, CH_2Cl_2) m/z: 236.0 (M^+), MW calculated $C_{14}H_8N_2O_2$ (MW^+) 236.23.

2,2'-(5,5'-(Ethyne-1,2-diyl)bis(pyridine-2,5-diyl))bis(4,4,5,5-tetramethylimidazolidine-1,3-diol) (89b)

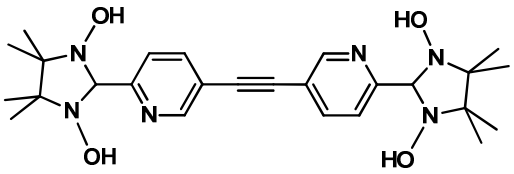

Biradical **89b** was synthesized in 67% yield from 0.1 g (0.4 mmol) of the starting dialdehyde **89a** and 0.14 g of BHA (0.96 mmol) following the general protocol **A2**. **^{1}H-NMR**[‡‡‡‡] ($(CD_3)_2SO$, 250 MHz, 298K, 16 scan), δ ppm: 1.09 (s, 24H, CH_3), 4.69 (s, H-7), 7.68 (d, 2H, ^3J = 8 Hz, H-3), 8.02 (dd, 2H, ^3J = 8 Hz, H-4), 8.71 (d, 2H, H-6). **MS-FD** (70 eV, CH_2Cl_2) m/z: 496.1 (M^+), MW calculated $C_{26}H_{36}N_6O_4$ (MW^+) 496.60.

2,2'-(5,5'-(Ethyne-1,2-diyl)bis(pyridine-2,5-diyl))bis(4,4,5,5-tetramethyl-4H,5H-imidazoline-1-oxyl-3-oxo) (89c)

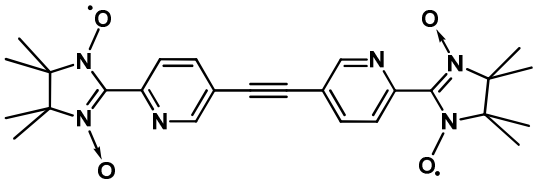

To a magnetically stirred solution of imidazolidine **89b** (0.133g, 0.27 mmol) in absolute methanol (3 mL) excess of MnO_2 (0.35g, 4 mmol, 15 eqivalents with respect to **89b**) was added. The process was monitored by TLC to avoid overoxidation, and formation of imino nitroxide radical. After reaction was completed MnO_2 was filtered off and methanol was evaporated. The radical was purified using thin-plate chromatography (SiO_2, chloroform/ethyl acetate, 2:1). After evaporation of the solvent blue crystals were obtained in 34% total yield. **M.p.**: 236-239°C. **UV-Vis** ($CHCl_3$) λ/nm (ε, $mol^{-1}\times cm^{-1}$): 591 (503), 341 (38929). **FT-IR** (powder, ν/cm^{-1}): 3048, 2985, 2933, 2868 (s, $Py_{\text{-C-H}}$ stretching), 2141 (w, C≡C), 1733 (m, C=O), 1588 (m, $Py_{C=C}$ stretching), 1560 (s, $C=N_{imid}$), 1360 (s, N-O). **Elemental analysis:** C 63.1; H 6.22; N 16.62; calculated for $C_{26}H_{30}N_6O_4$: C 63.66; H 6.16; N 17.13.

Biphenyl-4,4'-dicarbaldehyde (99a)

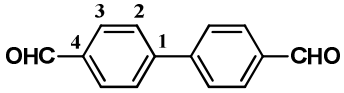

[‡‡‡‡] The ^{13}C-NMR spectr was not obtained, as the sample appeared to be not stable in DMSO and began to oxidize in the NMR tube during the measurements.

n-BuLi (10 mL, 1.6 M solution in hexane, 16 mmol) was charged into a flame-dried flask filled with argon through a septum. Dry TMEDA (2 mL, 0.013 mmol) was added. After stirring at room temperature for 15 minutes the mixture was cooled to -78°C (dry ice/*i*-PrOH), and solution of 4,4'-dibromo-biphenyl **101** (2 g, 6.4 mmol) in dry THF (20 mL) was added slowly dropwise within 30 min. The temperature was slightly increased (to -50°C), due to dramatic decrease of the solubility of the starting substrate at a lower temperature, and kept at this level for 25 minutes. After that the temperature was lowered again to -78°C, and dry dimethylformamide (1.25 mL, *d* = 0.94 g/mL, 16.1 mmol) was added. The temperature was kept constant for 1 h, and than it was allowed to rise slowly. The obtained dense mixture was decomposed with NH_4Cl saturated aqueous solution and extracted with diethyl ether (3×50 mL). The combined organic extracts were dried over $MgSO_4$, and the solvents were evaporated under the reduced pressure. The orange residue was recrystallized from dimethylformamide/water (1:2), yielding 0.78g (58%) of yellowish dialdehyde **99a**. **^{1}H NMR** ($CDCl_3$, 250.13 MHz), δ ppm: 7.71-7.75 (d, 4H, ^3J=8.0 Hz, H-2), 7.92-7.95 (d, 4H, ^3J=8.0 Hz, H-3), 10.02 (s, 2H, -CHO). **^{13}C-NMR** ($CDCl_3$, 63 MHz, 298K, 206 scan), δ ppm: 128.1 (C-1), 130.4 (C-2), 136 (C-3), 145.6 (C-4), 191.7 (-CHO). **MS-FD** (70 eV, CH_2Cl_2) m/z: 210.1 (M^+), MW calculated $C_{14}H_{10}O_2$ (MW^+) 210.1.

2,2'-(Biphenyl-4,4'-diyl)bis(4,4,5,5-tetramethylimidazolidine-1,3-diol) (99b)

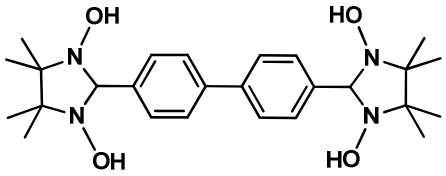

Compound **99b** was synthesized in accordance with the general procedure **A1** from 0.305 g (1.5 mmol) of biphenyl-4,4'-dicarbaldehyde **99a** and 0.64 g of BHA (4.3 mmol) in quantitative yield (0.65 g, 95%). **^{1}H NMR** ($(CD_3)_2SO$, 250.13 MHz), δ ppm: 1.11 (s, 12H, CH_3), 1.13 (s, 12H, CH_3), 4.59 (s, 2H, N-C<u>H</u>-N), 7.42-7.76 (m, 8H, ArH), 7.83 (s, 4H, -OH). **^{13}C NMR** ($(CD_3)_2SO$, 63 MHz, 298K, 256 scan), δ ppm: 17.6, 24.8 (CH_3), 66.5 (<u>C</u>-CH_3), 90.4 (N-<u>CH</u>-N), 126.3, 129.5 (CH_{Ar}), 139.8, 141.4 (C_{Ar}). **MS-FD** (70 eV, CH_2Cl_2) m/z: 470.1 (M^+), MW calculated $C_{26}H_{30}N_6O_4$ (MW^+) 470.60.

2,2'-(Biphenyl-4,4'-diyl)bis(4,4,5,5-tetramethylimidazolidine-1-oxyl) (99d):

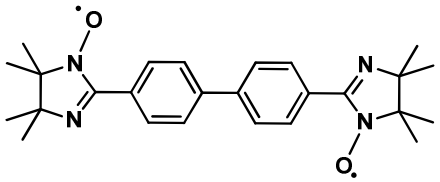

Oxidation of the precursor **99b** (0.3 g, 0.64 mmol) with excess of MnO_2 (0.83 g, 9.5 mmol, methodology **C**) was completed in 20 minutes. The radical **99d** was purified on a chromatographic column with hexane/ethyl acetate gradient solvent mixture (5:1, 3:1). Yield of the orange crystalline **99d** was 0.14 g (47%). **M.p**.: 248.5-250°C. **UV-Vis** ($CHCl_3$) λ/nm (ε, $mol^{-1}\times cm^{-1}$): 461 (1090), 486 (1016). **FT-IR** (powder, ν/cm^{-1}): 3069, 2973, 2926, 2862 (s, Ph-C-H stretching), 1611 (s, Ph C=C stretching), 1567 (w, C=N), 1364 (s, N-O). **Elemental analysis:** C 71.86; H 7.32; N 12.66; calculated for $C_{26}H_{32}N_4O_2$: C 72.19; H 7.46; N 12.95.

Bipyridine-2,2'-dicarbaldehyde (100a)

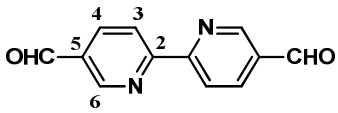

A solution of dimethyl bipyridine **102** (1 g, 5.38 mmol, 1 eq.), NBS (2.49 g, 14 mmol, 2.6 eq.), and benzoyl peroxide (0.29 g, 1.2 mmol, 0.22 eq.) in CCl_4 (50 mL) was refluxed under argon for 14 h. The precipitated succinimide was removed from the hot mixture by filtration. The precipitate was washed with CCl_4 (2×10 mL), and the combined CCl_4 extracts were evaporated in *vacuo*. The resulting yellowish solid containing 5,5'-bis(bromomethyl)-2,2'-bipyridine **103** (1 g, 2.95 mmol, 1 eq.) was refluxed with hexamethylenetetramine (1.65 g, 11.8 mmol, 4 eq.) in 100 mL of ethanol/water (1:1) for 60 h. The mixture was extracted with ethyl acetate/toluene (1:1) (4×50 mL) to afford effective phase separation. The organic extracts were collected and dried over $MgSO_4$. The filtrate was concentrated in *vacuo* to a volume of ca. 2 mL, placed on a column with silica, and eluted with ethyl acetate/hexane gradient solvent mixture (1:4, 1:3). The colorless fractions were collected, affording after solvents evaporation the product **100a** in 57% overall yield. **^{1}H NMR** ($CDCl_3$, 63 MHz, 298K, 256 scan), δ ppm: 7.60-7.64 (d, 2H, ^3J=8.02 Hz, H-4), 7.94-7.98 (dd, 2H, ^3J=8.02 Hz, H-6), 8.76 (d, 2H, ^3J=1.6 Hz, H-3), 10.02 (s, 2H, -CHO). **^{13}C-NMR** (THF-d^8, 63 MHz, 298K, 338 scan), δ ppm: 121.3 (C-3), 127.6 (C-5),

129.4 (C-4), 131.9 (C-6), 136.4 (C-2), 189.7 (-CHO). **MS-FD** (70 eV, CH_2Cl_2) m/z: 211.6 (M^+), MW calculated $C_{14}H_{10}O_2$ (MW^+) 212.1.

2,2'-(Bipyridine-1,1'-diyl)bis(4,4,5,5-tetramethylimidazolidine-1,3-diol) (100b)

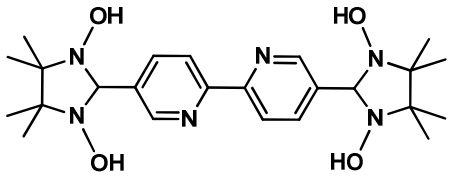

Derivative **100b** was synthesized employing the methodology **A1**. Thus, the imidazolidine **100b** was obtained from 0.15 g (0.71 mmol) of biphenyl-4,4'-dicarbaldehyde **100a** and 0.28 g of BHA (1.85 mmol) in 88% yield (0.30 g). **^{1}H NMR** ($(CD_3)_2SO$, 250.13 MHz), δ ppm: 0.84-0.87 (d, 24H, CH_3), 4.40 (s, 2H, N-C<u>H</u>-N), 7.68 (s, 4H, -OH), 7.73-7.77 (d, 2H, ArH), 8.12-8.15 (d, 2H, ArH), 8.48 (s, 2H, ArH). **^{13}C NMR** ($(CD_3)_2SO$, 63 MHz, 298K, 256 scan), δ ppm: 17.3, 20.8 (CH_3), 66.3 (<u>C</u>-CH_3), 87.9 (N-<u>CH</u>-N), 125.8, 127.9, 131.9 (CH_{Ar}), 137.4, 146.5 (C_{Ar}). **MS-FD** (70 eV, CH_2Cl_2) m/z: 471.8 (M^+), MW calculated $C_{26}H_{30}N_6O_4$ (MW^+) 472.28.

2,2'-(Bipyridine-1,1'-diyl)bis(4,4,5,5-tetramethylimidazolidine-1-oxyl) (100d)

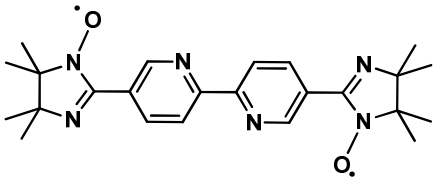

The biradical was achieved using similar procedure as was described earlier for the biradical **99d** in 44% overall yield. **M.p.**: compound started to decompose at 253°C. **UV-Vis** ($CHCl_3$) λ/nm (ε, $mol^{-1}\times cm^{-1}$): 448 (625), 476 (548). **FT-IR** (powder, ν/cm^{-1}): 3087, 3043, 2981 (s, $Py_{\text{-C-H}}$ stretching), 1603 (s, $Py_{C=C}$ stretching), 1562 (s, $C=N_{imid}$), 1366 (s, N-O). **Elemental analysis:** C 65.36; H 7.02; N 19.11; calculated for $C_{24}H_{30}N_6O_2$: C 66.34; H 6.96; N 19.34.

3-Hydroxy-4-ethynyl-trimethyl-silyl-benzaldehyde (110)

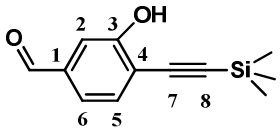

To a mixture of 3-hydroxy-4-iodobenzaldehyde **109** (0.419 g, 1.7 mmol, 1 eq.), $Pd(PPh_3)_2Cl_2$ (35 mg, 0.05 mmol, 0.03 eq.), CuI (30 mg, 0.16 mmol, 0.09 eq.), diisopropylamine (0.24 mL, 1 eq.) in dearated toluene (8.5 mL) ethynyl-trimethyl-silan (0.38 ml, 2.68 mmol) was added. The resulting solution was stirred at room temperature

for 18 h. The mixture was pressed through a short pad of celite and the solvent was removed *in vacuo*. The residue was dissolved in ethyl acetate and the solution was washed with water, dried over $MgSO_4$, concentrated to a smaller volume under the reduced pressure, and purified by a column chromatography over silica gel (hexane/dichloromethane/toluene, 1:2:3). The target compound **110** was obtained in 75% yield. **^{1}H-NMR** ($CDCl_3$, 250 MHz, 298 K, 16 scan), δ ppm: 0.24 (s, 9H, -CH_3), 6.0 (s, 1H, -OH), 7.31-7.38 (td, 2H, $^3J_1$ = 7.5 Hz, $^3J_2$ = 1.5 Hz, H-5, H-6), 7.42-7.45 (d, 1H, ^3J = 8.3 Hz, H-2), 9.89 (s, 1H, -CHO). **^{13}C-NMR** ($CDCl_3$, 63 MHz, 298 K, 1024 scan), δ ppm: 0 (-CH_3), 97.9 (C-8), 106.4 (C-7), 115.1 (C-2), 115.6 (C-4), 121.4 (C-6), 132.2 (C-5), 137.7 (C-1), 157.4 (C-3), 191.3 (-CHO). **MS-FD** (70 eV, CH_2Cl_2) m/z: 216.2 (M^+), MW calculated $C_{12}H_{14}O_2Si$ (MW^+) 218.08.

3-Hydroxy-4-ethynyl-benzaldehyde (111)

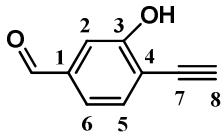

Solution of 3-hydroxy-4-ethynyl-trimethyl-silyl-benzaldehyde **110** (0.25 g, 1.6 mmol) in dearated THF (10 mL) was treated with TBAF (1.72 mL, 1M solution in THF, 2.4 mmol) at room temperature. After 20 min the reaction was complete. The mixture was diluted with diethyl ether (50 mL) and washed with brine (25 mL). Aqueous layer was additionally extracted with ethyl acetate (2×25 mL). The combined organic fractions were dried over Na_2SO_4 and concentrated in *vacuo*. The residue was separated using flesh column with silica and hexane/ethyl acetate (10:3) eluent mixture, yielding the titled compound **111** (69%). **^{1}H-NMR** (THF-d^8, 250 MHz, 298 K, 16 scan), δ ppm: 3.71 (s, 1H, H-8), 7.16-7.19 (m, 2H, H-5, H-6), 7.34-7.38 (d, 1H, ^3J = 8.2 Hz, H-2), 9.77 (s, 1H, -CHO). **^{13}C-NMR** ($CDCl_3$, 63 MHz, 298 K, 1024 scan), δ ppm: 78.5 (C-8), 84.5 (C-7), 114.2 (C-2), 115.3 (C-4), 120.0 (C-6), 133.4 (C-5), 137.5 (C-1), 159.0 (C-3), 189.8 (-CHO). **MS-FD** (70 eV, CH_2Cl_2) m/z: 146.2 (M^+), MW calculated $C_9H_6O_2$ (MW^+) 146.04.

2-(4-Formyl-2-hydroxyphenyl)-6-formyl-benzofuran (112a)

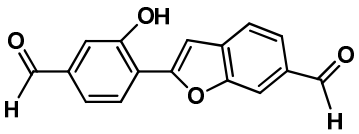

Route A. Following the literature procedure[§§§§] the titled dialdehyde was obtained in 23%.

Route B. 3-Hydroxy-4-iodobenzaldehyde **109** (0.25 g, 1 mmol), $Pd(PPh_3)_2Cl_2$ (14 mg, 0.02 mmol), CuI (3.8 mg, 0.02 mmol), and PPh_3 (10.5 mg, 0.04 mmol) were placed in a flame-dried and argon-filled Schlenk tube. After addition of *i*-Pr_2NH (1.0 mL) and toluene (6.0 mL), the mixture was stirred at 25°C for 5 min and (trimethylsilyl)acetylene (0.17 mL, 1.2 mmol) was added. This mixture was stirring at room temperature for 18 h, then solution of KOH (0.113 g, 2.00 mmol) in water/methanol (15:70, 0.85 mL) was added in one portion and the mixture was stirred for additional 3 h. After that 3-hydroxy-4-iodobenzaldehyde **109** (0.25 g, 1 mmol) was added to the reaction mixture in argon stream, and the stirring was continued for 16 h. The resulting mixture was quenched with saturated NH_4Cl solution (60 mL) and extracted with CH_2Cl_2 (3×50 mL). The combined organic layers were washed with HCl (2N, 30 mL), water (50 mL), and brine (50 mL). After concentration under vacuum, the residue was purified by flash chromatography on silica (dichloromethane/ethyl acetate, 10:1) to give **112a** (0.13 g, 49%) as a light orange solid.

Route C. 3-Hydroxy-4-iodobenzaldehyde **109** (0.68 g, 2.7 mmol), $Pd(PPh_3)_2Cl_2$ (0.114 g, 0.16 mmol) and CuI (51.4 mg, 0.27 mmol) were placed in a flame-dried and argon-filled Schlenk tube. Septum was parafilmed after solids were added. While stirring, sparged with argon dry benzene (13.5 mL) and 1,8-diazabicyclo[5.4.0]undec-7-ene (DBU, 2.5 mL, 1.018 g/mL, 6 eq.) were added by a syringe. The resulting mixture was additionally purged with argon. Ice-chilled (trimethylsilyl)acetylene (0.195 mL, 1.37 mmol) was then added through the septum, followed immediately by distilled water (20 µL, 1 mmol). The reaction flask was covered in aluminum foil and left stirring at a high rate of speed for 18 h. The mixture was diluted with diethyl ether and decomposed with NH_4Cl. The organic phase was separated and washed with brine (50 mL). Water was extracted with dichloromethane (3×40 mL). The combined organic extracts were dried over $MgSO_4$, and the solvents were removed in *vacuo*. The crude product was purified by silica gel column chromatography with dichloromethane/ethyl acetate (10:1) eluent mixture (0.566 g, 78%). **^{1}H-NMR** (CD_3OD, 250 MHz, 298 K, 64 scan), δ ppm: 5.42 (s, 1H, -OH), 7.36 (d, 1H, ^3J = 1.4 Hz), 7.42-7.46 (dd, 1H, $^3J_1$ = 8 Hz, $^3J_2$ = 1.5 Hz), 7.65 (d, 1H, ^3J = 0.9 Hz), 7.72 (m, 2H), 8.0 (d, 1H, ^3J = 0.9 Hz), 8.09-8.13 (d, 1H, ^3J = 8 Hz), 9.86 (s, 1H, -CHO), 9.96 (s, 1H, -CHO).

[§§§§] R. Severin, J. Reimer, S. Doye, *J. Org. Chem.*, **2010** (75), 3518–3521.

^{13}C-NMR (CD_3OD, 63 MHz, 298 K, 215 scan), δ ppm: 109.5 (=CH), 113.0, 115.7, 125.3, 126.01, 128.3, 135.3, 136.3, 138.9, 155.03 (=C-O-), 156.5 (=C-O-), 156.7 (-C-OH), 191.9 (-CHO), 192.0 (-CHO). **MS-FD** (70 eV, CH_2Cl_2) m/z: 266.2 (M^+), MW calculated $C_{16}H_{10}O_4$ (MW^+) 266.06.

2-[4-(4,4,5,5-tetramethyl-4H,5H-imidazoline-1-oxyl-3-oxo)-2-hydroxyphenyl]-6-(4,4,5,5-tetramethyl-4H,5H-imidazoline-1-oxyl-3-oxo)-benzofuran (112c)

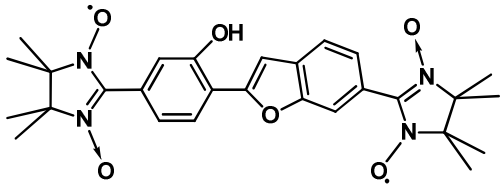

The condensation between the carbaldehyde **112a** and BHA was realized in deaerated methanol/toluene mixture (1:1). Full conversion of the starting dialdehyde **112a** into the corresponding imidazolidine **112b** was achieved after 15 days of stirring at room temperature. Oxidation of the imidazolidine **112b** with sodium periodate in DCM/water mixture (3:1) at ~0-5°C following the procedure described previously (**B**) granted the titled benzofuran biradical **112c** in 24% total yield. **M.p**.: 352-353°C. **UV-Vis** (toluene) λ/nm (ε, $mol^{-1}\times cm^{-1}$): 610 (938), 372 (55833). **FT-IR** (powder, v/cm^{-1}): 3260 (broad m, OH), 2981, 2930 (s, Ar_{-C-H} stretching), 1614 (m, C=N), 1578 (s, C=C), 1357 (s, N-O), 1136 (s, C-O-C). **Elemental analysis:** C 64.9; H 6.22; N 11.2; calculated for $C_{28}H_{32}N_4O_6$: C 64.60; H 6.20; N 10.76.

4-Amino-3-bromobenzaldehyde (117)

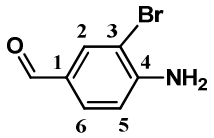

A mixture of 2-bromoaniline **116** (0.86 g, 5 mmol) dissolved in DMSO (100 mL), conc. aqueous HCl (5 mL) and dried CuCl (1.35 g, 10 mmol) was heated at 90°C for 6 h. The reaction was quenched with ice-water, and the pH of the mixture was adjusted to ~8 using NaOH (10%) solution. The mixture was extracted with diethyl ether (4×250 mL). The combined extracts were dried over Na_2SO_4 and the solvent was evaporated. The product was purified on a column with silica and toluene/ethyl acetate (40:1) solvents mixture. Yield: 47% (0.47 g). **^{1}H-NMR** ($CDCl_3$, 250 MHz, 298 K, 16 scan), δ ppm: 6.71-6.75 (d, 1H, ^3J = 8.3 Hz, H-5), 7.55-7.59 (dd, 1H, $^3J_1$ = 8.3 Hz, $^3J_2$ = 1.8 Hz, H-6), 7.88 (d, 1H, ^3J = 1.8 Hz, H-2), 9.64 (s, 1H, -CHO). **^{13}C-NMR** ($CDCl_3$, 63 MHz, 298 K, 256 scan), δ ppm: 114.6, 130.7,

135.1, 144.1, 149.5, 189.2. **MS-FD** (70 eV, CH_2Cl_2) m/z: 199.0 (M^+), MW calculated C_7H_6BrNO (MW^+) 198.96.

4-Amino-3-cyanobenzaldehyde (118)

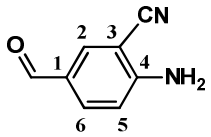

A mixture of 4-amino-3-bromobenzaldehyde **117** (0.1 g, 0.5 mmol, 1 eq.), zinc cyanide (35 mg, 0.3 mmol, 0.6 eq.) and $Pd(PPh_3)_4$ (0.023 g, 0.02 mmol, 0.04 eq.) in deaerated DMF (20 mL) was heated at 80°C under argon for 12 h until TLC showed absence of the starting material. The mixture was then cooled to ambient temperature, diluted with toluene (50mL), and washed twice with 2N ammonium hydroxide (50 mL). Afterwards the organic fraction was washed with brine (25mL) and concentrated in *vacuo* with silica. Purification on a silica chromatographic column with hexane/ethyl acetate gradient eluent mixture (3:1, 2:1) provided the titled product **118** in 70% yield. **^{1}H-NMR** ($CDCl_3$, 250 MHz, 298 K, 64 scan), δ ppm: 6.72-6.75 (d, 1H, ^3J = 8.3 Hz, H-5), 7.55-7.59 (dd, 1H, $^3J_1$ = 8.3 Hz, $^3J_2$ = 1.8 Hz, H-6), 7.80 (d, 1H, ^3J = 1.8 Hz, H-2), 9.65 (s, 1H, -CHO). **^{13}C-NMR** ($CDCl_3$, 63 MHz, 298 K, 256 scan), δ ppm: 108.5, 114.6, 128.5, 128.6, 130.7, 135.1, 189.2. **MS-FD** (70 eV, CH_2Cl_2) m/z: 146.2 (M^-), MW calculated $C_8H_6N_2O$ (MW^+) 145.05.

4-Iodo-3-cyanobenzaldehyde (119)

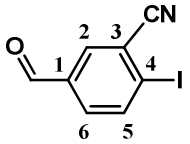

Conc. hydrochloric acid (4 mL) was added to a solution of 4-amino-3-cyanobenzaldehyde **118** (0.4 g, 2.8 mmol) in acetic acid (45 mL), and the resulting suspension was cooled using an ice-NaCl bath. Sodium nitrite aqueous solution (0.22 g, 3.1 mmol) in water (10 mL) was added slowly, keeping the internal temperature <5°C. On complete addition, the solution was stirred for 30 min, and then the resulting mixture was poured into a solution of potassium iodide (0.92g, 5.5 mmol) and iodine (0.1 g, 0.78 mmol) in water (50 mL). The mixture was left stirred for 90 min. Water (100 mL) and dichloromethane (50 mL) were added. The organic phase was separated, and water solution was extracted with dichloromethane (2×50 mL). The combined extracts were washed with sodium 10% thiosulfate aqueous solution (2×25 mL), 1.0M sodiumhydroxide

(2×25 mL), brine (30 mL), and dried over anhydrous Na_2SO_4. Evaporation of the solvent in *vacuo* afforded the title compound **119** (0.64 g, 87%) as a pale-brown solid. **^{1}H-NMR** ($CDCl_3$, 250 MHz, 298 K, 64 scan), δ ppm: 7.67-7.71 (dd, 1H, $^3J_1$ = 8.2 Hz, $^3J_2$ = 2 Hz, H-6), 8.01 (d, 1H, ^3J = 2 Hz, H-2), 8.10 (d, 1H, ^3J = 8.2 Hz, H-5), 9.92 (s, 1H, -CHO). **^{13}C-NMR** ($CDCl_3$, 63 MHz, 298 K, 256 scan), δ ppm: 105.3, 117.3, 121.1, 132.1, 133.7, 135.0, 139.7, 188.2. **MS-FD** (70 eV, CH_2Cl_2) m/z: 257.2 (M^+), MW calculated C_8H_4INO (MW^+) 256.93.

1,4-Diethynyl-trimethyl-silyl-benzene (133)

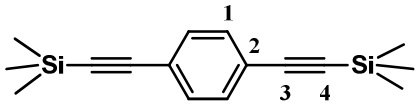

To achieve the target molecule **133** Sonogashira-Hagihara cross-coupling methodology was applied. Thus, a mixture of 1,4-dibromobenzene **127** (2.5 g, 10.6 mmol, 1 eq.) dissolved in dry CH_3CN/NEt_3 (30 mL, 1:1 v/v) solvent mixture was deaerated using argon bubbling for 20 min, and then the catalytic mixture of $Pd(PPh_3)_2Cl_2$ (0.74 g, 1.1 mmol, 0.1 eq.), PPh_3 (0.556 g, 2.1 mmol, 0.2 eq.), CuI (0.2 g, 1.1 mmol, 0.1 eq.) was added at once in argon stream. The reaction mixture was protected from oxygen with an air balloon, and ethynyl-trimethyl-silan (3.6 mL, 25.4 mmol, 2.4 eq.) was added through the septum. The reaction was complete after 18 h stirring at room temperature. Typical work-up (in accordance to the procedure (**I**)), and purification on a chromatographic column with silica gel (hexane) provided compound **133** in 80% yield (2.3 g). **M.p.**: 122-123°C. **FT-IR** (powder, v/cm^{-1}): 2956 (m, C-H_{Ar}), 2898 (w, -CH_3), 2156 (s, -C≡C-), 1492 (s, -C=C_{Ar}), 1244 (s, -Si-C), 826, 753 charateristic pair for Si-CH_3. **^{1}H-NMR** ($CDCl_3$, 250 MHz, 298 K, 16 scan), δ ppm: 0.27 (s, 18H, -CH_3), 7.42 (s, 4H, Ar-H). **^{13}C-NMR** ($CDCl_3$, 63 MHz, 298 K, 256 scan), δ ppm: 0 (-CH_3), 96.4 (C-4), 104.6 (C-3), 123.2 (C-2), 131.8 (C-1). **MS-FD** (70 eV, CH_2Cl_2) m/z: 269.3 (M^+), MW calculated $C_{16}H_{22}Si_2$ (MW^+) 270.13.

1,4-Diethynyl-benzene (134)

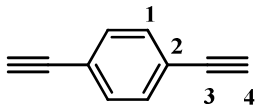

A solution of **133** (1.18 g, 4.4mmol) and NaOH (0.8 g, 20 mmol) in deaerated THF/water mixture (45 mL, 2:1 v/v) was stirred at room temperature for 6 h. The mixture was diluted with diethyl ether (100 mL), brine was added (75 mL), and the organic phase was separated. The aqueous layer was extracted with diethyl ether (2×50 mL). The combined organic layers were dried over $MgSO_4$, the solvents was evaporated under the reduced

pressure. The product **134** was obtained as a yellowish solid in 93% yield. **M.p.**: 87-88°C. **FT-IR** (powder, ν/cm^{-1}): 3260 (s, C-H_{Ar}), 2953, 2925, 2855 (w, ≡CH), 2105 (w, -C≡CH), 1495 (s, -C=C_{Ar}). **^{1}H-NMR** (THF-d^8, 250 MHz, 298 K, 16 scan), δ ppm: 3.65 (s, 2H), 7.39 (s, 4H). **^{13}C-NMR** (THF-d^8, 63 MHz, 298 K, 256 scan), δ ppm: 79.9 (C-4), 82.6 (C-3), 122.8 (C-2), 131.8 (C-1). **MS-FD** (70 eV, CH_2Cl_2) 125.3 (100%), MW calculated 126.05 ($C_{10}H_6$).

1,4-Bis-phenylpropargylaldehyde diethyl acetal (135)

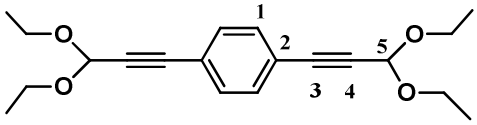

Into a reaction flask equipped with a thermometer and a 25-cm fractionating column 1,4-diethynyl-benzene **134** (0.25 g, 2 mmol), zinc iodide (0.06 g, 0.19 mmol), triethyl orthoformate (1.4 mL, *d* = 0.89 g/mL, 8.4 mmol) were charged. Ethanol was slowly distilled (at 175°C) from the reaction mixture, which was heated to about 131°C (inner temperature) before refluxing in the still-head has begun. The reaction mixture was cooled down to ambient temperature and diluted with acetone. Silica gel was added and the solvent was evaporated. The residue was then purified on a chromatographic column (SiO_2) with gradient hexane/dichloromethane/toluene mixture (5:3:2, 5:4:2, 1:1:0, 1:2:0). A total of 0.33 g (51%) of the product as yellow solid **135** was collected. **FT-IR** (powder, ν/cm^{-1}): 2976 (m, C-H_{Ar}), 2927, 2880 (w, -CH_3), 2240, 2222 (m, -C≡C-), 1505, 1442, 1355, 1325 (s, -C=C_{Ar}), 1014 (s, -C-O-C). **^{1}H-NMR** ($CDCl_3$, 250 MHz, 298 K, 16 scan), δ ppm: 1.17-1.23 (t, 12H, -CH_3), 3.52-3.80 (m, 8H, -CH_2), 5.41 (s, 1H, H-5), 7.34 (s, 4H, Ar-H). **^{13}C-NMR** ($CDCl_3$, 63 MHz, 298 K, 32 scan), δ ppm: 15.1 (-CH_3), 61.0 (-CH_2), 84.6 (C-3), 86.3 (C-5), 91.7 (C-4), 122.3 (C-2), 131.8 (C-1). **MS-FD** (70 eV, CH_2Cl_2) m/z: 329.5 (M^+), MW calculated $C_{20}H_{26}O_4$ (MW^+) 330.18.

1,4-Bis-phenylpropargylaldehyde (121a)

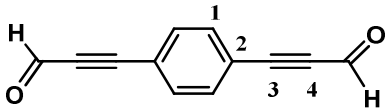

A solution of 1,4-bis-phenylpropargylaldehyde diethyl acetal **135** (0.6 g, 1.8 mmol) and $Ce(OTf)_3{\cdot}xH_2O$ (0.11 g, 0.18 mmol) in CH_3NO_2 (15 mL) saturated with water (3.0 mL) was stirred at room temperature under argon. After 1 h the reaction was complete, and CH_3NO_2 was removed in *vacuo*. The residue containing precipitate and water was filtered, washed with water (2×20 mL) and hexane (2×15 mL). The isolation by flash

chromatography (hexane/toluene/dichloromethane, 50:5:2) afforded the titled carbaldehyde **121a** in 94% yield (0.311 g). **FT-IR** (powder, ν/cm^{-1}): 2892 (w, -CH_3), 2191 (s, -C≡C-), 1650 (-C=O), 1498, 1406, 1387 (m, -C=C_{Ar}). **UV-Vis** (THF) λ/nm (ε, mol^{-1}×cm^{-1}): 302 (29069), 320 (31906). **^{1}H-NMR** (THF-d^8, 250 MHz, 298 K, 16 scan), δ ppm: 7.62 (s, 4H, ArH), 9.31 (s, 2H, -CHO). **^{13}C-NMR** ($CDCl_3$, 63 MHz, 298 K, 32 scan), δ ppm: 89.9 (C-4), 91.6 (C-3), 122.1 (C-2), 133.2 (C-1), 176.2 (-CHO). **MS-FD** (70 eV, CH_2Cl_2) m/z: 181.5 (M^+), MW calculated $C_{12}H_6O_2$ (MW^+) 182.04.

1,4-Di[2-(1-hydroxy-4,4,5,5-tetramethyl-2-ylidene)ethanone]-benzene (136)

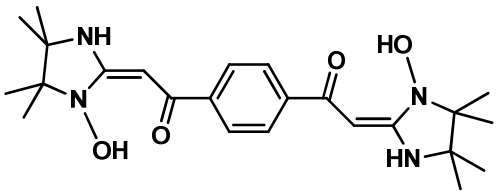

Following the general procedure **A2** compound **136** was obtained as yellow solid in 82% yield. **M.p**.: compound started to decompose at 272°C. **UV-Vis** (DMSO) λ/nm (ε, mol^{-1}×cm^{-1}): 351 (9818). **FT-IR** (powder, ν/cm^{-1}): 3300, 3118, 2792 (-NH, -OH), 2975 (-CH_3), 1586, 1522, 1492 (s, HN-C=C-C=O stretching). **^{1}H-NMR** (DMSO-d^6, 250 MHz, 298 K, 64 scan), δ ppm: 1.08 (d, 24H, -CH_3), 5.49 (s, 2H, HC=), 7.79 (s, 4H, ArH), 8.98 (s, 2H, NH), 9.39 (s, 2H, OH). **Elemental analysis:** C 71.86; H 7.32; N 12.66; calculated for $C_{26}H_{34}N_4O_4$: C 65.14; H 7.74; N 12.66.

Appendix

The the changes in the fluorescence intensities of the pyrene probe **80c** upon reaction with various chemical agents.

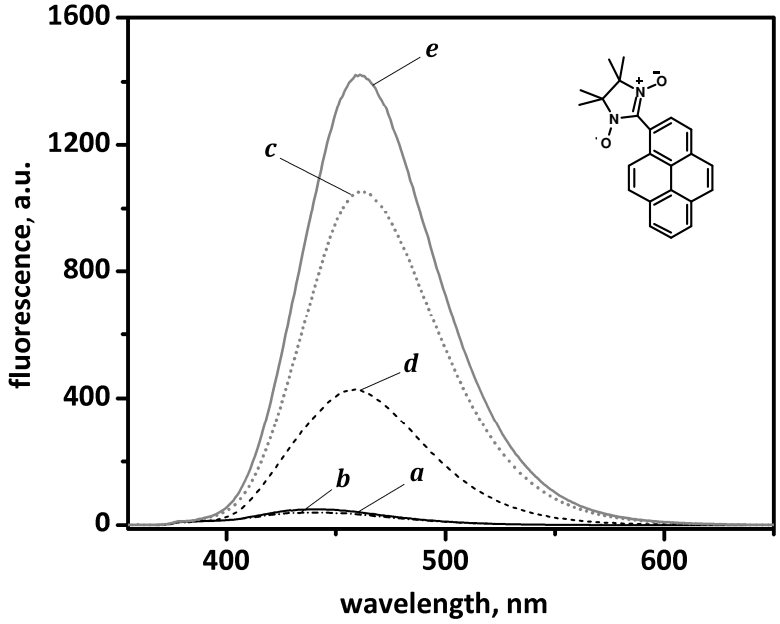

Figure A1. Fluorescence spectra of the pyrene nitronyl nitroxide **80c** in MeOH with the concentration 2.5×10^{-6} M and an excitation wavelength of 346 nm under different conditions: (*a*) pure solution of the radical; (*b*) after reaction with CF_3COOH (1.8×10^{-5} M); (*c*) after reaction with cysteine (5×10^{-4} M); (*d*) after reaction with ascorbic acid (5×10^{-4} M); (*e*) after sequential reactions with cysteine (5×10^{-4} M) and CF_3COOH (1.8×10^{-5}M).

Behaviour of the spin-coated nitronyl nitroxide radical **57c** in aqueous media is shown in *Figure A2* as a typical example. A small decay in the fluorescence intensity was attributed to the decrease of the radical layer thickness, which occurred, most probably, due to the drying of the films with compressed air.

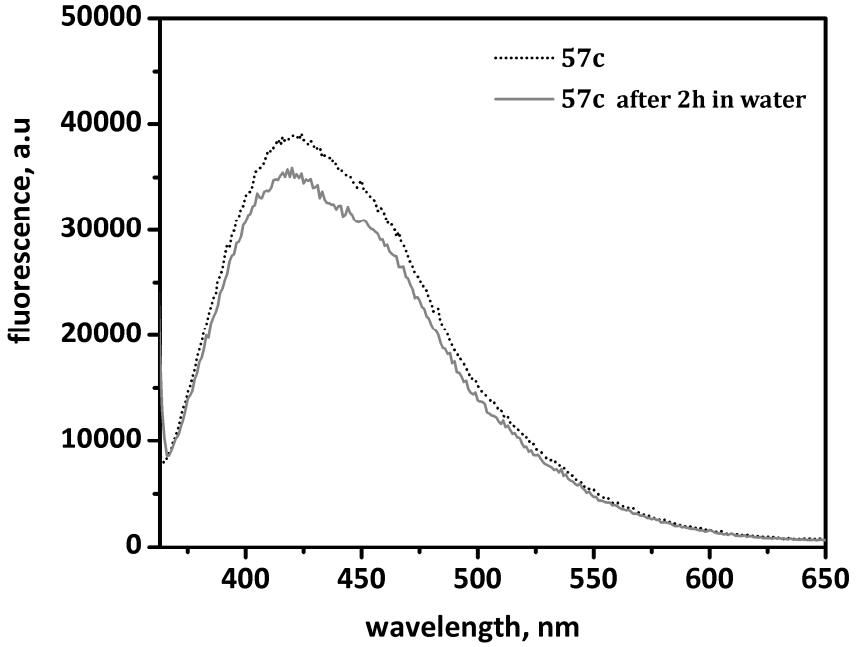

Figure A2. Stability of the spin-coated radical **57c** film in aqueous media.

List of publications

1. Bernd Wolf, Pham T. Cong, Katarina Remović-Langer, *Yulia B. Borozdina*, Evgeny A. Mostovich, Martin Baumgarten, Michael Lang "Coupled spin S = 1/2 dimer systems based on nitronyl-nitroxide biradicals" *J. Phys. Conf. Ser.* **2010**, 200, 1-4.

2. Evgeny Mostovich, *Yulia Borozdina*, Volker Enkelmann, Katarina Remović-Langer, Bernd Wolf, Michael Lang, Martin Baumgarten "Planar Biphenyl-Bridged Biradicals as Building Blocks for the Design of Quantum Magnets" *Cryst. Growth Des.* **2012** (12), 54–59.

3. Yulia B. Borozdina, Valentin Kamm, Frédéric Laquai, Martin Baumgarten "Tuning the Sensitivity of Fluorophore-Nitroxide Radicals" accepted for *J. Mat. Chem.*

4. Yulia B. Borozdina, Evgeny A. Mostovich, Volker Enkelmann, Bernd Wolf, Pham T. Cong, Katarina Remović-Langer, Michael Lang, Giorgio Zoppellaro, Martin Baumgarten "Synthesis and Physical Characterization of Interacting Networks of Purely Organic Spin-½ Dimers" submitted for *J. Org. Chem.*

5. Yulia B. Borozdina, Evgeny A. Mostovich, Volker Enkelmann, Bernd Wolf, Pham T. Cong, Michael Lang, Giorgio Zoppellaro, Martin Baumgarten "Low-dimentional spin networks architecture - tuning the magnetic exchange properties in the bulk" *manuscript in preparation.*